DISSERTATION

ANALYSIS OF HISTORICAL ISLAMIC GLAZES AND THE
DEVELOPMENT OF A SUBSTITUTION MATERIAL

SUBMITTED BY

RENA GRADMANN
2016

INSTITUTE OF GEOGRAPHY AND GEOLOGY
DEPARTMENT OF GEODYNAMICS AND GEOMATERIAL
RESEARCH

UNDER THE SUPERVISION OF
PROF. DR. ULRICH SCHÜSSLER
JULIUS MAXIMILANS UNIVERSITY WÜRZBURG

Statutory declaration

I hereby declare that this dissertation is my own original work and that I have fully acknowledged by name all of those persons and organisations that have contributed to the research for this dissertation. Any thoughts from others or literal quotations are clearly marked.

Acknowledgements

CONTENT

1 Motivation

Historical Islamic buildings impress by their filigree architecture and colourful facades and many of them therefore belong to the UNESCO world cultural heritage. Particularly the carefully arranged and gorgeous glazes of the facade tiles give the buildings their typical and imposing appearance (fig.1). But the mosques and Islamic schools (madrassas) lose their impressive image, when the glazed tiles are damaged and the glazes are chipped off (fig.2). In the architectural monuments, the influences of climate, groundwater and environment pollution can lead to deterioration of the building materials and to the chipping of the tile glazes (Allan *et al.*, 2000). Unfortunately this applies to lots of historical buildings in wide parts of the Islamic cultural area, and restoration of glazes becomes a matter of urgency to save the brilliant facades from irreversible destruction.

Figure 1: Cupolas and portal of the madrassa Mir-i Arab in Bukhara, Uzbekistan (picture kindly provided by Alexey Protchenkov).

Figure 2: Damaged tiles on the top of a column of the mosque Khoja Zainuddin in Bukhara, Uzbekistan, Badr *et al.* (2010).

As art and monuments in general, the buildings of Islamic culture are exposed to the risk of destruction by human or environmental influence, whereby long-kept knowledge and skills threaten to get lost. In order to preserve the knowledge of sophisticated craftsmanship and to develop a suitable supplement material for restoration of the glazes, the chemical compositions and processing parameters of the glazes are investigated in a first topic of this study. Especially for the creation of a similar optical effect of the restoration material, the colouring agents in the glazes have to be known. Apart from this, knowledge of the glaze compositions reveals trends and developments which result not only from the availability of raw materials but also from the adaption of production technology. In this study, samples from imposing Islamic buildings in Central Asia, the Middle East, Asia Minor, and North Africa and from a period of the 10th-18th century were taken for electron probe micro analysis (EPMA) and µ-XRD[2] analysis. The focus lies on the investigation of the glazes from inner and outer wall tiles, from pillars and archways, floors and prayer niches. Additionally, some glazes of ceramic tableware are included into the study. A comparison between the different locations, centuries, and dynasties gives the possibility to distinguish between well-established techniques, regional preferences, and temporal characteristics. The extent of the sample set, as well as the methodology of pigment analysis is new in the investigation of Islamic glazes.

On the field of Islamic ceramic tableware glazes several studies were carried out, primarily for particular sites or epochs, e.g. for Jordanian glazes of the 12th-13th century (Al-Saad, 2002), for

Yemenite glazes of the 12th-15th century (Hallett *et al.*, 1988), glazes from the south west Iran of the 13th century (Hill, 2004), and glazes from Akshiket, Uzbekistan from the 9th-13th century (Henshaw, 2010), but also comparative studies of several sites are found (Tite, 2011). Islamic tile glazes are sporadically investigated, i.e. Moroccan tile glazes from the 14th-18th century (Zucchiatti *et al.*, 2009), Turkish glazes from Iznik of the 16th century (Simsek *et al.*, 2010), Iranian glazes of the 13th century (Osete-Cortina *et al.,* 2010), and north Indian tile glazes from the 17th century (Gill & Rehren, 2011).

A second, analytical issue concerns the possibility to measure large quantities of glazes on site, as it is the need for tiled facades. The portable XRF is tested here for the first time to study historical glazed tiles. It is a controversially discussed device, which gives results of a not prepared sample within a few minutes without any destructive intervention. It is an important invention for the restorers and archaeometers and allows much better evaluation of the present material composition. For the analysis of historical material, this point makes it reasonable to test the tool on the glazed ceramics and to describe the possibilities and limits of application. The precision and the reliability of the measurements are investigated for the main composition as well as for the colouring agents in the glaze.

The third topic is the development of an adapted glaze restoration material for the use on site. High demands are imposed on the properties of such a substitution material in order to ensure its stability and reversibility, but also an appearance which fits into the overall picture of the object of art (Brandi *et al.,* 2006; Davison & Newton, 2008). The aim is to introduce the colouring agents into the material and to ensure the colour fastness and the resistance to different weathering conditions. The hybrid polymer ORMOCER® is taken as basis for the substitution material. This is already used as coating and stabilizing material in the restoration of glass (Müller-Weinitschke, 1995; Leißner *et al.,* 1998). Different adaptations of the material to the original colouring are performed, in order to get a suitable substitution material for the restoration of the historical glazes. The colour adaption of the modern material is done as far as possible according to the analysis of original colouring agents. Where the original colouring agents are not possible to be imitated, optically suitable substitutes are used. In a next step, the restoration material is tested in climate chambers under different weathering conditions. These conditions are adapted to known climatic data of the sampled regions in order to ensure a successful application of the substitute material in possible future restoration projects. This adaption of ORMOCER® material to Islamic tile glazes is a completely new approach and involves

modern technology of dispersion methods and particle integration. With the ORMOCER®
material of the Fraunhofer Institute for Silicate Research, a very promising and already
successfully applied restoration material builds the foundation for the substitution material.

In the beginning of the study, theory and background of the relevant contents are sketched in
chapter 2. The glass structure and composition is described including the methods of glass
colouring and the history of glaze making. The theory of restoration as well as the fundamentals
of the ORMOCER® material is explained here. Chapter 3 outlines the sample recovery and the
historical embedding of the historical glazes. The next chapter 4 elucidates the sample
preparation procedure and the essentials of the analytical methods. The study is than divided in
the three parts: sample analysis, analytical method, and restoration material development
investigation. The results of EPMA are described in chapter 5 and are subdivided into the results
from different regions and ages of the sample origin. Furthermore, the analysis of the historical
glazes brings along the description of theoretical firing temperatures in chapter 6, calculated
from the analysed composition. The chapter 7 outlines the colouring agents in the particular
groups of samples, investigated with EPMA and µ-XRD^2. The whole set of samples is investigated
with the EPMA method, whereas only part of the Uzbek samples are investigated with the µ-
XRD^2 concerning the colouring pigments of the glazes. A discussion of element composition,
firing temperatures and colouring agents is given in chapter 8.

The advantages and limits in the use of the portable XRF for the in-situ analysis on glass and
glazes are described in chapter 9. It is carried out on those 28 historical glazes from Uzbekistan
and Morocco which have a sufficiently large surface area. Two different measurement modes
are tested in the application of glazed ceramic. In addition, the data from synthetic glass samples
as bulk glass and glass layer are compared with the original glaze data.

The approaches of ORMCOER® colouring methods are sketched in chapter 10, beginning with
the consideration of former restoration projects with coloured ORMOCER® on terracotta
medallions in northern Germany. The colouring pigments for the ORMOCER® material include
coloured glass of historical composition, mineral pigments and nano scaled metal oxides, which
are additionally treated with a surface modification. Different methods of homogenization and
dispersion are tested. A summary of all results is given in chapter 11.

2 Theory and background

The theoretical embedding of the investigations is divided in the following subchapters: at the first place are the structural and chemical properties of glass and the calculation of glass processing temperature as well as a description of glass production technology. The second chapter describes the relevant options for glass colouring such as ion colouring, pigmentation, colloid technique, and lustre technology. In the third chapter, the specification of glaze and the history of glaze making are sketched, considering the early glazes in Egypt and Mesopotamia, the ancient glazes of the Greek and Roman Empire and the specifics of Islamic glaze making. In the fourth chapter, the theory for modern restoration approaches is explained and the options of supplement materials are sketched. The ORMOCER® material, which is tested in this study, is presented in its general composition and its specifications for glaze restoration.

2.1 Main components of glass

2.1.1 Glass structure

The basis of the glass composition is an amorphous network of SiO_4-tetrahedrons, which is enhanced with network modifying agents in the interstitial places of the network. These are traditionally the alkali ions Na^+ and K^+ as well as the alkali earth ions Ca^{2+} and Mg^{2+}. The so-called intermediates are not pure network formers or modifiers but can act as both, such as Al_2O_3, PbO, TiO_2, ZrO_2, ZnO or CdO (Scholze, 1965). The charges of network former ions are neutralised by non-bridging oxygen bonds in the silica network, respectively Al^{3+} ions on the network positions of Si^{4+}. The modifying agents lower the melting point of the silica. Because of their interstitial positions in the network, they prevent the silica structure to re-crystallise. In opposite to a crystalline structure with three dimensional translational symmetric arrays of atomic positions, the atomic array in glass has no long-range order but only short-range structure of mean atomic distances. These are defined by the lengths of the atomic bondings and the resulting sphere of nearest neighbours. The Si^{4+} ions have, according to the ionic radii ratio to O^{2-}, tetrahedral coordination polyhedrons, which are connected over the corners of tetrahedrons to a three dimensional network. Some other network formers such as BO_3 are too small and form triangles as coordination polyhedron.
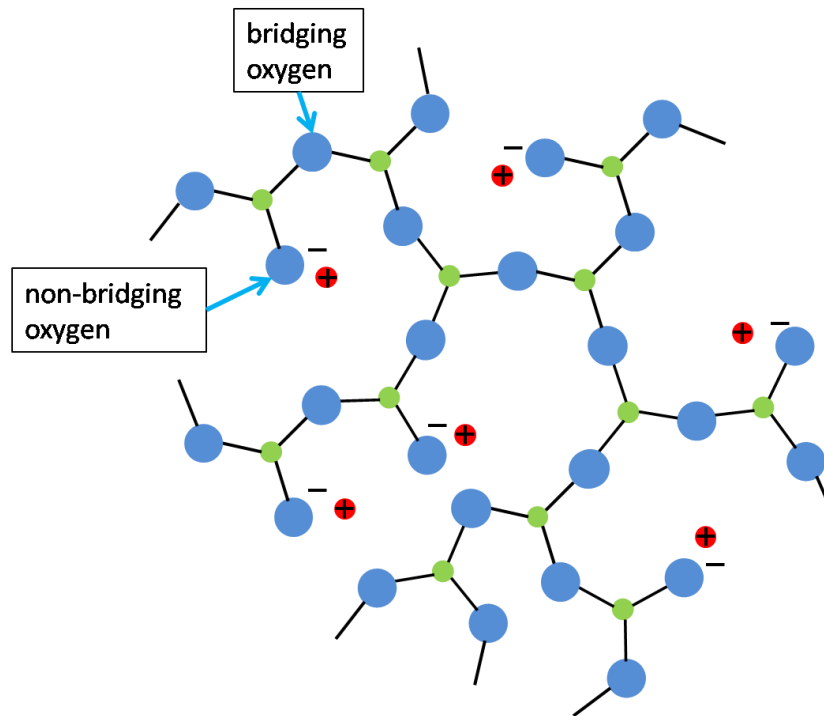
Figure 3: Two-dimensional representation of the three-dimensional structural network in a sodium silicate glass. Red = sodium, blue = silicon, green = oxygen (Hull & Clyne, 1996).

Other cations which are no network-formers have higher coordination numbers and are surrounded by other polyhedrons: Fe^{3+}, Fe^{2+}, Mn^{3+}, Mg^{2+}, and Ti^{4+} are commonly surrounded by an octahedron of six nearest neighbours, Ca^{2+}, Na^+ and Zr^{4+} by a cube with eight nearest neighbours and K^+, Pb^{2+} and Sr^{2+} by a cuboctahedral sphere of twelve nearest neighbours (Klockmann *et al.*, 1978). Because the structure of glass has no three dimensional translational periodicity, the occupation of the sites does not result in any defined stoichiometry. The network is therefore much more flexible to incorporation of other ions; different valences, ion radii, and electronegativities can be integrated, at least up to a particular amount. The glassy network can be therefore regarded as a solvent, in which the different cations are dissolved. The exact amount of incorporation depends among others on the main composition and the firing conditions of the glass (Scholze, 1965; Paynter *et al.*, 2004; Tanimoto & Rehren, 2008).

2.1.1.1 Chemical bondings in glass

Closely connected with the coordination sphere of nearest neighbours is the bonding energy and bonding character which determines the bonding length (Volceanov, 2008). The different

cations in the network have different ionicity of the bonding with O^{2-}. According to the concept of electronegativity of Linus Pauling, a higher ionic part of bonding corresponds to a larger difference in the electronegativity (McNaught & Wilkinson, 1997). In the covalent bonding, a binding electron pair is shared by the two involved atoms to fulfil the demand of a full outer electron shell, like e.g. the dominating part of the network-formers´ bonds Si-O or B-O. In the ionic bonding, the valence electrons of the one atom fill the outer shell of the other atom like the dominating part in Ca-O, Na-O, and K-O bonds. The occurring electron charge difference of resulting ions is the basis of the bonding. The covalent bonding is directional and much stronger than the not directed binding force of ionic bonds (Pauling, 1960). The both concepts are theoretical models, of which every bonding tends to the one or the other, but a pure ionic or pure covalent bonding does not exist. In a glass, more ionic bonds are formed when the content of Ca, Na, and K is high and the part of "bridging oxygen's" decreases (fig.3). A higher concentration of non-bridging oxygen ions (O^{2-}), which forms more ionic bonds can be understood as source of basicity, analogue to the concentration of H^+ which determines the acidity in aqueous solutions (Conradt, 2012). In this model, higher contents of CaO, Na_2O, and K_2O result in a higher basicity of the glass. Higher contents of SiO_2 result in higher acidity.

2.1.2 Chemical properties of glass

The variety of bonding types and bonding lengths in glass leads to a widened temperature interval of melting temperature instead of the sharp melting point T_m as it is in a crystalline material. The viscosity of a glass-melt increases with reduction of temperature. In terms of volumetric and viscosity changes, there is no sharp phase transition from the highly viscose melting to the solid state glass; therefore glass is regarded as a "sub-cooled liquid" (Debenedetti & Stillinger, 2001). In calorimetric measurements, the transition between liquid and "sub-cooled liquid" can be seen in a discontinuity of the specific heat capacity. With these measurements, the so-called glass transition point T_g can be determined. In a volumetric measurement, two different slopes of volume change with temperature are observable above and below the region of T_g (fig.4). The intersection point of the slopes can be also taken as T_g. The glass transition point or interval is additionally depending on the cooling rate of the material and therefore determined with a cooling/heating rate of 10 K/min by standard. For a sodium silicate glass, the transformation temperature is at 670-710 °C (Angell *et al.*, 2000).
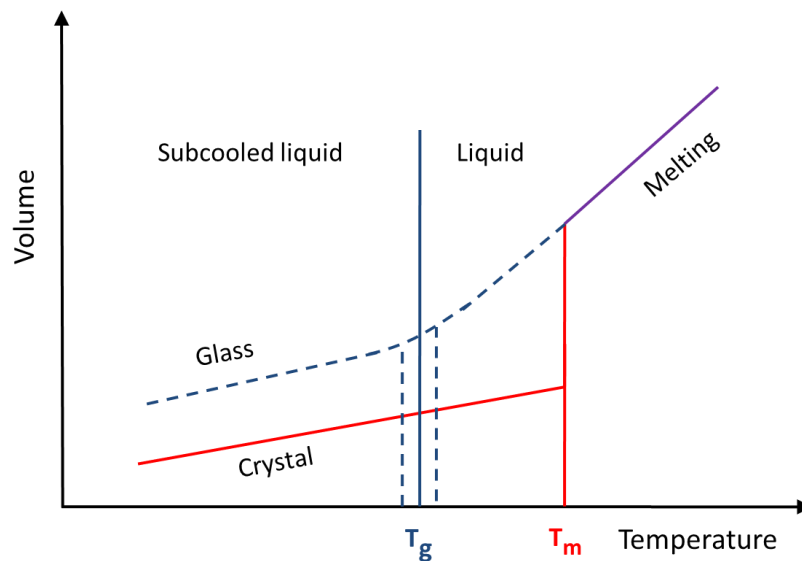
Figure 4: Different behaviour of volume changes with temperature of crystalline and amorphous solid (adapted from Debenedetti & Stillinger, 2001, and Ross *et al.*, 2013). Crystalline materials have a sharp melting point at T_m, whereas sub-cooled melts have a temperature interval of glass transformation around the point T_g.

Beside the transition point, many mechanical and chemical properties such as viscosity, transition temperature, density and chemical stability are influenced by particular ingredients e.g. alumina, alkali and alkali earth oxides (Scholze, 1965). The viscosity as well as the transition temperature is strongly related to the amount of non-bridging oxygen bonds which increases with the part of alkali and alkali earth metals. The more the network is modified, the lower is the viscosity, and the lower is T_g. The density is increased with the incorporation of alkali oxides in the amorphous network of SiO_2. Whereas the pure silica glass has a density of 2.2 g/cm^3, the density increases almost linear up to 2.4 g/cm^3 during addition of about 20 mol% of Na_2O, K_2O and to 2.3 g/cm^3 when Li_2O is added. The chemical stability of glass is reduced, when only Na_2O and K_2O as flux are brought in, because of the ionic-pronounced and therefore weaker bondings. Especially alkali glass can easily be attacked by acids, which can replace an alkali cation by a hydrogen atom and leave hydrogen bondings in the glass. Hydrogen groups of basic solutions can replace the Si-O bondings with Si-OH or Si-R compounds (Conradt, 2011 a and b). In contrast, CaO, MgO, ZnO, Al_2O_3 and also B_2O_3 up to 2.0 mol% enhance the chemical stability because some of the non-binding oxygens are for example cross-linked to Si-O-Al bonds (Brow, 2004; Fluegel, 2007). The glass composition is therefore a balance between temperature lowering and stabilising agents. Common agents in modern glass are e.g. B_2O_3 for the improvement of

mechanical stability or BaO, ZnO for better mechanical hardness (Rawson, 1967; Hinz, 1970; Matthes, 1990). In modern day glass, elements like Tl, F, Se, Ge, and Te additionally increase the chemical stability and the mechanical properties.

2.1.3 Possible silica sources

As historical silica source, sand or quartz pebbles are the typical raw materials, from which quartz pebbles are commonly purer than coastal or fluvial sand. In the latter, calcium carbonate from shells, alumina from feldspars and many other contaminations from minerals such as iron oxide can be found (MacCarthy, 1933). Antonio Neri describes in "arte vetraria" from 1663 for some regions of Europe, especially Italy, that pebbles were crushed after being quenched in order to sort the contaminated, coloured parts from the clean, white parts (Neri, 1663). For the glass production in Central Asia, the use of quartz pebbles from dry river beds and ravines is also reported (Allan *et al.*, 2000). The contaminations, primarily iron, are undesired because of the unintentional colouring effect which makes a transparent white glass impossible and a purposeful colouring difficult. The alumina, which acts as well as network former in the glass, is also generally brought in with a contamination of the silica source, especially by feldspar in sand (Herron, 1988).

2.1.4 Fluxes in glass

2.1.4.1 Mineral natron

Historically, alkali and alkali earth oxides were added either as mineral compounds or in the form of ashes from plants or parts of plants which will be treated in chapter 2.1.4.2. As mineral compounds, the lake Wadi-el-Natrun (today lake Fazda) yielded a very pure soda-mineral salt with very low amounts of potassium or alkali earth metals for e.g. Roman glass making. The most exploited mineral in the Wadi-el-Natrun is the sodium hydrogen carbonate "trona" with the formula $Na_2CO_3*NaHCO_3*2H_2O$. The mineral halite, NaCl, is also common, but not as useful for the glass production as trona. Another mineral, which is present in major amounts, is the sodium sulphate thenardite, Na_2SO_4. Less common, but also known from other lakes in the Nile Delta are the sodium carbonates burkeite ($Na_6CO_3*2SO_4$), gaylussite ($Na_2Ca*2CO_3*5H_2O$), and thermonatrite ($Na_2CO_3*H_2O$) (Shortland *et al.*, 2006). Another lake in the western Nile delta

bearing especially sodium carbonate was the lake el-Barnuj but the importance for glass production is not clarified yet (Shortland *et al.*, 2006; Shortland & Eremin, 2006).

In the Roman Empire, the mineral natron was the dominant alkali flux in glass (Lemke, 1998). Flux compositions displaying a clear mineral natron source are also found in glass findings from Nimrud of the 8th-9th century BC (Reade *et al.*, 2005) and Hellenistic glass from Rhodos and Syria, from the 3th-2th century BC (Brill, 1999). Shortages in the supply of natron from Wadi-el-Natrun led to the replacement of mineral natron by plant ash flux in Egypt, Europe, and the Middle East (Shortland *et al.*, 2006). After Sayre & Smith (1974), the exploitation of soda from Wadi-el-Natrun ends in the middle of the 9th century AD which leads to the introduction of plant ash flux in the Egyptian glass making (Sayre & Smith, 1974). This is probably due to the higher demand of glass, which couldn't be fulfilled anymore with mineral natron. Other deposits of mineral natron evaporites are known from India and could have been exploited in the medieval Islamic period (Allan *et al.*, 2000).

2.1.4.2 Plant ashes

For plant ashes, stems or leafs of halophytes, ferns, wood and bark are common source material. The characteristic glass based on plant ash flux in is set to ≥ 2.0 wt% K_2O and MgO by taking the sample of early Egyptian glass findings (Sayre & Smith, 1974; Lilyquist *et al.*, 1993). It is suggested that in Mesopotamia, Iran, and Central Asia, the early use of plant ash as flux in vitreous materials has never been interrupted by the Roman mineral natron glass making (Sayre & Smith, 1974).

The sodium oxide content of the plant is highly sensible to the soil on which the plant grows and to the water, with Na contents strongly depending on the vicinity to a sea coast or salt lake (Barkoudah & Henderson, 2006). In contrast to coastal and desert plants, the wood, cereal and fern ashes have much higher potash than sodium oxide content (Bezborodov, 1975). Both, potassium and sodium are present as carbonates, chlorides or sulphates in the plants, from which the carbonates are incorporated into the glass in more or less the same proportion as they are in the plant ashes (Rehren, 2008). Carbonatic alkali compounds are therefore very suitable for glass production.

The chlorides of the plant ashes are not incorporated directly into the glass melt. In contrast, a coherence between the presence of chloride and the take-up of potassium at an expense of sodium is observed (Rehren, 2008). Furthermore, chlorides tend to evaporate instead of being

incorporated into the glass melt (Turner, 1956; Barkoudah & Henderson, 2006). The composition of the glass batch therefore depends on the respective chemical compound in which the alkalis are present. Considering temperature dependant reactions and migration of ceramic compounds with the glaze layer, the glazes composition is influenced by the firing profile, too (Rehren & Yin, 2012).

In some cases the plant ash was purified before use in order to increase the content of sodium and potassium related to magnesium and calcium (Tite *et al.,* 2006). For that reason, the plant ash was partly dissolved in water, where the quasi unsolvable alkali earth contents of carbonate were filtered (Shortland *et al.,* 2006). In contrast, it is assumed by Pernicka & Malissa (1976) that the Iranian glazes of the 13th were produced with an additional dolomitic or calcareous component, which is mentioned in the treatise about Iranian ceramic production of the 14th century by Abu´l-Qasim (Allan *et al.*, 1973). The Na/K ratio of the plant ash raw material also can be increased by solution process, taking the advantage that Na_2CO_3 has a lower solubility (217 g/l) than K_2CO_3 (1120 g/l). The solution must be evaporated so that the sodium-rich precipitates first and therefore can easily be enriched.

2.1.4.3 Lead flux

The other important flux agent which was used already in ancient glass making technology is the lead oxide. In Islamic glass it is e.g. reported for Moroccan and Syrian glass from the 8th century AD (Sayre & Smith, 1974; Robertshaw *et al.*, 2010). The lead was commonly added as natural galena (PbS), litharge (PbO), lead red (Pb_3O_4), lead silicate or as other reaction product from smelting processes (Tite *et al.*, 1998). Traditional ceramic techniques in Central Asia used "red-lead", probably a Pb^{2+}/Pb^{3+} oxide, as addition to the quartz in the ratio 2:3 (Allan *et al.*, 2000). Henshaw (2010) describes roasting of PbS to PbO and the subsequent mixing with sand or quartz pebbles, too. Lead oxide has a very low melting point of 888 °C and therefore acts very effectively as flux agent. The use of lead as flux has to be deployed carefully, especially in the production of glazes: too high contents can result in a too runny liquid but too low Pb contents evoke high surface tension and bad wetting of the ceramic (Pérez-Arantegui *et al.,* 1999). More detailed information about the history of the lead use in glaze production is given in chapter 2.3.4.

2.1.5 Calculating the process temperature of glass

It has always been of great interest to improve the predictability of glass firing temperatures but this topic has for a long time been treated as an empirical science. Calculations on this matter were first made at the end of the 19th century by Otto Schott, who assumed an ideal mixture and suggested the additive principle of a glass property *X*, e.g. firing temperature (Winkelmann & Schott, 1894). Under this assumption, a composition with *n* different components *i* occurring in the concentrations C_i and with the properties *b* has the total characteristic of

$$X_{Glass} = \sum_{i=1}^{n} b_i C_i.$$

This approach for glass property prediction is suitable for small changes in compositions and a limited number of components. A more widely applicable approach was developed in multiple studies: Bottinga & Weill (1972) calculated the viscosity of complex natural rock and mineral systems with an accuracy of about $1\text{-}10^6$ P. Kucuk *et al.* (1999) used a multiple linear regression approach for the calculation of surface tension. Priven (2004) separated the glass properties into "structure sensitive" (heat capacity and surface tension) and "structure insensitive" (viscosity, density, thermal expansion coefficient, refractive index, average dispersion and Young´s modulus). Fluegel (2007) developed polynomial functions for the viscosity behaviour of silicate glass and included the non-linear "mixed-alkali effect", regarded as a behaviour primarily originating from a silica-alkali interaction. The linear regression modelling, which keeps linearity in the used coefficients, is also applied in the approach of Lakatos *et al.* (1972) based on the Fulcher-Tammann-Equation for viscosities of sub-cooled liquids:

$$T = T_0 + \frac{B}{\log \eta + A}$$

T_0, B and A are melt coefficients, T the temperature in °C and η the viscosity in poise (1 poise = 1P = 0.1 Pa*s). The coefficients, which are apllied in the calculation by Lakatos *et al.* (1972), include the molar contents of alkali and alkali earth oxides (Li_2O, Na_2O, K_2O, CaO, MgO and BaO) and of the metal oxides ZnO and PbO and Al_2O_3 in the glass composition. They are calculated from the ratios between the metal oxides and SiO_2 content ("MeO" $\triangleq \frac{mol\% \, MeO}{mol\% \, SiO_2}$) and are given as

$$B = 2830.0 \text{ "Al}_2O_3\text{"} - 6802.0 \text{ "Na}_2O\text{"} - 4566.7 \text{ "CaO"} - 611.6 \text{ "Li}_2O\text{"}$$
$$- 3622.9 \text{ "BaO"} + 1121.1 \text{ "ZnO"} - 3650.3 \text{ "PbO"} - 1519.0 \text{ "K}_2O\text{"}$$
$$+ 6590.0 \text{ "MgO"} + 5991.5$$

$$A = 1.29799 \text{ "Al}_2O_3\text{"} - 1.37112 \text{ "Na}_2O\text{"} - 1.22366 \text{ "CaO"} - 0.90151 \text{ "Li}_2O\text{"}$$
$$- 1.73879 \text{ "BaO"} + 3.13803 \text{ "ZnO"} - 1.32178 \text{"PbO"}$$
$$- 0.90479 \text{ "K}_2O\text{"} + 5.63513 \text{ "MgO"} + 1.50848.$$

For the calculation of process temperatures of window glass and alumo-silicate glass, the model of Fulcher-Tammann is more accurate than calculations of Avramov & Milchev (1988) or Mauro *et al.* (2009). The model of Fulcher-Tammann is transferred to the alkali glazes, as well as to the partly lead-containing compositions. For the viscosity behaviour, the linearity of coefficients is suitable. Because of nonlinearity of phase transitions, other properties such as liquidus temperature or phase separation in contrast have to be calculated with other approaches such as the modelling with disconnected peak functions (Fluegel, 2007). The viscosities of the historical glazes are calculated through the approach of Lakatos *et al.* (1972) with an assumption of a suitable processing viscosity of $\eta=10^4$ P for the curing of glaze (Hamer & Hamer, 2004).

In general, the degree of grain size and homogeneity has to be taken into account for the estimation of the processing temperature. The smaller the grains are and the higher the degree of mixing is, the closer is the real processing temperature to the value of ideal conditions. In the case of medieval glazed ceramics, a homogeneous distribution of components in the raw material is assumed, because the frit was commonly prepared with ground ingredients (Al-Saad, 2002; Tite & Shortland, 2003).

2.1.6 Glass production technology

In order to obtain a glass with a good processability and high stability, a homogeneous base material is needed. The raw materials have to be carefully selected, milled where required and mixed in right proportions. The melting of raw materials to a glass batch can either be directly done in the kiln, or with an intermediate step of a so-called glass frit. The frit is produced from a mixture of the raw materials, which can be fired at temperatures far below the melting point of silica (Henderson, 1985). It is then cooled or quenched in water and used as base material for the glass production. The intermediate step of fritting has the advantage of further

homogenization and out-gassing of e.g. water and carbonatic parts from the raw materials (Shelby, 2005). Furthermore, the effect of melting point reduction is enhanced in the frit, because the fluxes are homogenously distributed in the glassy phase. A disadvantage can be gas bubbles which rise from pores in the loosely cemented powder of the frit. This can especially occur in case of very fine milled raw materials (Shelby, 2005). In every case, the glass melt has to be heated until gas bubbles are driven out and the batch is homogenized. Central Asian potters report from the historical glaze production to use one part of powdered quartz and one to one and a half part of plant ashes (Vandiver *et al.*, 2010).

2.2 Colouring in glass

The colouring agents of glass and glazes are distinguished in ions which are integrated in the glass network, particles which colour the glass as pigments, colloids, which affect the colour by their size of the particles and lustre colouring which covers the top of a glaze with a metallic shine.

2.2.1 Colouring ions

For the generation of colour from ions, it is essential to have narrow energy levels in the electron shells of the ion. This is e.g. the case in the split levels of transition metal ions which are embedded in a coordination polyhedron. The colours produced by transition metal ions in the glass network are determined by the energy levels of outer electrons, between which an electron can change and absorb a certain wavelength of visible light´s radiation. The surrounding of the colouring ions produces an electrostatic field, in which the levels of the outer electrons are more or less attracted by the ligands. The colour of the polyvalent ions additionally depends on the valence and coordination sphere of the ion and on the specific splitting of the outer electron energies by the ligand field (Conradt, 2012). The *ligand field theory* allows an understanding of the different splitting variations and their resulting energy levels (Bamford, 1977; Nassau, 2001).
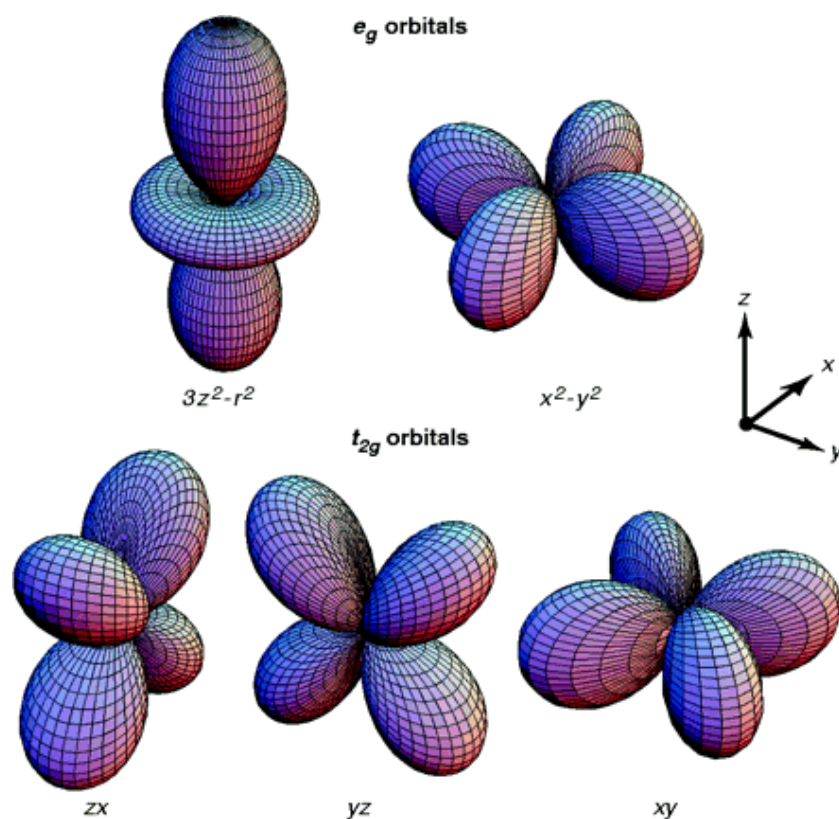
Figure 5: d-orbitals of transition metals. The e_g-group has high electron density distribution (EDD) along x,y and z axis and has the higher energy levels in an octahedral coordination sphere of the central atom. The t_{2g} orbitals have high EDD each between two axes and have the higher energy levels in a tetrahedral coordination sphere. This fine splitting leads to an easy transition of electrons, which causes the absorption of visible light © (Fjellvåg & Kjekshus, 2001).

The most important group of elements for such a colouring effect are the 3d-transition metals, whose five different d-orbitals are in slightly different energy levels, as soon as the ion is surrounded with a coordination polyhedron of e.g. O^{2-} ions. This effect, called crystal field splitting (also ligand field splitting), occurs because the five outer electron orbitals are in different geometric relations to the ligands. In the case of octahedral coordination, the d_{x2-y2} and the d_{z2} orbital (e_g orbitals, fig.5) point directly towards the oxygen ions (along x,y and z axis), whereby they raise in their energy level because of the strong repulsion of the electron charges. In opposite, the tetrahedral coordination leads to an enhancement of energy level in the t_{2g} orbitals (d_{xy}, d_{yz} and d_{xz}) which point toward the oxygen ions in this case.

The energy splitting in the tetrahedral coordination is much lower (4/9 of the splitting in octahedral coordination) and leads therefore to absorption of light with higher wavelength when an electron is excited to the higher energy state (Nassau, 2001). The absorption of lower

energies (e.g. red light) results in a glass colour with enhanced proportion of transmitted light with high energy (e.g. purple). For example, a glass with $Co^{2+}_{(T)}$ incorporated as network former (tetrahedrally coordinated with O^{2-}) appears in the typical blue colour, because the energy absorbed by electron transitions between two split orbitals is in the range of orange light. As a network modifier, the $Co^{2+}_{(O)}$ makes the glass appearing pink, because of the higher transition energy between split orbitals in this coordination sphere (Weyl, 1967). It is therefore obvious, that also the change of ligands, e.g. a replacement of oxygen by a sulphur ion or the occupation of other network positions influences the resulting colour of a transition metal ion. The ligand field strength changes with the type of ligands, depending on their position in the *spectrochemical* sequence (Nassau, 2001). The ligand field strength of a six fold coordinated Cr^{3+} is e.g. with 2.2 eV lower within oxygen ligands than within CN^- ligands for the same ion coordination (3.3 eV). Higher ligand field strength shifts the absorption maxima to higher energy levels resulting in a shift of the transmitted light to shorter wavelength (Nassau, 2001). The most prominent effect of O^{2-} replacement is the so-called amber glass, in which the tetrahedral coordination of a Fe^{3+} ion includes one sulphur ion at the place of one oxygen. The processing is rather difficult because of a small window of oxygen partial pressure in which the Fe is present as Fe^{3+} and the S^{2-} is not yet oxidised to SO_4^{2-} ($10^{-8} > PO > 10^{-10}$, Weyl, 1967). The conditions can be easier controlled with the addition of carbon to the melt ("carbon-sulphur-amber") and low oxygen availability during firing. The oxygen fugacity is closely connected with the oxidation state of the metal ion, which is for many ions reduced when less oxygen is available (e.g. Cr, Mn, Cu, and Fe). Most of the colours do not require oxygen-deficient atmosphere because they have the desired colouring effect in the highest oxidation state (Fe^{3+}, Mn^{4+}, and Cu^{2+}). Nevertheless, a reducing firing is needed for the Mn^{3+} in violet samples, which otherwise would turn into the brown colouring Mn^{4+}. This could be achieved by additional charcoal from wood or plants in the firing furnace, or by a special furnace with air seal.

The firing temperature also influences the valence, resulting in a higher oxidation with higher temperature (Bamford, 1977). Different oxidation states and the corresponding wavelengths of transmission are given in table 1. The basicity and acidity of a glass can be understood as molar concentration of O^{2-} ions in the system, analogous to the concentration of H^+ ions in the pH model. The higher the concentration of oxygen, the higher is the acidity with which the number of O^{2-} ligands and therefore the coordination number tend to increase (Bamford, 1977).

The main composition of the glass also influences the absorption spectra of the transition metals. The spectra of Co^{2+} in a Roman glass has already slightly different absorption bands (535 nm) than in post medieval glass (absorption band at 520 nm) which contains less soda but more potash and magnesia (Green & Hart, 1987). The Cu^{2+} ion colours the alkali-rich glass light blue, whereas in a lead glass with more than 30 wt% PbO it turns into green (Weyl, 1976). The role of the absolute absorptivity of an ions´ bonding (molar extinction coefficient ε) is also crucial for the resulting tint. The Fe^{3+}-S bonding in the amber glass for example has a very high transition probability of electrons in the orbitals, which makes only a few 100 ppm of sulphur on the oxygen positions in the glass sufficient for a yellow colouring. Furthermore, a glass with few per cent Cu but only small amounts of Co (few 1000 ppm) result in a dark blue colouring because of the rules of transition probabilities in electron bondings: whereas the transition of an octahedrally coordinated Cu^+ ion has an extinction coefficient of $\varepsilon=20$ L/mol*cm, the transition of the Co^{2+} in a tetrahedral coordination sphere lies at $\varepsilon=150$ L/mol*cm, which explains the blue colour despite the presence of Cu even in lead-rich samples where the Cu would normally produce a green colour.

Further, a decolourising effect is described already in early literature of glass making (Rottländer, 2000; Hoover, 2003). An elimination of all colouring agents, including smallest contamination of iron was almost impossible with the antique techniques but the demand for clear colourless glass was high. For decolouration, manganese in a four-valent state (MnO_2) was added to the melt and reduces there partly to Mn^{3+} and partly further to Mn^{2+}. Simultaneously, it oxidizes the present Fe^{2+} into Fe^{3+} (Nassau, 2001). The Fe^{3+} in the glass has a maximum of light transmission similar to the absorption band of Mn^{3+} (at ca. 480 nm, Bamford, 1977; Thiemsorn *et al.*, 2006). The yellowish Fe^{3+} is therefore extinguished by Mn^{3+} and the bluish-green colouring of the Fe^{2+} is eliminated through the oxidation to Fe^{3+}.

$$Mn^{4+} + e^- \rightarrow Mn^{3+}$$

$$Mn^{3+} + e^- \rightarrow Mn^{2+}$$

$$Fe^{2+} \rightarrow Fe^{3+} + e^-$$

$$2MnO_2 + 2FeO \rightarrow Mn_2O_3 + Fe_2O_3$$
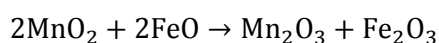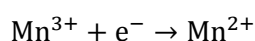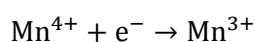
Table 1: Overview of metal ion colours in different oxygen coordinations in the glass matrix (Brow, 2004).

Me	complex	colour	λ (trans-mission) /nm	Comment
Fe	[$Fe^{II}O_6$]	Bluish-green	1050	Very intense colour, broad absorption range
	[$Fe^{III}O_4$]	Pale yellow	380-435	
	[$Fe^{III}O_6$]	Pale pink		In high acidity glass
Co	[$Co^{II}O_4$]	Deep blue	530;645	Very intense colour, two absorption ranges
	[$Co^{II}O_6$]	Green		In high acidity glass
	[$Co^{III}O_6$]	Pink		In high basicity glass
Ni	[$Ni^{II}O_6$]	Greyish-brown	450;930; 1800	Broad absorption range
	[$Ni^{II}O_4$]	Brown	560;530	
Cr	[$Cr^{III}O_6$]	Green	450;650	Very intense colour, two absorption ranges
Cu	[$Cu^{II}O_6$]	Cyan	780	
	[$Cu^{I}O_6$]	Colourless		
Mn	[$Mn^{III}O_6$]	Purple	490	
	[$Mn^{II}O_6$]	Colourless		

After aging and sunlight exposure, this decoloured glass can re-colour and get a slight purple tint. This is because parts of Mn^{2+} in the glass return to Mn^{3+} under radiation energy and produces a purple colour which can be often observed in ancient glass. This process of photo-oxidation is known as solarisation of glass and is e.g. described by Abd-Allah (2009). For the ochre colouring with Fe_2O_3, the firing temperature must be high enough and an oxidising atmosphere in the production process is necessary, in order to avoid a greenish colour of Fe^{2+} (Nassau, 2001).

2.2.2 Colouring pigments

Pigments in glazes can consist of all metal compounds with a proper colour and have beside the colouring function an opacifying effect to the glassy matrix. The colouring agents can be either added as ready-made pigments and remain in their original solid state during melting, or they are newly formed by recrystallization from the melt during glaze cooling. Hydrogen carbonates like azurite $Cu_3(OH)_2(CO_3)_2$ and malachite $Cu_2(OH)_2CO_3$ would decay already at low temperatures of 250-350 °C and are not suitable for a pigment colouring in glaze (Frost *et al.*, 2002). The colour

of pigments originates from electron transitions in the molecule of a pigment which absorbs specific wavelengths. For example, a Co-Al spinel has three absorption bands of 590, 1200 and 1320 nm, resulting in the typical dark blue colour (Fernández & Pablo, 2002).

The pigments can be homogeneously distributed in the glaze matrix or agglomerated in clusters. Often, an accumulation near the ceramic-glaze interface is observed, when the particles settle to the bottom of the glaze or crystalline phases rise from diffused ceramic elements. Those precipitates from ceramic elements cannot be counted as deliberately pigments, but can also cause an opacification of the glaze. In the case of recrystallized pigments, the particle size is commonly in range of several μm, the ready-made pigments are normally in the size of 50-100 μm.

For opacifying, a white colour of minerals such as SnO_2 and SiO_2 is desirable. For example, the opacifying SnO_2 is commonly dissolved in the melt and recrystallizes when the glaze cools down (Molera *et al.*, 2001).

Table 2: Selection of common historical pigments for glass or glaze.

Colour	Pigment	Example of occurrence
White	$Ca_2Sb_2O_7$, $CaSb_2O_6$	In prehistoric times in Egypt and Mesopotamia (Moorey, 1999)
	SiO_2	Moroccan tile glaze from early modern times (this study)
	SnO_2	Persian or Late Sassanid/early Islamic glazes (Kleinmann, 1986; Hill, 2004)
Yellow	$Pb_3(SbO_4)_2$	Early Babylonian glaze pigment (Moorey, 1999)
	$Pb_2Sn_2O_7$	Medieval pigment (Kühn & Feller, 1986)
Black	Carbon black	First occurrence in Neolithic ceramic glazes (Colomban, 2013)
	MnO_2	Colouring for medieval tile glazes (Hansen, 2008)
	FeO	Colouring in medieval glass (Hansen, 2008)
	CuO	Medieval glass and glaze colouring (Holleman & Wiberg, 1995)
Red	Cu_2O	Middle East glass, 1st and 2nd Millennium BC (Freestone, 1987)
	Fe_2O_3	Burnt sienna, medieval Pigment (Lewis & Edwards 2001)
Blue	$CaCuSi_4O_{10}$	Glass-ceramic pigment in Ancient Egypt (Chase, 1971)

The recrystallized SnO_2 particles are finely distributed in the matrix; this leads to further whitening because of the higher amount of phase boundaries, on which the reflected light is scattered. A short overview of common colouring particles in glass and glazes is given in table 2. SiO_2 can also be used as opacifier, but has to be added as a milled powder. It can hardly be dissolved and wouldn't recrystallize in the pure form, but only in compounds with other elements of the glaze. A suitable particle size and a refractive index differing from the glass´ one is crucial for a good opacifying result. A high refraction index of the pigment material leads to high colour intensity. The oxides and sulphates of e.g. Pb and Cd have refraction indices between 2.4 and 2.6. The opacifiers TiO_2 and SnO_2 also have refractive indices above 2.0 (Nassau, 2001). The particle size is ideally between 1 and 10 µm, a finer grinding would lead to a loss of colour (Nassau, 2001). For Islamic glazed ceramic, the most common pigments are the whitening SnO_2 and the calcium antimonate ($Ca_2Sb_2O_7$ and $CaSb_2O_6$), the yellow lead tin oxide $Pb_2Sn_2O_7$, the yellow lead antimonate $Pb_3(SbO_4)_2$) as well as manganese and iron oxides for black colour (Hansen, 2008).

2.2.3 Colloid colouring

The invention of colloid colouring possibly dates back to the 4th century AD, when the famous red Roman Lycurgus cup was manufactured (Freestone *et al.*, 2007). The documented production of ruby glass took place much later in early modern times (Neri, 1633; Cassius, 1685). A widespread use of ruby glass followed in Europe in the manufacturing of glass tableware, stained-glass windows and painting of porcelain (Molera *et al.*, 2007). The colloid colouring bases on a dispersed systems of two solid phases of matrix and particles, in which the dispersed particles have not more than 100 nm size and consist of about 10^3-10^9 atoms which results in a large surface area between the two phases (Stilgebauer, 1996). Commonly, the particle material is a metal phase such as Cu, Ag, or Au. The particles at this size cannot develop the highly reflecting properties of a bulk metal, and therefore the absorption of light dominates. In the case of a conducting particle material, the interactions between the electrons of the particle material and an incident electromagnetic wave increases further (Liz-Marzan, 2007). An incoming wave of electromagnetic radiation excites the charge distribution of one particle and leads to an oscillation of the charge around the particle centre. For the metals Au, Ag, and Cu, this oscillation is in the frequency of visible light and leads to the colouring effect. These metals are therefore the common agents for colloid colouring. The best particle diameter for colloid

colouring for e.g. gold particles is between 1 and 10 nm, commonly shaped as octahedrons (Kreibig & Vollmer, 1995). For the effect of gold ruby glass, a content of only 0.1 wt% Au in the glass is sufficient. For the ruby glass production, the metal has to be dissolved in the glassy medium. Then, the glass with dissolved metal is annealed at around 600-700 °C and the metal precipitates. With reducing agents e.g. like carbon, the nucleation of crystals can be promoted (Nassau, 2001). The process of annealing and size matching of the particles is quite complicate and made the ruby glass to a luxury ware, especially in the case of gold ruby.

2.2.4 Lustre

Lustre colour is described as the iridisation effect of a thin layer of elemental metals on the surface of a glass or glaze. The lustre glazing technology is based on slurry of metal salt and clay which is applied to the glazed ceramic ware as painting dye. A reducing firing leads to elemental state of the metal and results in the shiny appearing. The unwanted parts of clay can be removed by simple polishing of the ceramic (Sentance *et al.*, 2008).

Lustre colouring technique was developed in the early Islamic times in Fustat, Egypt (Pinder-Wilson, 1995) or in Iraq of the 9th century (Pradell *et al.*, 2008). A common lustre layer in Egypt, Syria and Iran but also Italy consists of a combination of Ag and Cu. The colour of the lustre layer is determined by the ratio of copper and silver (Padovani *et al.*, 2003; Padovani *et al.*, 2004; Pradell *et al.*, 2008).

The metal particles commonly vary between 5 and 50 nm and can be embedded in the upper glassy matrix or in a separate layer on the top of the glass (Pradell *et al.*, 2006; Pradell *et al.*, 2008). As metals, primarily copper, silver, and gold are used. The copper and gold particles absorb wavelengths above 520 respectively 590 nm, resulting in the typical yellow and red colours. Other metal layers absorb all wavelengths of visible light, which leads to an opaque and colourless appearing (Pradell *et al.*, 2008). Nano-particles of metals absorb only in one frequency which is called Plasmon resonance frequency, as described in the colloid chapter. Elemental gold can also be found as upper glaze layer, but is probably added as a readymade gold foil and not reduced from Au-compounds. The production of lustre ware requires reducing firing conditions which leads to the elemental state of the metals, either in the separate layer on the glaze or in a redox-reaction with the uppermost layer of glass matrix elements (Padovani *et al.*, 2004). The reducing atmosphere creates a deficiency of oxygen in the glass composition and all metal ions which diffuse from the surface into the glaze are reduced. The sheet of nano-particles on the

top layer of the glaze appears with a metal shine, particularly in combination with a lead-rich glaze compound, whereas on alkali glazes the lustre has an ochre or brown colour (Molera *et al.*, 2007). Therefore, most of the lustre ware glazes have lead containing compositions (Pradell *et al.*, 2006).

2.3 History of glazes

2.3.1 Specification of glaze

Glazes are characterized as thin laminar and glassy coatings, which are fused onto the underlying surface of a ceramic body. A glassy coating is necessary to seal the ceramic surfaces off from gases and liquids and to make them easily cleanable, to increase the stability and to provide an aesthetic affect. The material of glaze is therefore very similar to a glass, the same raw materials, the same fluxes and similar colouring agents can be used. In contrast to a homogeneous glass, a glaze can be a combination of the amorphous matrix and crystalline parts and may contain gas bubbles or relics of included slurry liquid.

Different ways of ancient glaze manufacturing are described; for the case of Ancient Egyptian faience, efflorescence, cementation, and direct application are mentioned (Tite & Bimson, 1986; Tite & Shortland, 2003). The efflorescence technique is based on migration of dissolved alkali salts, which are within the raw, quartz-rich ceramic body. Through the evaporation of water, the alkali ions migrate to the surface and form a glaze layer together with the quartz grains of the ceramic. The cementation technique comprise the firing of the ceramic body, buried in the glaze mixture, consisting of alkalis, copper compounds, calcium oxide or hydroxide, and/or quartz (Sparavigna, 2012). The application method uses a suspension of glaze or glaze components and typically water as liquid phase. The suspension can be applied by dipping, brushing, or pouring to the ceramic body (Parmelee & Buckles 1942). For easier application of the slurry, clay, gum, or starch may be added (Tite *et al.*, 1998). The efflorescence technique can be tracked by contents of colouring ions in the ceramic body, as it is described for copper coloured Egyptian faience (Tite & Shortland, 2003). In the present glazes, no such hint is found in the analysed ceramic compositions. The cementation method produces a monochrome glaze layer around the whole covered piece of ceramic, which cannot be assumed for the tile glazes and the polychrome glazed tableware. The application method is assumed to be the typical glazing technique for the present sample set.

For the Ancient Egyptian faience bodies, the use of an organic binder such as gum or resin is assumed, in order to achieve high enough viscosity and plasticity of the paste. In the case of lead glaze, the lead compound may be solely applied to the ceramic and fuses with the underlying body to form a glaze layer, as it is described for ancient glazes from the Middle East (Parmelee & Harman, 1973; Tite *et al.*, 1998).

The alkali and alkali lead glazes have to be applied as suspension of ground frit, because the separate alkali compounds would dissolve in the water of the application slurry (Mason, 2004). The glazing mixture of lead glazes can be applied as raw materials or with the pre-step of a fritting and milling (Tite & Shortland, 2003). When raw materials are applied directly, a preferably low melting temperature must be achieved by addition of sufficient flux. Thus, the viscosity of the melt is low enough to ensure homogenization of the material and a degassing of all volatile compounds. In case of frit technology, the volatile components are already evaporated and only little flux must be added. The frit is then again milled and applied in a suspension, described as it is above.

The application can be carried out on pre-fired, biscuit-fired, or raw ceramic bodies (Tite *et al.*, 1998, Molera *et al.*, 2001). As Molera *et al.*, (2001) demonstrate, the glazing of raw clay-based body results in more migration from the ceramic body into the glaze and therefore to a broader interface. However, extend and structure of the interface also depends on parameters like ceramic composition or firing profiles (Molera *et al.*, 2001; Rehren & Yin, 2012).

The glaze slurry can be applied directly on the ceramic, or with a layer between ceramic and glaze, called slip or engobe. The slip is based on clay and water and serves as smoothing of the body surface or a colouring of the ceramic (Dodd, 1994). Additionally, it can reduce a misfit between the expansion coefficients of ceramic and glaze. In this study, slipware is not observed, beside one case of Bulgarian tableware glaze.

The firing of glazes takes commonly place in so-called updraft kilns, in which the fire is at the bottom and the ceramic pieces are in a separate chamber above. This is reported e.g. for ancient Egypt pottery (Nicholson, 2010) or traditional Uzbek glaze making (Vandiver *et al.*, 2010). The updraft kilns can be covered or uncovered, whereas the downdraft kilns are usually covered (Nicholson, 2010). For the heating in reducing atmosphere, a covered kiln system is necessary. In the less common downdraft kilns, the heat source is above the ceramic ware.

When the glaze cover is not completely homogeneous, turbidity occurs because the incident light is scattered on phase boundaries of different refraction indices. These phase transitions

can be pigments, which are added to the pre-fritted raw materials or recrystallize intentionally from the glaze melt, undesired precipitations of crystallites during the cooling, remained gas bubbles from raw materials and frit pores, or decompositions of the melt, e.g. liquid-liquid dispersions (Matthes, 1990). The last ones have only little opacifying effect, because of similar refractive indices. A crystallisation of the glaze melt can occur when the cooling rate is too low and the composition contains insufficient SiO_2 compound. Common undesired precipitates in CaO-Al_2O_3-SiO_2 dominated glaze compositions are anorthite $CaAl_2Si_2O_8$ and wollastonite $CaSiO_3$. In Na_2O-Al_2O_3-SiO_2 dominated glaze compositions nepheline $(Na,K)AlSiO_4$ occurs. Diopside $CaMgSi_2O_6$, cordierite $Mg_2Al_4Si_5O_{18}$ and indialite $Mg_2Al_4Si_5O_{18}$ may form when MgO occurs at the place of CaO or is additionally present (Rasteiro *et al.*, 2007). In lead containing compounds, the unintended precipitation of Pb_2SiO_4 is observed (chapter 7.2). Fe-compounds like olivine, fayalite, or hematite and Al-compounds like mullite or corundum are found as crystallisation products, also in modern glazes.

2.3.2   Early glazes

Earliest man-made glazes are found in Mesopotamia from the 4th millennium BC on, covering stones like steatite or quartz (Moorey, 1999; McCarthy, 1996). Simple glassy beads are known from ca. 3000 BC from Mesopotamia (Colomban, 2013). The earliest glaze colours are green and blue, but also black in the Mesopotamian prehistoric culture.

The Egyptian faience is the earliest known glaze material. The faience consists mainly of sintered quartz grains, which are additionally connected with a matrix of alkali rich glassy phase (Pernicka *et al.*, 1977; Lilyquist & Brill, 1993). The body is typically covered with a layer of copper coloured alkali glaze. This material can be treated as early glazed ceramic and it was the basis for many different objects such as beads, amulets, vessels, or figures in the early Egyptian culture.

Moorey (1999) describes the occurrence of white glazes 2900 BC in Egypt, produced by an alkali glaze on a light ceramic body. In Mesopotamian glaze finds, a yellow lead antimonate pigment occurs in the third millennium BC. Black glazes of this time in Mesopotamia are coloured by enhanced contents of Fe and Ni (Moorey, 1999). From the second millennium BC, blue coloured faience from Amarna, Egypt, is reported to be produced with copper, but also with cobalt values up to 0.45 wt% CoO (Shortland & Tite, 2000; Tite & Shortland, 2003). The Co content can be ascribed to a Co-containing alum deposit in the western Egyptian Oases Dakhla and Khagra. Co

from these Oases was identified through the accompanying elements Al, Mg, Mn, Ni and Zn (Kaczmarczyk & Hedges, 1988; Shortland & Tite, 2000).

The first evidence for glazed terracotta is found in the Mesopotamian region around the 18th century BC in the times of the kingdom of Arrapha (Moorey, 1999). Glazes on bricks for sculptured reliefs or murals are not recorded until the Neo-Assyrian period from the 17th to the 10th century BC. Studies of Moorey (1999) and McCarthy (1996) show, that the glazing technology continued in the Kassite period (1531-1155 BC) in Mesopotamia and became more common in the first millennium BC. In the Kassite and Mittanian times, the variety of colours increased further with the spreading of glazing technology (Moorey, 1999).

2.3.3 Ancient glazes

The antiquity is commonly accepted to begin in the 8th century BC with the time of the Greek colonisation in the Mediterranean region. The classical ancient cultures comprise the Greek culture and the Roman Empire, but also the cultures of Egypt, Turkey, Syria, Mesopotamia, and Persia in the time between 800 BC and 500-600 AD.

Regarding the development of glaze making, the Seleucid Empire from 312 to 63 BC had an important influence to the ancient glazing technology. As colorants in Seleucid glazes, copper and iron were applied to produce green and brown hues in glazes (McCarthy, 1996). Additionally blue, yellow, white, and black monochrome glazes and polychrome combinations of these are found on sherds of the Parthian period (3rd century BC- 3rd century AD). In early Islamic times, the variety increases further and several innovations in glaze technology like the production of high lead glazes with more than 50 wt% PbO (Mason, 2004) and the imitation of Chinese porcelain with blue-white colouring and splashed glaze decoration (McCarthy, 1996). As described by Mason and Tite (1997), the Islamic potters inherited the tradition of lead glaze and created tin-opacified lead alkali glaze. In medieval times, the glaze technique was highly cultivated in the Islamic cultures like e.g. the Mamluk Dynasty (11th -13th century AD, Colomban *et al.*, 2012).

2.3.4 Flux

The contents of alkali and alkali earth oxides in glazes can give some indication of the raw materials and origin of the material. It can e.g. be differentiated between a high sodium

characteristic, typical for Islamic glass and glazes, a high lime type which is primarily found in Turkish and Chinese glazes and the high potash type, which is known from the medieval Europe (Henshaw, 2010). Mixed alkali compositions are found e.g. in alkali glazes from Ferghana/Tashkent and Merv (Wang, 2009).

The relative amounts of alkali and alkali earth oxides are often used to indicate whether the flux derives from a mineral alkali source or a plant ash one (Lilyquist & Brill 1993; Henshaw, 2010). However, the alkali contents in vitreous materials, originating from plant ash flux depend on the plant species, the composition of groundwater and soil, and on the specific chemical compound in the ash (Mohr & Schopfer, 1978; Clemens, 2002; Rehren, 2008). Furthermore, a purification of the plant ash can increase the alkali contents in comparison to the alkali earth values (Shortland *et al.,* 2006). Direct conclusions from the glass composition to the plant species are therefore difficult.

2.3.4.1 Plant ash glazes

The glazes from early Mesopotamia in the second millennium BC are primarily based on plant ashes as flux, bearing higher MgO and K_2O contents than glaze produced with mineral natron fluxes (Sayre & Smith, 1974; Shortland *et al.*, 2006; Rehren, 2008).

The alkali ashes are commonly mixed and pre-fritted with the quartz grains, in order to increase the homogeneity of the glaze coating (Tite & Shortland, 2003). For example, from the Central Asian production with plant ash flux from the 9th-11th century, the roasting of flux together with silica is described by Henshaw (2010). After heating, the mixture is quenched with water and ground to a frit powder which is then used for the glaze slurry. The use of plant ash flux and the attendant fritting procedure is also documented for medieval glass production in the Middle East (Barkoudah & Henderson, 2006).

In Mesopotamian Kassites, Mittanian Seleucid, Parthian and Sassanid cultures and in Middle East and Central Asia plant ash as alkali source was used throughout the first millennium BC until medieval times. Glazes from the Seleucid, Parthian, and Sassanian periods in Nippur, Iraq, are based on plant ash flux (McCarthy, 1996).

Analyses of the Hellenistic glass of the 6th century BC from the northern part of the Black sea reveal a Na-Ca-basis as flux. Whether the alkalis are obtained from plant ashes or mineral natron cannot be ultimately clarified here. The contents of K_2O are between 0.0 and 1.4 wt% and the MgO values are between 0.7 and 2.4 wt%.

Black Hellenistic glazes of the 5th-4th century BC are described to have very low contents of <1 wt% Na_2O and plant ash characteristics with 2-3 wt% high K_2O values (Wolff *et al.*, 1986). The Seleucid ceramics from the 4th-1st century BC have sodium oxide dominated glazes with 5-12 wt% Na_2O and high K_2O and MgO values typical for alkali glazes with plant ash flux, too (3-4 wt% K_2O and 3-5 wt% MgO, McCarthy, 1996). Ceramic wares of the Archaemenid, Parthian and Sassanid periods in the 6th century BC -7th century AD have glazes which deviate from this recipe primarily with a lower Na_2O content (Debevoise, 1934; McCarthy, 1996). These glazes have Na_2O and CaO values of about 6-8 wt%. Nevertheless, their MgO and K_2O content of each 2-4 wt% suggest a plant ash as flux (Moorey, 1999). From Central Asia from the 5th century BC until the 9th century AD, glass with high Na_2O and CaO on the basis of plant ashes are also reported to be traded to the Far East (Liu *et al.*, 2012).

2.3.4.2 Mineral natron glazes

The earliest use of mineral natron in glazes and vitreous materials is known from the early Egyptian faience production, based on the salt deposits of the lake Wadi el Natrun (chapter 2.1.4.1). In the Islamic glaze compositions, alkali glazes from Syria and Iran from the 7th-13th respectively 14th century are reported to have mineral natron characteristics (Mason, 2004). This stands in contrast to the commonly plant ash based Islamic glass compositions (2.1.4.2). The use of mineral natron is also reported from Turkish Iznik glazes. Possible sources for the salt compound are assumed to be alkali borax deposits in the western part of turkey (Tite *et al.*, 2016).

High alumina alkali glazes with mineral natron characteristic also occur in Indian Islamic tile glazes from the 14th-17th century, but with at most 7.4 wt% Al_2O_3 wt% (Gill *et al.*, 2014).

2.3.4.3 Lead and lead alkali glazes

The use of lead as flux has the advantage of a lower expansion coefficient, matching better the expansion properties of the fired ceramic body (Henshaw *et al.*, 2007). The raw materials of lead, oxides or sulphides, are easier to process and less variable in composition than plant ashes (Tite *et al.*, 1998). Because of the high diffraction index of a lead glass, the glaze appears thicker and shows a more brilliant colour. The addition of alkalis to the lead glazes increases the hardness of the material and makes the colour more clear (Al-Saad, 2002).

Tite (2008) finds the earliest high lead compositions (45-60 wt% PbO) in glazes of the 1st century AD from the eastern part of present day´s Turkey (45-60 wt% PbO). From there, the technology is taken up in the Roman and Byzantine imperia and continues into the medieval Islamic culture of the 8th-9th century in Syria and Iraq (Mason & Tite, 1997; Caiger-Smith, 1991). The high lead glazed wares are also known from the 8th-10th century on in Egypt (Wolf *et al.*, 2003).

It is remarkable, that the traditional pure alkali glazes are continued to be produced throughout the early and the medieval Islamic period, although lead glaze technology was established. The so-called "Samarra" glazes from Iran (Hill *et al.*, 2004) can be sub-divided into a group of alkali glazes with low PbO below 1 wt% and high lead glazes with ca. 40 ± 18 wt% PbO as it is seen in other medieval glaze compositions from Iraq, Jordan, Iran and Uzbekistan and India (McCarthy, 1996; Al-Saad, 2002; Vandiver, 2005; Gill & Rehren, 2011; Holakooei *et al.*, 2014). Tite (2011) describes a subdivision of glazes from Egypt, Iran, Syria and Iraq into alkali lime glazes (<2 wt% PbO), low lead-alkali glazes (2.0-9.9 wt% PbO, lead-alkali glazes (10-35 wt% PbO) and high lead glazes (>35 wt% PbO). The sources of the alkali portion are plant ashes of the respective region. The incoming parts of CaO from plant ash flux have additionally the effect of an increase of the lead oxide solubility in SiO_2 (Al-Saad, 2002). In the middle ages, the main composition of Islamic glazes seems to develop from alkali compositions towards lead alkali compositions, as it is described for Syrian, Egyptian and Iraq glazes of the 8th-14th century (Hallett *et al.*, 1988; O´Kane, 2011). Only the Iranian glazes of the 8th-14th century show more alkali than lead alkali compositions. The part of pure lead glazes stays more or less constant (Mason *et al.*, 2001).

2.3.5 Typical decoration techniques of glazed ceramic

2.3.5.1 Tin opacification

Tin opacification was a very wide spread technology through the medieval times in the Middle East and Central Asia. Some studies suppose, that the white colouring with SnO_2 pigments was an Islamic invention to imitate the imports of Chinese white wares (Caiger-Smith, 1991). For glass opacification instead, tin oxide is reported from Roman glass of the 2nd century BC (Turner & Rooksby, 1961).

Mason & Tite (1997) describe the tin oxide opacification already in glazes of the pre-Islamic Basra, Iraq. Nevertheless, the imports of Chinese porcelain ware are dated to the 8th or 9th century and could be one reason for the wide spreading of the tin opacifying technology.

Primarily in Egypt, Syria, and Iran, tin opacification is reported (Allan *et al.*, 1973; Mason & Tite, 1997; Shokouhi *et al.*, 2002). In the Iraq region, the production of tin opacification decreases quickly in the 10th century (Mason, 2004). This is possibly due to an escape of Iraqi potters to the Fatimid Egypt because of crusades or due to shortage of tin (Mason & Tite, 1997).

Together with the opacification of glazes, the development of paintings on glazes occurs, where the tin oxide whitens the background glaze on which the colourful glazes in Cu-green and Co-blue are applied. From the 9th century of Samarkand, lead glazes are known which are painted with the so-called "splashed decoration" (Lane, 1947). They imitate the imported Chinese wares with splashed glaze of the 8th-9th century (Henshaw, 2010).

In many cases, an increase of lead content is observed together with the increase of tin content. This corresponds to the descriptions of pottery manufacturing by Abu´l-Qasim, who was a member of one of the most important lustre producing families of Kashan, Iran, of the 13th and 14th century. He wrote in his recipe for opaque glazes, "three parts of good white lead and a third part of tin, or if one wants a better and finer mixture up to one half of tin" has to be mixed at high temperature (Allan *et al.*, 1973). He mentioned deposits of tin in Europe, in the Volga region and in China, which were available especially from Iran. For Syria and Egypt, the obtaining of tin from these regions was less developed and the tin technology was therefore introduced later (Allan *et al.*, 1973). The early 13th century is treated as the blooming period for Islamic faience, which was then interrupted by the Mongolian conquests.

2.3.5.2 Lustre

The earliest development of lustre wares is described for the early Islamic period, namely in Iran of the 9th century. Here, the lustre is applied on tin opacified lead-alkali-glazes (Mason, 2004; Pradell *et al.*, 2006; Henshaw, 2010). Watson (1985) describes lustre as an Egyptian (Fustat) innovation under the Fatimids in the late 8th century. Accordingly, the technique resulted from the development of a Roman colouring technique which is similar to the lustre technique (Lamm, 1941; Jones & Michell, 1976; Watson, 1985).

Craftsmen from Egypt had then transferred the technology to Samarra, Iraq, during the time of the Abbasid Caliphs in the 9th century (Kleinmann, 1986). In the times of the Ayyubid dynasty in the second half of the 12th century, the lustre production expires in Egypt in the context of the end of the Fatimid dynasty. Lustre production is then found in Tel Minis and Raqqa, Syria, and the Seljuq Iran (Watson, 1985). Especially the assimilation of Egyptian frit ware instead of clay

body ceramics improved the quality and the fineness of lustre in Persia from the middle of the 10th century on (Philon *et al.*, 1980; Watson, 1985). A white slip is also observed in earlier glazes from Iraq of the 9th century. Later, the slip technology was also spread into central Asia for polychrome painted glazes (Mason, 2004; Henshaw, 2010). The lustre production lasted until the Mongolian invasion in the 13th century at a high level of popularity. The Mongolian period caused an interruption of lustre production, which flourished again in the 13th and 14th century during the Il-Khanid dynasty. From this time on, the lusterware production varies from dynasty to dynasty, depending on the respective sovereign, craftsmen and resources.

2.3.5.3 *Cuerda seca* technique

C*uerda seca* is a Spanish invention of the 10th century. Glazes of different colours are painted to ornaments and pictures and are prevented to run into each other by lines of oil or wax (Bernar & Martín, 1987). The lines between the different glazes are black coloured, commonly with manganese and iron oxides (Chapoulie *et al.*, 2005; Holakooei *et al.*, 2014). The distribution from Spain to the eastern Islamic world took probably place across Turkey to Central Asia and India, undergoing regional changes in design and composition (Chapoulie *et al.*, 2005; O´Kane, 2011). From the Bulgarian period it is known that *cuerda seca* was used also for tiles in Hurasan and Bursa (Golombek, 1996). Further prominent uses of *cuerda seca* are known from the Mameluck period and from the Timurid dynasty on the mausoleums Amir-Zadah and Ustad Alim in Uzbekistan from ca. 1385. The Safavid production site Tabriz was 1514 absorbed by the Ottomans. This adaption revealed a high level of artisan facility and revived the use of *cuerda seca* in the Ottoman Empire. In the later periods of Timurids and Sheibanides, the technique is said to be less common. Instead, the under-glaze painting becomes a wide spread method, especially in the Ottoman ceramic production (Golombek, 1996).

2.3.5.4 Champlevé technique

Champlevé (French for "raised field") is a medieval decoration technique, where the surface of a metal or ceramic object is carved, edged, or casted and filled out with vitreous enamel (Victoria and Albert Museum, 2014). The technique is primarily known from the ancient Roman and Greek cultures, but it was extensively used in the medieval European and Islamic glazing technique, too (Hildburgh, 1936; Campbell, 1983).

2.3.5.5 Lajvardina technique

The word lajvardina comes from the Persian word lajvard, meaning "cobalt". The technique was invented in the 12th century in Iran and implies the application of a cobalt-blue glaze on the body of the vessels and tiles (Fehervari, 2012). On this glaze the decoration was painted in black, red, or white, while the frequently used gold was cut out of thin gold leafs and then glued to the body. The decorative themes were restricted to floral designs and palmettes (Fehervari, 2012).

2.3.5.6 Glazed tiles

From the 2nd Millenium BC, decoration of clay in architectural context with glaze material is reported from Mesopotamia (Paynter, 2009). Glazed terracotta wall plaques are known from the Neo-Assyrian period from the 9th century BC in Nimrud, Ba'shiqa, and Arban, Iraq (Freestone, 1991). From Nimrud, glazed bricks are reported from outer walls of the fort Shalmaneser from the 7th century BC (Nadali, 2006). The typical colours of Assyrian glazed ceramics are blue, white, green, and yellow (Nadali, 2006). The Babylonian Ishtar gate from the 6th century BC is probably one of the most famous examples for glazed bricks in Mesopotamia. In ancient Egypt, the use of faience or stone seems to be the common choice for building material (Paynter, 2009).

Glazes on building tiles can be generally classified according to their ceramic body into clay-based and stone paste ones (Grazhdankina, 2006). The clay-based ceramic bodies have a natural colour of red or brown hue, depending on the particular iron content and firing temperature (Kreimeyer, 1987; Molera *et al.*, 1998). The stone paste bodies, consisting mainly of quartz grains and a carbonatic or clay binder, have a lighter beige or white colour.

Since approximately the end of the 12th century AD, glazing is used for the decoration of buildings on glazed tiles on inner and outer walls in the Islamic culture (Watson, 1985). This is contemporaneous to the fall of the blooming period of the fine lustre painted Kashan glazes from Iran, which consequently influenced the ornamental style of the first tile glazes (Mostafawy, 2007). A noteworthy work for an early large-scale application of glazed tiles was done by the two potters Muhammad ibn Abi Tahir and Abu Zaid. In the beginning of the 13th century they decorated tomb-chambers and sarcophaguses with painted tile glazes (Watson, 1985). Commonly, the applied tiles have the shape of stars, octagons, or double pentagons. Other forms are crosses or rectangulars, either monochrome, polychrome and often lustre painted. The high standard of tile glaze production was interrupted by the Mongolian invasion around 1220. Nevertheless, the technique was not forgotten under the Mongolian rule and in

1270, the Mongol Sultan Abaqa Khan decorated his palace Takht-i-Suleiman with colourfully painted glazed tiles and lusterware. After a few decades of less activity and virtuosity, another highlight of the tile glazing is the prayer niche "mihrab" in Qumm, Iran. It was decorated in the 1330s by a certain "Master Jamal", "the most noble, the most excellent master" as it is recorded on two pieces of glazed tiles; (Watson, 1985). In the early modern times, i.e. the 15th century and later, Ottoman tile glazing style reached a high level of popularity due to its great fineness and high purity of materials (Paynter *et al.*, 2004; Yousef Jameel Centre, 2013). In European culture, the use of glazed tiles or bricks is e.g. known from the red brick Gothic in the Northern and Baltic Sea region or from the Islamic influenced cultures in Spain and Portugal (Turnbull, 2003; Figueiredo *et al.*, 2009).

2.4 Ideals of present day´s restoration

The conservation of a material can be done by a passive and an active conservation approach. The passive approach focuses on the control of the environment and prevents further deterioration. In the active conservation, the material itself is treated to preserve it from decay (Thomson, 1986; Davison & Newton, 2008). In the active conservation, it has to be distinguished between the pure consolidation of the material in the status quo, and the full conservation including also repair and supplement of the original state. The complementing of parts of an object is in every case a delicate issue because of the risk to modify the original state. It is stated e.g. for modern restoration in Central Asia by Allan *et al.* (2000), that non-adequate investigations of original material and "inappropriate use of traditional techniques" can result in irreversible defects of the historical building. The supplement of missing parts has to stop at the point of conjecture, when the original state doesn´t show enough reference for an unambiguous reconstruction (Brandi *et al.*, 2006). Further, the aim of modern conservation is not to bring the object to the exact state of its creation date. An important part of the objects impression is the history it has undergone since its completion. This part is also worthy to be protected. The aging marks from the time of an objects existence shall not be made undone by an intervention of a restorer (Brandi *et al.*, 2006). The most important document of conservation principles, the Venice Charta of 1964, still keeps its validity until present days. About the topic of restoration (article 9) it states: "Its aim is to preserve and reveal the aesthetic and historic value of the monument and is based on respect for original material and authentic documents.

It must stop at the point where conjecture begins, and in this case moreover any extra work which is indispensable must be distinct from the architectural composition and must bear a contemporary stamp. The restoration in any case must be preceded and followed by an archaeological and historical study of the monument." (International Council on Monuments and Sites, 1964). A supplement material for a historical object must therefore follow the optic and aesthetic style of the original, but it has to be distinguishable from the original substance. It is desirable, that the supplement material can be applied on site without removing parts of the historical bulk. Further, no act of restoration may prevent or even prevent later restorations (Brandi *et al.*, 2006). This results in the demand of complete reversibility of each intervention in the original material. A more detailed description of conservation and substitution materials for glass and glazes is given in the following chapter.

2.4.1 Substitution materials for restoration

In the conception of active restoration, the supplement materials have to fulfil particular requirements. In general, the conditions for glass restoration materials which are listed by Davison & Newton (2008) also hold for glazes. For supplement materials such as adhesives, consolidants and lacquers, following criteria are listed;

- The material has to show a reasonable adhesion to the substrate, for example glass or ceramic.

- In the state of application, the supplement must be fluent or at least elastic, after application is has to be easily curable either with temperature, light or with a curing agent.

- The mass has to stand strains and stress during application and curing, as well as after the curing process.

- The intervention has to be reversible, if it is possible without any detectable chemical or mechanical changes or leftovers in the original material.

- For the supplement of glass, the material should match the refractive index of the original glass and should have a lasting clear and transparent appearing without yellowing.

Among the conventionally used materials, the oldest one is probably a cellulose nitrate, which was developed in 1838 and which was industrially produced from 1845 on (Davison & Newton, 2008). Paraloid, also known as soluble nylon, is also widely used as consolidant of vessels and

window glass, but tends to attract particles such as dust from the atmosphere, which darken the material with time. Different epoxy-resins, commonly formed of a two component system build a very stable epoxy and polyamine network, which has good adhesion and low shrinking percentage. In some epoxy resins, a disadvantage is the tendency to yellow and the susceptibility to moisture. Further, it is irremovable from porous original materials such as ceramic or damaged glass surfaces. One of the often used epoxy resins is Araldite 2020, which has a remarkable good transparency. Different polyester resins are used for glass in optical instruments because of their adjustable refractive index (Davison & Newton, 2008). Acrylic resins, acrylates, and especially met-acrylates have very high resistance to oxidation and light deterioration (Davison & Newton, 2008). Silicones and silanes form another important material group for glass restoration. It includes all silicon molecules with organic radicals such as CH_3 or other functional groups. They react strongly and form a weathering resistant material with good adhesion, but have the disadvantage to be irreversible in their application (Davison & Newton, 2008). Additionally, dust is attracted to the silicone surfaces and makes the appearing dirty during weeks. Especially for glazes, an urea- or melamine-formaldehyde mixture is widely used under the name "Rustin´s Clearglaze", but it is almost irreversible and can´t be removed without damaging the original surface (Davison & Newton, 2008). The need for a reversible material with good adhesion and weathering characteristics is obvious. In the following section, the very versatile material ORMOCER® is presented which has suitable properties to become an important restoration material.

2.4.2   ORMOCER® composition

For a most careful, historically reasonable treatment of an ancient monument, a material for a sensible restoration needs to fulfil essential requirements, as discussed above.

The basis for the substitution material in this study is the material group of ORMOCER®s. ORMOCER® is an acronym for ORganic MOdified CERamic and is a hybrid polymer, developed by the Fraunhofer Institute in the 1980s (Schmidt, 2010). The basic component of the material is a combination of an inorganic network of Si-O-Si bounds with an organic polymer network. Additionally, different functional groups can be integrated (fig.6). The inorganic network is built from silicon alkoxides, which are generally the product of an alcohol anion and metal cation. The alkoxides are hydrolysed and afterwards condensed in a sol-gel process. In the hydrolysis reaction, the silicon alkoxides $Si(OR)_m$ reacts with the water molecules to form a hydroxide

Si(OR)$_{m\text{-}n}$(OH)$_n$ where m is the number of initial (OR) groups per Si ion and n the number of hydroxide groups. The other part (m-n) is the number of ligand molecules, remaining on the silicon bound:

$$\mathrm{Si(OR)_m + n\,H_2O \rightarrow Si(OR)_{m-n}(OH)_n + n\,ROH}$$
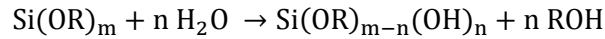
The parallel condensation reaction excludes the water molecules, in the following way:

$$\mathrm{\equiv Si - OH + \equiv Si - OH \rightarrow \equiv Si - O - Si \equiv + H_2O}$$
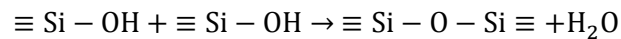
Because of the coincidence of the two reactions, a third one between the hydroxide and the alkoxides appear, excluding an alcohol:

$$\mathrm{\equiv Si - OH + \equiv Si - OR \rightarrow \equiv Si - O - Si \equiv + ROH}$$
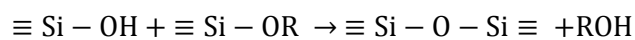
In the step of gelation, the cross-linking of the single clusters forms the complete network. The remaining solution of the solvent of water or alcohol is included in the network and evaporates until the final curing. The resulting structure is formed at low temperatures and with a high degree of chemical homogeneity (Haas *et al.*, 1999; Declerck, 2010). The organic compounds can be for example acrylic, vinyl or epoxy resin. It polymerises commonly under UV radiation or thermal treatment, but some types of ORMOCER® also cure at room temperature (Pilz & Römich, 1997). Functional groups do not act as a network former but influence the characteristics of elasticity, surface energy, and gas permeability of the material. They can be added to the hydrolyzed alkoxides as depicted in figure 7 (Schmidt *et al.*, 1998; Haas *et al.*, 1999). The composition of organic polymers with inorganic basic structure covers a wide range of mechanical and thermal properties. Additionally, the sol-gel materials can be prepared in many different processing variations, leading to different products such as e.g. powders, fibres, films, gels or dense ceramics. The applications reach from coloured coatings over protective coatings to coatings for electronic applications (Brinker & Scherer, 1990; Declerck, 2010).

The material has an appropriate viscosity for the easy use on-site which allows the applications by brush or spatula. The material cures on the historical building without any heating step and is stable against temperature and humidity for a long time. In addition, the claimed reversibility of present day´s restoration (Viñas, 2002; Brandi *et al.*, 2006) is fulfilled.
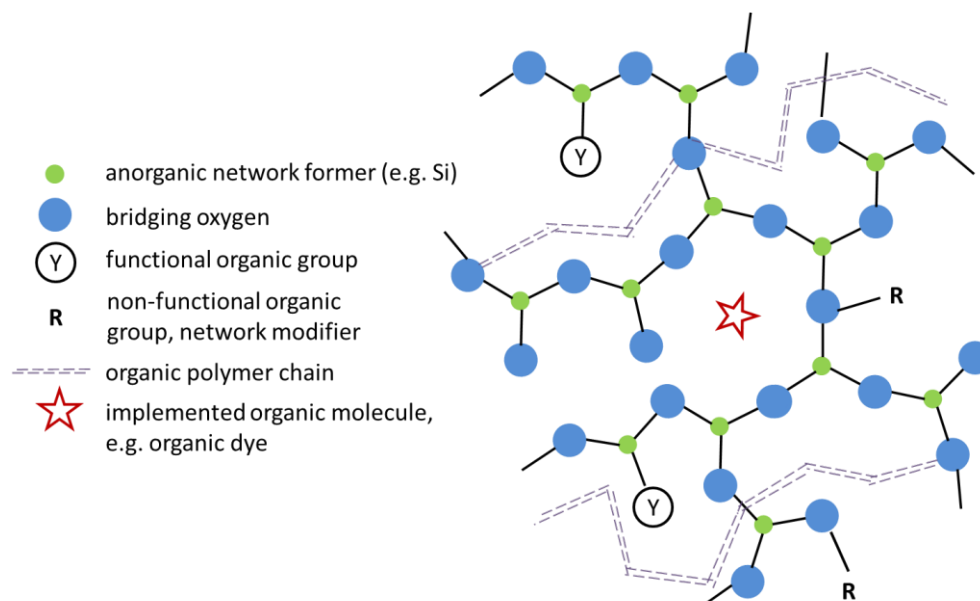
Figure 6: Sketch of the ORMOCER® components, adapted from Kasemann *et al.* (2010).

2.4.3 ORMOCER® "G", "B" and "E"

Two different kinds of ORMOCER® are tested in this study; the ORMOCER® "G" which is developed as a glass substitution material and the ORMOCER® "E" which is developed for enamel substitution. Both do not need a heating step for curing and form a stable coating after ca. 24 h. No shrinkage or crack formation occurs after the curing time as it is known from other hybrid polymers (Attin *et al.*, 1995). The formation of the ORMOCER® E requires the addition of a curing agent of ethoxy silane and e.g. di-ethylene-tetramine (Pilz & Römich, 1998). The hardener is given in the proportion of 1:200 to the ORMOCER® E.

For the restoration of vitreous materials, commonly the ORMOCER® G is used, which is based on the silicone-acrylate polymerizate "Paraloid B72" and a sealing resin. The resin consists of a pyrrole-ketone (C_5H_9NO) and a benzophenone ($C_{17}H_6O_7$). The solvents are butoxyethanol and ethyl acetate. First, the ethyl acetate is given in mass ratio 2:1 to the polmerizate Paraloid B72. In a 50 °C water bath it becomes a clear and transparent solution.

One after the other, one part of butoxyethanol and the resin is added until the solution gets transparent under stirring. The ORMOCER® E is a mixture of the ORMOCER® G and another ORMOCER® for bronze "ORMOCER® B" in the volume ratio of 85:15. The ORMOCER® B consists of a methoxy silane (GLYMO) and diphenyl silane diol as network formers (Pilz & Römich, 1997). With the GLYMO, different functional groups can be cross linked.
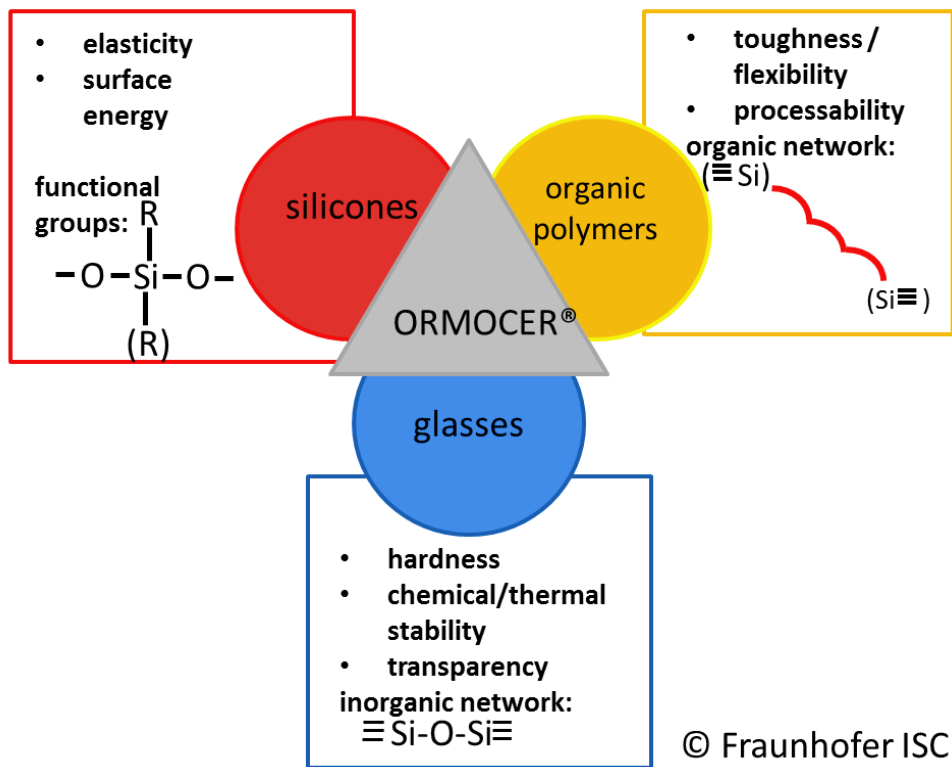
Figure 7: Schematically sketched diagram for the components of the ORMOCER® hybrid polymer. © Fraunhofer Institute for Silicate Research

3 Sample recovery and historical background

A total of 243 glaze samples is analysed, stemming from 216 sherds or tiles, a few of which are differently coloured glazes from one polychrome sherd or tile. The set includes 55 samples from Uzbekistan, 22 from Afghanistan, 39 from Iran, nine from Turkey, 37 from Bulgaria and 81 from Morocco (fig.8). The determination of sampling regions started with the purpose to increase the knowledge and understanding of Uzbek tile glazes from the ancient city of Bukhara, which is part of the UNESCO world heritage. The further purpose, to develop a restoration material which is adapted to the glaze composition and colouring gave rise to the widening of the random test. Glazes of adjacent and distant Islamic cultures were included in order to figure out more generally valid characteristics. At the same time, this sample set allows the comparison of glassy matrix components and colouring agents within the ancient glazed ceramics of different Islamic cultures.

The sampling of most of the Uzbek sherds and tiles is done by R. Drewello and J. Badr and documented by Badr *et al.* (2010) and in Gradmann *et al.* (2012). The samples from the mausoleum Ishrat Khane in Samarkand, Uzbekistan, are collected by the group of Steffen Laue at the University of Applied Sciences in Potsdam, Germany. The Afghan, Iranian, Turkish, and some of the Uzbek glazes were provided by the German Islamic Museum in Berlin; the Bulgarian ones are from the historical Museum of Silistra, Bulgaria, and the Moroccan tiles were collected by myself during field trips in 2013. The majority of the glaze samples derive from facades and interiors of Islamic buildings. In addition, part of the Uzbek and Bulgarian samples and all from Herat, Afghanistan are glazed tableware. The choice of tableware glazes is partly made according to the poor availability of glazed tiles (in Bulgaria and the 10th and 11th century in Uzbekistan), and with the aim to test the general comparability with regard to the application of a restoration material. Because it turns out that the compositions of tableware glazes are within the same compositional range as the glazed tiles, they are similarly considered in this investigation. The bodies of both ceramic types, tableware and tiles, are partly quartz-rich stone paste (quartz frit) and partly clay ceramics. In the tile ceramics, the quartz-rich stone paste build the majority; in the tableware ceramics, the clay bodies dominate. Detailed information is given in the list below.

Figure 8: Geographical sites of the sampled buildings and ceramics.

Short summary of the sample set; if not specified, the glaze samples have stone paste ceramic bodies.

The 55 Uzbek samples are subdivided into:

- 6 tableware glazes of the 10th-11th century from the ancient town of Afrasiab in the eastern part of Uzbekistan, close to the present-day city of Samarkand, Seljuq period, all glazes are on clay-based ceramic bodies
- 4 tile glazes from a Mongolian time building dated to the 13th century, Samarkand, 3 of the glazes are on clay-based tiles, 1 is on stone paste body
- 3 tile glazes originating from the mausoleum Ishrat Khane from 1464, Timurid dynasty, Samarkand
- 31 samples from tiles of the mosque Khoja Zainuddin from 1520-30, Bukhara, Sheibanid period (Badr *et al.*, 2010)
- 5 samples from the madrassa Mir-i Arab from 1535/6, Bukhara, Sheibanid period
- 1 samples from the mosque Baland, 16th century, Bukhara, Sheibanid period
- 5 samples from the madrassa Abdul Aziz Khan, 1652, Bukhara, Dshanide dynasty.

All the Bukhara samples derive from the centre of the city, which is an UNESCO world heritage since 1993.

The 22 Afghan samples originate from the western town of Herat and are all tableware glazes. They can be distinguished concerning their age:

- 2 glazes from the 13th-15th century, Mongolian period, 1 glaze is on clay-based body, 1 on a stone paste body
- 14 glazes from the 15th-16th century, Timurid dynasty, 4 of the glazes are on clay-based bodies, the remaining 10 are on stone paste bodies

39

- 6 glazes from the 16th-17th century, Safavid dynasties, 2 of the glazes are on clay-based bodies, 4 glazes are on stone paste bodies.

37 out of the 39 Iranian samples are from tiles from the building complex Takht-i-Suleiman in the north of Iran, two are newer, restored tiles from the central Iran:
- 5 glazes of tableware date to the 12th and early 13th century, Khwarezmid dynasty, and predate the Mongolian time which initiates in this part of Iran around 1237, 2 of the glazes are on a common clay-based ceramic sherd, the other ones on stone paste bodies
- 32 tile glazes date to the second half of the 13th century, particularly to the Ilkhanate dynasty, 8 of the 32 glazes are on clay-based tiles, the other ones on stone paste bodies
- 2 date into the early 20th century and are restored tiles from a prayer niche in Isfahan in the central Iran.

The Turkish samples are from tiles from the cities of Konya in central Anatolia and Kayseri in Cappadocia from the 12th and 13th century, i.e. the Seljuq period:
- 3 are tile glazes from on sherd from the 12th or early 13th century, from the city of Konya
- 5 are tile glazes from the 13th century, from the mosque Ata Hanka in the city of Konya
- 1 is from the second half of the 13th century from an unknown building of the city of Kayseri.

The 37 Bulgarian samples of the fortress Dristra in the north of present day´s Bulgaria represent with a range from the 11th-12th century, pre-Islamic Second Bulgarian Empire and from the 14th-18th century, Ottoman period (personal communication, Atanasov, 2013):
- 10 tableware glazes from the 11th and 12th century from Bulgaria, Second Bulgarian Empire
- 3 tableware glazes of monochrome tableware from the 14th and 15th century, Ottoman period
- 11 tableware glazes of monochrome tableware from the 16th and 17th century, Ottoman period
- 6 tableware glazes from 2 polychrome sherds (BG 1-3 and BG 11-13), probably imported tableware objects dated to the 16th-17th century, Ottoman period (pers. comm. Atanasov, 2013)
- 7 tableware glazes, monochrome tableware, 17th and 18th century, Ottoman period.

The 81 Moroccan samples of tile glazes originate from different buildings and dynasties between the 14th century and the 18th century:
- 10 tile glazes from the madrassa Bou Inania in Meknes from the 14th century, Marinid dynasty

- 14 glazes from the madrassa Bou Inania in Fes from the 14th century, Marinid dynasty
- 5 glazes from a school building in Salé from the 14th century, Marinid dynasty
- 9 glazes from the madrassa Abu al Hassan in Salé from the 14th century, Marinid dynasty
- 10 glazes from the necropolis Chellah in Rabat from the 14th century, Marinid dynasty
- 10 younger ones, deriving from the Saadian tombs in Marrakesh from the 16th century, Saadian epoch
- 4 even younger tile glazes of the Sultans palace in Tangier, 17th century, Alaouite dynasty
- 6 glazes from the fountain in Tangier, 17th century, Alaouite dynasty
- 13 latest samples from the mausoleum of Moulay Ismail in Meknes, built in 1727, Alaouite dynasty.

3.1 Uzbek glazes

The glazes from Uzbekistan are in the majority tile work from mosques and madrassas of the 13th-17th century. A smaller part is clay-based tableware from the 10th-11th century. These early ones are six samples from an excavation in Afrasiab, an ancient town in the north of Samarkand. The town Afrasiab was strongly influenced by its geographical location on the Silk Road and possesses a tradition of ceramic production which was well established since the 9th century (Pugachenkova & Rtveladze, 2009). During the 10th and the 11th century, Uzbekistan was governed by the Early Islamic dynasty of the Samanides and later by the Turkish tribes of the Karakhanides and the Seljuqs (Fragner, 2007). The rich city Afrasiab was part of a vassal state of the Seljuqs, which became independent in the late 11th century and was then ruled by the Khwarazmian dynasty (Spuler & Marcinkowski, 2003). During the 11th and 12th century, the capital of this dynasty was Urgench, but it was Samarkand from 1212 on (Grousset, 1970). In this region, the distribution of glazed tiles is known from the 12th century on (Grazhdankina *et al.*, 2006).

Seven newer samples are taken from tiles of historical buildings in Samarkand. Four tile glazes date to the Mongolian epoch in the 13th century, from which three are clay-based ceramic and one stone paste ceramic. They are not clearly assigned to a building and are treated as "tiles from Samarkand" in the present work. Three samples from the 15th century originate from the building Ishrat Khane, which is dated to 1460-1464, when Samarkand was the capital of the Timurid Empire (Kasch, 2009).

37 even younger samples of glazed tiles of stone paste ceramic are from the period of the Sheibanides, beginning in the late 15th century. The Sheibanides are named after their ruler Muhammed Sheiban, a grandson of Genghis Khan, and have their origin in Mongolian and Turkish tribes which converted in the 13th century to the Islam (Bukharaev, 2000; Lapidus, 2002; 'Izzatī & Ezzati, 2002).

The samples originate from the mosque Khoja Zainuddin in Bukhara, which was built in the middle of the 16th century and from the madrassa Mir-i Arab and the mosque Baland of the same period (Badr *et al.*, 2010). The newest five samples from ca. 1640 are on a *cuerda seca* tile from the madrassa Abdul Aziz Khan in Bukhara, which is the only polychrome tile of the set (fig.9, Abri & Wallasch, 2008).

The numbers of glaze samples of different locations in Uzbekistan are given in table 3.
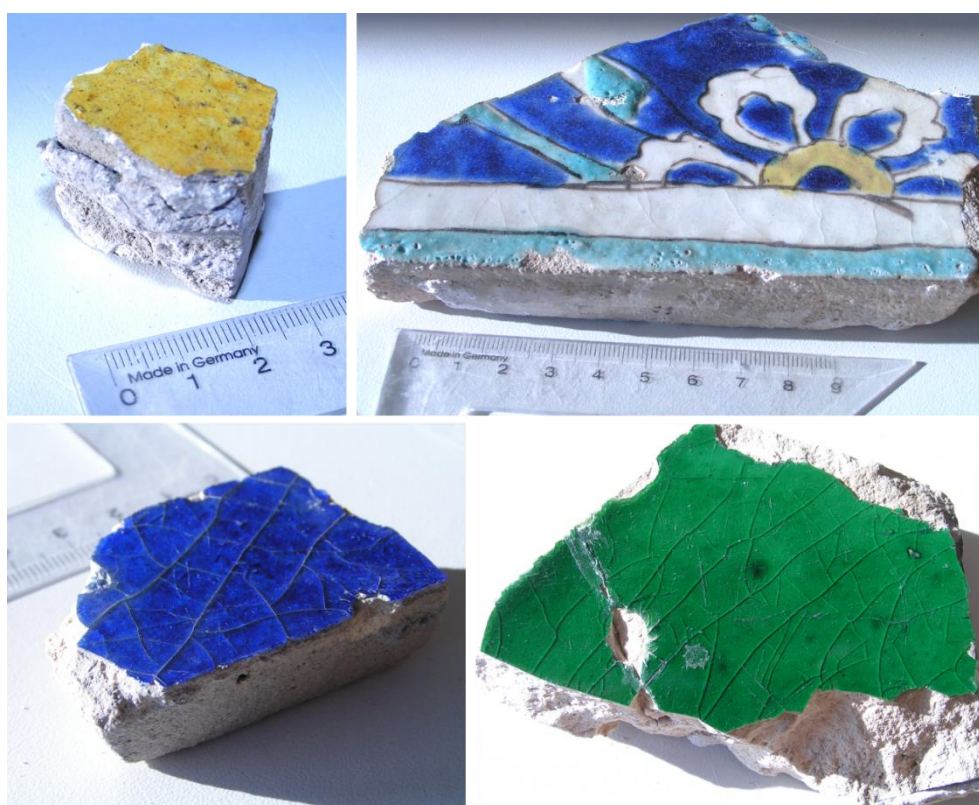
Figure 9: Four tiles from historical Uzbek buildings from Bukhara; top left: yellow glazed tile from the mosque Khoja Zainuddin, top right: polychrome *cuerda seca* tile from the madrassa Abdul Aziz Khan, bottom left: blue glazed tile from the mosque Khoja Zainuddin; bottom right: green glazed tile from the mosque Baland.

Table 3: Overview of the historical classification, the locations, and the number of glazes for each colour for the Uzbek samples.

	Afrasiab	Samarkand	Mausoleum Ishrat Khane	Mosque Kohja Zainuddin	Madrassa Mir-i Arab	Mosque Baland	Madrassa Abdul Aziz Khan
Century	10th-11th	13th	15th	16th	16th	16th	17th
Black	1			1	1		1
Blue		2	1	8	1		1
Yellow				2			1
Green	2		1	4		1	
Red	1	1					
White	2			4	1		1
Purple				3			
Ochre/ Brown				3	1		
Turquoise		1	1	6	1		1

3.2 Afghan glazes

The group of Afghan glazes consists of 22 samples which are commonly transparent, turquoise, or green glazes from tableware ceramics. Within the ceramic bodies, 15 are stone paste bodies made of quartz frit and seven are clay-based bodies. The subdivision does not correlate with the age, colour, or flux composition of the glazes. The excavation site is Herat, which had a stable economy and was an important centre of art in this region (Arjomand, 1999; Meyer, 2014). From 1505 to 1507, Herat was even the capital of the Timurid Empire. Two samples date to the 13th-15th century, the period of the Kurt dynasty which was a vassal state of the Mongolian Empire (Bosworth, 2004). The largest group of 14 samples originates from the 15th and early 16th century, when the Timurids were the rulers in the present day Afghanistan. A number of six younger samples from the 16th and 17th century originates from the Persian Safavid Dynasty (1502-1722), established by Shah Ismail (Fragner, 2007). In these times, Herat was a provincial

capital with less importance, lying in the debatable territory between Safavids and Uzbeks (Newman, 2006; Savory, 2007). Table 4 sketches the numbers of glazes in different colours from different centuries.

Table 4: Colours and historical classification of the samples from Herat, Afghanistan.

	Herat	Herat	Herat
Century	13th-14th	15th-16th	16th-17th
Black		1	1
Blue		4	1
Green		2	1
White		2	
Ochre/Brown	1	1	1
Turquoise	1	4	2

3.3 Iranian glazes

Among the 39 Iranian glazes, 37 are taken from the historical building Takht-i-Suleiman in the northern part of the modern-day Iran. Five of the glazes date to Khwarazmian times of the 12th century and are from bichrome decorated tiles, the so-called "Champlevé" technique (see 2.3.5.4). Two of the seven tiles are clay-based, the other five are stone paste bodies. The dynasty of Khwarazmians ruled in the 11th and 12th century in the area of present day´s Iran, Iraq, Syria, and Anatolia before the Mongolian conquest. The Khwarazmians are a Turkish tribe, converted to the Islam in the 10th century and strongly influenced by Persian language and art (Adas, 2001; Hillenbrand, 2005). The largest part of the samples, 32 glazes, date to the Mongolian period in the second half of the 13th century (tab.5). Eight of the 32 tiles are clay-based, the remaining ones are stone paste bodies. In particular, they belong to the Mongolian vassal state "Il-Khanate", where the Islamic religion was re-established after the invasion of the Mongols in 1227 (Morgan, 1988). Furthermore, art and craftsmen-ship were supported by the Mongolian rulers and further developed. Different colours like white, blue, and turquoise, but also few

brown, red and yellow-greenish colours are found among the glazes. Some of the tiles are polychrome sherds with lustre painting areas and metallic glance.

Two more samples in the stock are from the prayer niche of a mosque in Isfahan which was restored in the early 20th century by local potters. These modern samples are black and blue coloured and are taken as a reference for the continuity or discontinuity of glazing technique tradition in the Iranian region up to the very young Qajar dynasty (1794 to 1925).

Table 5: Colours and historical classification of the samples from Iran.

	Takht-i-Suleiman	Takht-i-Suleiman	Isfahan
Century	12th	13th	20th
Black			1
Blue		10	
Light blue			1
Yellow	1		
Green	3		
Red		1	
White		9	
Ochre/Brown		2	
Turquoise	1	10	

3.4 Turkish glazes

From the nine Turkish samples, one glaze is from a tile of an unknown building in Kayseri and eight glazes are from three tiles of the mosque Ata Hanka in Konya. All nine ceramic tiles are stone paste bodies. Both cities are in the area of present day´s central Turkey. The tiles from the mosque Ata Hanka are polychrome sherds with black, ochre, blue, and turquoise glazes. The samples date to the 12th and 13th century when the region was under the regiment of the Seljuqs,

before the Ottoman Empire rose in the early 14th century (tab.6). Kayseri and Konya, together with Sivas, were the three Seljuq capitals of this time.

Table 6: Colours and historical classification of the samples from Turkey.

	Konya	Konya	Kayseri
Century	12-13th	13th	13th
Black		1	
Blue	1		
Green	1		
Ochre/Brown		1	
Turquoise	1	3	1

3.5 Bulgarian glazes

The 37 Bulgarian samples split into 10 pre-Islamic and 27 Islamic glazes. The ten earliest are from the Second Bulgarian Empire in the 12th century of Bulgaria (pers. comm. Atanasov, 2013). The glazes are taken from clay-based tableware sherds. On the basis of these samples, the later Ottoman influence on the craftsman work and glazing technology in the conquered regions can be estimated. 27 samples of the 14th-18th century date to this Ottoman period in Bulgaria which lasted from 1396 to 1829 (tab.7). They originate from the fortification Dristra on the Danube riverside in the centre of the modern city Silistra. Three glazes date into the 14th-15th century, but most of the samples are from the 16th and 17th century, according to the local archaeologist Prof. Atanasov (pers. comm. 2013). Six of these glazes are from two polychrome painted sherds; one has blue and green paintings, the second one has violet and blue paintings, both on white background. Eleven glazes are green coloured, six samples of the set are beige coloured. Additionally, there are 15 ochre and brown glazes and one black glaze.

Table 7: Colours and historical classification of the samples from Bulgaria.

	Dristra	Dristra	Dristra	Dristra polychrome sherds	Dristra
Century	12th	14th-15th	16th-17th	16th-17th	17th-18th
Black			1		
Blue		1		2	
Green		1	6	1	3
White/Beige		1	1	2	2
Purple				1	
Ochre/Brown	10		3		2

3.6 Moroccan glazes

81 samples of nine different sites in Morocco are collected in total. Nine different colours are found on the consistently monochrome tiles. The entirety of the tiles is made of stone paste ceramics. The localities and shades are depicted in table 8. Most of the tile glazes are from the 14th century from buildings of the Marinid dynasty which lasted from the 13th-15th century. Ten glazes are from the Saadian tombs in Marrakesh and date into the time of the sultan Ahmad al-Mansur of the 16th century. The Saadians were the rulers in Morocco from 1554 to 1659. Another ten glazes are from the palace and a nearby fountain in the city Tangier and date into the early Alaouite dynasty of the 17th century. The 13 later samples from the mausoleum of Moulay Ismail in Meknes from 1727 (fig.10) belong to this dynasty, too, which lasts with the reign of King Mohammed VI until today. The ages for the particular buildings are given by archaeologists on-site and the ministry of cultural affairs of Morocco (pers. comm. Abdelkader Chergui, 2013; Achaari, 2010). The sample taking was carried out with big caution, in order to conserve the tile glazes appearing as much as possible (figs.11 a and b).
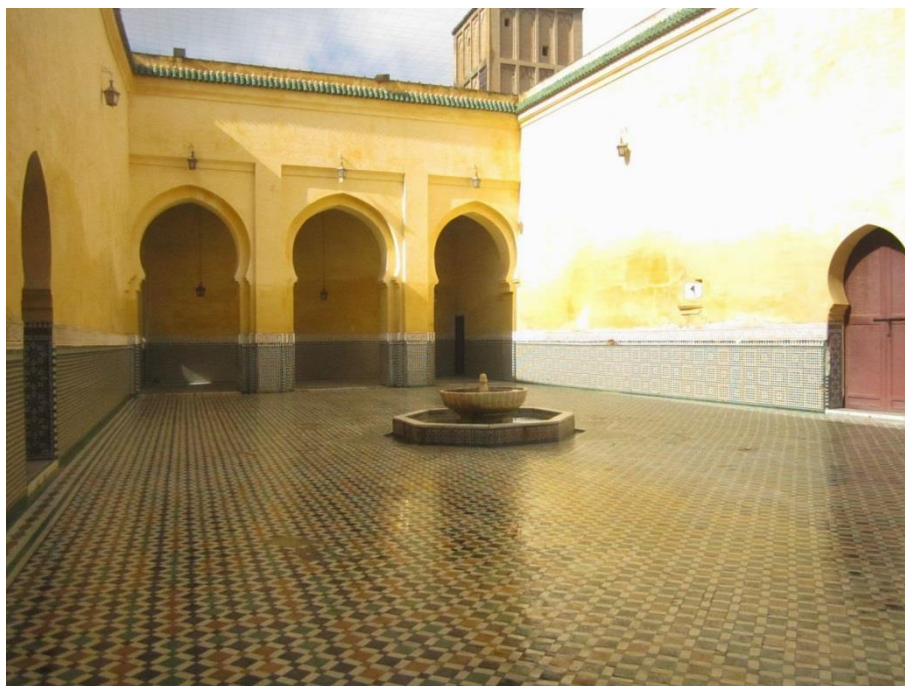
Figure 10: Inner yard of the mausoleum of Moulay Ismail in Meknes from 1727.
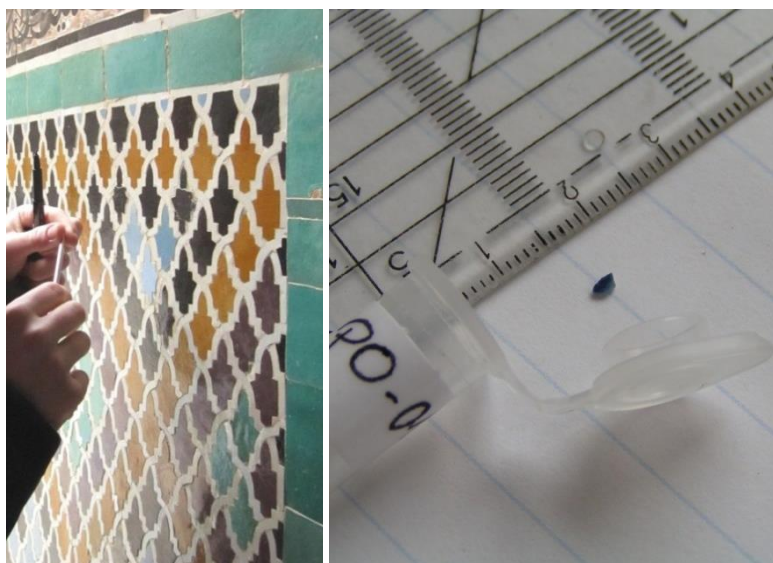
Figure 11 a, and b): Sampling of wall tiles in the madrassa Bou Inania in Fes (left). The small pieces of glazed tiles are chipped with a screwdriver and encapsulated in plastic tubes (right).

Table 8: Colours and historical classification of the samples from Morocco.

	Necropolis Chellah Rabat	Marinid School Salé	Bou Inania Fes	Bou Inania Meknes	Abu al Hassan Salé	Saadian Tombs Marrakesh	Fountain Tangier	Sultans Palace Tangier	Mausoleum Meknes
Century	14th	14th	14th	14th	14th	16th	17th	17th	18th
Black	2	1	1	2	3	2	1	1	2
Blue				1			1	1	1
Light blue	1		1			2	1		1
Yellow	1	1				1			
Green	2	2	1	2	1			1	2
White	1	1	3	2	2	2	1	1	2
Purple	1		4						1
Ochre/Brown	1		2	2	1	1	1		2
Turquoise	1		2	1	2	2	1		2

4 Sample preparation and experimental methods

4.1 Sample preparation

Taking a glaze sample from a ceramic fragment or from a historical building has to be carefully carried out in order to minimize the intervention of the object. It has to be considered that the sample is in the optical appearing representative for a larger part of the object material. The sampling is done on a hidden part of the object or at already damaged areas. Obviously weathered parts are not suitable for the investigation of the original components because of changes in the chemical composition by deterioration. The particular piece of the desired area can be carefully forced away by pressing a small spatula or screwdriver on the surface close to the glaze rim. Each sample consists of an area of about 1-2 mm² glaze with the appending part of ceramic body or slip below. This piece of material is mounted with the cross section on the top on a glass substrate and is fixed with epoxy resin. For better control of the upright position of the sample, it is stabilized by small cubes of cured epoxy resin. The surface is polished for the measurement in the EPMA device and sputtered with carbon for a better conductivity.

4.2 Electron probe microanalysis (EPMA)

The electron probe microanalysis is used for the analysis of the matrix phase of the glaze materials and for solid inclusions of more than a few μm in the glazes. The method is based on an electron beam, which is focussed by several magnetic lenses to the sample surface. As electron source is commonly used a W-cathode with 15 kV acceleration voltage and about 20 nA electron beam current. As a first interaction with the sample, the electrons of the beam kick out electrons from the atoms on the sample surface. These secondary electrons are collected in a detector and depict the relief of the sample, when the electron beam is scanning across a defined area of the sample surface. Another part of the beam electrons, the so-called backscattered electrons, enter the sample and are deflected by the atoms of the upper ca. 100 nm of the material and are released from the sample surface again. The higher the atomic weight of the surface near elements, the higher is the detected signal of backscattered electrons. Therefore, these backscattered electrons depict the differences in average atomic numbers of the scanned phases. Furthermore, the electron beam generates characteristic X-ray

emission from the sample material down to ca. 500 nm depth. In the case of wavelength dispersive X-ray analysis (WDX), these element-characteristic X-ray signals are separated in four crystal spectrometers with different monochromator crystals according to the Bragg equation and detected in gas flow counters with commonly Ar-methane gas-mixture. The method is suitable for phases which are homogenous within 1 µm depth and several µm lateral extents. The sample chamber is evacuated in order to avoid interaction from the electron beam or the emitted X-ray signal with gas molecules. The EPMA measurements are primarily performed with a JEOL JXA 8800L device with wavelength-dispersive analysis at the University of Würzburg. One part of the analyses was carried out with a JEOL 8900L at the University of Cologne. A 15 µm beam size is used in order to minimize the sodium migration in the analysed spot.

Measurements on ceramic bodies were carried out with a row of 20 µm beam size, overlapping 10 µm, in order to get mean values of the non-homogeneous material. Due to the very little amount of ceramic material, the analysis with more standardised methods like X-ray fluorescence could not be carried out.

For matrix correction, the ZAF method is applied. The analytical error of the analyses is determined by repeated measurements on the relevant standards to <1% relative for major elements, <2% rel. for Na. It increases for trace elements. The detection limit is estimated to 0.05 wt%. For the analysis, the Kα-line is used for the determination of Na, Mg, Al, Si, Ca, K, Ti, Mn, Fe, Co, Cu, Ni, S, Zn, P, and Cl the Lα for Ba and Sn and the Mα−line for Pb. The measurement is adjusted to 20 s on the peak and 20 s on the background. As standards, natural and synthetic silicates, oxides, and sulphides are used: Albite for Na, MgO for Mg, Corundum for Al, Andradite for Si and Ca, Orthoclase for K, $MnTiO_3$ for Mn and Ti, Fe_2O_3 for Fe, metallic Co and Cu, NiO for Ni, ZnS for S and Zn, Apatite for P, Vanadinite for Cl, $BaSO_4$ for Ba, SnO_2 for Sn, and PbS for Pb.

4.3 Portable X-ray fluorescence analysis

The portable X-ray fluorescence analysis (p-XRF) was applied to the Uzbek and Moroccan glaze samples with a sufficiently large glaze surface (7 mm^2). In addition, synthetic glass samples were measured in order to estimate the accuracy of the device in glass and glaze analytic. The measurements were carried out with the devices of the Paz Laboratories for Archaeometry in Bad Kreuznach, Germany and in the Institute of Earth Sciences in Heidelberg, Germany.

The method is based on the emission of characteristic X-ray fluorescence of X-ray-exited atoms and is commonly used for the elemental analysis from sodium ($_{11}$Na) to uranium ($_{92}$U) of bulk samples. The excited atoms emit radiation in a combination of wavelengths which is specific for the respective chemical element (fig.12). An incident X-ray with the energy h*ν_i hits an electron e$^-$ out of its atomic electron shell of a sample atom. ν_i is the frequency of the electromagnetic wave, h is the Planck constant of 4.136×10^{-15} eV*s. The vacancy of the kicked electron is than occupied by another electron from an outer-lying shell when the energy difference between both electron positions in the shells is emitted in form of an element-characteristic X-ray signal, the so-called fluorescence radiation. The released radiation has the characteristic frequency ν_f and the energy h*ν_f, which is then used for the qualitative and quantitative element analysis.

The radiation energies are the higher the larger the distance between the two energy levels. Therefore, primarily the higher energies released from transitions to the very inner shells of the atom are taken as main signal. According to the nomenclature of electron shells, this signal is called Kα-line.

The p-XRF is a gun-like device (fig.13), which is a quick and easy to handle instrument to determine the major element composition in a high number of samples. The non-destructive measurement makes the method to a tempting tool for the investigation of historical objects (Tite, 2002; Orfanou & Rehren, 2015). The measurements theoretically include the elements from U down to Mg. The lighter elements Mg and Al have higher relative errors than the heavier ones. With a vacuum or He-flush system, which reduces the absorbing air between sample surface and detector, the precision of the measurements is improved and even Na can be detected (Meyer *et al.*, 2014). However, in the upper layer of historical glass and glaze samples, the Na content is commonly depleted, so the measurements are not diagnostic for the bulk glass composition (Gianoncelli & Kourousias, 2007).

The depth of the detectable signals depends on the specific element and the particular absorption coefficients of the elements in the analysed material composition. The depth from which the signal of a particular element reaches the surfaces is in the range from a few µm for lighter elements up to several mm of heavy elements (Duve & Schmottlach, 2012). The p-XRF analysis was carried out with the XL3 Hybrid device from *Analyticon Instruments*. The device works with an Ag-anode; measurement conditions were up to 40 kV accelerating voltage and 40 µA tube current.
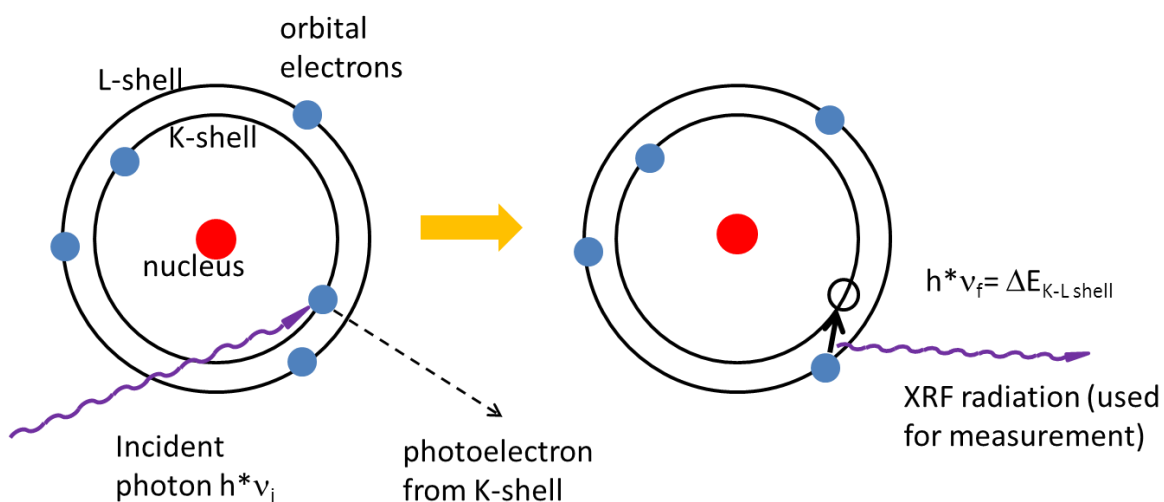
Figure 12: Sketch of the X-ray fluorescence principle. An incident X-ray hits an electron out of its atomic electron shell. The vacancy is than occupied by another electron from an outer-lying shell. The energy difference between these two shells is emitted in a characteristic electromagnetic radiation (adapted from Fisher, 2014).

Figure 13: Portable XRF device with movable display. © Thermo Scientific

The signal is collected with an energy dispersive silicon drift detector (SDD detector). The device is used without helium flush system, accepting the lower precision for the light element Mg with the benefit of easier handling. The measuring area is adjustable between 7 mm² with a spot

diameter of 3 mm, and about 50 mm^2 with a spot diameter of 8 mm. In this work, the spot diameter is chosen to 3 mm in order to enhance the number of possible measuring spots without surface inhomogeneities like pinholes or cracks. The measurement area is visible during the measurement thanks to an integrated camera system. For the finely distributed pigments such as SnO$_2$, the area of 7 mm^2 is large enough to measure a reproducible average of matrix and pigments.

The details of the internal settings of the device, such as background fitting or measuring line are not published by the producer. Nevertheless, the use of the Kα-lines for the lighter elements Mg, Al, Si, P, S and Cl and Sn, and the Lβ-lines for Pb can be deduced from the given spectra. The device is equipped with different measuring programs; alloys, noble metals, plastics, dusts, minerals and soils, which are specialized to specific types of material. Two of the measuring programs, called "mining" and "soil", are suitable for the analysis of glass. The matrix correction is differently done by these particular programs; the correction of the "mining" program uses the fundamental parameter method. It assumes not only linear, but also nonlinear behaviours of absorption, attenuation coefficients and fluorescence effects, in contrast to older methods which used linear approximations (van Sprang, 2000; Rousseau, 2004). The non-determined elements like elements with atomic weights below Mg are calculated in a "balance" value, which is then used for matrix correction (Han *et al.*, 2006; pers. comm. H.P. Meyer, 2013). This program is appropriate to measure K, Ca, Si, Al and the transition metals like Fe, Cu, and Co.

The "soil" program in contrast measures these elements together with Th and U, but neglects the elements below S. The program "soil" uses the Ag-Kα-Compton peak for matrix correction, which is obtained from the incoherent scattering of primary X-rays. The calculation uses calibrations of pure elements and their ratio to the Compton peak and therefore includes differences in matrix or surfaces texture of the sample (Van Grieken & Markowicz, 2001; Agency, 2006). The program is first of all recommended for trace elements and heavy elements. The measurements of lighter elements are commonly less precise.

The calibration of the programs is done in the factory adjustment with standard measurements. The calibration cannot be carried out by the user, so external standards must be used to test the suitability of a particular measurement program. The measurement procedure is divided in four measuring modes (called "filters") for the particular elements: Main (40 kV), low (20 kV), high (40 kV) and light (8 kV). The different elements are choosen from these different filters in order to get optimum results. The "Main" mode measures most of the transition metal elements

together with Rb, Sr, As, Se, and Pb. The "Low" mode includes the elements from K to Cr. In the "High" mode, Pd, Ag, Cd, Sn, Sb, and Ba are measured. The "Light" mode includes all elements from Mg to Cl.

The "mining" program uses all four modes, whereas the "soil" program skips the "Light" modus. The measurement times of each modus can be selected in all programs. In this investigation, 20 sec for all modes in "mining" and "soil" measurements were applied. The Uzbek and Moroccan glazes with sufficient surface area of 7mm* are measured. For the selection of Uzbek glazes, the "mining" program is chosen, for the selected Moroccan samples, both programs are applied. The programs are carried out one right after the other, so that the selected measurement areas are identical.

4.4 Two-dimensional micro X-ray diffraction device (µ-XRD²)

The two-dimensional micro X-ray diffraction (µ-XRD²) is applied to several samples from Uzbekistan in order to determine the µm and sub-µm sized crystalline phases such as precipitations and inclusions. The measurements were carried out at the Institute of Mineralogy and Geodynamic in Tübingen, Germany.

The µ-XRD² is based on the same principle as a conventional powder diffraction device; X-ray radiation interacts with the structure of lattice planes in a crystalline material. The lattice planes in the crystalline material result from the three dimensional periodic array of atoms in a crystal structure (fig.14). A monochromatic X-ray beam is reflected on these lattice planes of the analysed sample. The combination of reflexion from different lattice planes of a particular crystalline material forms the characteristic reflexion pattern.

In detail, the X-ray beam with wavelength λ is reflected in one part in the angle of its incidence *(θ).* Another part of the beam crosses some lattice planes before it is reflected on a deeper lying plane. For each distance between lattice planes *d*, the additional length of *d*sin(θ)* is travelled twice (fig.14). When this additional path length is a multiple of the X-ray wavelength (*n*λ*), the minima and maxima of the differently reflected waves are added and reinforced. In this case, constructive interference occurs and the reflected radiation is detected as a peak of high intensity. In knowledge of the angles of reflection, the distances of the lattice planes can be calculated from the following formula

$$2 * d \sin \theta = n * \lambda$$

It is developed by the British physicists William Lawrence Bragg and William Henry Bragg (Bragg & Bragg, 1915). From the distances of the lattice plane, the lattice parameters themselves can be calculated. The totality of reflexes is diagnostic for one crystal structure with crystallographic point group and lattice parameters. In powder diffraction measurement, the crystal grains are statistically orientated and the signal is detected only in one section of the sample surrounding. In single crystal analysis the crystal must be movable in both angles of the polar coordinate system in order to detect all lattice reflexes.
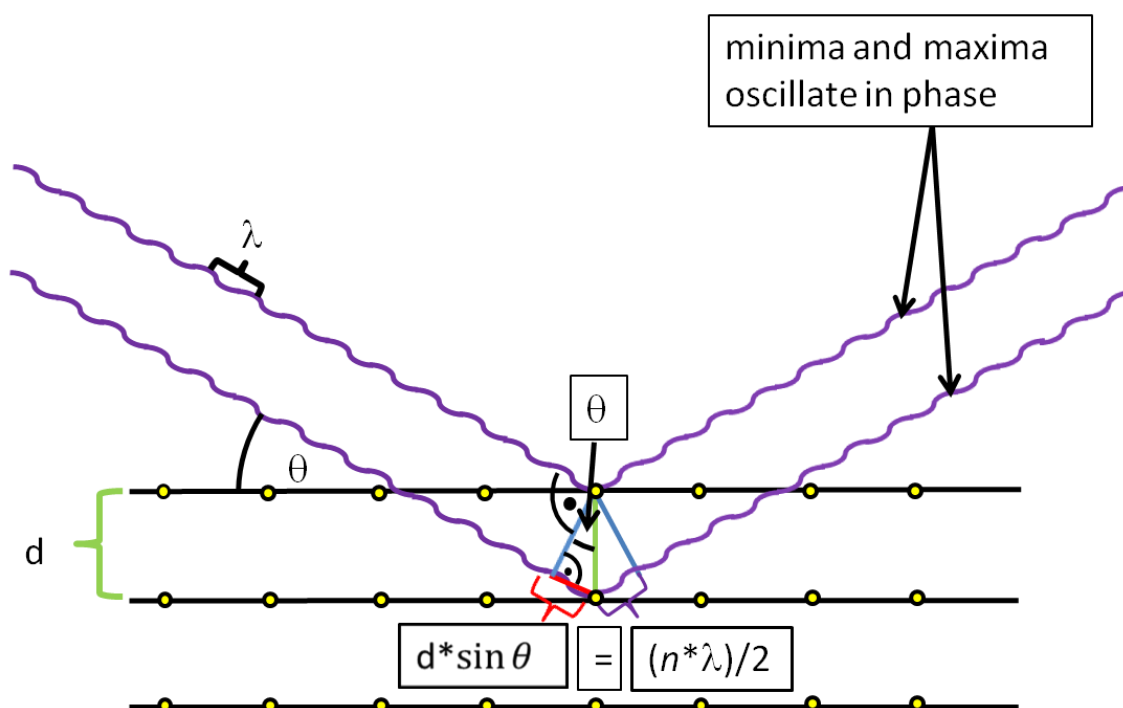

Figure 14: Sketch of the Bragg formula with θ = angle of incidence, d = lattice spacing, λ = wavelength and n = order of positive interference (with n = part of the natural numbers). © Online lessons of the University of Göttingen, Germany

The most common approach of powder diffraction analysis is the Bragg-Brentano geometry, where the focus of the X-ray source, the detector, and the plane sample lies on one orbit. The detector moves with an angular speed of $2*\theta$ along the circular path; the sample rotates with angular speed of θ around the own axis. All X-ray signal of one angle converge in one point in the detector.

In the µ-XRD[2] method, small crystal grains down to a few 100 nm can be analysed in a variable spot diameter (Tholey *et al.*, 2010). The samples do not need a foregoing preparation and can

be shaped in any geometry up to about 25 cm. The samples are mounted on a XYZ-movable stage of the company Universal Moving Components (UMC) with additional rotation function around the Z-axis to increase the measurement statistics.
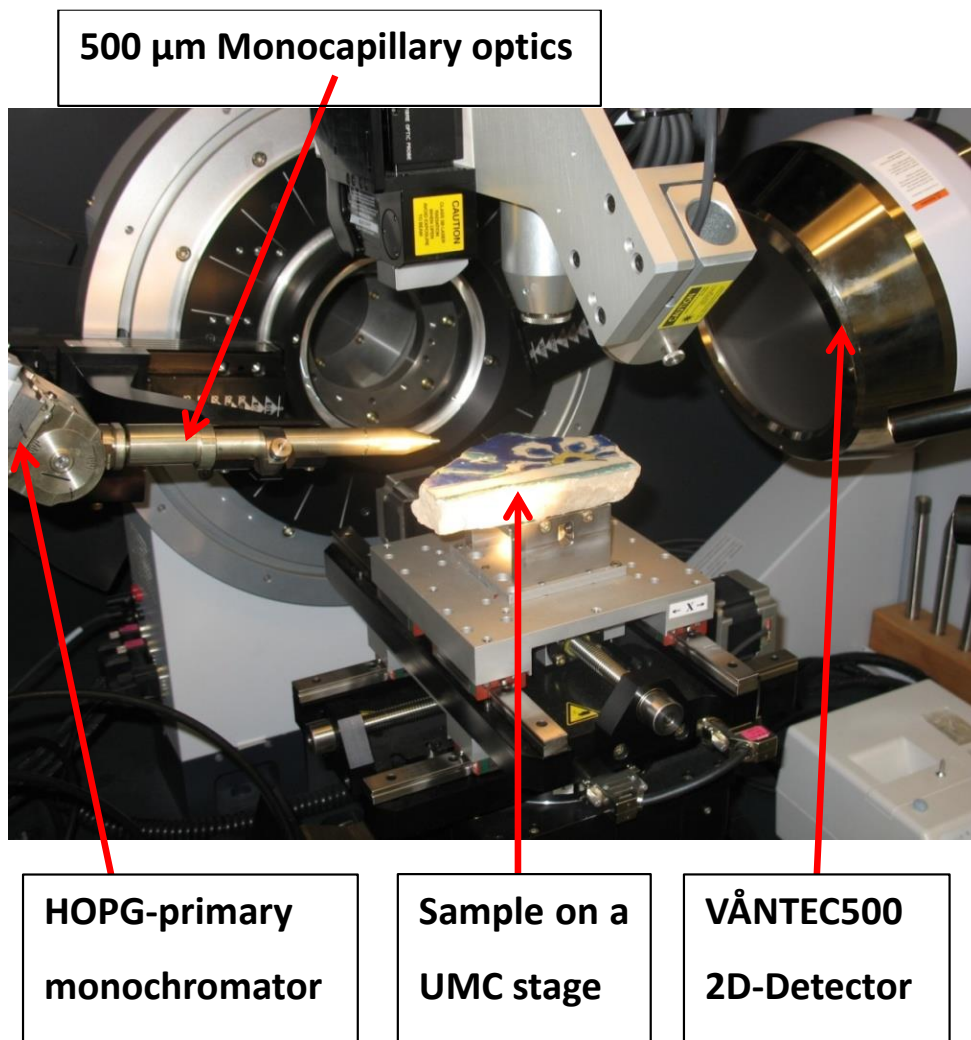

500 µm Monocapillary optics

HOPG-primary monochromator

Sample on a UMC stage

VÅNTEC500 2D-Detector

Figure 15: The BRUKER D8 XRD[2], equipped with: HOPG-primary monochromator, 500 µm monocapillary optics, a stage of the company universal motion components (UMC) and a VÅNTEC500 2D-Detector.

Instead of Bragg-Brentano geometry, all reflections are captured simultaneously in a 2D detector. The method is suitable for surface near measurements. In the detector patterns, a random distribution of crystals can be distinguished from larger single crystals in the material. The applied µ-XRD[2] device is a Bruker D8 with a monochromatic X-ray beam of Co-Kα (30 kV, 10

mA) which is focussed in a 500 µm monocapillary optic with a 300 µm pinhole (fig.15, Berthold *et al.*, 2009). The monochromator uses highly ordered pyrolytic graphite (HOPG) for the wavelength selection. The X-ray beam intensity is sufficient to detect small numbers of crystallites in the material, although the statistics is not sufficient to ensure the typical ratios of reflexion intensities. The device comprises a large 2D-detector with 140 mm diameter window, covering an angle 40° 2θ and 40° ψ, which is perpendicular to θ in the spherical geometry. The measuring times for the 50 µm spot size here used are between 120 and 240 sec per diffractogram. With X-ray micro-lenses and higher spot sizes, the measurement time is even reduced (Berthold *et al.*, 2009).

4.5 Micro-Raman spectroscopy

The Micro-Raman spectroscopy is used to characterize the chemical bondings within a given sample. The Raman technique is suitable for organic and inorganic solid samples such as minerals, ceramics, or proteins. Liquids like e.g. aqueous solutions can also be investigated. A very small spot of <1 µm diameter can be analysed and special focussing add-ons can increase the resolution of the measurement down to 250 nm (Bowley *et al.*, 1989; Anslyn & Dougherty, 2006; Atkins & Friedman, 2011). In this study, Micro-Raman spectroscopy is used to detect the alterations in ORMOCER® coatings of a former restoration approach (chapter 10.1). The relative changes in the intensity of the organic bondings of the ORMOCER® reveal the effect of deterioration of the material (fig.16). The samples are few mm^2 sheets of pigmented ORMOCER® material, which can be measured in the micro Raman spectrometer without sample preparation. In this study, the micro-Raman device LabRam of the company Horiba is used. It is equipped with a charge coupled device (CCD) detector and allows a spatial resolution of 2-4 cm^{-1}, suitable for common laser excitations between 400 and 800 nm. The signal of scattered light is detected in a CCD detector or photo-multiplier. The investigations are carried out at the Fraunhofer Institute for Silicate Research ISC in Würzburg, Germany. The method of Raman spectroscopy is based on the inelastic scattering process of photons with phonons, which represent the lattice vibrations within a substance. The photons of a monochromatic laser beam excite the bonding electrons of a chemical compound to a higher vibrational mode. In this process, the photon is reduced by the energy of excitation and shows an energy shift, which is characteristic for the chemical bond it interacted with. The energy-loss of photons is called stokes scattering.
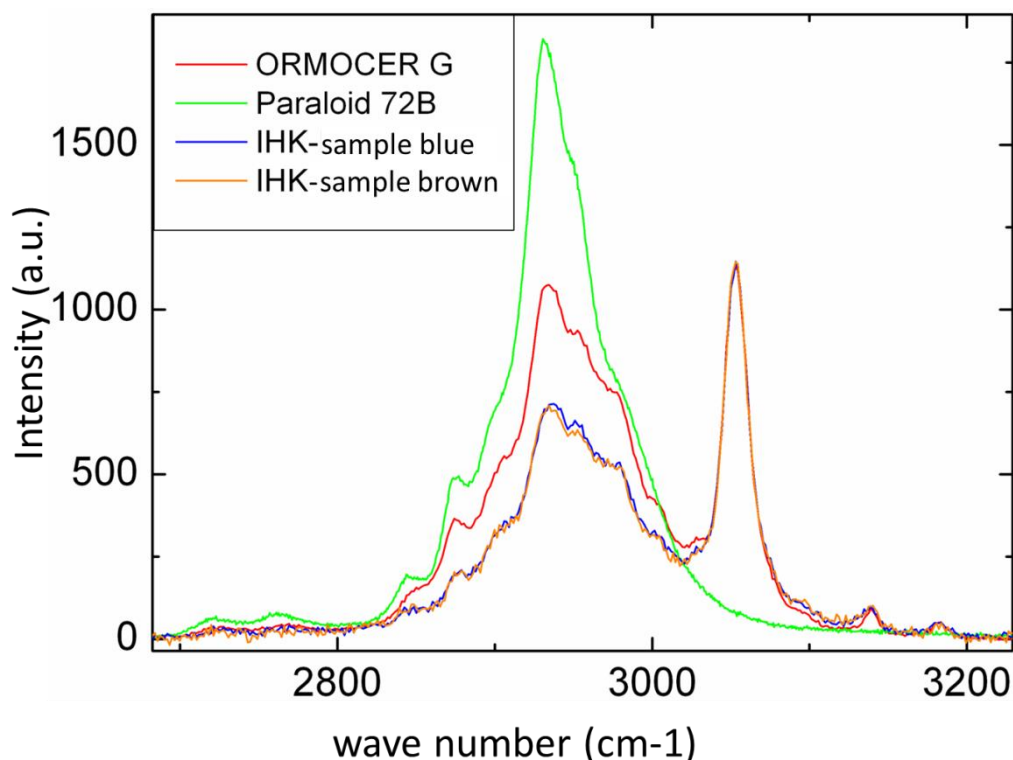
Figure 16: Typical spectra of a Micro-Raman measurement of new ORMOCER® G material, of the main components of the ORMOCER® Paraloid 72B, and of aged ORMOCER® coatings (IHK sample blue and brown).

The opposite case, when the energy of an excited state of the bonding is transferred to the incident photon, the process is called anti-stokes scattering (Raman, 1928; Masters, 2009). For Raman spectroscopy, the bondings have to reveal polarizability of their charge distribution in the electron cloud of the atom or molecule. The method is therefore complementary to the infra-red spectroscopy. Here, only chemical bonds are detected whose vibrations go hand in hand with a change of the electrical dipole moments.

4.6 Ultraviolet and visible spectrometry

The ultraviolet and visible spectrometry characterizes the wavelength dependent absorption and transition of light and is used to investigate the light-fastness of the coloured restoration materials before and after weathering. The measurements are carried out at the Fraunhofer Institute for Silicate Research in Bronnbach, Germany.

The method of ultraviolet and visible (UV-Vis) spectrometry measures the transmission and reflexion properties of a material in the range of ultraviolet and visible electromagnetic waves. The UV-Vis spectrometry is used for the characterisation of absorption and transmission properties, but also for the quantitative determination of e.g. specific colouring ions or organic compounds.

From the initial source of light, a monochromator selects the particular wavelengths, which are than guided through the sample and through a reference material. The incident light excites electrons of the material from the ground state to a higher energy level. This transition absorbs particular wavelengths in the initial radiation and the transmitted light is reduced by these energies (Skoog *et al.*, 1980). Spectra of the UV-Vis measurements are shown in figure 17.

For the UV-Vis measurements, a Cary® 100 Bio of VARIAN® is used. The data in the range of 360-830 nm is collected with a 2 nm step width and 1 sec integration time. The signal is detected in a photo multiplier, a photodiode, or a CCD detector.
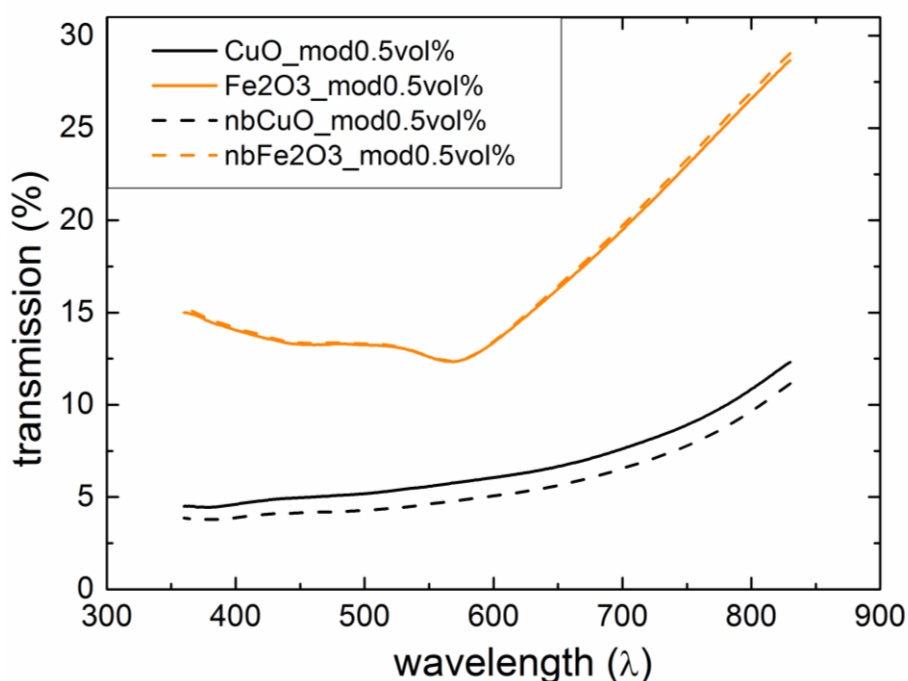

Figure 17: UV-Vis spectra of 0.5 vol% CuO and Fe_2O_3 particles in ORMOCER® G before and after weathering (nb).

5 Results of EPMA analysis

This chapter presents the compositions of the glassy matrix of the glazes. Additionally, the glaze microstructures and the ceramic-glaze interfaces are described by reference to backscattered electron pictures. Furthermore, the ceramic-glaze interface is investigated by EPMA line scan analyses. For statistics, the quantitative measurements on the glassy phase are done on at least 5 different spots in the homogeneous parts of the sample. The given results are the average values of the at least 5 single measurements. The error is given as standard deviation in the supplementary tables. The data is classified according to the elemental compositions and to different sample provenances and ages in the following. In the case of Uzbek samples, a further distinction into the different localities is given.

5.1 Observations in backscattered electron (BSE) images

The EPMA measurements analyse the glassy matrix of the glazes, but also the inclusions and precipitates, if these are sufficiently large. In addition to that, BSE pictures reveal the homogeneity of the glassy matrix, the distribution of inclusions, cracks and bubbles and the characteristics of the transition area between ceramic and glaze. Further, the BSE pictures give insight to the texture and porosity of the underlying ceramic.

A rough estimation of the average atomic weight of a particular phase is given by its brightness in the BSE image. Higher atomic numbers lead to more backscattered electrons and consequently to a brighter area in the picture. Lead- or tin- bearing compounds therefore appear brighter than alkali- and silica-dominated phases (fig.18 a). From the part of ceramic body, which is inherent to the glaze, the amount of quartz grains and clay or feldspar minerals can be roughly estimated. The observation of the shape of quartz grains in ceramic bodies gives hint to whether the source of the silica is crushed quartz pebbles (sharp grain shapes in the ceramic) or sand (rounded grains) (Gill *et al.,* 2014). The quartz grains of the bodies in this study normally show sharp edges, suggesting quartz pebbles as the likely silica source (fig.18 b).
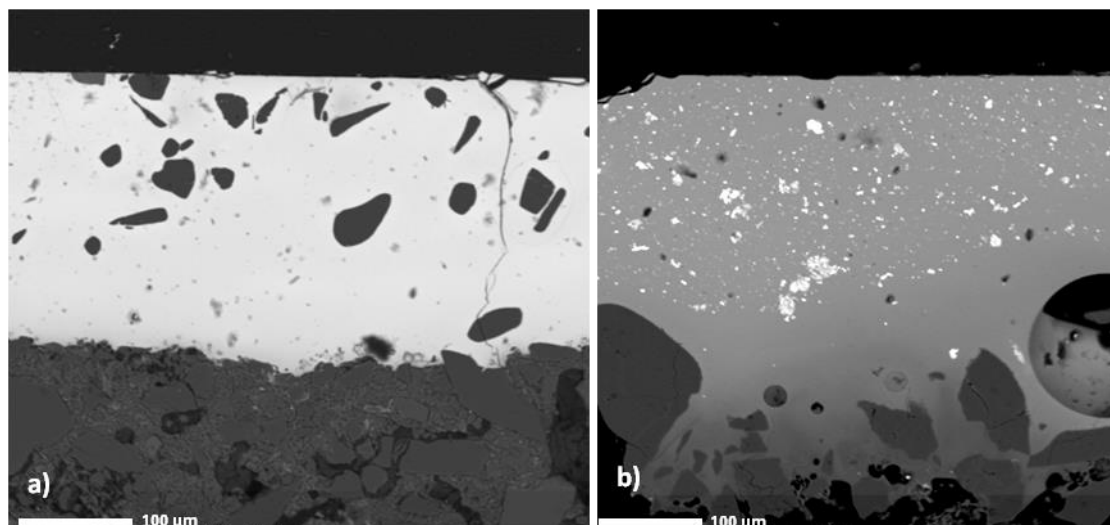
Figure 18 a) and b): Backscattered electron images of two examples of ochre (left) and turquoise (right) glazes of the mosque Khoja Zainuddin, Uzbekistan in BSE pictures. The brighter glaze phase in picture a) results from an enhanced PbO content, the darker glaze in picture b) results from an alkali rich composition with lower atomic numbers. Crystalline phases in the glaze of the left picture are occasional and rounded quartz grains. The ceramic quartz grains instead show sharp edges. In the right one, white cassiterite precipitates in small grain sizes are used as opacifier. The transition between ceramic body (on the bottom) and glaze layer is sharp in the left picture and diffuse in the right one.

5.2 Ceramic-glaze interfaces

In the present sample stock, the ceramic bodies are either quartz-rich stone paste (quartz frit) or clay-based ceramics, from which the latter ones are only 40 of the overall 233 samples. On both ceramic types different groups of glaze compositions are found. However, only three alkali glazes (two from Herat, Afghanistan, one from Samarkand, Uzbekistan) and only two of the alkali lead glazes (Takht-i-Suleiman, Iran) are on clay bodies, i.e. 35 of the 40 clay ceramic samples are covered by lead glaze.

The interfaces between ceramic and glaze show large variation in dimension, from several μm up to 500 μm, which is influenced by the particular compositions of ceramic and glaze and by the heating steps of the tile or sherd. Rehren & Yin (2012) can show on an example of lime-rich glazes that the interaction layer formation strongly depends on the duration of dwell time below the liquidus temperature of the glaze. The production in two firing steps is reported to result in a reduced diffusion of elements from the ceramic body into the glaze layer during the glaze

maturing and therefore leads to a narrower ceramic-glaze interface (Molera *et al.*, 2001; Coentro *et al.*, 2014). A well-defined interface like in figure 18 a, indicates a production obviously done in at least two steps of firing, from which the first (biscuit) one cures the ceramic body and the second one melts the applied glaze layer. The biscuit firing of the body drives out any gaseous parts from calcareous or H_2O-bearing components in the ceramic; this reduces the bubble formation in the glaze and therefore increases the transparent appearing (Domenech-Carbó *et al.,* 2008). The second step is assumed to be at lower temperatures than the first one, in order to avoid further reaction of the underlying ceramic. The matching of expansion coefficients of ceramic and glaze, which reduces misfits and cracks in the glaze, is improved through the biscuit firing (Matthes, 1990; Henshaw *et al.,* 2007). Cracks and bubbles are rarely observed in the investigated glazes, especially in those with clay ceramic body. Particularly, alkali glazes are more affected by cracking compared to lead glazes; this is ascribed to the lower expansion coefficient in lead-silica than in alkali glaze, which matches better the low thermal expansion coefficient of the fired ceramic body (Ghoneim & El Badry, 1983; Henshaw *et al.,* 2007). The clay or siliceous layer of a slip between ceramic and glaze would compensate a potential misfit, but is not observed in the investigated samples. A disadvantage of a biscuit firing is the higher effort of double firing as well as the weaker contact between glaze and ceramic, which decreases the stability of the ceramic-glaze connection.

A wider and diffuse transition area between ceramic and glaze suggests a single heating step, when the glaze layer is applied to the unbaked ceramic body. However, the appearance of a broad interface is not an unambiguous evidence for a single heating step but can also reveal an insufficient first one of a two-step procedure. A tendency towards broader interfaces is visible in the alkali glazes as opposed to lead compositions. Lead glazes, which have commonly lower curing temperatures, result in less digestion of the ceramic parts and therefore a smaller interface of only several µm.

Another important question concerning the ceramic-glaze interface is a possible influence of the ceramic body to the glaze composition caused by element diffusion into the glassy layer. Ceramic grains of quartz, feldspar, or clay may be dissolved in the glaze during the maturing, and particularly Si, Na, K, Ca, Mg, Al, and Fe may diffuse into the melt. In the case of element diffusion, an enrichment of the diffusing element(s) is expected in the vicinity of the interface. Therefore, EPMA line-scans including the critical elements have been carried out across the interfaces and the complete glaze layers on all ceramic-glaze interface types. The

inhomogeneities within the glaze layers are due to compositional differences in ceramic and glaze, to the firing conditions, and on the stability of the glaze composition.

In the line scans of alkali glaze on stone paste bodies, a diffusion of Si is observed from the body into the glaze composition. Al and K contents are either enhanced near to the ceramic body or they don´t show any gradient, which also suggests diffusion from the ceramic body, compensating the relative dilution by the migrated Si. The dilution by Si input is observed in the line scans of Na, Mg, and Ca. The counting rates of Fe are low in total, but a small dilution can be observed. Exemplarily, the alkali glaze Sam14 is shown in figure 19 b, where diffusion of Si, K, Ca, and Al can be seen in the 50-80 µm next to the ceramic body. In contrast, Na, Mg, and Fe seem not to have additional input from the ceramic body and are therefore decreased in their counting rate. In the quantitative EPMA analyses of the alkali glaze on stone paste body KhZ 162, the SiO_2 values increase from 71.8 wt% in the upper glaze area to 77.1 wt% close to the interface. Simultaneously, Mg, Na and Ca contents decrease relatively to the total composition near to the ceramic (MgO 3.5-2.9 wt%, Na_2O 5.3-3.6 wt%, CaO 6.2-5.0 wt%).

The alkali glazes on clay-based bodies, a similar picture of Si, Al, and K diffusion into the glaze is observed. The Na and Ca concentrations are relatively reduced. The dilution of Fe cannot be observed on the clay-based body, which suggest Fe-input from the ceramic. The line scan of the alkali glaze on clay body (Sam 17) shows the migration from the ceramic into the glaze (fig. 19 b). The Si in the glaze is enriched in the vicinity of the ceramic; Na and Ca are relatively diluted. The lack of gradient in K, Al, and Fe scans suggest migration of these elements into the glaze. In the work of Molera *et al.* (2001), the diffusion of alkali, alkali earth, and silica into the glaze is found to be reduced at higher Al contents in the glaze, which increase the stability of the glaze composition. This tendency is not observed in our samples, showing the same diffusion in glazes with high Al_2O_3 (7.8-8.0 wt%) as in Al_2O_3-poor ones (0.9-2.9 wt%).

In the lead glazes on stone paste bodies as well as on clay-based bodies, little or no diffusion gradient of Si is observed. In the glazes on stone paste body, the low contents of Na, Ka, Ca, Al and Fe are very sensible to input from the ceramic body. In some cases (Turkish tile Kon 35c), dilution of K and Ca is observed near to the ceramic, corresponding to the little Si input. In other glazes, increased counting rates of Al and Fe are observed close to the ceramic-glaze interface, as it is seen in the lead glaze on the stone paste body Mau 47 (fig. 19 c).

The diffusion from clay-based ceramics into the lead glazes is driven by the large concentration difference of the minor elements and depends largely on the clay composition. Diffusion profiles
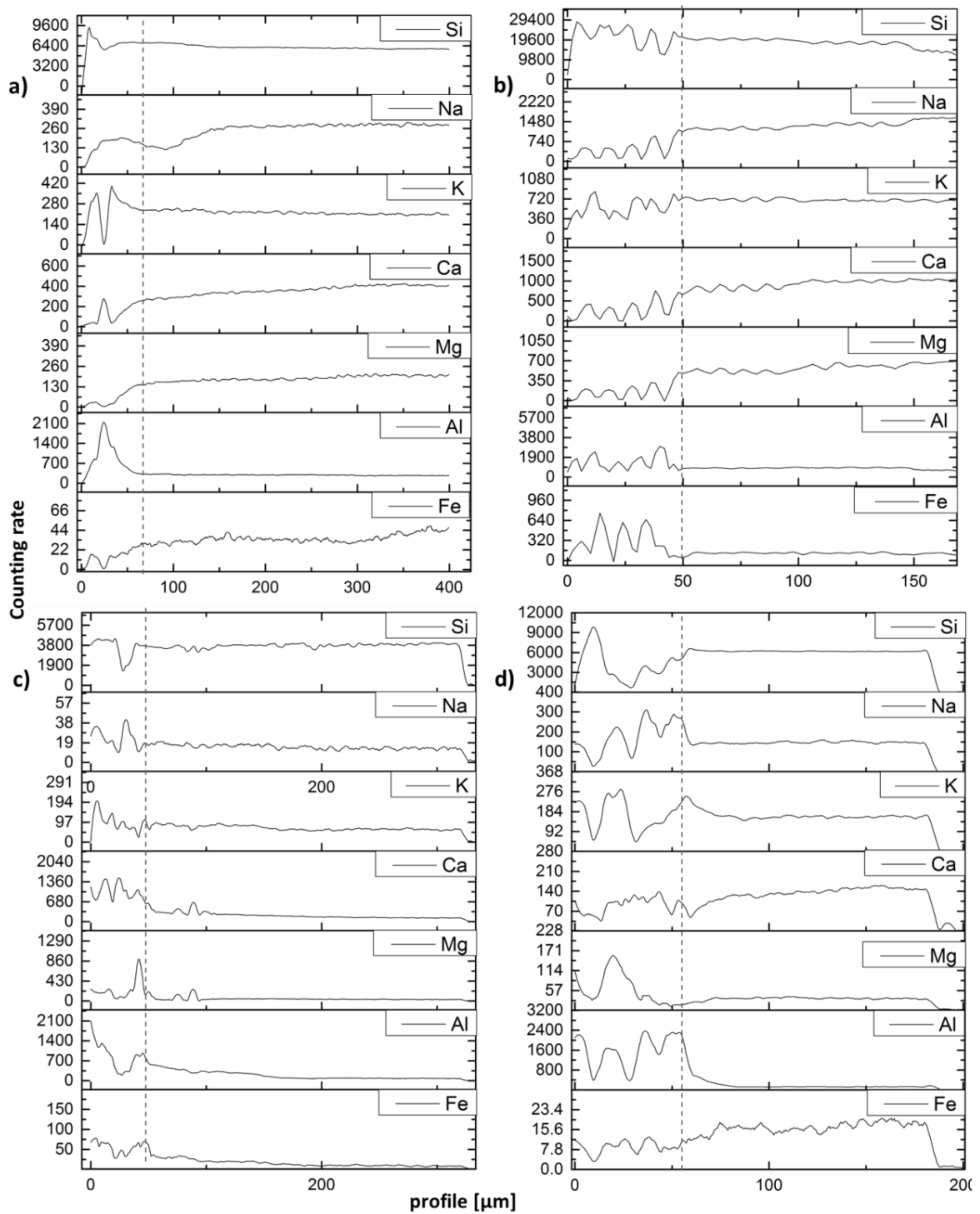
64

Figure 19 a-d: Profiles of selected elements across the ceramic-glaze interface and the glaze composition. The dotted lines mark the approximate starting point of glassy phase. a) alkali glaze on quartz frit (Uzbek tile Sam 14), b) alkali glaze on clay ceramic (Uzbek tile Sam 17), c) lead glaze on quartz frit (Moroccan tile Mau 47) and d) lead glaze on clay ceramic (Bulgarian sherd BG 2).

are primarily seen in Al and K counting rates, which suggest an illitic part of the clay body. Ca, Mg, and Fe are relatively decreased respectively. The lead glaze on clay-based body BG 2 which is shown in figure 19 d, also has increased values of K and Al close to the ceramic body, whereas Si, Ca, Mg, and Fe seem to be diluted. The Na-profile does not show any gradient, which suggest element migration compensating the input of K and Al.

Because of the minimal invasive sampling, the parts of ceramic body which adhere to the glazes mostly consist of only a few grains which are often blended with parts of the glaze material. A statistical evaluation of the ceramic material could therefore not be carried out here. Exemplarily, a few samples of ceramic with sufficient ceramic material were analysed with a widened beam diameter of 20 µm in order to get mean values of the inhomogeneous composition. A line array of 20-30 measurements is carried out with a spot distance of 10 µm, of which the mean value is calculated. The analysed elements are Si, Al, Na, K, Ca, Mg, and Fe. The stone paste ceramic bodies primarily consist of quartz grains, and are therefore not further investigated. Normalised mean values of selected clay-based bodies are given in table 9. Due to the highly porous structure of the ceramic, the analyses have low totals of 60-70 wt% and are normalised to 100%.

Table 9: Selected mean values of analysed ceramic compositions from Afrasiab and Samarkand (Uzbekistan), Takht-i-Suleiman (Iran), Herat (Afghanistan), and the second Bulgarian Empire and one monochrome and polychrome sherd each from the Ottoman period in Bulgaria

	Afr., Uzb	Sam., Uzb.	TiS., Iran	Herat, Afg.	2. BG. Emp.	Ottom. BG monochr.	Ottom. BG, polychr.
Oxide	Afr 36	Sam 16	Tis 13	Her 50	Zar 8	BG7	BG 2
SiO$_2$	68.0	70.4	40.3	37.0	79.1	74.5	58.7
Fe$_2$O$_3$	2.9	0.1	4.25	3.4	4.5	5.3	0.7
Al$_2$O$_3$	22.0	21.4	27.6	9.7	11.0	13.0	21.1
CaO	0.3	0.1	0.3	17.5	1.3	2.1	11.6
MgO	0.5	<0.05	19.6	3.5	1.6	1.4	1.2
Na$_2$O	1.1	4.9	4.8	0.3	0.5	0.8	3.1
K$_2$O	5.2	3.0	3.3	1.3	2.1	3.0	3.6

5.3 Main composition

The elemental composition of the glaze matrix is quantitatively analysed by EPMA. The individual elements can be divided into different groups, performing different functions in the

glaze; beside the network formers SiO_2, and Al_2O_3, the major elements and network modifiers Na, K, Ca, Mg, and Pb are measured together with P, S, Cl, Ba and the transition metals Cr, Mn, Fe, Cu, Co and Zn. The main fluxes, i.e. melting temperature decreasing agents, are Na, K, and Pb. The Pb amount is acts as flux, but also has a colouring function e.g. in the copper-coloured green glazes and the yellow glazes above 50 wt% PbO (Wedepohl *et al.*, 1995; Nassau 2001). The ions of Cr, Mn, Fe, Cu, Co and the opacifying SnO_2 usually occur only in small quantities in the glass network (0.5-5 wt%) and do not influence the melting temperature significantly. Especially the minor elements P, S and Cl cannot be treated as representative for the original composition due to their possible escape during the melting process (Heide *et al.*, 2000).

Three different major groups of glazes can be distinguished on the basis of the alkali and lead contents. These are alkali glazes, alkali lead glazes, and lead glazes. Hereby, the total alkali and lead contents behave roughly anti-proportional as can be seen in figure 20. The average of alkali oxides of the alkali group exceeds that of the alkali lead and lead group, compensating the missing lead flux. With only a few exceptions, this classification is valid in almost all parts and periods of the Islamic sphere investigated in this study. In a few cases, the lead content is more continuously distributed among the investigated samples (e.g. glazes from Turkey), or one lead-rich group predominates (e.g. glazes from Afrasiab and Morocco). The lowest lead contents are between 0 and 3 wt% PbO and define the alkali glazes, varying within these boundaries in 57 glazes from different locations (tabs.10 a and b). The upper limit is set to 3 wt% PbO in order to include the Iranian glazes with 3.0 wt% PbO, which seem to scatter around to the Iranian glazes with 0.4-2.0 wt% PbO. The next higher amount of PbO in Iranian glazes is at 9.7 wt% and therefore clearly isolated. The group of Uzbek alkali glazes also show a narrow scattering of 0.0-1.5 wt% PbO, well demarcated from the next higher PbO values in Uzbek glazes (4.8-9.6 wt%). The alkali lead group with PbO values between 5 and 30 wt% is represented by 51 glazes. The lower limit of the alkali lead group is set to 5 wt% because of the little scattering Uzbek subgroup of lead contents between 4.8 and 9.6 wt%. The glaze with 4.8 wt% PbO belongs to a group of 4 glazes from one polychrome sherd of the madrassa Abdul Aziz Khan with 4.8-5.2 wt% PbO and is therefore counted to the alkali lead group. The upper limit of the alkali lead group is not easy to be set. The continuous scatter of Iranian glazes with medium lead content reaches up to 27 wt% PbO. One Turkish glaze lies with 27.5 wt% close enough to be assigned to this group. The lead glaze group is dominated by the Moroccan glazes, which start at compositions of 29.7 wt% PbO. The gap of more than 2 wt% is than used to set the upper limit of alkali lead glazes and the

boundary between the alkali lead and the lead group is set to 30 wt%. Beside the more or less continuous distribution of Moroccan glaze compositions, the high lead group of Uzbek and Afghan glazes start with 31.2, respectively 31.8 wt% PbO after a gap of more than 15 wt%. The Iranian and Bulgarian lead glazes have higher lead contents, which start at 55.7, respectively 48.1 wt% PbO.

In the alkali and the alkali lead group, most glazes are turquoise, blue, and white coloured. The lead component in the glazes can be assumed to be fairly pure due to a pre-treatment and purification (Tite *et al.*, 1998). This allows subtracting the amount of lead oxide from the alkali and alkali lead compositions and normalizing to 100 wt% in order to compare the remaining alkali and alkali earth values. The lower alkali and alkali earth values of the alkali lead glazes increase by re-casting relatively to those of the alkali glazes. The similarity of the re-cast values would suggest a dilution of the pure alkali composition with lead oxide in order to obtain the alkali lead compositions. A comparison of the alkali and alkali lead glazes of the particular locations will be given in the following sub-chapters.

The largest group of 136 samples is the lead group with lead oxide values above 30 wt% PbO. Glazes with high lead contents are found in all sets of samples, even if represented only by a few samples like in the Iranian and Samarkand sample set (chapter 5.6.3). The lead glazes are predominately green and brown coloured, the few yellow samples also belong to this group.

In the alkali-rich samples, the Na_2O/K_2O ratio is above 1 in almost all cases, which agrees with the general observation that Islamic alkali glazes are richer in soda than in potash (Brill, 1999; Shortland & Eremin, 2006; Rehren, 2008). The samples from Bukhara, Takht-i-Suleiman, and the Turkish localities 15 samples have Na_2O values of up to 10-15 wt%, which are the highest Na_2O values observed in this study. However, they are still moderate in comparison to other analyses of e.g. Indian glazes which have consistently values between 10 and 19 wt% (Rehren, 2008; Gill & Rehren, 2011). The potash values underlie large variations, especially in the case of plant ash source as alkali flux. In the compositions with mineral natron, the potash contents are usually below 1.5 wt% (chapter 2.1.4). An overview of the classification into alkali, alkali lead, lead glazes, and sample locations is given in chapter 8.3. The alkali glazes can be further subdivided into mineral natron and plant ash flux, according to their K_2O and MgO content (chapter 5.8 and 8.2).
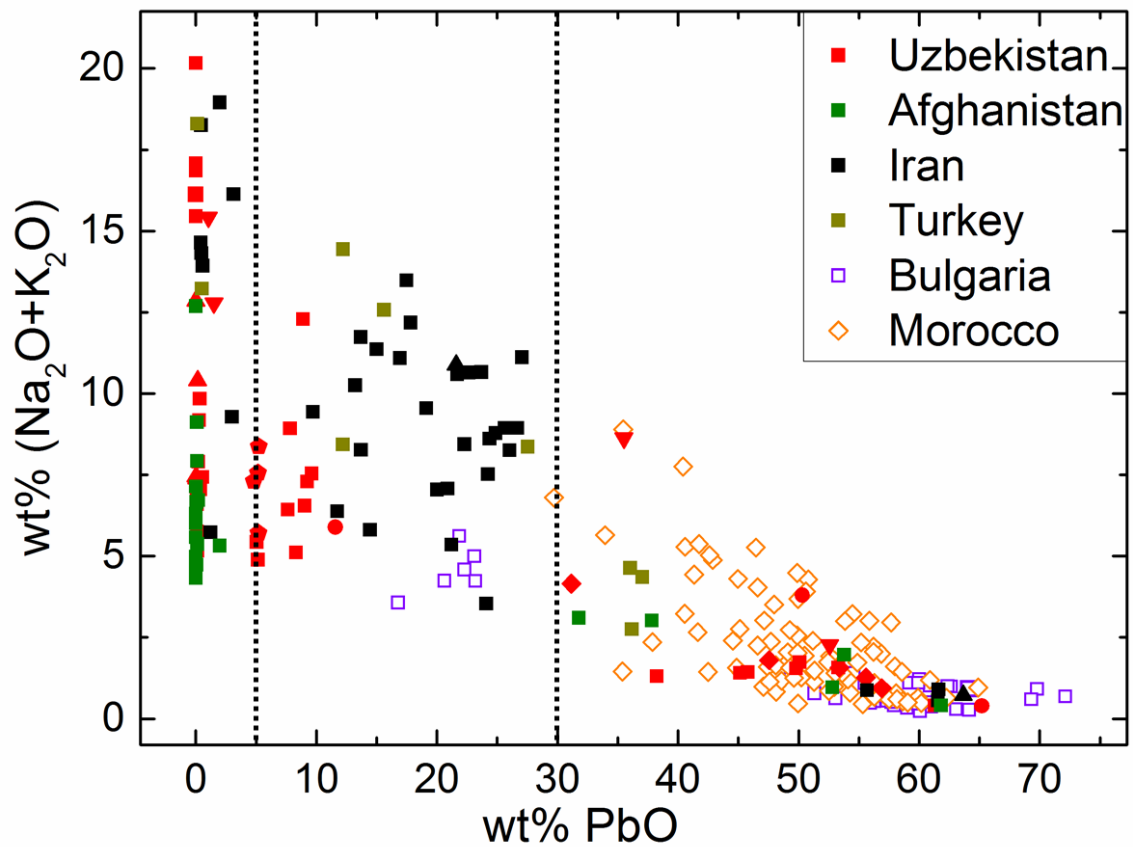
Figure 20: Subdivision of the glazes into an alkali group with lead contents below 3 wt% PbO, an alkali lead group with medium lead contents (5-30 wt% PbO) and a lead group with more than 30 wt% PbO. The Uzbek samples are subdivided into squares (mosque Khoja Zainuddin), circles (Ishrat Khane), triangles top up (madrassa Mir-i Arab), triangles top down (Samarkand), pentagons (madrassa Abdul Aziz Khan), and diamonds (Afrasiab). The Iranian data points are subdivided into squares (Takht-i-Suleiman) and triangles (restoration glazes from Isfahan).

Tables 10 a) and b): Overview over the lead contents in glazes of different sites and epochs, given in wt%. The alkali samples range within 0-3 wt%, the alkali lead glazes within 5-30 wt% and the lead glazes from 30 to 72 wt% PbO. The abbreviations are Unk for unknown, Afr for Afrasiab, IK for Ishrat Khane, KhZ for Khoja Zainuddin, MMA for madrassa Mir-i Arab, BM for Baland mosque, MAK for madrassa Abdul Aziz Khan, TiS for Takht-i-Suleiman and MAH for madrassa Abu al Hassan.

	Uzbekistan								Afgh.	Iran		Turkey	
City	Samarkand		Bukhara						Herat	TiS	Isfahan	Kon-ya	Kay-seri
Building	Afr	Unk	IK	KhZ	MMA		BM	MAK	Unk	TiS	Prayer Niche	Ata Hanka	Unk
Century	10-11th	13th	15th	16th	16th	20th	16th	17th	15-17th	12-13th	20th	13th	13th
Alkali		1-2		0-1	0-1				0-2	0-3		0-1	
Alkali lead			11	5-11		22-26		5		10-27	22	12-28	16
Lead	31-57	36-53	48-62	38-61	56	31-36	56		32-62	56-62	64	36-37	

	Bulgaria		Morocco								
City	Dristra		Salé		Rabat	Fes	Marra-kesh	Tangier		Meknes	
Building	Fortress		MAH	Meri-nide School	Necro-polis	Bou Inania	Saadian Tombs	Sultans Palace	Foun-tain	Bou Inania	Mauso-leum
Century	11-13th	13-17th	14th	14th	14th	14th	16th	17th	17th	14th	18th
Alkali											
Alkali lead		17-23									
Lead	55-70	48-72	36-54	30-51	34-57	49-59	42-65	49-56	45-54	38-60	35-60

5.4 Uzbek glazes

5.4.1 Alkali glazes

The alkali group in the Uzbek samples contains 0-0.6 wt% PbO and comprises most of the blue, black, and violet samples and a few white and turquoise ones. Aside from the silica, the alkali (earth) oxides are the most important ingredients in alkali glazes.
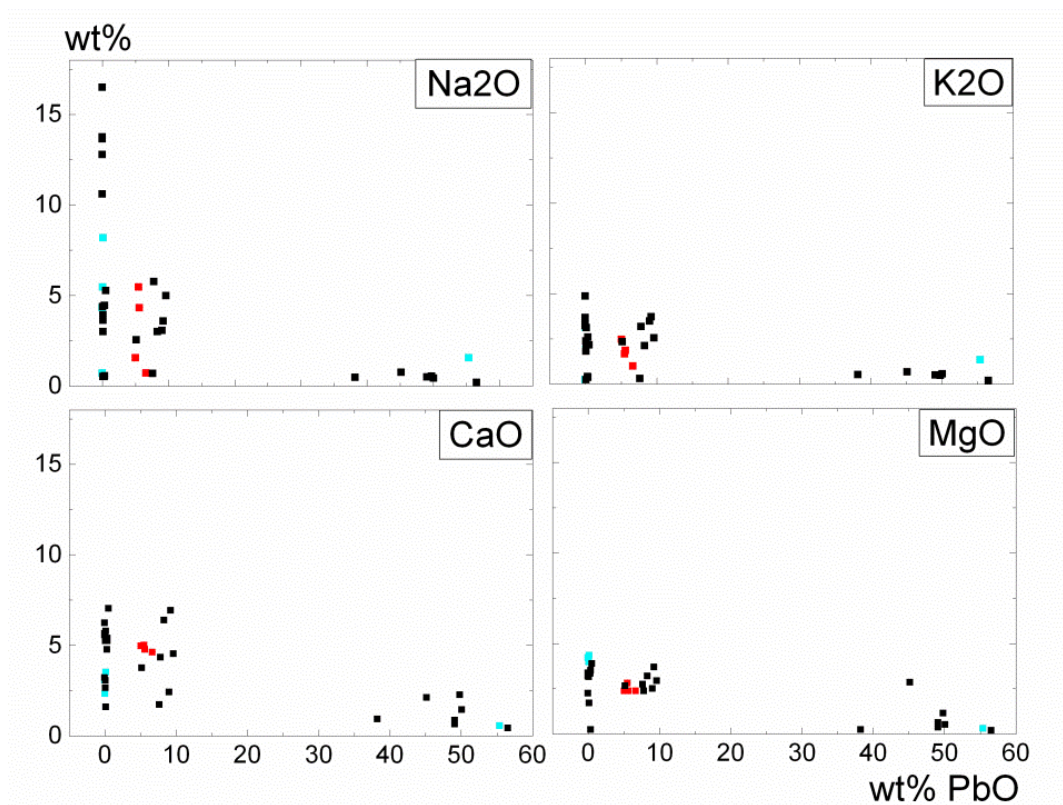

Figure 21: Classification of Uzbek glazes on the basis of lead content (black: mosque Khoja Zainuddin, red: madrassa Abdul Aziz Khan, turquoise: madrassa Mir-i Arab). Three different groups appear with (i) alkali (0-0.6 wt% PbO), (ii) alkali lead (4.8-10.6 wt% PbO) and (iii) lead glazes with more than 38 wt% PbO here.
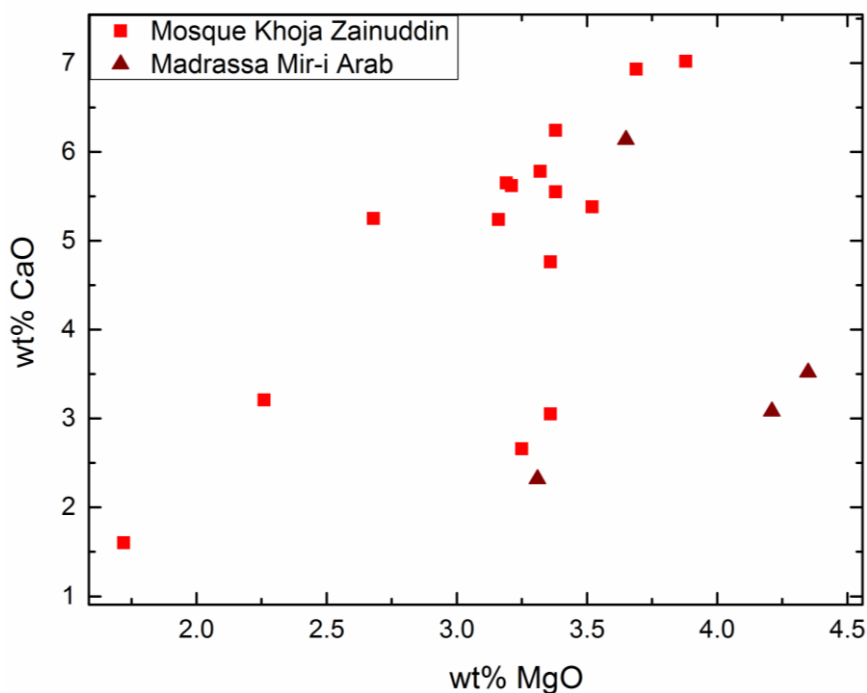
Figure 22: CaO/MgO ratios in the alkali glazes from Uzbekistan. In most of the samples of the Mosque Khoja Zainuddin, the CaO/MgO ratio higher than in the glazes from the madrassa Mir-i Arab.

The ratio of Na_2O to K_2O varies between 1.2 and 4.5. The alkali group is subdivided into a Na_2O-rich one, containing more than 10 wt% Na_2O, and a Na_2O-poor one with Na_2O values below 5 wt% (fig.21). The CaO and MgO values of the alkali glazes from the mosque Khoja Zainuddin show a correlation with CaO/MgO ratios of 1.0-2.0. Two of the glazes, KhZ 160 and KhZ 161 have lower CaO/MgO ratios <1, which is close to the ratios in glazes from the Madrassa Mir-i Arab (fig. 22). The two buildings are built in the 16th century in Bukhara, which makes common raw materials and techniques presumable.

5.4.2 Alkali lead glazes

The alkali lead group with 4.8-10.6 wt% PbO in the Uzbek samples is represented by most of the white and turquoise glazes. Whereas the alkali group shows a large variation in sodium oxide content, the respective values of the alkali lead group are less scattered (fig.23). The sum of alkali and alkali earth oxides is between 11 and 21 wt%, the sum of alkali oxides is between 5 and 12 wt%. The Na_2O/K_2O ratio is at 1.7 with a standard deviation of 0.75. In the comparison

of re-cast data from the alkali and alkali lead glazes, the difference of K_2O and CaO is not significant, whereas the Na_2O values are with 5.9 wt% in average lower than the alkali glazes with 8.3 wt% average value. The MgO contents of the alkali glazes split in two groups, whereas the re-cast values of alkali lead glazes plot only in the high MgO group. The simple addition of lead to the alkali glaze recipe cannot be ruled out for some glazes, but is definitely not the case for the entirety of Uzbek alkali lead glazes.
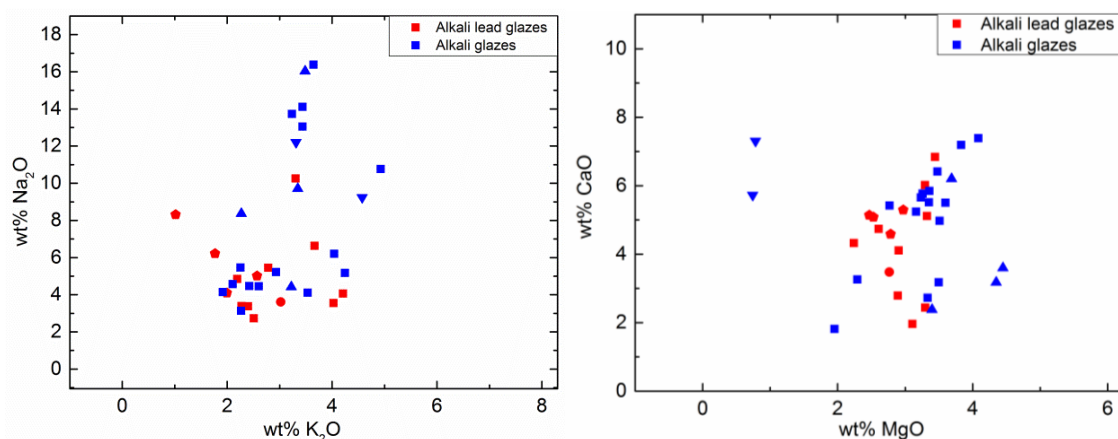
Figure 23 a and b: Alkali and alkali earth oxides from alkali and alkali lead glazes from Uzbekistan. The data points are subdivided into squares (mosque Khoja Zainuddin), circles (Ishrat Khane), triangles top up (madrassa Mir-i Arab), triangles top down (Samarkand), and pentagons (madrassa Abdul Aziz Khan).

5.4.3 Lead glazes

The third of the major glaze groups is the lead group with 31-61 wt% PbO, including green, ochre and yellow glazes. The silica content is, as expected, inversely proportional to the lead content. In the lead group, alkali oxides form only minor components with less than 3 wt% in total. These low values make it difficult to classify and determine correlations, but a first-order correlation between MgO and CaO is detectable. The Na_2O/K_2O ratio of the 13th century and younger tiles is about 1.0 ± 0.4; that of the older tiles from the 10th and 11th centuries is 0.6 ± 0.2 and thereby the lowest in the group of Uzbek tiles.

5.4.4   Subgroups of Uzbek localities

Afrasiab: The samples from the 10th-11th century (Afrasiab) show a lead composition (31.2-56.9 wt%), which is also observed in some of the Uzbek samples of the newer epochs. In these glazes SiO_2-values are commonly below 40 wt% in contrast to 44 and 51 wt% in younger samples. Alkali values are with a total alkali and alkali earth content of <10 wt% very low (fig.24).
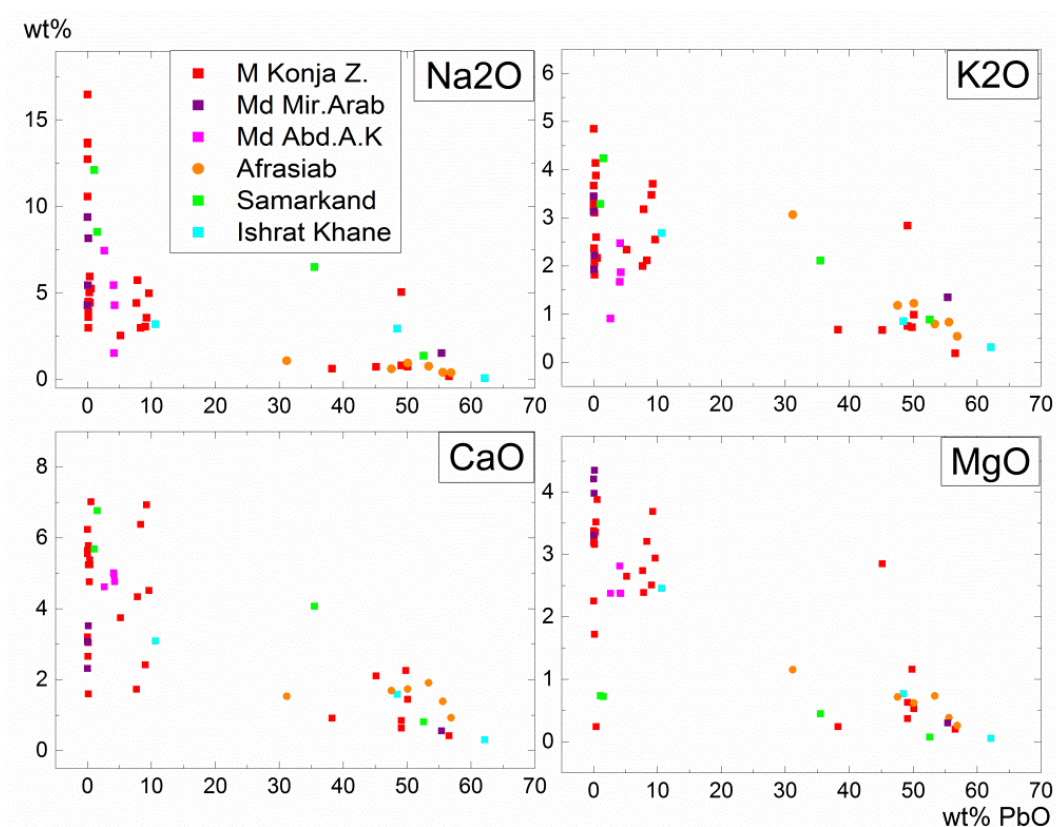

Figure 24: Depiction of the alkali and alkali earth content of glazes from all Uzbek localities.

Samarkand: The samples from Samarkand of the early Mongol period (13th century) show both lead-rich as well as pure alkali compositions. This shows the continuity of alkali glaze production despite the upcoming lead glaze technology. The tiles have a dark blue and a turquoise lead-rich glaze, and a blue and orange coloured almost lead free glaze with 1-1.5 wt% PbO (fig.25). The two samples from the mausoleum Ishrat Khane in Samarkand belong with 48.5 and 62.1 wt% PbO to the lead group and have green and blue colours. The third, turquoise glaze of the mausoleum Ishrat Khane has a medium lead content (10.6 wt% PbO) and an enhanced content of Na_2O (2.9 wt%) in comparison to the lead glazes. The glazes from Samarkand, including alkali,

alkali lead, and lead glazes, show a correlation of K_2O and CaO contents (fig.25). The six samples from Afrasiab, which is located close to Samarkand fit also into the correlation.
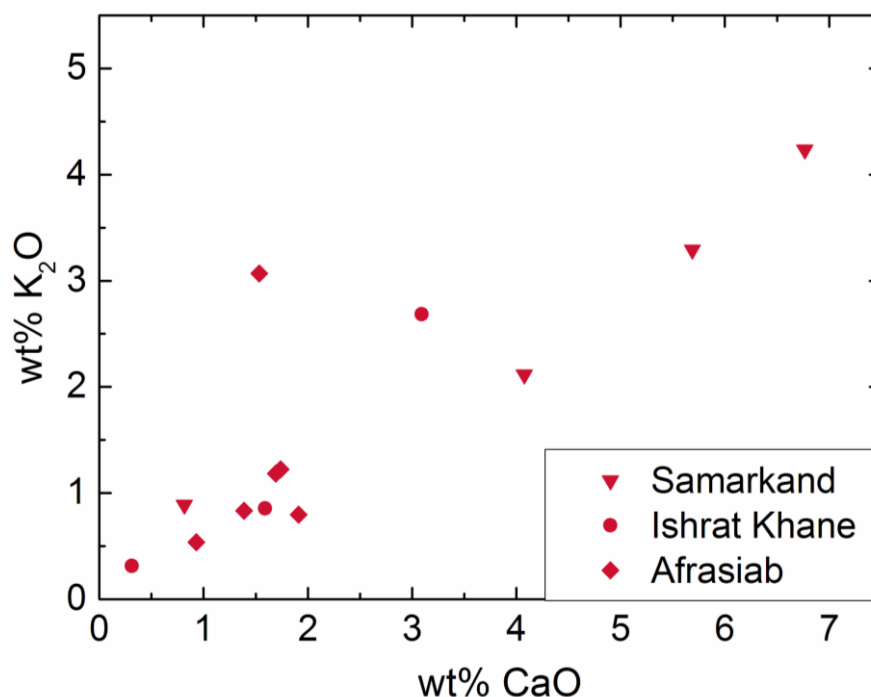

Figure 25: Correlation of CaO and K_2O in the samples of a building from Samarkand. The Ishrat Khane and Afrasiab samples do not show a clear correlation on its own but fit fairly well with that of the Samarkand samples.

Bukhara: The turquoise, one white and two green samples of the mosque Khoja Zainuddin from the early 16th century are with 4.8-10.6 wt% PbO in the group of the alkali lead glazes. The green, ochre, and yellow coloured samples belong with 38.2-61.3 wt% PbO to the lead group. In the alkali and alkali lead groups, Na_2O is again the dominant element with a Na_2O/K_2O-ratio between 1.3 and 3.5. Enhanced contents of K_2O (up to 5 wt%) and MgO (between 2 and 4.5 wt%) are present in all alkali samples (fig.24).

Most of the samples of the younger dated madrassa Abdul Aziz Khan (1652) have medium lead contents. Only in the samples of the madrassa Mir-i Arab, the blue, black, turquoise, and white glazes belong with PbO contents of 0.0-0.6 wt% to the alkali group.

Table 11: Analyses of Uzbek glazes in wt%. The abbreviations are the following: Afr for tableware glazes from Afrasiab, SAM for tile glazes from a building in Samarkand, IK for tile glazes from the mausoleum Ishrat Khane in Samarkand, MMA for tile glazes from the madrassa Mir-i Arab in Bukhara, BM for a tile glaze from the mosque Baland in Bukhara, KhZ for tile glazes from the mosque Khoja Zainuddin in Bukhara, and MAK for tile glazes from the madrassa Abdul Aziz Khan in Bukhara. All values are averages from at least 5 single measurements.

Alkali glazes																						
sample	ceramic body	century	colour	SiO_2	Al_2O_3	PbO	MgO	CaO	Na_2O	K_2O	SnO_2	Cr_2O_3	MnO_2	Fe_2O_3	CoO	CuO	ZnO	P_2O_5	SO_3	TiO_2	Cl	Sum
KhZ246	quartz	early 16th	blue	74.5	4.2	0.1	3.5	5.4	4.4	2.4	<0.05	<0.05	<0.05	2.1	0.3	0.1	<0.05	0.6	0.2	<0.05	<0.05	95.96
KhZ162	quartz	early 16th	purple	74.7	3.5	0.1	3.3	5.8	4.5	2.1	<0.05	<0.05	2.3	1.7	<0.05	<0.05	<0.05	0.6	<0.05	<0.05	<0.05	99.4
KhZ244	quartz	early 16th	blue	71.2	4.2	0.1	3.9	7.0	3.9	1.8	0.6	<0.05	<0.05	1.9	0.4	0.1	<0.05	<0.05	0.2	<0.05	0.2	97.7
KhZ199	quartz	early 16th	blue	70.8	5.3	0.1	1.7	1.6	3.6	3.1	<0.05	<0.05	<0.05	1.4	0.2	<0.05	<0.05	<0.05	<0.05	0.2	0.2	100.6
KhZ250	quartz	early 16th	blue	74.6	4.1	0.1	3.4	4.8	3.0	2.2	<0.05	<0.05	<0.05	1.1	0.2	0.1	<0.05	2.0	0.2	0.2	0.1	100.32
KhZ133.1	quartz	early 16th	blue	74.3	4.0	0.2	2.7	5.3	5.1	2.8	8.0	<0.05	<0.05	1.7	0.5	0.2	<0.05	<0.05	<0.05	<0.05	0.4	99.4
KhZ161	quartz	early 16th	purple	74.5	4.3	0.3	3.3	2.7	5.0	4.1	3.1	<0.05	0.7	2.1	<0.05	0.1	<0.05	<0.05	<0.05	<0.05	0.5	95.42
KhZ160	quartz	early 16th	purple	73.5	3.6	0.3	3.4	3.1	6.0	3.9	1.6	<0.05	0.8	1.7	<0.05	0.1	<0.05	<0.05	<0.05	0.1	<0.05	97.4
KhZ171	quartz	early 16th	white	77.3	3.8	0.4	3.2	5.2	4.5	2.6	3.0	<0.05	<0.05	1.2	<0.05	<0.05	0.1	1.7	0.1	0.1	0.2	98.9
KhZ247	quartz	early 16th	blue	69.9	4.5	0.6	3.7	6.9	5.3	2.2	6.4	<0.05	<0.05	2.5	0.4	0.1	<0.05	<0.05	0.2	<0.05	0.2	101.22
MMA5	quartz	16th	turquoise	69.2	4.3	0.1	4.4	3.5	8.2	2.2	0.2	<0.05	<0.05	1.5	<0.05	3.8	<0.05	<0.05	<0.05	0.3	0.4	96.9
14SAM	quartz	13th	blue	71.0	3.4	1.1	0.7	5.7	12.1	3.3	<0.05	<0.05	0.1	2.7	0.4	<0.05	<0.05	<0.05	<0.05	0.1	<0.05	98.1
17SAM	clay	13th	orange	68.8	2.2	1.5	0.7	6.8	8.6	4.2	<0.05	<0.05	<0.05	1.2	<0.05	0.1	<0.05	<0.05	<0.05	0.1	<0.05	98.3

Results of EPMA analysis

Alkali lead glazes

sample	ceramic body	century	colour	SiO$_2$	Al$_2$O$_3$	PbO	MgO	CaO	Na$_2$O	K$_2$O	SnO$_2$	Cr$_2$O$_3$	MnO$_2$	Fe$_2$O$_3$	CoO	CuO	ZnO	P$_2$O$_5$	SO$_3$	TiO$_2$	Cl	Sum
MAKschw	quartz	17th	black	75.8	4.1	4.8	2.4	5.0	4.8	2.5	<0.05	<0.05	<0.05	0.8	<0.05	<0.05	<0.05	<0.05	<0.05	0.1	0.3	98.1
MAKbl	quartz	17th	blue	73.5	4.1	5.2	2.8	5.0	5.9	1.7	<0.05	<0.05	<0.05	0.7	<0.05	<0.05	0.1	<0.05	<0.05	0.2	0.6	97.44
MAKwei	quartz	17th	white	74.9	4.2	5.2	2.4	4.8	3.8	1.9	0.5	<0.05	<0.05	0.7	<0.05	<0.05	0.0	<0.05	<0.05	<0.05	0.5	99.0
MAKtü	quartz	17th	turquoise	67.5	2.9	5.2	2.5	4.1	7.5	0.9	<0.05	<0.05	<0.05	1.0	<0.05	1.6	<0.05	<0.05	<0.05	0.1	1.3	98.3
KhZ031	quartz	early 16th	green	72.5	3.0	5.1	3.2	5.8	3.3	2.2	<0.05	<0.05	<0.05	1.0	<0.05	2.1	<0.05	0.5	0.2	<0.05	0.3	96.5
KhZ198	quartz	early 16th	green	67.0	3.4	5.2	3.2	6.4	2.6	2.3	<0.05	<0.05	<0.05	1.2	<0.05	2.6	0.1	0.6	0.1	<0.05	<0.05	97.7
KhZ196	quartz	early 16th	turquoise	67.5	3.5	7.6	2.7	3.8	4.4	2.0	2.3	<0.05	<0.05	1.2	<0.05	1.9	<0.05	1.1	0.1	<0.05	<0.05	99.5
KhZ135	quartz	early 16th	turquoise	63.4	2.7	7.8	2.5	2.4	5.8	3.2	<0.05	<0.05	<0.05	0.8	0.6	1.8	<0.05	<0.05	<0.05	0.2	<0.05	96.83
KhZ201tü	quartz	early 16th	turquoise	65.7	2.8	8.3	2.9	4.5	3.0	2.1	0.5	<0.05	<0.05	1.2	<0.05	2.4	<0.05	<0.05	<0.05	0.2	0.1	99.0
KhZ032.2	quartz	early 16th	white	59.3	3.2	8.9	2.0	3.9	9.3	3.0	3.5	<0.05	<0.05	0.8	<0.05	<0.05	<0.05	0.4	0.2	0.1	0.4	94.48
KhZ133.2	quartz	early 16th	turquoise	61.9	3.0	9.0	2.9	2.1	3.1	3.5	<0.05	<0.05	<0.05	1.2	<0.05	4.5	<0.05	1.2	<0.05	0.1	<0.05	97.45
KhZ197	quartz	early 16th	turquoise	68.4	2.3	9.2	2.7	1.7	3.6	3.7	<0.05	<0.05	<0.05	1.2	<0.05	2.4	<0.05	<0.05	<0.05	0.1	0.4	96.81
KhZ032.1	quartz	early 16th	white	65.7	2.2	9.6	2.4	4.3	5.0	2.6	3.5	<0.05	<0.05	0.9	<0.05	<0.05	<0.05	1.8	0.1	0.1	0.3	96.7
IK03	quartz	15th	turquoise	69.6	3.2	10.6	2.5	3.1	3.2	2.7	<0.05	<0.05	<0.05	0.9	<0.05	1.5	<0.05	<0.05	<0.05	0.2	<0.05	97.9

Lead glazes

sample	ceramic body	century	colour	SiO$_2$	Al$_2$O$_3$	PbO	MgO	CaO	Na$_2$O	K$_2$O	SnO$_2$	Cr$_2$O$_3$	MnO$_2$	Fe$_2$O$_3$	CoO	CuO	ZnO	P$_2$O$_5$	SO$_3$	TiO$_2$	Cl	Sum
15SAM	clay	13th	dark blue	40.9	2.9	52.6	0.1	0.8	1.4	0.9	<0.05	<0.05	0.1	0.4	0.5	<0.05	<0.05	<0.05	<0.05	0.1	<0.05	96.81
16SAM	clay	13th	turquoise	43.6	3.1	35.5	0.5	4.1	6.5	2.1	<0.05	<0.05	<0.05	1.0	<0.05	1.6	0.1	<0.05	<0.05	0.2	<0.05	97.44

Results of EPMA analysis

sample	ceramic body	century	colour	SiO₂	Al₂O₃	PbO	MgO	CaO	Na₂O	K₂O	SnO₂	Cr₂O₃	MnO₂	Fe₂O₃	CoO	CuO	ZnO	P₂O₅	SO₃	TiO₂	Cl	Sum
39Afr	clay	10-11th	black	51.4	8.0	31.2	1.2	1.5	1.1	3.1	<0.05	<0.05	0.1	3.5	<0.05	<0.05	<0.05	0.3	<0.05	0.2	<0.05	96.83
37Afr	clay	10-11th	white	44.4	3.9	47.5	0.7	1.7	0.6	1.2	1.2	<0.05	<0.05	0.8	<0.05	<0.05	<0.05	0.2	<0.05	0.1	<0.05	100.6
38Afr	clay	10-11th	white	44.3	3.4	50.1	0.6	1.7	1.0	1.2	2.3	<0.05	<0.05	0.6	<0.05	<0.05	<0.05	0.2	0.2	<0.05	<0.05	99.5
41Afr	clay	10-11th	green	37.2	3.3	53.4	0.7	1.9	0.8	0.8	<0.05	<0.05	<0.05	0.7	<0.05	1.6	<0.05	0.2	<0.05	0.1	<0.05	97.45
40Afr	clay	10-11th	green	36.6	2.9	55.6	0.4	1.4	0.4	0.8	0.5	<0.05	<0.05	1.3	<0.05	1.0	<0.05	0.1	<0.05	0.2	<0.05	99.0
36Afr	clay	10-11th	red	37.9	3.6	56.9	0.3	0.9	0.4	0.5	<0.05	<0.05	<0.05	0.3	<0.05	<0.05	<0.05	0.1	<0.05	<0.05	<0.05	99.4
IK02	quartz	15th	blue	41.7	1.9	48.5	0.8	1.6	3.0	0.9	<0.05	<0.05	<0.05	0.5	0.6	<0.05	<0.05	<0.05	<0.05	0.2	<0.05	97.7
IK01	quartz	15th	green	32.4	1.3	62.1	0.1	0.3	0.1	0.3	<0.05	<0.05	<0.05	0.1	<0.05	2.6	<0.05	<0.05	<0.05	0.2	<0.05	97.1
KhZ201oc	quartz	early 16th	ochre	50.1	1.1	38.2	0.2	0.9	0.6	0.7	<0.05	<0.05	<0.05	4.3	<0.05	0.1	<0.05	0.2	0.1	<0.05	<0.05	99.9
KhZ029	quartz	early 16th	yellow	41.6	1.7	45.2	1.2	2.3	0.7	0.7	<0.05	<0.05	<0.05	3.7	<0.05	<0.05	<0.05	0.5	<0.05	0.2	<0.05	97.78
KhZ029.1	quartz	early 16th	yellow	43.4	1.8	45.8	1.1	2.4	0.7	0.7	<0.05	<0.05	0.1	3.7	<0.05	<0.05	0.1	0.1	<0.05	<0.05	<0.05	96.39
KhZ163	quartz	early 16th	green	38.8	1.1	49.8	0.5	1.5	0.8	0.7	0.1	1.9	<0.05	0.7	<0.05	<0.05	<0.05	<0.05	<0.05	<0.05	<0.05	96.7
KhZ200	quartz	early 16th	ochre	38.0	1.3	50.1	0.4	0.6	0.8	1.0	0.6	<0.05	<0.05	5.3	0.1	<0.05	<0.05	<0.05	<0.05	0.2	<0.05	101.2
KhZ134	quartz	early 16th	ochre	34.9	1.2	53.3	0.5	1.5	0.8	0.8	0.3	<0.05	<0.05	3.5	<0.05	0.1	<0.05	<0.05	<0.05	<0.05	<0.05	94.9
KhZ164	quartz	early 16th	green	30.6	0.8	61.3	0.4	1.3	0.2	0.2	<0.05	<0.05	<0.05	0.6	<0.05	1.7	<0.05	<0.05	<0.05	0.2	<0.05	98.98
BM0001	quartz	16th	dark green	34.7	2.0	56.0	0.5	1.1	0.5	0.5	0.1	<0.05	<0.05	0.4	<0.05	2.1	<0.05	0.3	<0.05	0.1	<0.05	97.55
MMA4	quartz	16th	ochre	32.5	1.4	55.4	0.3	0.6	1.5	1.4	<0.05	<0.05	<0.05	3.5	<0.05	0.1	<0.05	<0.05	<0.05	<0.05	<0.05	97.2

5.5 Afghan glazes

The Afghan glazes can be attributed to two of the three major glaze types. The alkali glazes have PbO contents of 0-2.0 wt%, the lead group glazes of 31.8-61.8 wt% PbO (fig.26). The alkali group dominates with 17 of 22 glazes. The lead content is not correlated with a specific age or century of the glazes, but in the correlation with the glaze colouring, the lead glazes show exclusively green (2 samples) and ochre (3 samples) colours.

5.5.1 Alkali glazes

The alkali glazes include the blue, black, white, and turquoise samples. The turquoise samples are characterized by absence of tin oxide, which is unusual for Cu coloured turquoise samples (see chapter 7.3).

The sample set shows varying alkali contents of 2.7-6.1 wt% Na_2O and 0.9-3.9 wt% K_2O. The alkali earth values are comparatively high (5.0-8.7 wt% CaO, 2.3-5.2 wt% MgO); the silica content is at about 70 wt% SiO_2. The Na_2O/K_2O ratio is 2.4±1.6. Within the alkali group, two samples have slightly lower SiO_2, Na_2O, and MgO contents, but at enhanced K_2O values (67-68 wt% SiO_2, 1.5 wt% Na_2O, 0.6 wt% MgO, and 9.3 wt% K_2O). The Al_2O_3 contents of the alkali group are between 0.5 and 3.9 wt%, the iron oxide values are at 0.5-2.4 wt% Fe_2O_3.

5.5.2 Lead glazes

The lead samples split into a lower PbO group of two ochre samples with 31.8-37.8 wt% PbO and one green and one ochre sample with >52 wt% PbO. The samples with minor lead have contents of 1.5-1.6 wt% Na_2O, 2.3-2.4 wt% K_2O, 3.8-5.5 wt% CaO, and 0.6-0.8 wt% MgO. In the samples with high PbO contents, the alkali and alkali earth values are commonly below 1.0 wt%. The ratio between Na_2O and K_2O is in both sub-groups about 0.7±0.2. The iron oxide and alumina contents of all lead-rich glazes are enhanced in comparison to the alkali samples and correlate roughly with the silica content (5.2-8.2 Al_2O_3 and 1.5-5.0 wt% Fe_2O_3).
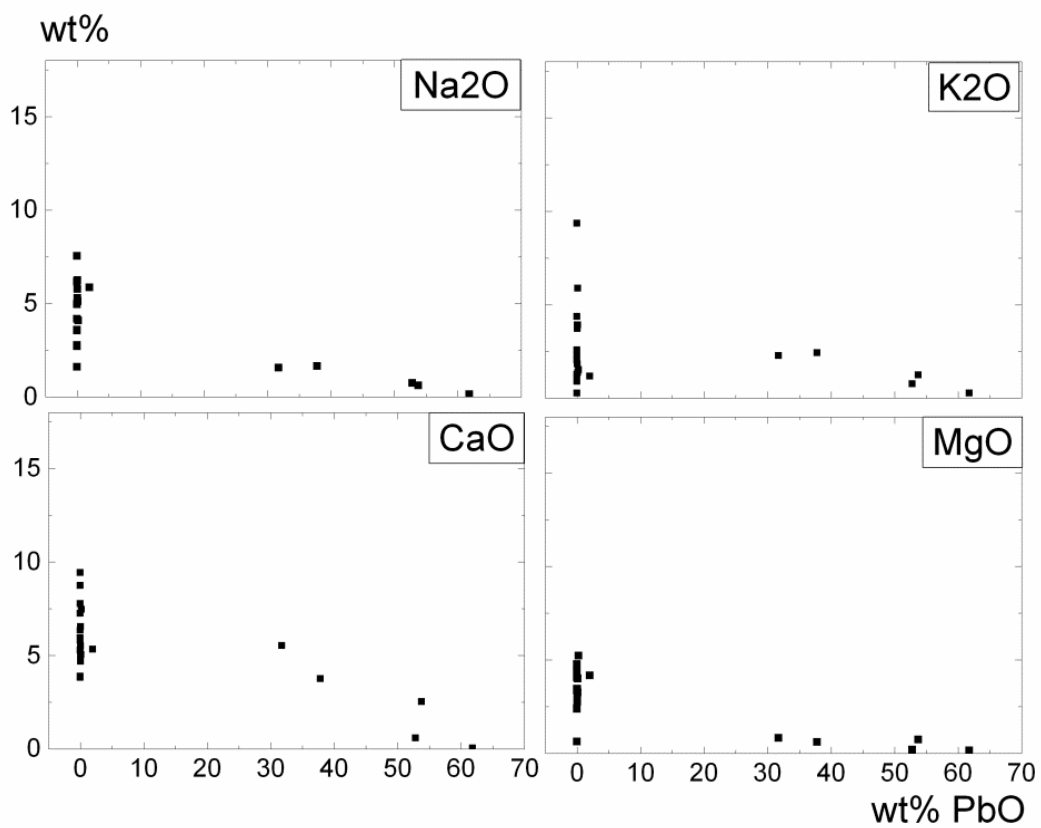
Figure 26: Alkali and alkali earth oxides versus PbO in the samples from Herat (Afghanistan) versus the PbO content. There is one alkali group with very low lead content and corresponding high alkali (earth) values, especially Na_2O and CaO. The other glazes belong to a lead group with lower alkali and alkali earth values. The glazes of the second group show a larger variation from 31.8 to 62.8 wt% PbO.

Table 12: Analyses of Afghan glazes in wt%. The abbreviation her stands for the glaze of tableware ceramic from Herat. All values are averages from at least 5 single measurements. Cr_2O_3, ZnO and TiO_2 are not listed, because of values consistently below the detection limit.

Alkali glazes																		
sample	ceramic body	century	colour	SiO_2	Al_2O_3	PbO	MgO	CaO	Na_2O	K_2O	SnO_2	MnO_2	Fe_2O_3	CoO	CuO	P_2O_5	SO_3	Sum
48her	quartz	16-17 th	blue	76.8	2.7	0.1	2.8	4.7	5.8	3.9	<0.05	0.1	1.4	0.1	<0.05	0.7	1.6	100.4
56bher	quartz	17th	black	76.4	3.3	0.1	2.9	5.0	5.3	1.8	0.1	0.2	1.2	<0.05	2.4	0.7	0.4	99.6
59aher	quartz	15th	light green	73.6	2.2	0.1	3.3	5.5	5.1	5.9	0.2	0.1	0.6	<0.05	2.0	0.3	0.3	99.0
49her	quartz	15th	turquoise	74.9	1.8	0.1	4.0	6.5	6.3	3.9	<0.05	<0.05	1.2	<0.05	1.7	0.2	0.3	100.8
42her	quartz	15th	turquoise	77.1	2.6	0.1	4.0	5.0	5.1	1.4	0.1	<0.05	1.1	<0.05	1.3	0.3	0.3	98.4
58her	quartz	13-14th	turquoise	75.6	1.9	0.2	5.2	7.5	4.1	1.5	<0.05	<0.05	0.5	<0.05	2.1	0.3	0.3	99.0
47her	quartz	15th	blue	74.2	1.4	2.0	4.2	5.3	5.9	1.2	0.5	0.2	1.9	0.1	1.9	0.2	0.4	99.1
Lead glazes																		
sample	ceramic body	century	colour	SiO_2	Al_2O_3	PbO	MgO	CaO	Na_2O	K_2O	SnO_2	MnO_2	Fe_2O_3	CoO	CuO	P_2O_5	SO_3	Sum
54her	clay	15th	brown	43.5	8.2	31.8	0.8	5.5	1.6	2.3	<0.05	<0.05	5.0	<0.05	<0.05	0.1	0.2	100.0
50her	clay	15-17th	ochre	41.9	7.7	37.8	0.6	3.8	1.6	2.4	<0.05	0.2	4.0	<0.05	<0.05	0.1	0.2	99.9
57her	clay	14-15th	ochre	33.7	6.4	52.8	0.2	0.6	0.7	0.8	<0.05	0.1	3.3	0.1	0.9	<0.05	<0.05	99.3
55her	clay	15-17th	green	33.8	5.2	53.8	0.7	2.5	0.6	1.2	<0.05	0.1	1.5	<0.05	0.6	<0.05	0.3	100.6
45her	quartz	15th	green	29.9	3.6	61.8	0.1	<0.05	0.1	0.3	<0.05	<0.05	1.6	<0.05	0.6	<0.05	1.2	99.1
43her	quartz	15th	beige	76.3	2.0	<0.05	4.8	7.8	6.2	1.3	<0.05	0.1	0.7	<0.05	<0.05	0.2	0.4	99.4
44her	clay	15th	blue	79.1	1.1	<0.05	3.5	3.9	4.9	0.9	0.1	<0.05	1.6	0.3	0.1	0.4	0.5	96.2
46her	quartz	15th	white	68.1	13.4	<0.05	0.6	9.4	1.6	4.4	<0.05	0.1	0.5	<0.05	<0.05	0.1	<0.05	98.1
51her	quartz	15th	turquoise	76.6	1.9	<0.05	4.5	5.8	2.7	1.1	<0.05	<0.05	0.8	<0.05	1.5	0.3	0.2	95.3

Results of EPMA analysis

sample	ceramic body	century	colour	SiO$_2$	Al$_2$O$_3$	PbO	MgO	CaO	Na$_2$O	K$_2$O	SnO$_2$	MnO$_2$	Fe$_2$O$_3$	CoO	CuO	P$_2$O$_5$	SO$_3$	Sum
52her	quartz	15-16th	turquoise	74.6	3.8	<0.05	3.4	6.3	4.2	3.7	0.1	0.3	1.7	<0.05	0.5	0.4	0.2	99.1
53her	quartz	15-17th	turquoise	77.9	3.6	<0.05	2.4	5.9	3.5	2.0	<0.05	0.1	0.9	<0.05	<0.05	0.5	0.3	97.2
56aher	quartz	17th	turquoise	75.1	0.5	<0.05	4.3	8.7	7.5	0.3	<0.05	<0.05	0.1	<0.05	<0.05	<0.05	0.2	96.7
59bher	quartz	15th	black	67.8	3.2	<0.05	3.3	7.2	5.0	9.3	0.1	0.1	2.4	<0.05	0.8	0.4	0.1	99.3
61her	clay	15th	dark blue	79.3	4.0	<0.05	2.4	3.8	2.8	2.6	<0.05	<0.05	2.0	<0.05	0.2	0.1	0.2	97.2
62her	clay	15-16th	blue	77.6	1.8	<0.05	4.1	5.3	3.6	2.2	<0.05	0.1	0.7	0.1	<0.05	0.5	0.3	96.1

5.6 Iranian glazes

The samples of Takht-i-Suleiman cover all three compositional glaze groups: an alkali group with 0.42-3.14 wt% PbO, a widely scattered alkali lead group with 9.7-27.1 wt% PbO and a lead group with 55.7-61.2 wt% PbO. The alkali and alkali lead glazes have SiO_2 between at 49.3-79.5 wt%, the lead group´s silica values are between 30.9 and 35.0 wt% SiO_2. In the alkali and alkali lead groups are a few painted samples with differing alkali earth characteristic, evident through much higher MgO values between 1.8 and 3.0 wt% MgO (TiS 31-34), in comparison to the rest of alkali and alkali lead glazes, which have MgO contents below 1 wt%.

5.6.1 Alkali glazes

The alkali group contains ten samples with blue, turquoise, and ochre colours and one sample with white colour. Beside the glazed tiles, also one of the bichrome tableware sherds of the 12th century with two different glazes (TiS 11a, TiS 11b) belongs to this group. No congruence between the glaze colour and the lead content is observed. Na_2O and CaO are dominant as flux and stabilizer (up to 15.7 wt% Na_2O and 7.4 wt% CaO); the contents of K_2O are less substantial (1.8-3.4 wt%). The MgO content is in most cases less than 1.0 wt%. Two samples of ochre and red glaze differ from the rest of the set with MgO values of 2.4 and 3.0 wt% (TiS 31 and TiS 32).

5.6.2 Alkali lead glazes

The second group contains 27 samples with a wide range of PbO content (9.7-27.1 wt%), varying strongly in the content of Na_2O (2.5-15.7 wt%) and CaO (2.4-7.4 wt%). In contrast, the K_2O contents are with 1.1-2.6 wt% comparatively well defined. The MgO contents are with values below 0.9 wt% similar to that of the alkali glazes. Again, a subgroup of two painted tiles with MgO 1.8-2.2 wt% in turquoise and white colour forms an exception (TiS 33 and TiS 34). Both, the alkali and the alkali lead groups show Na_2O/K_2O ratios of 4.6 ± 1.8. In the comparison of re-cast alkali and alkali earth data, no significant difference can be observed between the alkali and the alkali lead glazes from Takht-i-Suleiman (fig. 27 a and b). A production of alkali lead glazes by addition of lead to the alkali glaze recipe seems likely here.
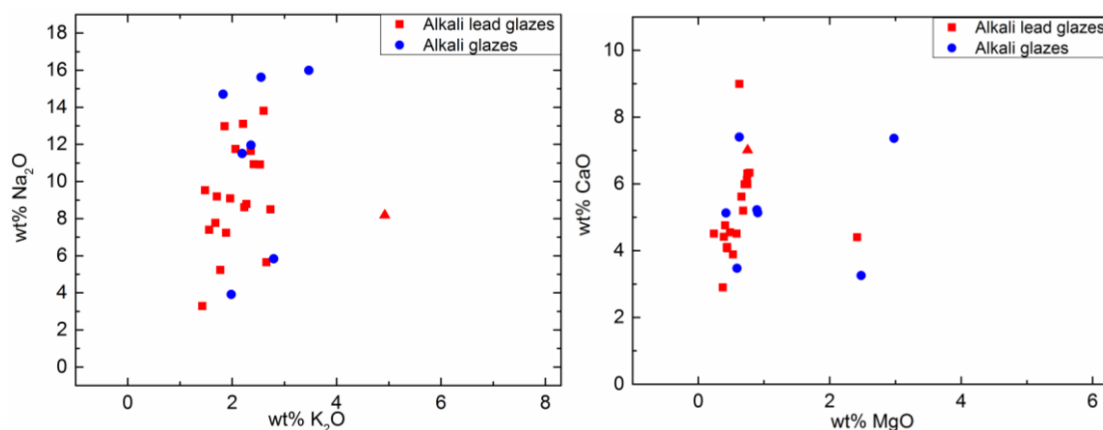
Figure 27 a and b: Alkali and alkali earth oxides from alkali and alkali lead glazes from Uzbekistan. The triangle within the group of alkali lead glazes belongs to a modern restored glaze from Isfahan

5.6.3 Lead glazes

The lead group consists of three samples of tableware (TiS 12, TiS 13a, TiS 13b), decorated with the "Champlevé"-technique in green and yellow-greenish colours (chapter 3.3). The main composition with 55.7-61.6 wt% PbO and 30.9-35.0 wt% SiO_2 is quite homogeneous. The alkali and alkali earth oxides have maximum values of 0.4 wt% Na_2O, 0.6 wt% K_2O, 2.0 wt% CaO, and 0.2 wt% MgO. The Na_2O/K_2O ratio is consistently around 0.6 ± 0.2.

5.6.4 20th century samples from Isfahan

From the two monochrome sherds of the restored prayer niche in Isfahan, one glaze with 63.7 wt% PbO matches the lead group, the other one with 21.6 wt% PbO fits into alkali lead group. The K_2O value of the alkali lead glaze is with 4.0 wt% higher than those of the old samples. This higher value is also found in the comparison of re-cast data (fig. 27 a) The Na_2O, CaO, and MgO values do not differ visibly from those of the historic Iranian samples with comparable lead content (fig.28).
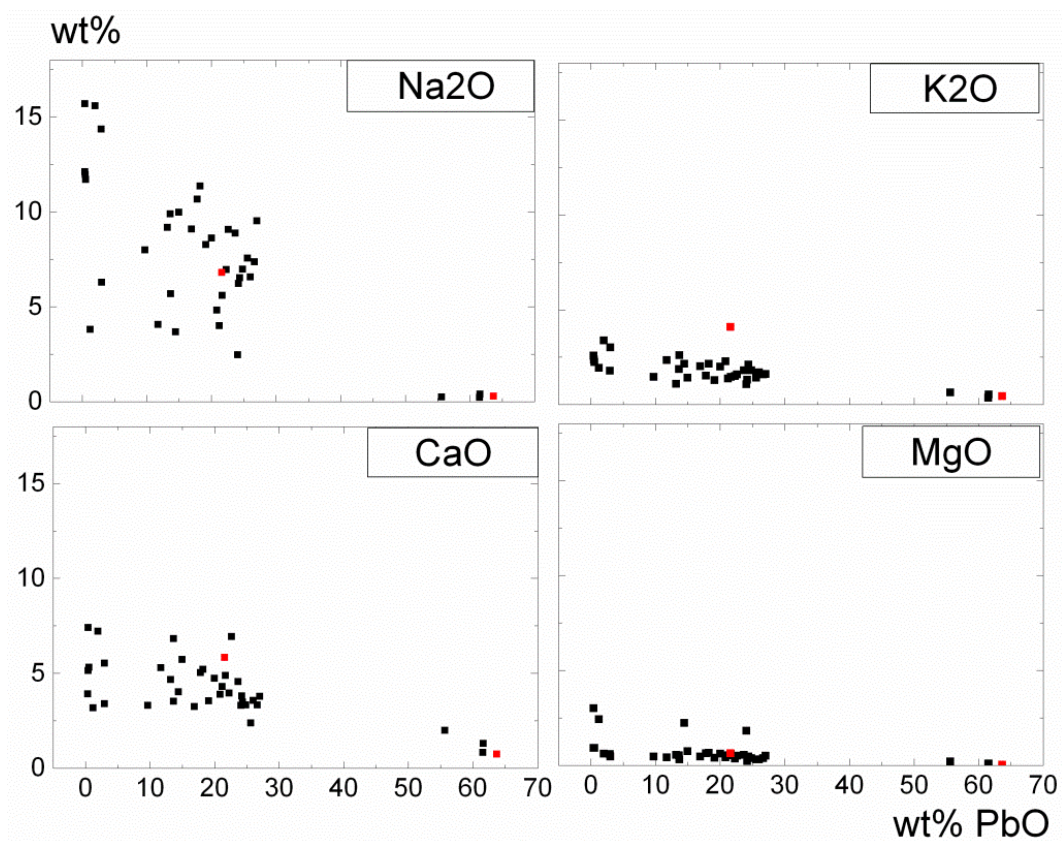
Figure 28: Alkali and alkali earth contents of the glazes from the Khwarazmian culture of the 12th century, the Ilkhanate dynasty of the 13th century and the modern restoration of the 20th century (black: historic samples, Takht-i-Suleiman, red: modern samples, prayer niche Isfahan). Except for one K_2O value, the two modern samples are within the scattering range of the two major groups of the Takht-i-Suleiman glazes.

Table 13: Analyses of Iranian glazes in wt%. the abbreviation TiS stand for the tile glazes of the building complex Takht-i-Suleiman. All values are averages from at least 5 single measurements. n.d. stands for not determined. Cr_2O_3, Cl, and TiO_2 are not listed, because of values consistently below detection limit.

Alkali glazes																			
sample	ceramic body	century	colour	SiO_2	Al_2O_3	PbO	MgO	CaO	Na_2O	K_2O	SnO_2	MnO_2	Fe_2O_3	CoO	CuO	ZnO	P_2O_5	SO_3	Sum
30bTiS	quartz	late 13th	blue	72.6	2.3	0.4	0.9	3.9	12.1	2.5	<0.05	<0.05	2.0	0.2	<0.05	<0.05	<0.05	0.2	97.0
31TiS	clay	late 13th	ochre	60.8	5.0	0.4	3.0	7.4	15.7	2.6	<0.05	3.3	1.7	<0.05	0.1	<0.05	0.7	0.3	100.9
11bTiS	quartz	12th	turquoise	74.3	1.8	0.5	0.9	5.1	12.0	2.4	0.1	<0.05	2.6	0.5	0.3	<0.05	<0.05	<0.05	100.2
11aTiS	quartz	12th	green	75.0	1.8	0.6	0.9	5.3	11.7	2.2	0.2	1.5	0.8	<0.05	2.2	<0.05	<0.05	<0.05	100.6
32TiS	quartz	late 13th	red	79.5	5.1	1.2	2.4	3.2	3.8	1.9	0.1	<0.05	1.1	<0.05	<0.05	<0.05	0.1	<0.05	98.5
10TiS	clay	late 13th	brown	60.5	4.8	2.0	0.6	7.2	15.6	3.4	0.3	<0.05	4.9	0.1	<0.05	<0.05	<0.05	<0.05	100.4
30aTiS	quartz	late 13th	white	73.0	3.4	3.0	0.6	3.4	14.4	1.8	0.3	<0.05	0.6	<0.05	0.1	0.1	<0.05	<0.05	100.5
4aTiS	clay	late 13th	blue	79.2	7.6	3.0	0.5	5.5	6.3	3.0	1.9	0.1	2.9	0.3	0.4	<0.05	<0.05	<0.05	98.5
Alkali lead glazes																			
sample	ceramic body	century	colour	SiO_2	Al_2O_3	PbO	MgO	CaO	Na_2O	K_2O	SnO_2	MnO_2	Fe_2O_3	CoO	CuO	ZnO	P_2O_5	SO_3	Sum
2aTiS	quartz	late 13th	white	76.2	3.6	9.7	0.5	3.3	8.0	1.5	2.4	<0.05	1.7	<0.05	0.1	<0.05	<0.05	<0.05	101.1
1bTiS	clay	late 13th	blue	75.2	2.1	11.7	0.4	5.3	4.1	2.3	2.5	<0.05	1.9	0.4	0.1	<0.05	<0.05	<0.05	99.2
2bTiS	quartz	late 13th	blue	70.2	1.6	13.2	0.5	4.7	9.2	1.1	3.7	<0.05	1.8	0.6	0.1	<0.05	<0.05	<0.05	100.5
26bTiS	clay	late 13th	blue	59.0	1.8	13.7	0.5	6.8	9.9	1.9	3.1	0.1	2.5	0.4	0.1	<0.05	<0.05	<0.05	99.5
3bTiS	quartz	late 13th	blue	72.8	2.5	13.7	0.3	3.5	5.7	2.6	3.7	0.1	3.2	1.2	<0.05	<0.05	<0.05	<0.05	99.5
34TiS	quartz	late 13th	white	65.9	2.8	14.4	2.2	4.0	3.7	2.1	2.6	0.1	1.1	<0.05	0.1	<0.05	0.1	<0.05	99.1
28TiS	quartz	late 13th	blue	58.9	1.1	15.0	0.7	5.7	10.0	1.4	3.7	<0.05	2.2	0.6	0.1	<0.05	<0.05	<0.05	99.1
23cTiS	quartz	late 13th	blue	58.0	1.3	16.9	0.4	3.2	9.1	2.0	5.6	<0.05	1.8	1.6	<0.05	<0.05	<0.05	0.1	100.0

sample	ceramic body	century	colour	SiO$_2$	Al$_2$O$_3$	PbO	MgO	CaO	Na$_2$O	K$_2$O	SnO$_2$	MnO$_2$	Fe$_2$O$_3$	CoO	CuO	ZnO	P$_2$O$_5$	SO$_3$	Sum
27TiS	quartz	late 13th	blue	56.9	1.4	17.8	0.6	5.0	10.7	1.5	3.5	0.1	1.3	0.7	0.5	0.1	<0.05	<0.05	99.8
24TiS	quartz	late 13th	turquoise	53.8	1.6	18.3	0.6	5.2	11.3	2.1	3.3	0.1	1.0	<0.05	3.0	0.1	<0.05	<0.05	100.2
5TiS	quartz	late 13th	blue	66.0	1.3	19.1	0.4	3.5	8.3	1.3	3.5	<0.05	1.7	0.7	0.1	<0.05	<0.05	<0.05	97.7
1aTiS	clay	late 13th	turquoise	67.0	1.9	20.9	0.4	3.9	4.8	2.3	2.7	<0.05	0.8	<0.05	1.4	<0.05	<0.05	<0.05	100.6
25TiS	quartz	late 13th	white	60.3	0.6	21.2	0.5	4.3	4.0	1.4	4.5	<0.05	0.7	<0.05	0.1	0.1	<0.05	0.1	97.6
29bTiS	quartz	late 13th	turquoise	53.6	1.4	21.7	0.6	4.9	5.6	1.5	6.5	0.1	0.9	<0.05	2.1	0.2	<0.05	<0.05	98.8
3aTiS	quartz	late 13th	white	63.3	1.7	22.3	0.4	4.0	6.9	1.5	10.6	0.1	1.0	<0.05	<0.05	<0.05	<0.05	<0.05	101.7
26aTiS	clay	late 13th	turquoise	49.3	1.5	22.6	0.5	6.9	9.1	1.6	5.1	0.1	1.2	<0.05	1.8	<0.05	<0.05	<0.05	99.6
23bTiS	quartz	late 13th	white	55.3	0.9	23.7	0.5	4.6	8.9	1.8	3.1	<0.05	1.0	<0.05	0.1	<0.05	<0.05	<0.05	99.7
33TiS	quartz	late 13th	turquoise	57.8	2.2	24.1	1.8	3.3	2.5	1.1	3.2	0.1	0.9	<0.05	2.2	<0.05	0.2	<0.05	99.3
4bTiS	clay	late 13th	turquoise	63.0	1.9	24.2	0.2	3.8	6.2	1.3	4.7	0.1	0.8	<0.05	1.9	<0.05	<0.05	<0.05	99.5
8TiS	quartz	late 13th	turquoise	55.7	1.5	24.4	0.5	3.5	6.5	2.1	3.2	<0.05	0.7	<0.05	3.0	<0.05	<0.05	<0.05	101.1
7bTiS	quartz	late 13th	white	62.0	1.8	24.9	0.4	3.3	7.0	1.8	3.8	<0.05	0.8	<0.05	<0.05	<0.05	<0.05	<0.05	101.1
6TiS	quartz	late 13th	turquoise	61.6	1.1	25.6	0.3	2.4	7.5	1.4	5.4	0.1	0.6	<0.05	1.8	<0.05	<0.05	<0.05	99.4
9TiS	quartz	late 13th	turquoise	53.7	2.3	26.0	0.3	3.6	6.6	1.7	3.1	0.1	1.3	<0.05	2.1	<0.05	<0.05	<0.05	100.6
7aTiS	quartz	late 13th	white	59.6	1.7	26.7	0.4	3.3	7.4	1.6	6.2	<0.05	0.7	<0.05	<0.05	<0.05	<0.05	<0.05	100.4
23aTiS	quartz	late 13th	white	51.9	1.3	27.1	0.5	3.8	9.5	1.6	2.9	<0.05	1.0	<0.05	0.1	<0.05	<0.05	0.2	99.5
18 Isf	quartz	early 20th	blue	56.33	1.65	21.60	0.62	5.82	6.80	4.09	0.67	4.88	0.81	1.05	0.30	n.d.	n.d.	n.d.	99.72
Lead glazes																			
sample	ceramic body	century	colour	SiO$_2$	Al$_2$O$_3$	PbO	MgO	CaO	Na$_2$O	K$_2$O	SnO$_2$	MnO$_2$	Fe$_2$O$_3$	CoO	CuO	ZnO	P$_2$O$_5$	SO$_3$	Sum
12TiS	quartz	12th	green	35.0	3.2	55.7	0.2	2.0	0.2	0.6	<0.05	0.1	1.6	<0.05	2.4	<0.05	<0.05	<0.05	100.9
13bTiS	clay	12th	green	30.9	2.8	61.6	0.1	0.8	0.2	0.4	0.1	0.1	0.5	<0.05	3.0	<0.05	<0.05	<0.05	100.3
13aTiS	clay	12th	yellow	32.8	3.2	61.6	0.1	1.3	0.4	0.5	<0.05	0.1	0.7	<0.05	0.9	<0.05	<0.05	<0.05	101.5

Results of EPMA analysis

sample	ceramic body	century	colour	SiO$_2$	Al$_2$O$_3$	PbO	MgO	CaO	Na$_2$O	K$_2$O	SnO$_2$	MnO$_2$	Fe$_2$O$_3$	CoO	CuO	ZnO	P$_2$O$_5$	SO$_3$	Sum
29aTiS	quartz	late 13th	turquoise	55.5	1.3	<0.05	0.6	4.7	8.6	2.0	2.9	<0.05	0.9	<0.05	2.1	0.3	<0.05	<0.05	98.8
19 Isf	quartz	early 20th	black	31.04	3.31	63.66	0.02	0.73	0.28	0.44	0.05	0.05	1.38	0.03	0.10	n.d.	n.d.	n.d.	100.90

5.7 Turkish glazes

All three groups of lead content are identified within the Turkish glazes; the alkali one with 0.1-0.5 wt% PbO, the alkali lead one with 12.2-27.5 wt%, and the lead group with values of 36.-37.0 wt% PbO (fig.29). The content of SiO_2 and alkali oxides is correspondingly decreasing with higher PbO. The eight samples from the mosque Ata Hanka in Konya are from three polychrome tiles. Within the glazes from two tiles, the compositions differ significantly in their lead content; Kon 20b and Kon 22a are alkali glazes, whereas Kon 20a, Kon 20c, and Kon 22b belong to the alkali lead group.

5.7.1 Alkali glazes

One black and one ochre sample (Kon 20b, Kon 22a) from the mosque Ata Hanka in Konya belong with 0.5 and 0.1 wt% PbO to the alkali group. The Na_2O values of 10.8 and 16.3 wt% are in the upper range of Na values of the entirety of analysed glazes of this study. The K_2O values of 2.4 and 2.0 wt% and CaO values of 4.0 and 4.3 wt% are comparable to other those of the rest of alkali glazes of the sample set. MgO is with 0.3 and 0.6 wt% comparatively low to alkali glazes from e.g. Uzbekistan more than 4.0 wt% MgO. The Na_2O/K_2O ratios vary between 4.4 and 8.2.

5.7.2 Alkali lead glazes

The alkali lead group with 12.2-27.5 wt% PbO comprises four turquoise glazes, three from the mosque Ata Hanka in Konya (Kon 20a, Kon 20c, Kon 22b) and the one from Kayseri (21 Kay). The samples from Konya are from polychrome tiles which have partly alkali and partly alkali lead glazes. In the alkali lead glazes are partly lower Na_2O, K_2O, and CaO values than in the alkali group (6.1-12.6 wt% Na_2O, 0.8-2.4 wt% K_2O and 0.5-4.7 wt% CaO). The MgO values instead are with 0.1-1.4 wt% MgO slightly higher. The Na_2O/K_2O ratios are between 2.7 and 6.8. The comparison between alkali and alkali lead glazes in re-cast data does not show any significant deviation. However, the data set is too small here to make any assumptions about the possible derivation of alkali leaf glazes from alkali glaze composition.

5.7.3 Lead glazes

The lead group is formed by glazes from three small tiles of turquoise, green and blue colour, combined in one piece of mortar. The sodium oxide contents are with 2.0-3.0 wt% Na_2O comparatively higher than those of lead glazes from Uzbekistan, Afghanistan, Iran, and Bulgaria (max. 1.6 wt% Na_2O). The CaO content is with 2.8-3.7 wt% also enhanced. The K_2O and MgO values do not differ significantly from those of the alkali lead group (0.7-1.6 wt% K_2O and 0.5-1.4 wt% MgO). The Na_2O/K_2O ratios are between 1.8 and 2.8.
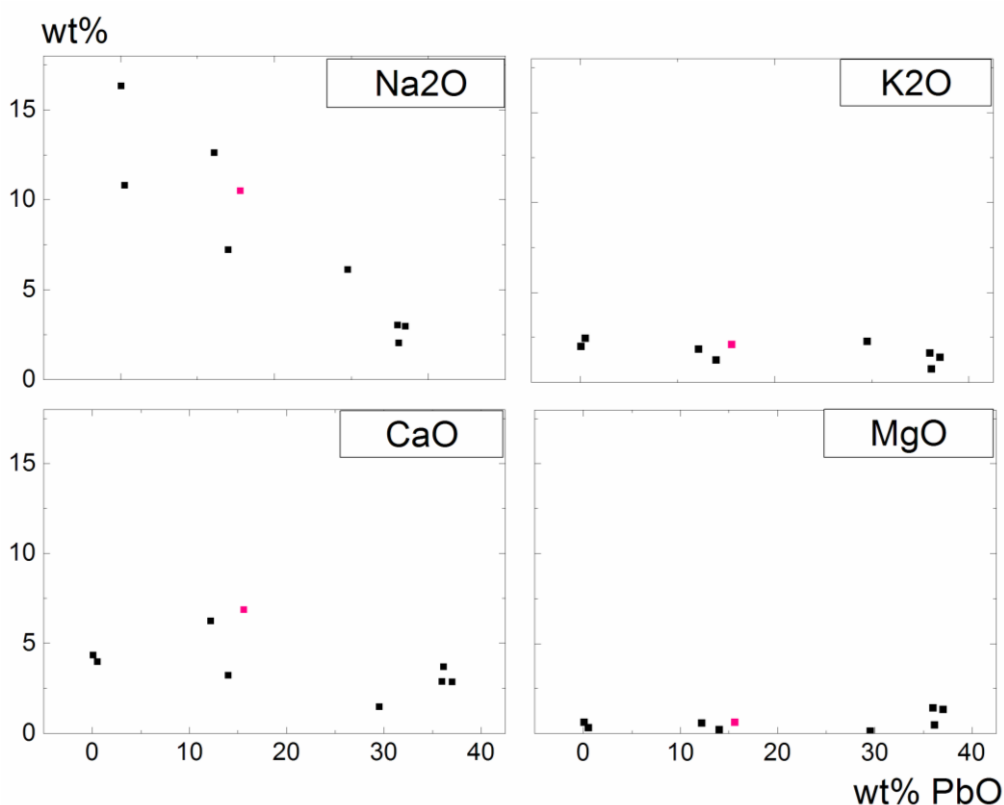
Figure 29: The glazes of tiles from the mosque Ata Hanka in Konya (black data points) and from Kayseri (red data point) from the late 12th and 13th century. The only sample from Kayseri has 15.1 wt% PbO and lies within the scattering of alkali lead glazes from Konya.

Table 14: Analyses of Turkish glazes in wt%. The abbreviations Kon and Kay stand for glazes from buildings of the cities Konya and Kayseri.All values are averages from at least 5 single measurements. Cr_2O_3, ZnO, Cl, and TiO_2 are not listed, because of values consistently below detection limit.

Alkali glazes																		
sample	ceramic body	century	colour	SiO_2	Al_2O_3	PbO	MgO	CaO	Na_2O	K_2O	SnO_2	MnO_2	Fe_2O_3	CoO	CuO	P_2O_5	SO_3	Sum
22aKon	quartz	13/14th	black	65.5	3.4	0.1	0.6	4.3	16.3	2.0	<0.05	<0.05	2.1	<0.05	0.1	<0.05	0.1	98.5
20bKon	quartz	13/14th	ochre	69.5	5.7	0.5	0.3	4.0	10.8	2.4	<0.05	0.3	2.1	<0.05	0.2	<0.05	<0.05	99.3
Alkali lead glazes																		
sample	ceramic body	century	colour	SiO_2	Al_2O_3	PbO	MgO	CaO	Na_2O	K_2O	SnO_2	MnO_2	Fe_2O_3	CoO	CuO	P_2O_5	SO_3	Sum
20cKon	quartz	13/14th	turquoise	63.1	4.7	12.2	0.2	3.2	7.2	1.2	4.9	3.9	1.6	<0.05	1.1	<0.05	<0.05	99.2
22bKon	quartz	13/14th	turquoise	56.4	2.1	12.2	0.6	6.2	12.6	1.9	4.1	4.2	1.2	<0.05	1.9	<0.05	0.1	99.1
21Kay	quartz	late 13th	turquoise	58.9	0.5	15.6	0.6	6.9	10.5	2.1	4.1	<0.05	0.6	<0.05	2.2	<0.05	0.1	101.8
20aKon	quartz	13/14th	turquoise	55.6	1.0	27.5	0.1	1.5	6.1	2.3	3.4	0.1	2.2	0.7	0.5	<0.05	<0.05	100.6
Lead glazes																		
sample	ceramic body	century	colour	SiO_2	Al_2O_3	PbO	MgO	CaO	Na_2O	K_2O	SnO_2	MnO_2	Fe_2O_3	CoO	CuO	P_2O_5	SO_3	Sum
35aKon	quartz	12/early13th	turquoise	48.3	1.0	36.0	1.4	2.9	3.0	1.6	3.8	0.1	0.5	0.1	1.2	0.2	0.1	100.2
35cKon	quartz	12/early13th	green	50.0	0.9	36.2	0.5	3.7	2.0	0.7	<0.05	<0.05	1.2	<0.05	5.5	0.1	<0.05	100.9
35bKon	quartz	12/early13th	blue	49.7	1.2	37.0	1.3	2.8	3.0	1.4	1.7	0.1	0.9	0.3	0.2	0.2	<0.05	99.8

5.8 Bulgarian glazes

The glazes from Dristra, Bulgaria split into one group of monochrome tableware and another group of glazes from polychrome tableware. The glazes from monochrome sherds are lead glazes, the glazes from polychrome sherds are alkali lead glazes. Ten of the monochrome glazes date to the pre-Islamic, Second Bulgarian Empire in the 11th-12th century and have consistently brown colours. The other monochrome and the polychrome samples are from the 14th-18th century (chapter 3).

5.8.1 Alkali lead glazes

This group of medium lead content (16.7-23.2 wt% PbO) comprises six samples from polychrome sherds with violet, blue, and green colour on white background. Each three of them belong to one painted polychrome sherd. The glazes BG 1-3 have blue and green colour with white background, the samples BG 11-13 are blue and violet glazes on a white basis. The dominating alkali and alkali earth values are 2.6-3.5 wt% Na_2O and 1.4-2.9 wt% CaO. MgO is consistently below 1 wt%. The K_2O contents are with 2.0-2.1 wt% enhanced in the three samples BG 1-3 compared to BG 11-13 with 0.8-0.9 wt% (fig.30).

5.8.2 Lead glazes

The group of lead glazes consists of the eleven monochrome glazes from the Second Bulgarian Empire and the 21 monochrome glazes of the Ottoman period. The glazes of this group cover a range of PbO contents between 48.1 and 72.1 wt% and are very poor in alkali and alkali earth contents, i.e. Na_2O <0.5 wt%, K_2O <0.9 wt%, CaO <2.0 wt% (except one sample with 2.88 wt% CaO) and MgO <0.9 wt%. The Na_2O/K_2O ratio is 0.3-0.5. Within the alkali and alkali earth contents, a correlation between MgO and NaO_2 is observed (fig.31). The Fe_2O_3 also roughly correlates with the Na_2O content, but will be discussed in chapter 8.4.5. The remaining part of the composition is SiO_2 at values between 17.1 and 39.6 wt% which are slightly correlating with the CaO content.

The occurrence of MgO and Fe_2O_3 in the Bulgarian lead glazes from the Second Bulgarian Empire and the Ottoman period can be influenced by diffusion of these components from the clay body

into the glaze. The normalised analyses of Bulgarian clay bodies show MgO values of 1-4 wt%; the Fe_2O_3 values are between 4 and 9 wt%.
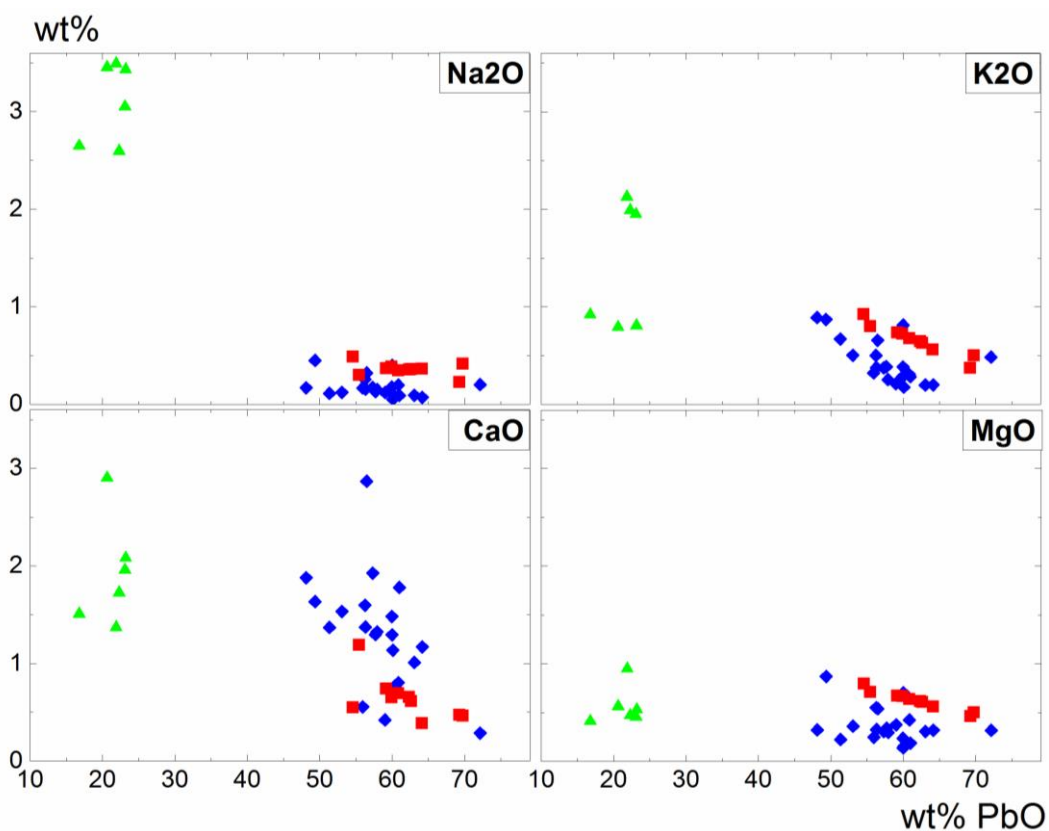
Figure 30: The alkali and alkali earth contents of Bulgarian glazes. The lead group consists of Ottoman (blue diamonds) and samples if the Second Bulgarian Empire (red squares). The Na_2O, K_2O, and MgO contents are below 1.0 wt% here. The Ottoman glazes show CaO values up to 3.0 wt%, the samples from the Second Bulgarian Empire rarely exceed the 1 wt% level. The probably imported ware (green triangles), are polychrome glazes with lower lead contents and enhanced Na_2O values. Three of them (BG 1-3) show enhanced K_2O values around 2 wt%.
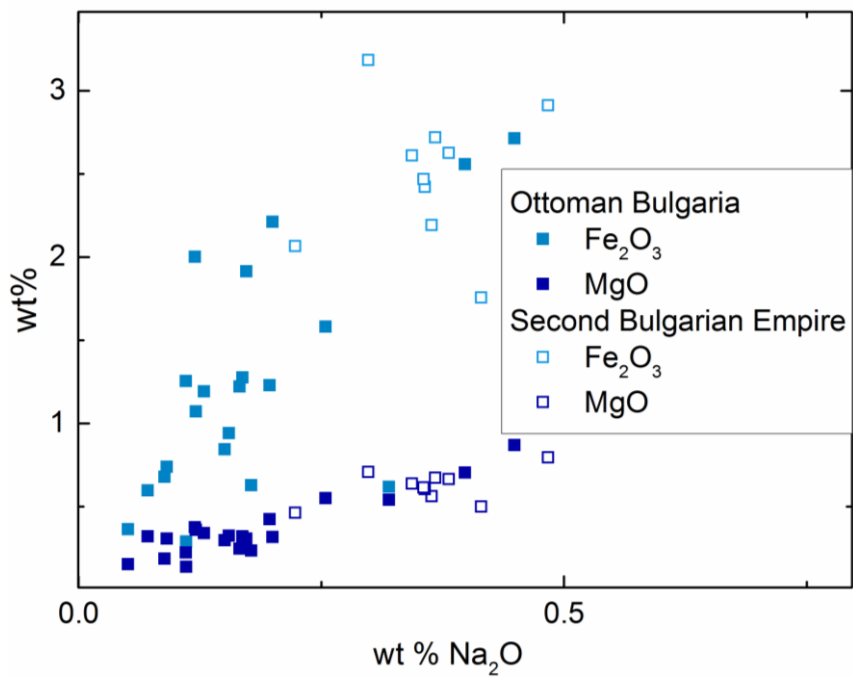
Figure 31: Correlation of MgO with Na₂O content in the lead glazes of the Ottoman and the Second Bulgarian Empire. The correlation with Fe₂O₃ is less distinct than the MgO-Na₂O correlation.
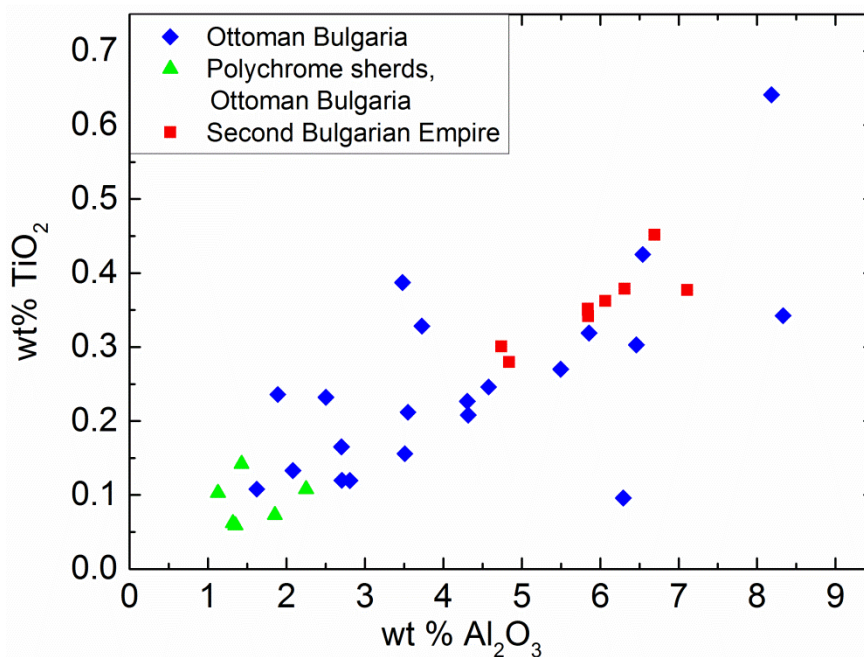
Figure 32: Al₂O₃ and TiO₂ correlation in Ottoman Bulgarian glazes (blue diamonds), polychrome sherds from the Ottoman Bulgaria (green triangles) and earlier glazes of the Second Bulgarian Empire (red squares).

All glazes have considerable content of TiO_2 in the matrix (0.1-0.4 wt%), correlating roughly with the Al_2O_3 content (fig.32). Titanium is found in contents of 0.5-1 wt% in the ceramic grain analyses of all Bulgarian subgroups, which cannot explain the differences in Ti contents in the glazes. Migration of Al from the clay body into lead glazes is already described in chapter 5.2. However, the mean value of the exemplarily analysed polychrome ceramic from Ottoman Bulgaria is 21 wt% Al_2O_3, whereas the mean alumina values of the monochrome sherd is at 13 wt% (tab. 9). A large influence of the ceramic body composition would lead to higher Al_2O_3 values in the polychrome glazes. Thus, the migration of Al from the ceramic body to the glaze is assumed to be minor compared to the original glaze recipe.

A beige glaze (BG 19) which generally has a similar composition to the other glazes (61.0 wt% PbO) has a separate layer at the interface to the ceramic body. This layer shows high contents of silica (54.3 wt%), Al_2O_3 (27.2 wt%), and K_2O (4.0 wt%) and low lead content (0.1 wt% PbO). This layer is probably a slip, which is applied to the ceramic body in order to have a light grounding or to avoid chipping due to different expansion coefficients. A deviation in Fe_2O_3 and MgO contents due to the slip layer cannot be observed; the values for BG 19 lay within the overall scattering. The TiO_2 contents of Bulgarian lead glazes are with 0.1-0.6 wt% slightly higher than those of e.g. Uzbek or Moroccan lead glazes (0.1-0.3 wt%).

The glazes from the Second Bulgarian Empire have high PbO contents as well, but differ from the younger Ottoman glazes primarily in the lower CaO content (0.6 wt% in average in contrast to 1.4 wt%, fig.30). The Na_2O, K_2O, and MgO contents are slightly enhanced in comparison to the Ottoman glazes. The TiO_2 and Al_2O_3 values fit into the correlation of younger Ottoman samples (fig.32).

Table 15: Analyses of Bulgarian glazes in wt%. The abbreviation BG stand for the tableware samples of the fortress Dristra, from Ottoman period (BG). The The samples BG1-3 and BG11-13 belong each to one polychrome sherd, probably imported ware. Abbreviation Zar stand for the glazes from the 12th century (Second Bulgarian Empire) from the fortress Dristra. All values are averages from at least 5 single measurements. n.d. stands for not determined. P_2O_5, SO_3 and Cl are not listed, because of values consistently below detection limit.

Alkali lead glazes																			
sample	ceramic body	century	colour	SiO₂	Al₂O₃	PbO	MgO	CaO	Na₂O	K₂O	SnO₂	Cr₂O₃	MnO₂	Fe₂O₃	CoO	CuO	ZnO	TiO₂	Sum
BG12	clay	17th	blue	60.6	1.9	16.8	0.4	1.5	2.7	0.9	<0.05	<0.05	0.3	4.1	0.9	1.0	0.1	0.1	90.7
BG13	clay	17th	purple	60.1	1.3	20.6	0.6	2.9	3.5	0.8	<0.05	<0.05	2.2	0.7	0.1	0.2	0.1	0.1	93.0
BG3	clay	16-17th	green	62.1	2.3	21.9	1.0	1.4	3.5	2.1	<0.05	1.0	0.1	2.0	<0.05	0.3	<0.05	0.1	97.5
BG1	clay	16-17th	blue	61.4	1.1	22.3	0.5	1.7	2.6	2.0	<0.05	<0.05	0.1	2.3	1.1	0.9	0.1	0.1	95.9
BG2	clay	16-17th	white	62.7	1.4	23.1	0.5	2.0	3.1	2.0	<0.05	<0.05	<0.05	1.0	<0.05	0.2	<0.05	0.1	96.0
BG11	clay	17th	white	59.9	1.4	23.2	0.5	2.1	3.4	0.8	<0.05	<0.05	<0.05	0.5	<0.05	0.2	<0.05	0.1	92.0
Lead glazes																			
sample	ceramic body	century	colour	SiO₂	Al₂O₃	PbO	MgO	CaO	Na₂O	K₂O	SnO₂	Cr₂O₃	MnO₂	Fe₂O₃	CoO	CuO	ZnO	TiO₂	Sum
BG14	clay	17th	green	38.0	4.6	48.1	0.3	1.9	0.2	0.9	0.2	<0.05	<0.05	1.3	<0.05	1.7	<0.05	0.3	97.3
BG26	clay	18th	ochre	37.5	6.5	49.3	0.9	1.6	0.5	0.9	<0.05	<0.05	0.1	2.7	<0.05	0.4	<0.05	0.4	100.5
BG21	clay	17/18th	beige	39.6	3.5	51.3	0.2	1.4	0.1	0.7	0.1	<0.05	<0.05	1.3	<0.05	0.3	<0.05	0.4	98.7
BG25	clay	18th	beige	35.1	8.3	53.1	0.4	1.5	0.1	0.5	<0.05	<0.05	<0.05	1.1	<0.05	0.3	<0.05	0.3	100.7
BG18	clay	17th	dark green	31.0	5.9	55.9	0.3	0.6	0.2	0.3	<0.05	<0.05	<0.05	1.2	<0.05	3.0	<0.05	0.3	98.6
BG23	clay	17/18th	ochre	34.2	3.7	56.3	0.6	1.6	0.3	0.5	<0.05	<0.05	0.1	1.6	<0.05	0.3	<0.05	0.3	99.2
BG15	clay	17th	green	33.5	2.5	56.3	0.3	1.4	0.2	0.4	0.3	<0.05	<0.05	0.9	0.1	1.4	<0.05	0.2	97.3
BG4	clay	16-17th	green	31.6	3.5	56.5	0.5	2.9	0.3	0.7	0.2	<0.05	<0.05	0.6	<0.05	1.3	<0.05	0.2	98.2

sample	ceramic body	century	colour	SiO$_2$	Al$_2$O$_3$	PbO	MgO	CaO	Na$_2$O	K$_2$O	SnO$_2$	Cr$_2$O$_3$	MnO$_2$	Fe$_2$O$_3$	CoO	CuO	ZnO	TiO$_2$	Sum
BG20	clay	17th	green	27.7	5.5	57.3	0.3	1.9	0.2	0.4	0.2	<0.05	<0.05	1.9	<0.05	2.3	<0.05	0.3	97.8
BG27	clay	18th	green	30.7	4.3	57.7	0.3	1.3	0.1	0.4	0.3	<0.05	<0.05	1.2	<0.05	4.5	<0.05	0.2	101.0
BG16	clay	17th	black	34.1	2.1	57.9	0.3	1.3	0.2	0.3	0.2	<0.05	<0.05	0.8	<0.05	1.5	<0.05	0.1	98.6
BG5	clay	16-17th	ochre	28.5	8.2	59.0	0.4	0.4	0.1	0.2	<0.05	<0.05	<0.05	2.0	<0.05	<0.05	<0.05	0.6	99.4
BG9	clay	16-17th	dark green	29.7	3.6	59.9	0.2	1.5	0.2	0.3	0.1	<0.05	<0.05	0.6	<0.05	3.9	0.1	0.2	100.3
BG6	clay	14-15th	green	30.3	6.3	60.0	0.1	1.3	0.1	0.4	<0.05	<0.05	<0.05	0.3	<0.05	1.4	<0.05	0.1	100.3
BG10	clay	16-17th	ochre	27.1	6.5	60.0	0.7	0.7	0.4	0.8	<0.05	<0.05	0.1	2.6	<0.05	0.2	<0.05	0.3	99.1
BG8	clay	14-15th	light green	32.0	2.7	60.1	0.2	1.1	0.1	0.2	<0.05	<0.05	<0.05	0.4	<0.05	0.3	<0.05	0.2	97.1
BG24	clay	17/18th	dark green	29.5	2.7	60.8	0.4	0.8	0.2	0.3	<0.05	<0.05	<0.05	1.2	<0.05	2.3	<0.05	0.1	98.4
BG19	clay	17th	beige	31.0	2.8	61.0	0.2	1.8	0.1	0.3	<0.05	<0.05	<0.05	0.7	<0.05	0.3	<0.05	0.1	98.2
BG7	clay	14-15th	ochre	32.2	1.9	63.1	0.3	1.0	0.1	0.2	<0.05	<0.05	<0.05	0.7	<0.05	0.1	0.1	0.2	99.9
BG22	clay	17/18th	green	29.3	1.6	64.2	0.3	1.2	0.1	0.2	0.1	<0.05	<0.05	0.6	<0.05	1.2	<0.05	0.1	98.7
BG17	clay	17th	ochre	17.1	4.3	72.1	0.3	0.3	0.2	0.5	<0.05	<0.05	<0.05	2.2	<0.05	0.1	<0.05	0.2	97.2
Zar1	clay	12th	ochre	24.4	5.8	64.1	0.6	0.4	0.4	0.6	0.0	0.0	0.0	2.2	n.d.	0.0	n.d.	0.3	98.7
Zar2	clay	12th	ochre	21.5	4.7	69.8	0.5	0.5	0.4	0.5	0.0	0.0	0.0	1.8	n.d.	0.0	n.d.	0.3	99.9
Zar3	clay	12th	ochre	22.0	4.8	69.3	0.5	0.5	0.2	0.4	0.0	0.0	0.0	2.1	n.d.	0.1	n.d.	0.3	99.9
Zar4	clay	12th	ochre	32.0	6.7	55.5	0.7	1.2	0.3	0.8	0.1	0.0	0.0	3.2	n.d.	0.0	n.d.	0.5	100.7
Zar5	clay	12th	ochre	32.4	7.1	54.6	0.8	0.5	0.5	0.9	0.0	0.0	0.1	2.9	n.d.	0.0	n.d.	0.4	99.9
Zar6	clay	12th	ochre	26.5	5.8	62.7	0.6	0.6	0.4	0.6	0.0	0.0	0.0	2.4	n.d.	0.0	n.d.	0.4	99.8
Zar7	clay	12th	ochre	26.9	5.8	62.4	0.6	0.7	0.4	0.6	0.0	0.0	0.0	2.5	n.d.	0.0	n.d.	0.4	100.1
Zar8	clay	12th	ochre	28.0	6.1	60.9	0.6	0.7	0.3	0.7	0.0	0.0	0.0	2.6	n.d.	0.0	n.d.	0.4	100.1
Zar9	clay	12th	ochre	29.1	6.3	59.2	0.7	0.7	0.4	0.7	0.0	0.0	0.0	2.7	n.d.	0.0	n.d.	0.4	100.1

sample	ceramic body	century	colour	SiO$_2$	Al$_2$O$_3$	PbO	MgO	CaO	Na$_2$O	K$_2$O	SnO$_2$	Cr$_2$O$_3$	MnO$_2$	Fe$_2$O$_3$	CoO	CuO	ZnO	TiO$_2$	Sum
Zar10	clay	12th	ochre	28.6	6.2	59.9	0.7	0.6	0.4	0.7	0.0	0.0	0.0	2.6	n.d.	0.0	n.d.	0.4	100.0
Zar1	clay	12th	ochre	24.4	5.8	64.1	0.6	0.4	0.4	0.6	0.0	0.0	0.0	2.2	n.d.	0.0	n.d.	0.3	98.7

5.9 Moroccan glazes

As can be seen in figure 33, the samples of Moroccan sites all show high contents of PbO, generally above 35 wt%. Na_2O and MgO values are commonly below 1 wt%, the CaO contents are in the majority below 4 wt% and the K_2O values below 3 wt%.

The Na_2O/K_2O ratios of the samples are generally between 0.4 and 0.8, but scatter up to 2.6. In both, alkali and alkali earth contents, a rough internal correlation is observed (Na_2O-K_2O and CaO-MgO, fig.34).
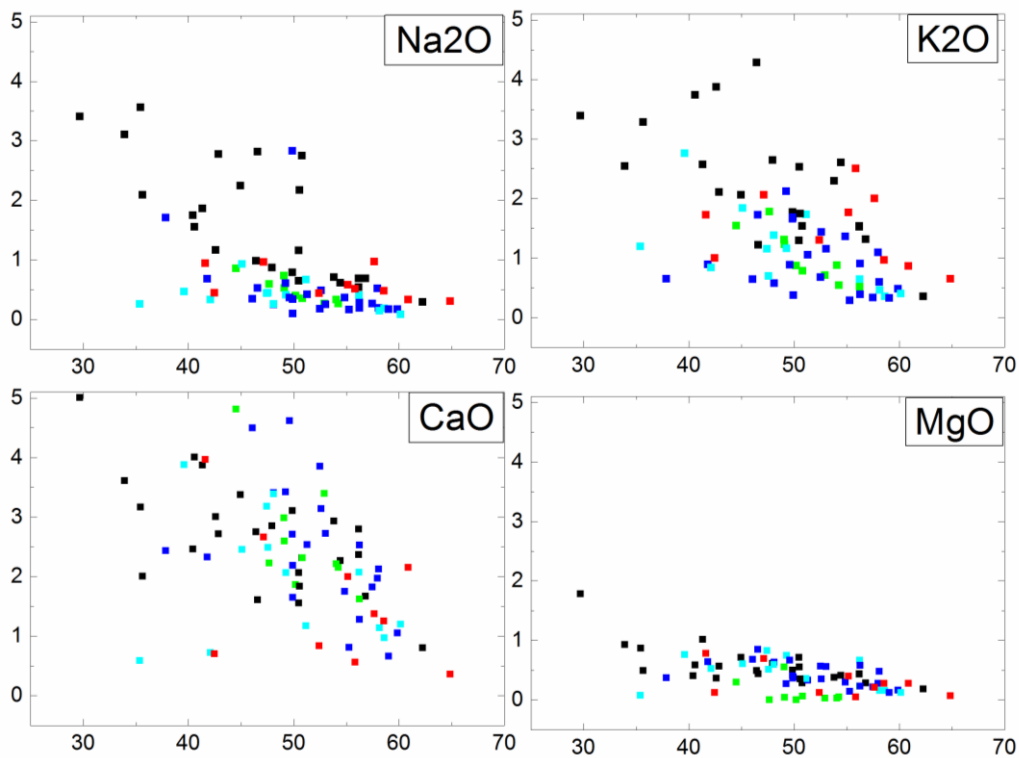
Figure 33: Plots of alkali and alkali earth contents versus PbO content in the samples of different sites in Morocco. The black data points are glazes from Necropolis Chellah, Marinid School, and madrassa Abu Al Hassan, blue data points are from the compositions of glazes from the madrassas Bou Inania in Meknes and Fes, and the red data points represent the glazes from the Saadian tombs in Marrakesh. Green dots belong to the glazes from Tangier (Sultans Palace and fountain). Finally, the turquoise ones represent the glazes from the mausoleum in Meknes.

The ZnO contents of the Moroccan glazes are with 0.3-0.4 wt% slightly enhanced, which is most obvious in the samples from the fountain and the sultan´s palace in Tangier. Similar ZnO contents are observed in Afghan samples. The older samples from the Marinid period of the 14th century (madrassa Abu Al Hassan, Marinid School in Salé and Necropolis Chellah in Rabat, near Salé), differ from the rest of Moroccan samples in alkali and alkali oxide contents. With 0.3-3.6 wt% Na_2O and 0.2-1.8 wt% MgO they have higher values and higher scattering than the rest with <1 wt%. The same tendency is observed for the K_2O higher contents of 0.4-6.0 wt% in Rabat and Salé´s samples in contrast to 0.3-2.9 wt% K_2O in the remaining samples. A few samples from Salé (madrassa Abu Al Hassan, Marinid School) and Fes (madrassa Bou Inania) show higher CaO values around 5 wt% or even up to 11.2 wt% (madrassa Abu Al Hassan in Salé).
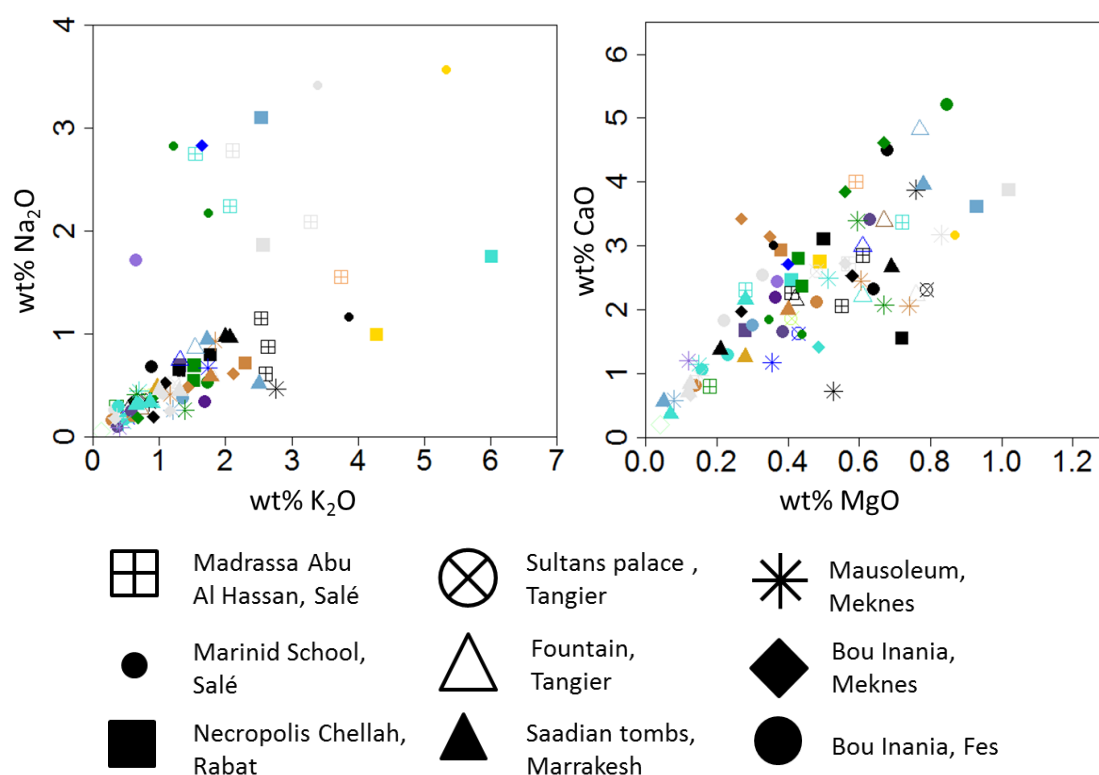
Figure 34: Correlation of element contents of alkali (left) and alkali earth oxides (right). The samples of the Marinid School and madrassa Abu Al Hassanin Salé and the Necropolis Chellah in Rabat show a wider scatter of Na_2O values. The colours of the data points represent the colours of the glazes.

Table 16: Analyses of Moroccan tile glazes in wt%. The abbreviations are the following: Sal for the madrassa Abu al Hassan in Salé, Nec for the necropolis Chellah in Rabat, Sul for the Sultans palace in Tangier, Bru for the nearby fountain, Ina for the madrassa Bou Inania in Fes, Mau for the mausoleum of Moulay Ismail in Meknes, InM for the madrassa Bou Inania in Meknes, Sad for the Saadian tombs in Marrakesh, and Eco for a school building in Salé. All values are averages from at least 5 single measurements, the fields with n.d. are not determined. Cr_2O_3 and TiO_2 are not listed, because of values consistently below detection limit.

sample	ceramic body	century	colour	SiO_2	Al_2O_3	PbO	MgO	CaO	Na_2O	K_2O	SnO_2	MnO_2	Fe_2O_3	CoO	CuO	ZnO	P_2O_5	SO_3	Cl	Sum
Lead glazes																				
1 Sal	quartz	14th	black	33.3	1.2	48.1	0.6	3.4	0.3	0.6	10.8	1.3	0.7	<0.05	<0.05	<0.05	n.d.	<0.05	<0.05	100.3
2 Sal	quartz	14th	turquoise	36.3	0.8	51.3	0.3	2.5	0.4	1.1	6.8	<0.05	0.6	<0.05	<0.05	<0.05	n.d.	<0.05	<0.05	100.0
3 Sal	quartz	14th	white	34.4	0.8	57.5	0.2	1.8	0.3	0.3	3.9	<0.05	0.4	0.1	<0.05	0.3	n.d.	<0.05	<0.05	100.0
5 Sal	quartz	14th	ochre	38.5	1.8	47.1	0.7	4.1	0.3	0.6	1.0	1.2	6.0	<0.05	<0.05	<0.05	0.1	0.1	<0.05	100.7
6 Sal	quartz	14th	black	32.1	0.7	56.3	0.2	1.3	0.3	0.4	7.6	<0.05	0.3	<0.05	1.0	0.4	n.d.	<0.05	<0.05	100.5
7 Sal	quartz	14th	turquoise	31.2	1.0	37.9	0.4	2.4	1.7	0.7	21.7	2.0	0.7	<0.05	0.1	<0.05	n.d.	<0.05	0.4	100.0
8 Sal	quartz	14th	green	29.8	0.8	55.3	0.1	0.8	0.2	0.3	7.4	0.1	5.0	<0.05	<0.05	<0.05	<0.05	0.1	n.d.	99.5
9 Sal	quartz	14th	white	30.9	0.5	50.0	0.4	1.7	0.1	0.4	11.5	1.3	0.2	<0.05	0.1	<0.05	<0.05	<0.05	<0.05	96.8
10 Sal	quartz	14th	black	39.2	2.4	46.6	0.9	5.2	0.5	1.7	0.8	<0.05	1.2	<0.05	1.8	0.2	<0.05	<0.05	<0.05	100.3
11 Nec	quartz	14th	white	35.5	1.6	49.9	0.4	2.2	0.3	1.7	0.2	2.8	2.0	0.1	0.1	<0.05	<0.05	<0.05	<0.05	96.6
12 Nec	quartz	14th	turquoise	43.7	0.8	47.5	0.8	3.2	0.4	1.2	2.7	<0.05	0.3	<0.05	<0.05	0.1	n.d.	<0.05	<0.05	100.7
13 Nec	quartz	14th	light blue	40.9	1.6	48.6	0.6	1.2	0.5	1.2	2.4	1.8	4.8	<0.05	<0.05	0.1	0.1	0.2	<0.05	101.5
14 Nec	quartz	14th	black	34.0	0.8	47.6	0.5	2.5	0.5	0.7	9.2	0.1	0.5	0.1	1.3	<0.05	n.d.	<0.05	<0.05	97.6
15 Nec	quartz	14th	ochre	34.4	0.7	51.2	0.4	1.2	0.7	1.7	6.0	<0.05	0.3	0.5	<0.05	<0.05	n.d.	<0.05	0.1	97.1
16 Nec	quartz	14th	green	41.0	0.9	45.1	0.6	2.5	0.9	1.8	0.7	<0.05	5.8	<0.05	<0.05	0.1	n.d.	<0.05	<0.05	98.9
17 Nec	quartz	14th	purple	40.1	4.7	48.1	0.6	3.4	0.3	1.4	0.5	<0.05	1.2	<0.05	<0.05	<0.05	n.d.	<0.05	<0.05	100.1

Results of EPMA analysis

sample	ceramic body	century	colour	SiO$_2$	Al$_2$O$_3$	PbO	MgO	CaO	Na$_2$O	K$_2$O	SnO$_2$	MnO$_2$	Fe$_2$O$_3$	CoO	CuO	ZnO	P$_2$O$_5$	SO$_3$	Cl	Sum
18 Nec	quartz	14th	green	38.7	2.8	40.6	0.6	3.7	0.4	2.9	0.1	1.8	8.6	<0.05	0.1	0.1	0.1	0.3	<0.05	100.8
19 Nec	quartz	14th	yellow	33.9	0.9	58.6	0.2	1.0	0.2	0.4	0.8	<0.05	3.9	<0.05	<0.05	0.2	<0.05	<0.05	<0.05	99.5
20 Nec	quartz	14th	black	37.9	1.3	49.3	0.7	2.1	0.4	1.2	0.4	1.3	5.2	0.1	0.1	0.1	<0.05	<0.05	n.d.	99.6
21 Sul	quartz	late 17th	black	27.2	0.6	58.2	0.2	1.1	0.1	0.5	10.4	<0.05	0.4	<0.05	0.9	<0.05	<0.05	0.4	n.d.	100.0
22 Sul	quartz	late 17th	dark green	33.4	0.5	60.2	0.1	1.2	0.1	0.4	1.8	0.9	0.3	<0.05	0.1	0.1	<0.05	<0.05	<0.05	99.1
23 Sul	quartz	late 17th	white	19.1	0.3	35.4	0.1	0.6	0.3	1.2	41.2	<0.05	0.5	0.1	<0.05	0.1	<0.05	<0.05	n.d.	98.7
24 Sul	quartz	late 17th	blue	34.9	1.5	56.3	0.7	2.1	0.4	0.7	0.9	0.1	0.5	<0.05	2.1	<0.05	<0.05	0.3	n.d.	100.4
25 Bru	quartz	late 17th	black	33.4	0.8	59.1	0.1	0.7	0.2	0.3	0.8	<0.05	4.3	<0.05	<0.05	0.3	<0.05	<0.05	<0.05	99.4
26 Bru	quartz	late 17th	ochre	36.6	1.4	52.6	0.4	3.1	0.5	1.4	<0.05	<0.05	3.9	<0.05	0.2	0.1	<0.05	<0.05	<0.05	99.8
27 Bru	quartz	late 17th	white	35.7	0.8	49.9	0.4	2.7	2.8	1.7	2.9	<0.05	1.1	0.1	<0.05	0.8	<0.05	<0.05	1.0	99.8
28 Bru	quartz	late 17th	turquoise	32.2	2.7	56.3	0.6	2.5	0.2	0.9	0.4	<0.05	3.9	<0.05	<0.05	0.1	<0.05	<0.05	n.d.	99.3
29 Bru	quartz	late 17th	light blue	31.3	1.0	53.6	0.5	1.4	0.3	0.7	9.9	<0.05	0.3	<0.05	0.7	0.3	0.1	0.3	<0.05	100.2
30 Bru	quartz	late 17th	blue	37.3	1.8	52.5	0.6	3.9	0.2	0.7	0.2	<0.05	1.0	<0.05	1.5	0.1	<0.05	<0.05	<0.05	99.6
31 Ina	quartz	14th	turquoise	37.8	0.8	53.0	0.6	2.7	0.3	1.2	4.0	<0.05	0.5	0.1	0.1	<0.05	<0.05	0.4	0.1	101.4
32 Ina	quartz	14th	black	37.6	3.1	49.6	0.7	4.6	0.4	0.9	0.7	<0.05	1.4	<0.05	1.2	<0.05	0.1	0.2	0.0	100.4
33 Ina	quartz	14th	light blue	33.1	2.3	58.0	0.3	2.0	0.5	1.1	0.1	1.7	1.0	<0.05	0.5	<0.05	<0.05	0.1	0.1	100.6
34 Ina	quartz	14th	ochre	40.4	0.9	49.3	0.3	3.4	0.6	2.1	<0.05	<0.05	3.7	<0.05	0.1	<0.05	0.1	0.3	0.1	100.9

sample	ceramic body	century	colour	SiO$_2$	Al$_2$O$_3$	PbO	MgO	CaO	Na$_2$O	K$_2$O	SnO$_2$	MnO$_2$	Fe$_2$O$_3$	CoO	CuO	ZnO	P$_2$O$_5$	SO$_3$	Cl	Sum
35 Ina	quartz	14th	purple	46.1	2.0	41.6	0.8	4.0	0.9	1.7	1.9	<0.05	0.7	0.2	<0.05	<0.05	n.d.	<0.05	<0.05	99.8
36 Ina	quartz	14th	white	31.7	0.4	52.4	0.1	0.8	0.4	1.3	11.8	<0.05	0.2	<0.05	<0.05	0.1	n.d.	<0.05	<0.05	99.4
37 Ina	quartz	14th	white	34.8	1.7	47.1	0.7	2.7	1.0	2.1	0.6	1.7	7.5	<0.05	<0.05	<0.05	n.d.	<0.05	0.2	99.1
38 Ina	quartz	14th	black	35.9	1.5	55.2	0.4	2.0	0.6	1.8	0.1	<0.05	2.7	<0.05	<0.05	0.1	n.d.	<0.05	0.9	99.9
39 Ina	quartz	14th	turquoise	32.3	1.0	60.9	0.3	2.2	0.3	0.9	1.0	<0.05	0.5	<0.05	0.8	<0.05	<0.05	<0.05	<0.05	100.1
40 Ina	quartz	14th	purple	32.4	1.7	58.6	0.3	1.3	0.5	1.0	0.7	<0.05	4.7	<0.05	<0.05	0.1	<0.05	<0.05	0.9	100.7
41 Ina	quartz	14th	ochre	38.0	0.5	55.9	0.1	0.6	0.5	2.5	1.5	<0.05	0.5	0.2	0.1	<0.05	<0.05	0.2	n.d.	100.4
42 Ina	quartz	14th	purple	28.1	0.2	64.9	0.1	0.4	0.3	0.7	3.0	<0.05	0.3	<0.05	1.5	<0.05	<0.05	<0.05	n.d.	99.2
43 Ina	quartz	14th	green	24.2	0.4	42.5	0.1	0.7	0.5	1.0	32.0	0.1	0.3	0.1	0.1	<0.05	<0.05	0.2	n.d.	102.0
44 Ina	quartz	14th	purple	37.2	1.3	57.7	0.2	1.4	1.0	2.0	0.4	1.3	0.5	<0.05	0.1	<0.05	0.1	0.3	n.d.	103.1
45 Mau	quartz	18th	white	36.1	0.8	50.6	0.4	1.8	2.2	1.7	2.2	0.1	0.5	<0.05	3.1	0.1	<0.05	<0.05	0.5	99.8
46 Mau	quartz	18th	black	40.7	1.0	42.6	0.4	3.0	1.2	3.9	0.1	5.5	0.6	<0.05	<0.05	0.1	<0.05	<0.05	0.1	99.1
47 Mau	quartz	18th	turquoise	50.7	2.0	29.7	1.8	5.0	3.4	3.4	1.9	0.1	1.1	<0.05	0.1	0.1	<0.05	<0.05	0.3	99.5
48 Mau	quartz	18th	blue	34.0	1.2	46.6	0.4	1.6	2.8	1.2	6.5	<0.05	0.7	<0.05	3.9	<0.05	<0.05	<0.05	1.3	99.9
49 Mau	quartz	18th	ochre	44.1	4.6	35.5	0.9	3.2	3.6	5.3	1.2	<0.05	1.4	<0.05	0.1	<0.05	<0.05	<0.05	0.7	100.0
50 Mau	quartz	18th	green	33.3	1.2	48.1	0.6	3.4	0.3	0.6	10.8	1.3	0.7	<0.05	<0.05	<0.05	<0.05	<0.05	0.7	100.3
51 Mau	quartz	18th	black	36.3	0.8	51.3	0.3	2.5	0.4	1.1	6.8	<0.05	0.6	<0.05	<0.05	<0.05	<0.05	<0.05	<0.05	100.0
52 Mau	quartz	18th	white	34.4	0.8	57.5	0.2	1.8	0.3	0.3	3.9	<0.05	0.4	0.1	<0.05	0.3	<0.05	<0.05	<0.05	100.0
53 Mau	quartz	18th	ochre	38.5	1.8	47.1	0.7	4.1	0.3	0.6	1.0	1.2	6.0	<0.05	<0.05	<0.05	0.1	0.1	<0.05	100.7
54 Mau	quartz	18th	turquoise	32.1	0.7	56.3	0.2	1.3	0.3	0.4	7.6	<0.05	0.3	<0.05	1.0	0.4	<0.05	<0.05	<0.05	100.5
55 Mau	quartz	18th	purple	31.2	1.0	37.9	0.4	2.4	1.7	0.7	21.7	2.0	0.7	<0.05	0.1	<0.05	<0.05	<0.05	0.4	100.0
56 Mau	quartz	18th	light blue	29.8	0.8	55.3	0.1	0.8	0.2	0.3	7.4	0.1	5.0	<0.05	<0.05	<0.05	<0.05	0.1	n.d.	99.5
56.1 Mau	quartz	18th	green	30.9	0.5	50.0	0.4	1.7	0.1	0.4	11.5	1.3	0.2	<0.05	0.1	<0.05	<0.05	<0.05	<0.05	96.8

Results of EPMA analysis

sample	ceramic body	century	colour	SiO$_2$	Al$_2$O$_3$	PbO	MgO	CaO	Na$_2$O	K$_2$O	SnO$_2$	MnO$_2$	Fe$_2$O$_3$	CoO	CuO	ZnO	P$_2$O$_5$	SO$_3$	Cl	Sum
57 InM	quartz	14th	white	39.2	2.4	46.6	0.9	5.2	0.5	1.7	0.8	<0.05	1.2	<0.05	1.8	0.2	<0.05	<0.05	<0.05	100.3
58 InM	quartz	14th	ochre	35.5	1.6	49.9	0.4	2.2	0.3	1.7	0.2	2.8	2.0	0.1	0.1	<0.05	<0.05	<0.05	<0.05	96.6
59 InM	quartz	14th	blue	43.7	0.8	47.5	0.8	3.2	0.4	1.2	2.7	<0.05	0.3	<0.05	<0.05	0.1	<0.05	<0.05	0.5	100.7
60 InM	quartz	14th	black	40.9	1.6	48.6	0.6	1.2	0.5	1.2	2.4	1.8	4.8	<0.05	<0.05	0.1	0.1	0.2	<0.05	101.5
61 InM	quartz	14th	turquoise	34.0	0.8	47.6	0.5	2.5	0.5	0.7	9.2	0.1	0.5	0.1	1.3	<0.05	0.1	<0.05	<0.05	97.6
62 InM	quartz	14th	green	34.4	0.7	51.2	0.4	1.2	0.7	1.7	6.0	<0.05	0.3	0.5	<0.05	<0.05	<0.05	<0.05	0.1	97.1
62.1 InM	quartz	14th	white	41.0	0.9	45.1	0.6	2.5	0.9	1.8	0.7	<0.05	5.8	<0.05	<0.05	0.1	<0.05	<0.05	<0.05	98.9
62.2 InM	quartz	14th	green	40.1	4.7	48.1	0.6	3.4	0.3	1.4	0.5	<0.05	1.2	<0.05	<0.05	<0.05	<0.05	<0.05	<0.05	100.1
62.3 InM	quartz	14th	black	38.7	2.8	40.6	0.6	3.7	0.4	2.9	0.1	1.8	8.6	<0.05	0.1	0.1	0.1	0.3	<0.05	100.8
62.4 InM	quartz	14th	ochre	33.9	0.9	58.6	0.2	1.0	0.2	0.4	0.8	<0.05	3.9	<0.05	<0.05	0.2	<0.05	<0.05	<0.05	99.5
63 Sad	quartz	16th	light blue	37.9	1.3	49.3	0.7	2.1	0.4	1.2	0.4	1.3	5.2	0.1	0.1	0.1	<0.05	<0.05	<0.05	99.6
64 Sad	quartz	16th	white	27.2	0.6	58.2	0.2	1.1	0.1	0.5	10.4	<0.05	0.4	<0.05	0.9	<0.05	<0.05	0.4	<0.05	100.0
66 Sad	quartz	16th	black	33.4	0.5	60.2	0.1	1.2	0.1	0.4	1.8	0.9	0.3	<0.05	0.1	0.1	<0.05	<0.05	<0.05	99.1
67 Sad	quartz	16th	ochre	19.1	0.3	35.4	0.1	0.6	0.3	1.2	41.2	<0.05	0.5	0.1	<0.05	0.1	<0.05	<0.05	<0.05	98.7
68 Sad	quartz	16th	turquoise	34.9	1.5	56.3	0.7	2.1	0.4	0.7	0.9	0.1	0.5	<0.05	2.1	<0.05	0.1	0.3	<0.05	100.4
69 Sad	quartz	16th	yellow	33.4	0.8	59.1	0.1	0.7	0.2	0.3	0.8	<0.05	4.3	<0.05	<0.05	0.3	<0.05	<0.05	<0.05	99.4
70 Sad	quartz	16th	light blue	36.6	1.4	52.6	0.4	3.1	0.5	1.4	<0.05	<0.05	3.9	<0.05	0.2	0.1	<0.05	<0.05	<0.05	99.8
71 Sad	quartz	16th	turquoise	35.7	0.8	49.9	0.4	2.7	2.8	1.7	2.9	<0.05	1.1	0.1	0.3	0.8	<0.05	<0.05	1.0	99.8
72 Sad	quartz	16th	white	32.2	2.7	56.3	0.6	2.5	0.2	0.9	0.4	<0.05	3.9	<0.05	<0.05	0.1	<0.05	<0.05	<0.05	99.3
73 Sad	quartz	16th	black	31.3	1.0	53.6	0.5	1.4	0.3	0.7	9.9	<0.05	0.3	<0.05	0.7	0.3	0.1	0.3	<0.05	100.2
74 Eco	quartz	14th	green	37.3	1.8	52.5	0.6	3.9	0.2	0.7	0.2	<0.05	1.0	<0.05	1.5	0.1	<0.05	<0.05	<0.05	99.6
75 Eco	quartz	14th	black	37.8	0.8	53.0	0.6	2.7	0.3	1.2	4.0	<0.05	0.5	0.1	0.1	<0.05	<0.05	0.4	<0.05	101.4
76 Eco	quartz	14th	white	37.6	3.1	49.6	0.7	4.6	0.4	0.9	0.7	<0.05	1.4	<0.05	1.2	<0.05	0.1	0.2	1.0	100.4

Results of EPMA analysis

sample	ceramic body	century	colour	SiO$_2$	Al$_2$O$_3$	PbO	MgO	CaO	Na$_2$O	K$_2$O	SnO$_2$	MnO$_2$	Fe$_2$O$_3$	CoO	CuO	ZnO	P$_2$O$_5$	SO$_3$	Cl	Sum
77 Eco	quartz	14th	green	33.1	2.3	58.0	0.3	2.0	0.5	1.1	0.1	1.7	1.0	<0.05	0.5	<0.05	<0.05	0.1	0.6	100.6
78 Eco	quartz	14th	yellow	40.4	0.9	49.3	0.3	3.4	0.6	2.1	<0.05	<0.05	3.7	<0.05	0.1	<0.05	0.1	0.3	0.9	100.9

6 Processing temperature

In this chapter, the processing temperatures of all sampled glazes are calculated, according to the approach of Lakatos *et al.* (1972). After a short overview over the whole data set, the groups of localities and epochs are separately described. As reasonable viscosity for a glassy material to form a glaze layer a value of $\eta = 10^4$ P is assumed (Bezborodov, 1975). This viscosity is higher than the viscosity necessary for pouring the glass melt (10^3 P), but on the lower edge of tenacity for the forming of glass (Bezborodov, 1975). The model used for viscosity calculation includes the most common oxides of Si, Al, Na, Ca, K, Mg, and Pb, as well as the minor elements, Ba and Zn (chapter 2.1.5, Lakatos *et al.*, 1972). The calculation of Lakatos *et al.* (1972) is chosen, because it integrates considerable contents of lead in contrast to modern glass calculations as done e.g. by Fluegel (2007).
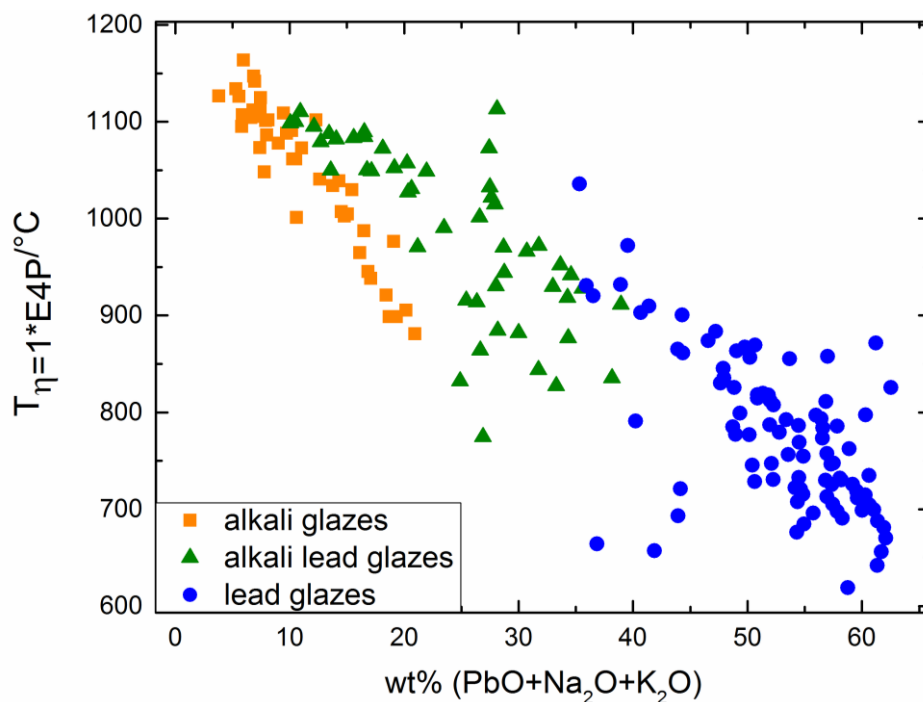
Figure 35: Calculated process temperatures at the viscosity of $\eta = 10^4$ P from the different sites versus the wt% of flux content (PbO + alkali oxides).

The Fulcher-Tammann calculation used by Lakatos *et al.* (1972) is with about 4% rel. error one of the most precise melting temperature estimations for glass (Mauro *et al.*, 2009). The analytical error is much smaller than the calculation error and can be neglected. The error of calculated values is estimated to be 25-50 °C (Mauro *et al.*, 2009). In the investigated set of glazes, Na_2O, K_2O, and PbO contribute the most to the reduction of firing temperature. The content of PbO is treated here as flux, although the intended function might have been a colouring one, especially in green and yellow glazes (chapter 5.3). The calculated ranges of processing temperature are given in table 16, sorted according to their lead content in wt%. Figures 35 and 36 depict the calculated firing temperatures versus the main flux contents. The depiction of firing temperatures in juxtaposition with the mol% of flux components is given in chapter 8.2.
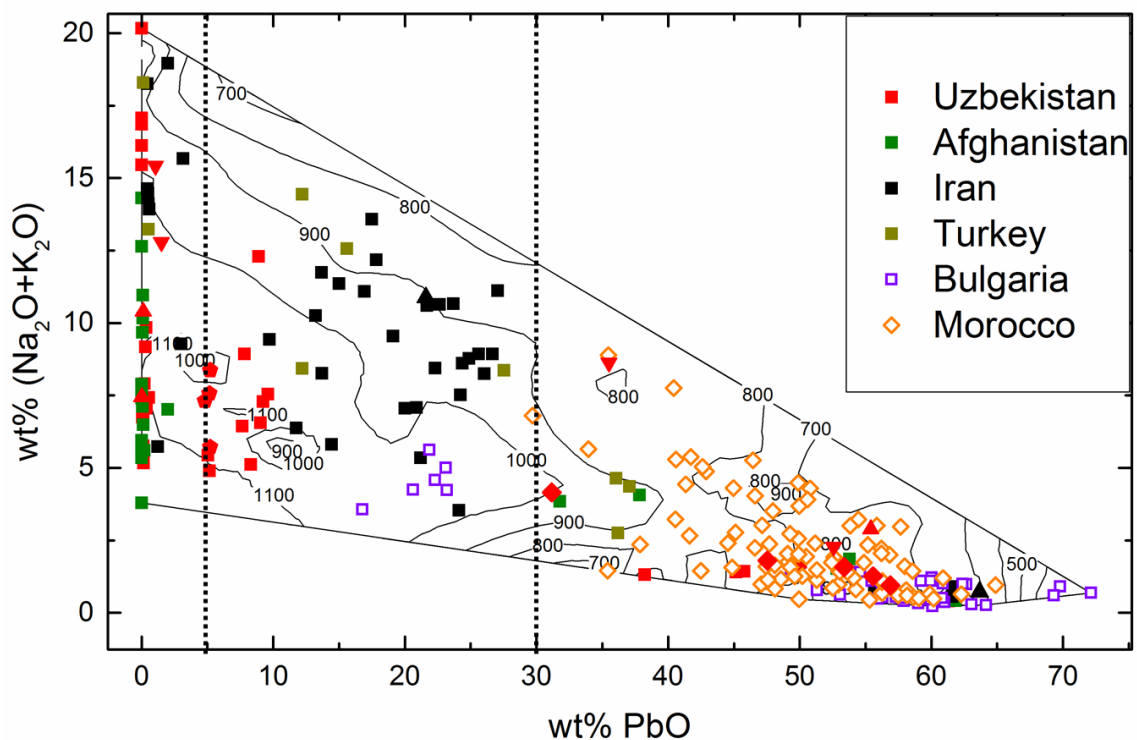
Figure 36: Temperatures at which the glaze reaches a viscosity of $\eta = 10^4$ P. The isotherms are interpolated along equal values of the entirety of proceeding temperatures. The highest processing temperatures of >1100°C results from the subgroup of alkali glazes with low sodium oxide and low total alkali oxide contents of ca. 7 wt% Na_2O+K_2O. High lead contents lead to the lowest heating temperatures around 660 °C.

An overview over the different temperatures with flux contents and locations is depicted in figure 36. The distinction of glazes into alkali, alkali lead, and lead compositions is found in the distribution of processing temperatures (tab.17). The three groups have overlapping ranges of 700-1160 °C for alkali glazes, 810-1100 °C for alkali lead glazes and 440-1100 °C for lead glazes. Because of the wide scattering, the average values of 1040±90 °C, 960±90 °C and 780±110 °C respectively with 1s-standard deviation better mirror the classification. A few of the localities have wide spectra of firing temperatures: especially the Uzbek glazes from the mosque Khoja Zainuddin and the madrassa Mir-i Arab of the 16th century; both have processing temperatures below 700 and above 1100 °C. The lead glazes from the Ottoman Bulgaria also show with 630-860 °C a wide range of temperatures.

Table 17: Overview of the calculated firing temperatures after Lakatos *et al.* (1972) in °C, separated in the three major compositional groups. The abbreviations are Unk for unknown, Afr for Afrasiab, IK for Ishrat Khane, KhZ for Khoja Zainuddin, MMA for madrassa Mir-i Arab, BM for Baland mosque, MAK for madrassa Abdul Aziz Khan, and TiS for Takht-i-Suleiman.

	Uzbekistan							Afgh.	Iran		Turkey	Bulgaria		Mor.
City	Samarkand			Bukhara				Herat	TiS	Isfahan	Konya Kay-seri	Dristra		Various
Building	Afr	Unk.	IK	KhZ	MMA	BM	MAK	Unk.	TiS	Prayer Niche	Ata Hanka	Fortress		Various
Century	10-11th	13th	15th	16th	16th	16th	17th	15-17th	12-13th	20th	13th	11-13th	13-17th	14-18th
T firing Alkali glaze		990-1010		700-1150	1050-1120			1040-1160	880-1140		920-1030			
T firing Alkali lead glaze			810	970-1100			890-1100		820-1070	910	860-1030		1020-1080	
T firing Lead glaze	790-1030	800-830	1090-1100	660-970	690	760		690-960	680-770	670	900-930	710-800	630-860	570-920
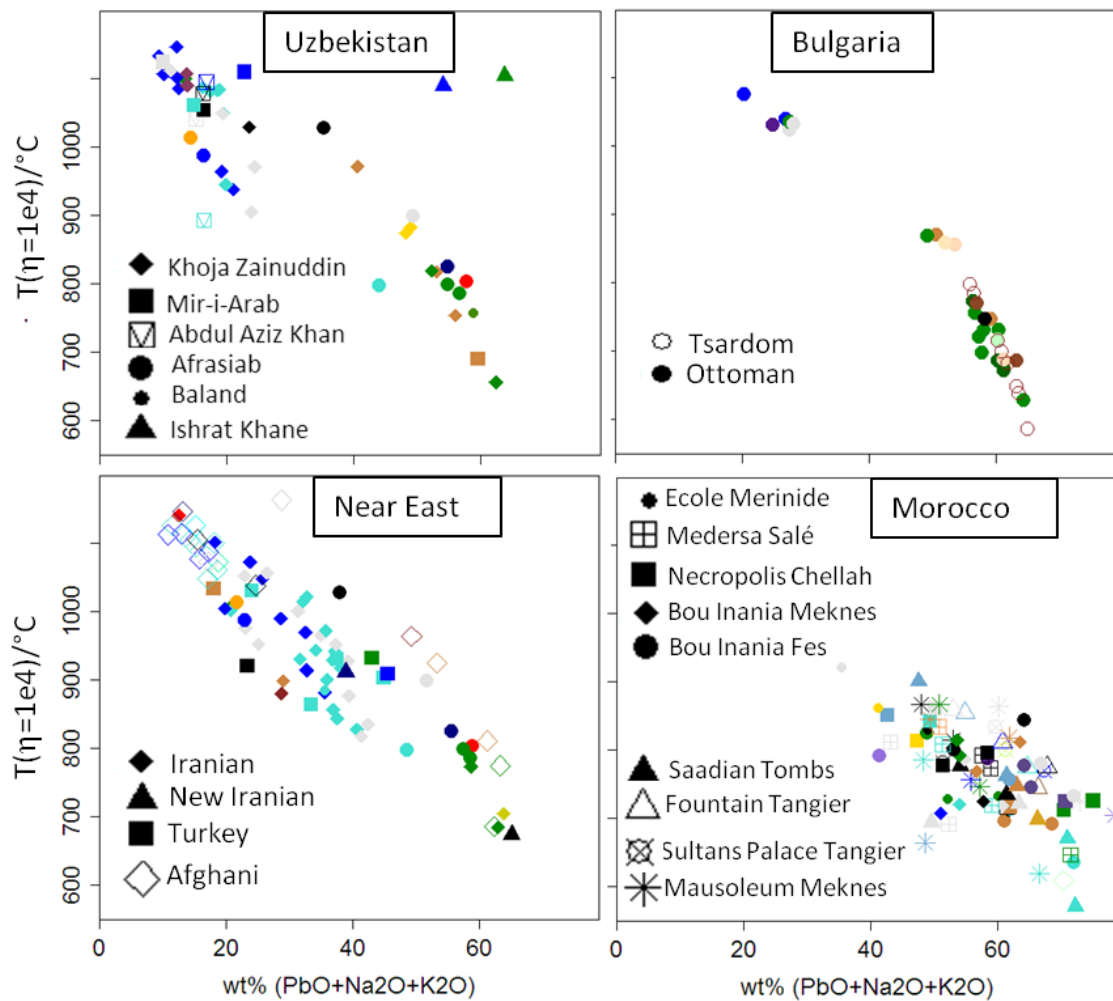
Figure 37: Calculated process temperatures at the viscosity of $\eta=10^4$ P from the different sites versus the flux content (PbO + alkali oxides). Each sample is plotted in its glaze colour.

The glazes from the Second Bulgarian Empire have with 440-800 °C an even larger scattering. The alkali lead samples found in Bulgaria have with 1020-1080 °C a narrower window, differing substantially from the lead glazes. A smaller interval of processing temperatures is also seen in the lead glazes from Samarkand of the 13th century with 800-830 °C and the lead-rich Iranian and Turkish ones with 680-770 °C and 690-960 °C. The lead groups, especially those from the Second Bulgarian Empire and Morocco, have the lowest values (440 °C for Bulgaria and 570 °C for Morocco). Some of the lead samples from Afrasiab show up to 1100 °C process temperatures, due to their high alumina content of ca. 8 wt% Al_2O_3. The lead glazes from the Uzbek mausoleum Ishrat Khane of the 15th century have noticeably high temperatures of 1090-1100 °C, too (fig.37). Firing temperatures of the alkali lead groups of Uzbekistan, Iran, and Turkey with ca. 1070-

1100 °C with 1070-1100°C do not significantly differ from those of the pure alkali group with 1030-1150 °C. This demonstrates that flux properties of PbO take effect primarily at higher percentages.

Uzbek glazes: The alkali and alkali lead group of Uzbek glazes has values between 700 and 1150 °C. Within this range, the sodium-poor alkali glazes have with 1050-1150 °C the highest calculated processing temperatures. These are primarily the alkali glazes from tiles from Bukhara of the 16th- 17th century (fig.38). The temperature range for the lead glazes is between 660 and 900 °C.
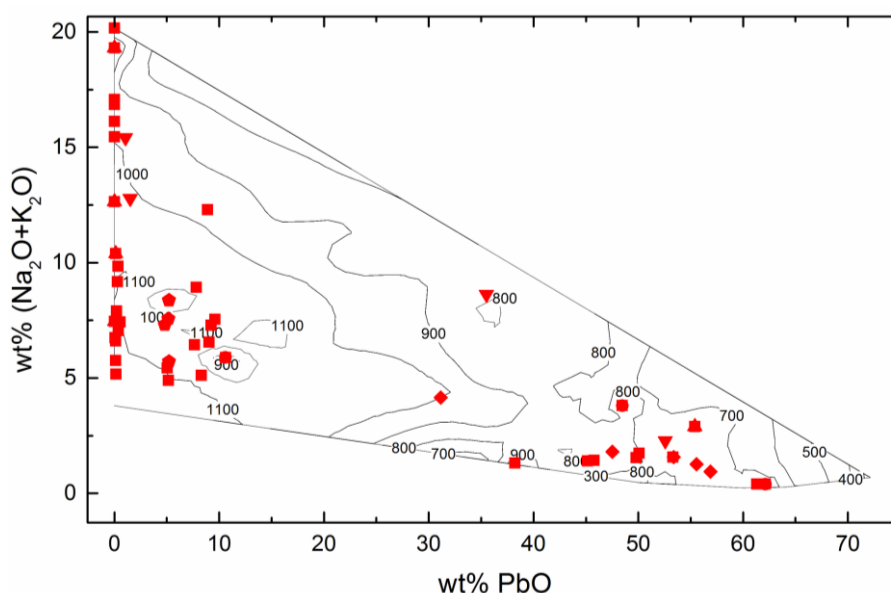
Figure 38: Flux composition of Uzbek glazes with isotherms of theoretical processing temperature. The data points are subdivided into squares (mosque Khoja Zainuddin), circles (Ishrat Khane), triangles top up (madrassa Mir-i Arab), triangles top down (Samarkand), pentagons (madrassa Abdul Aziz Khan), and diamonds (Afrasiab).

Afghan glazes: In the set of Afghan samples, the classification into two groups of alkali and lead glaze can be also observed in the processing temperatures (fig.39). The calculated firing temperatures of the alkali group are between 1040 and 1160 °C. The lead glazes have the lowest calculated firing temperatures at 690-960 °C.
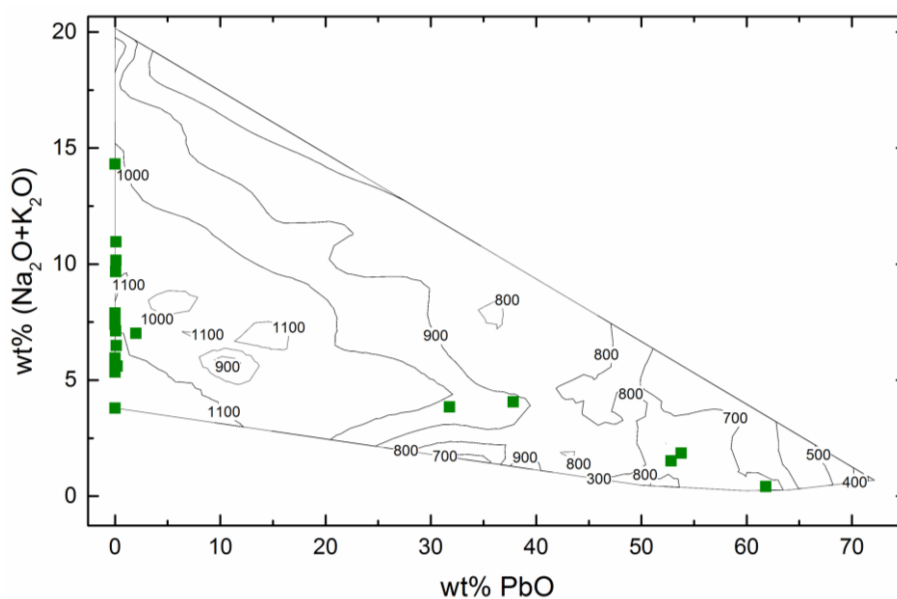
Figure 39: Flux composition of Afghan glazes with isotherms of theoretical processing temperature.

Iranian glazes: In the samples from Iran, alkali and alkali lead glazes have the highest calculated processing temperatures of 880-1140 °C (fig.40). Na_2O and K_2O flux compensate only a part of the missing or reduced PbO content. The highest value of 1140 °C belongs to a glaze with 1.2 wt% PbO and 11.3 wt% Na_2O+K_2O. The glazes of the alkali lead group have with 820-1070 °C the widest range of processing temperatures which is due to the wide range of PbO and alkali contents (9.7-27.1 wt% PbO and 2.5-15.7 wt% Na_2O). The lead glazes have the lowest values of calculated firing temperature with 690-770 °C.

From the two samples from the 20th century, the lead glaze has a calculated process temperature of 670 °C, slightly lower than those of the older Iranian lead glazes. The alkali lead glaze of the 20th century lies with 910 °C within the overall scatter of the Iranian alkali lead group.
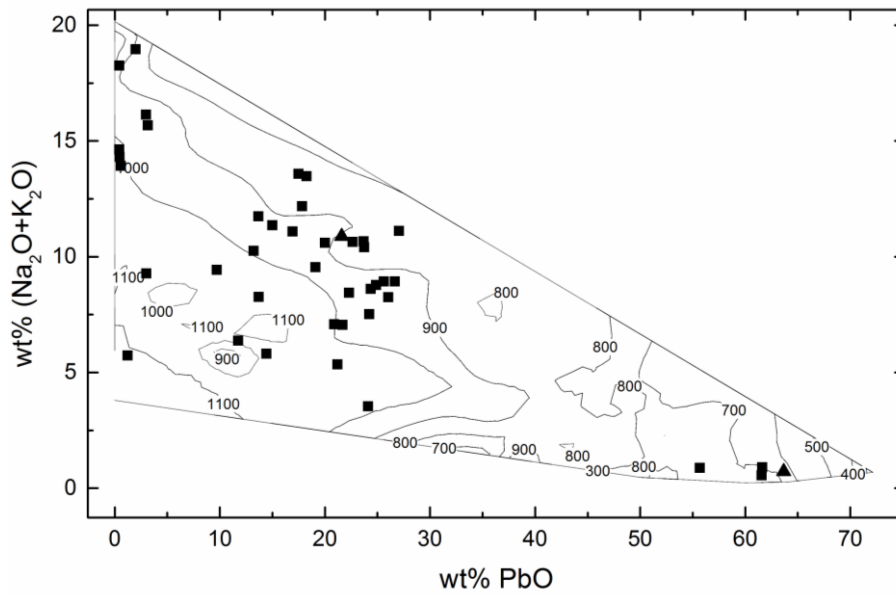
Figure 40: Flux composition of Iranian glazes with isotherms of theoretical processing temperature. The data points are subdivided into squares (Takht-i-Suleiman) and triangles (restoration glazes from Isfahan).

Turkish glazes: The values of calculated firing temperatures show less distinct separation into the three groups of alkali, alkali lead and lead glazes.
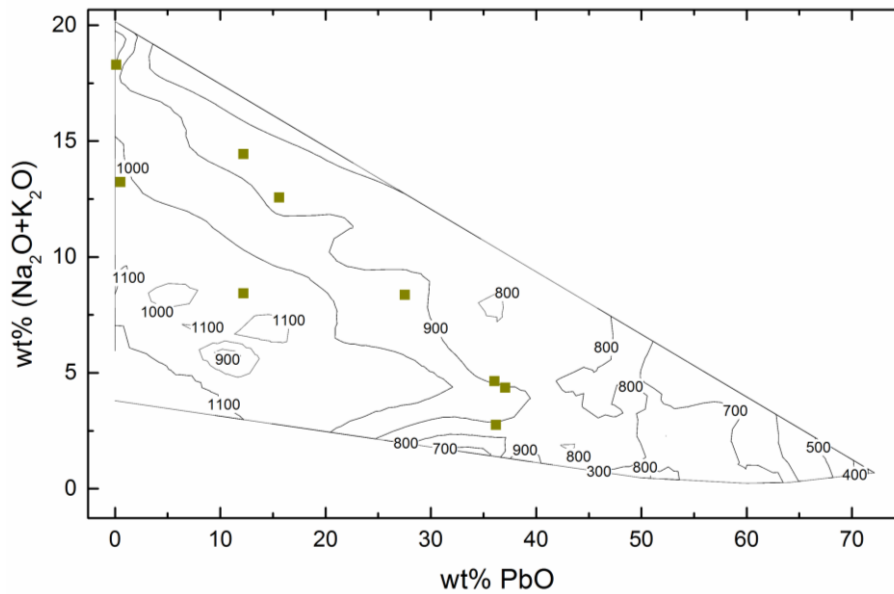
Figure 41: Flux composition of Turkish glazes with isotherms of theoretical processing temperature.

The alkali samples have values down to 920 and up to 1030 °C (fig.41). The alkali lead group with 12.2-27.5 wt% PbO has a very wide scattering of 860-1030 °C. The lead group with 36.0-37.1 wt% PbO shows temperatures of 900-930 °C and is therefore within the region of alkali lead glaze compositions.

Bulgarian glazes: Within the set of Bulgarian samples, the differences between alkali lead and lead compositions are very distinct. In the group of lead glazes, the large distribution of PbO contents leads to a wide range of processing temperatures, down to 680 °C (fig.42). The samples with about 50 wt% PbO give highest calculated values within the lead group of 860-870 °C. The very few and probably imported alkali lead glazes of the Ottoman period show higher processing temperatures of 1020-1080 °C. The glazes of the Second Bulgarian Empire have lead contents and processing temperatures within the scattering of the Ottoman lead glazes.
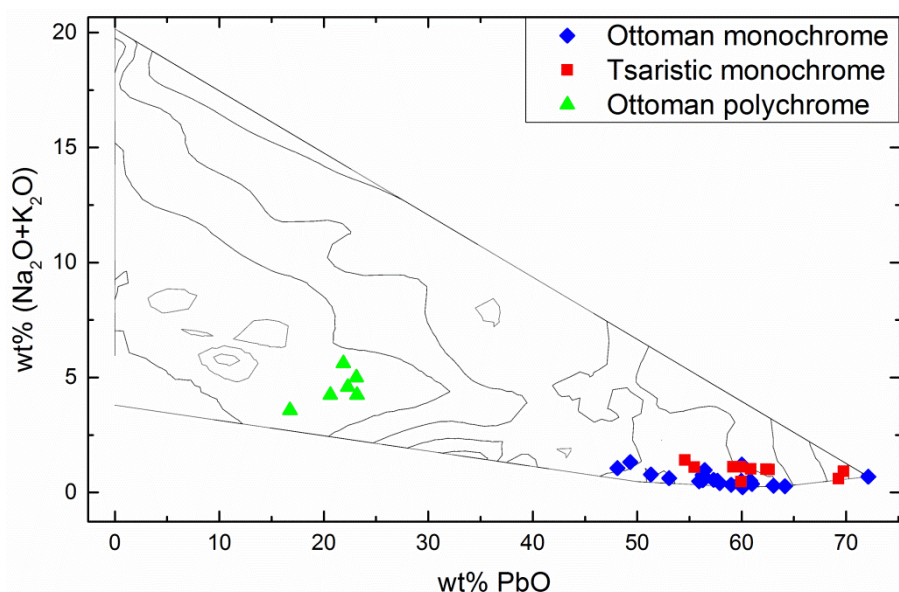
Figure 42: Flux composition of Bulgarian glazes with isotherms of theoretical processing temperature.

Moroccan glazes: The calculated firing temperatures are scarcely higher than 900 °C because of the continuously high or medium lead contents (fig.43). The lowest calculated temperatures at ca. 570°C result from glazes with approximately 60 wt% PbO.

113
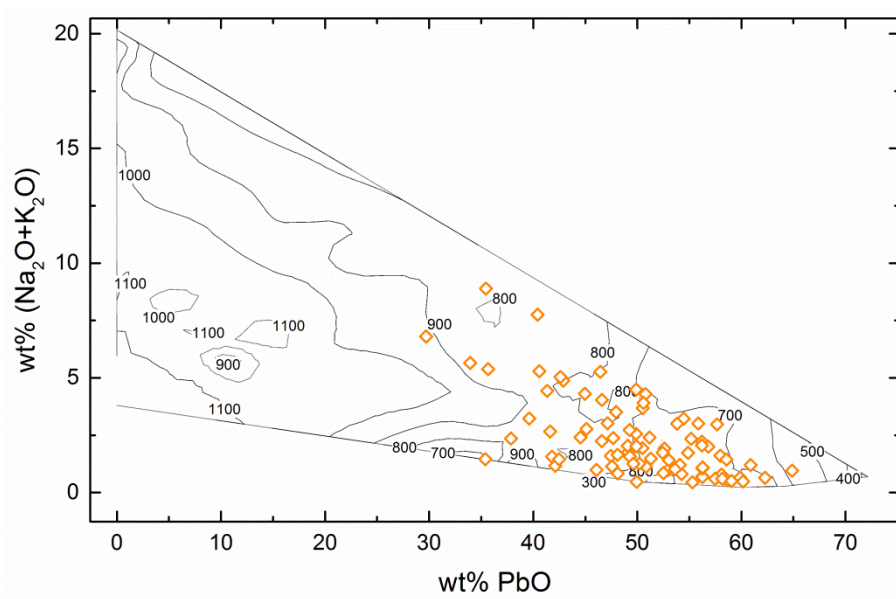
Figure 43: Flux composition of Moroccan glazes with isotherms of theoretical processing temperature.

7 Colouring

This chapter treats the colouring agents in the glazes, comprising the transition metal ions in the glassy matrix and the pigments in the glaze layers. Additionally, the relation between colouring agents and flux compositions of the glazes is considered.

Table 18: EPMA analyses of eight Uzbek glazes from the mosque Khoja Zainuddin as examples for different colours. The ions and relevant matrix components which are responsible for the colouring are highlighted. The resulting colour shade of the transition metal ions is also a result of the valence, the interaction with the matrix composition, the trace elements, and the network position of the transition metal itself. n.d. stands for not determined.

Oxide	KhZ 029	KhZ 164	KhZ 032	KhZ 090	KhZ 133.1	KhZ 135	KhZ 162	KhZ 200
SiO_2	43.44	30.56	65.65	70.01	74.30	63.96	74.65	38.00
Al_2O_3	1.83	0.78	2.22	5.39	3.98	2.53	3.53	1.29
Fe_2O_3	3.36	0.57	0.90	1.76	1.71	0.96	1.71	5.32
MgO	1.14	0.40	2.39	2.42	2.68	2.26	3.32	0.37
CaO	2.36	1.33	4.34	3.56	5.25	4.05	5.78	0.64
CuO	<0.05	1.66	<0.05	0.40	0.19	2.08	<0.05	<0.05
PbO	45.78	61.30	9.61	0.10	0.22	7.28	0.11	50.08
Na_2O	0.74	0.22	4.99	10.25	5.06	8.52	4.52	0.75
K_2O	0.69	0.19	2.55	4.68	2.84	3.41	2.08	0.99
P_2O_5	0.10	<0.05	1.77	<0.05	<0.05	<0.05	0.63	<0.05
Sb_2O_3	<0.05	<0.05	<0.05	<0.05	<0.05	<0.05	<0.05	<0.05
MnO_2	0.06	0.01	<0.05	1.02	<0.05	<0.05	-	<0.05
Mn_2O_3	-	-	-	-	-	-	2.32	-
BaO	0.11	<0.05	<0.05	<0.05	<0.05	<0.05	0.11	<0.05
CoO	<0.05	<0.05	<0.05	<0.05	0.54	<0.05	<0.05	0.09
SnO_2	0.10	<0.05	6.43	<0.05	<0.05	3.02	<0.05	<0.05
TiO_2	0.06	0.00	n.d.	0.10	0.00	0.11	0.17	<0.05
S	<0.05	<0.05	0.11	<0.05	<0.05	<0.05	<0.05	<0.05
Cl	<0.05	<0.05	0.27	<0.05	0.38	0.09	<0.05	<0.05
Sum	97.55	97.65	101.22	99.65	97.16	98.15	98.98	97.70

The transition metal ions occur as oxides of commonly 0.2-4.0 wt% in the samples. The shade of the resulting colour of transition metal oxides depends on the overall matrix composition, on trace elements and on the valence of ions (chapter 2.2.1). The oxidation states of the colouring ions cannot be determined in the EPMA measurements and have to be assigned according to the optical appearing of the glaze. Most of the colours can be assigned to the analysed main compositions and pigments. The black, violet, blue, green, and ochre colours are caused by the network integrated transition metal ions Mn^{4+}, Mn^{3+}, Co^{2+}, Cu^{2+}, and Fe^{3+} (Weyl, 1967). The manganese has different roles, depending on its valence (Bamford, 1977) ; Mn^{4+} as a dissolved compound or as MnO_2 pigment is used as a black colorant; Mn^{3+} ions are used for the colouring of violet glazes. The colouring of Cu^{2+} ions depends critically on the composition of the matrix. In alkali glazes, it causes a light blue colouring which turns into turquoise in combination with white pigments. In a high lead matrix, Cu^{2+} leads to an intense green colour (tab.18; Weyl 1976; Colomban, 2013).

Besides the ion colouring, pigments play an important role in glass colouring and go hand in hand with an opaque appearance of the glaze. The pigments are determined whether by separate EPMA measurements or with the μ-XRD^2, when the crystalline particles are too small for the measurement spot of EPMA.

In the present samples, the most common pigments are the opacifying SnO_2 and SiO_2 in white and turquoise glazes. As black pigment, Cr-Cu-Mn-oxides, Fe-rich pyroxenes and Cr-diopside occur, primarily in the Uzbek glazes from the 16th century. In a yellow glaze from the same location and period, $Pb_2Sn_2O_6$ is the colouring pigment.

7.1 Correlation of main composition and colour

The subdivision into three major groups of matrix composition partly corresponds to the colour of the glazes (fig.44). Turquoise, blue, and white colours are cumulated in the alkali and the alkali lead glazes. The turquoise glazes from Herat have pure alkali compositions without lead, those from Uzbekistan are in a range between 0.0 and 9.2 wt% lead. The turquoise samples from Turkey and Iran have partly higher PbO contents of 0.5-36.0 wt%. One Turkish turquoise sample is a lead glaze and is part of a polychrome tile with blue, green, and turquoise colours. It should be noted that the other polychrome glazes from the mosque Ata Hanka in Konya, Turkey, and

Takht-i-Suleiman, Iran, reveal different lead contents on one and the same tile. On the other hand, polychrome tiles with similar lead contents are found in different colours on an Uzbek tile from the 16th century (4.8-5.2 wt% PbO, madrassa Abdul Aziz Khan, MMA 1-5) and on the imported tableware of Bulgaria (BG 1-3, BG 11 and BG13: 20.6-23.2 wt% PbO with the outlier BG12 at 16.8 wt% PbO). Blue glazes from Herat and Bukhara also have pure alkali compositions, whereas blue glazes of most of the Iranian samples and of the imported tableware from Bulgaria belong to the alkali lead group. The attribution of white coloured samples is largely the same as for blue ones.
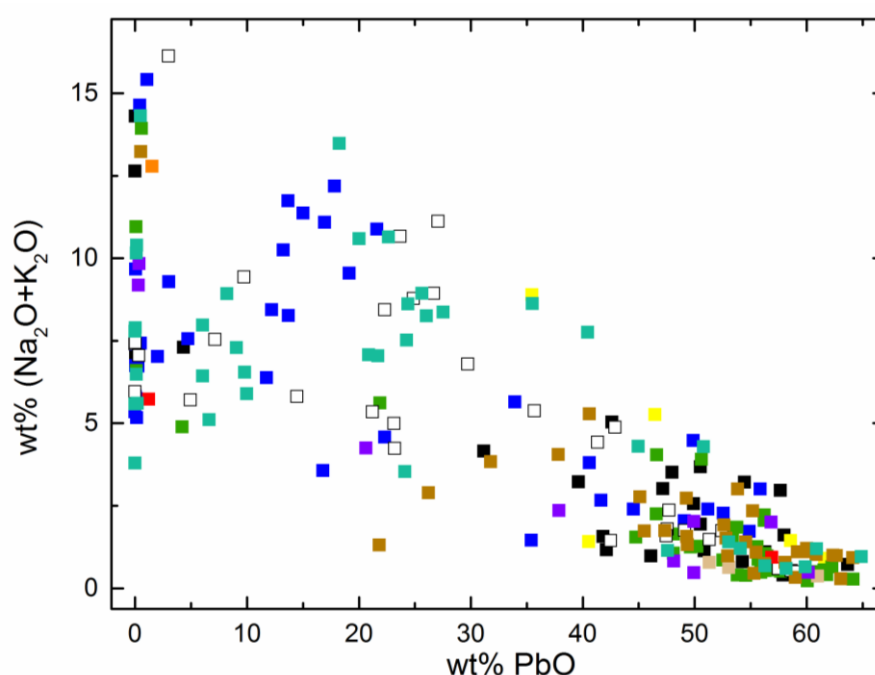
Figure 44: Total alkali oxides versus lead content of the glazes, depicted in their original colour.

Green glazes occur primarily in the lead glaze group. This can be easily explained by the origin of the green colour as a combination of the colouring Cu^{2+} ion and a high lead matrix. Yet, green glazes are also found in the lead alkali group, like in glazes from Uzbekistan (Bukhara) and imported ware of Bulgaria, the latter in combination with white and blue colours on one polychrome sherd. Brown and black glazes are generally clustered either in the pure alkali or in the lead glaze groups. Ochre glazes from Herat and Bukhara belong to the lead glaze group, those from Iran, Turkey and Samarkand do not exceed 1.5 wt% PbO. All investigated yellow glazes originate either from Morocco or from the mosque Khoja Zainuddin in Bukhara and can

be attributed to the lead glaze group. The violet samples from the same mosque in Bukhara instead have pure alkali compositions.

7.2 Uzbek glazes

The oldest tableware glazes from Uzbekistan from the 10th and 11th century from Afrasiab have primarily white and black glazes occur, additionally two green and one red glaze. The tile glazes from the 13th century from Samarkand are blue, turquoise, and red; the glazes from the mausoleum Ishrat Khane from the 15th century are blue, green, and turquoise. In the glazes from the mosque Khoja Zainuddin of the 16th century, blue, green, turquoise, and white glazes are most numerous; black, purple, ochre, and yellow glazes are less common. The glazes from the madrassa Mir-i Arab from Bukhara of the 16th century, glazes are blue, turquoise, white, black and ochre; from the mosque Baland from the same city and the same century, only one green glaze is sampled.

The glazes from the glazed pottery of the Timurid period in 14th-16th century are thought to be strongly influenced by the Chinese culture, copying the design of blue paintings on white background (Golombek, 1996). However, the Uzbek tile glazes of this work instead are almost consistently monochrome and not painted. Nevertheless, blue is the dominating colour in the glazes from Samarkand and Bukhara, followed by turquoise tiles. From the madrassa Abdul Aziz Khan from Bukhara from the 17th century, the glazes belong to one polychrome tile and have blue, turquoise, white, black, and yellow colour. In general, the colours in this group are produced by the ions and pigments as described above.

The blue colouring in the glazes is affected by CoO, occasionally concentrated in up to 0.7 wt% in the glassy matrix (KhZ 133.1). The average CoO value of the blue Uzbek glazes is 0.4±0.2.

The green glazes have all lead or alkali lead compositions and the CuO contents vary between 1.7 and 2.6 wt%. The turquoise glazes from the younger Uzbek tiles of the 13th century and later show a homogeneous picture. The glazes have CuO contents of 1.8-4.5 wt% in an alkali or alkali lead composition. High amounts of crystalline SnO_2 whiten the glaze to the opaque turquoise colour (fig.45).

One white glaze KhZ 032 from the mosque Khoja Zainuddin has SnO_2 particles as opacifying agent. In contrast, the white sample KhZ 171 from the same building and
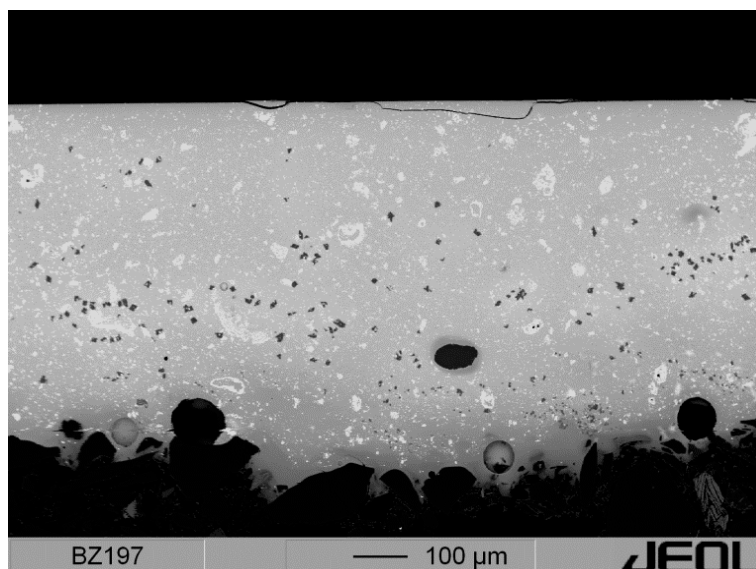
Figure 45: BSE image of a turquoise sample from the mosque Khoja Zainuddin in Bukhara (KhZ 197). The matrix is an alkali lead glaze with considerable content of CuO (2.4 wt%). The light particles are recrystallized SnO_2-phases, which, together with the Cu^{2+} coloured greenish-blue glass matrix, result in an opaque and turquoise appearance. The dark particles are calcium-magnesium silicates with considerable amounts of Na, Cu, Fe and Sn (2-9 wt%).
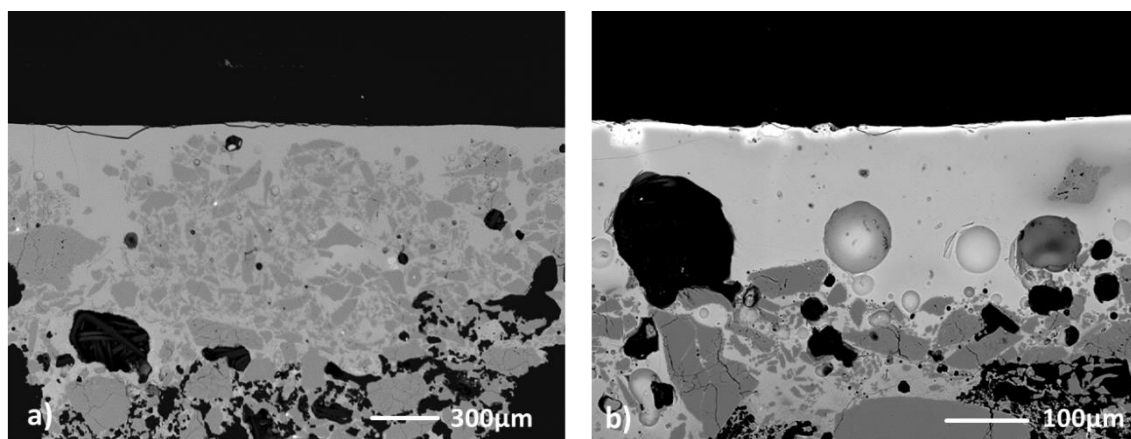
Figure 46 a and b: White glazes MMA 3 (a) from the madrassa Mir-i Arab and MAK w (b) from the madrassa Abdul Aziz Khan from Bukhara, Uzbekistan. The sharp edged particles are quartz grains, which are assumed to originate from the quartz frit body and which contribute to the white appearing of the glaze. The bright zone on the top of the right glaze shows an enrichment of lead oxide and low analysis totals which suggest a leaching out of light elements due to corrosion.
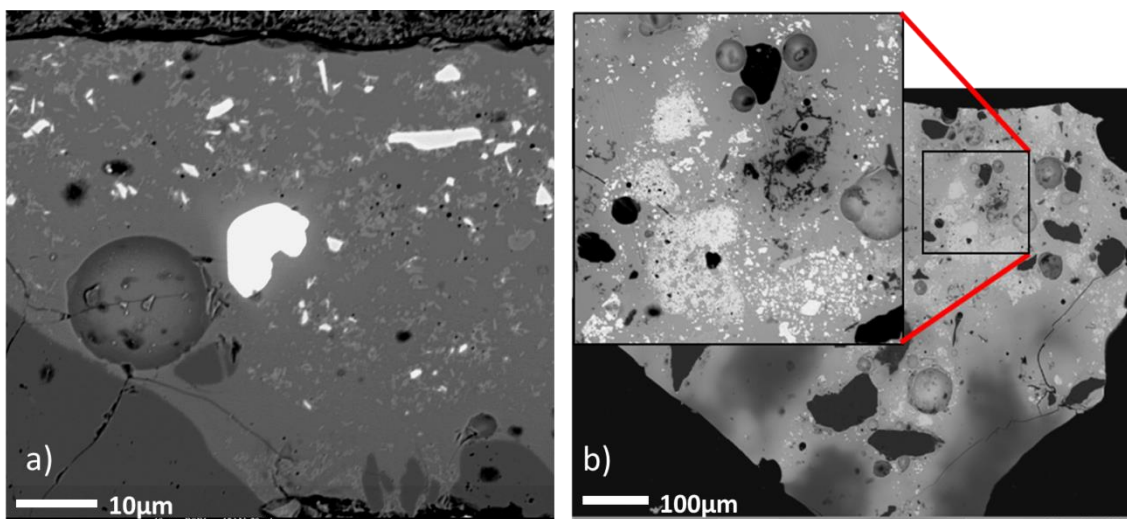
Figure 47 a) and b): a): Pigments in a black glaze of the mosque Khoja Zainuddin (KhZ 090) are large Cr-rich crystals (EPMA) and iron-rich diopside (μ-XRD^2 analysis). b): Pigments in a yellow glaze of the madrassa Abdul Aziz Khan (MAK g) are lead tin oxide and lead silicate (determined by μ-XRD^2).
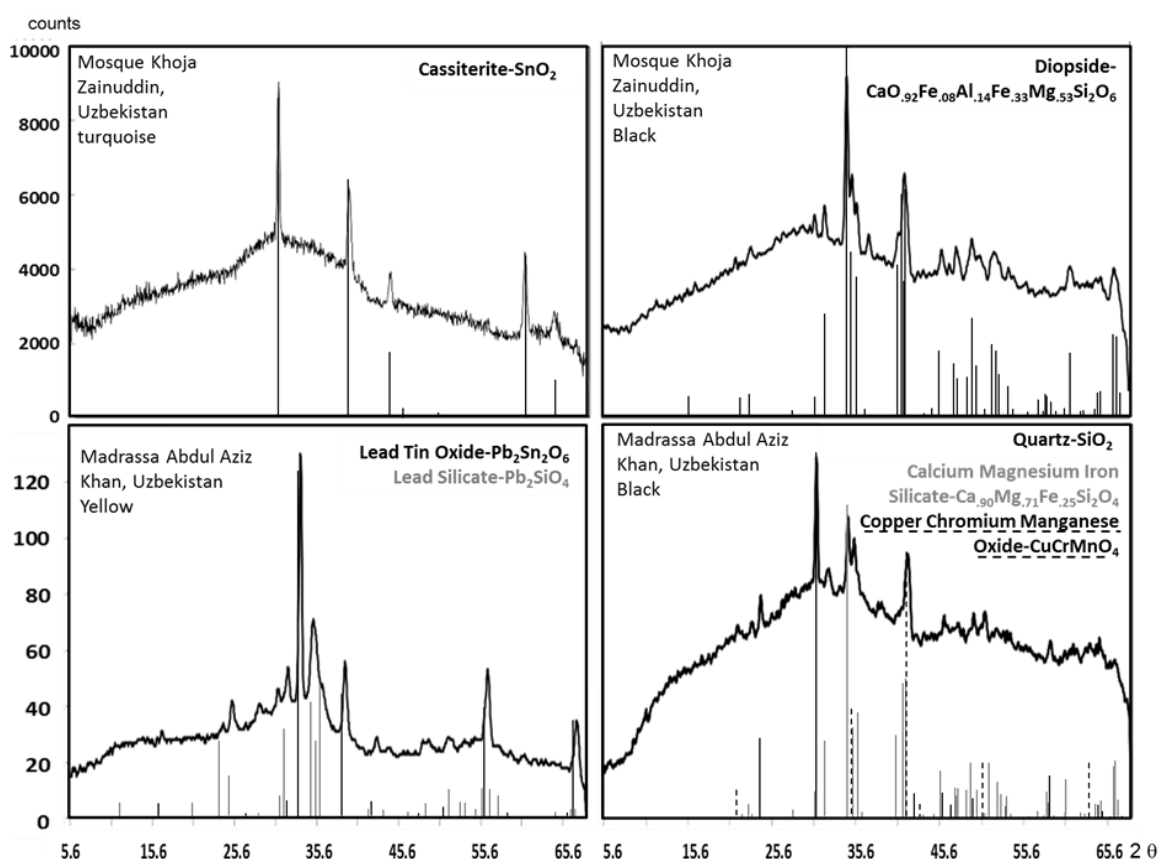
Figure 48: Diffractograms of two samples from the mosque Khoja Zainuddin (turquoise, KhZ 196 and black, KhZ 090) and two from the madrassa Abdul Aziz Khan (yellow, MAK g and black, MAK s), both from Bukhara, Uzbekistan and dated to the 16th century. The crystalline phases are cassiterite in the turquoise and clinopyroxene in black sample from the mosque Khoja Zainuddin. In the madrassa Abdul Aziz Khan, the yellow sample contains lead tin oxide and lead silicate; in the black sample is quartz beside a Ca-Mg-Fe-silicate and an oxide of Cu, Cr, and Mn.

the white samples from the madrassas Mir-i Arab (MMA 3) and Abdul Aziz Khan (MAK w) have quartz grains as opacifiers. The grains seem to arise as undissolved relics from the ceramic body, which is in the remaining part dissolved by the glaze layer (fig.46 a and b).

The black colours in samples from the madrassa Abdul Aziz Khan and the mosque Khoja Zainuddin are produced by contents of Mn^{4+}, but also by particles of copper-chromium-manganese oxide, iron-containing clinopyroxene or Cr-rich crystals (figs.47 and 48, μ-XRD[2] and EPMA analysis). The manganese, which is found in the glazes, cannot be distinguished regarding its oxidation state by the EPMA. Nevertheless, it is known that manganese produces a purple

121

colour in glass when it is present as Mn^{3+} and a black colour when it is present as Mn^{4+} (Bamford, 1977; Nassau, 2001).

In the analyses, it has to be separated into Mn^{3+} and Mn^{4+} according to the given glaze colour. In the violet glazes there are up to 2.47 wt% Mn_2O_3, the black glazes have up to 1.0 wt% MnO_2. The ochre coloured glazes from Uzbekistan (KhZ 134, KhZ 200, KhZ 201oc, and MMA 4) have enhanced Fe_2O_3 contents of 3.5-5.3 wt% in combination with a high PbO content of 32.6-50.1 wt%. The lead rich matrix have an own slightly yellow colour (Wedepohl *et al.*, 1995). This shifts the red-brownish colour of the Fe^{3+} ion to an ochre combination colour.

Pigments of $Pb_2Sn_2O_6$ and Pb_2SiO_4 are found in the yellow glazes from the madrassa Abdul Aziz Khan (MAK g) where the tin compound produces yellow colouring and the silicate $PbSiO_4$ a whitening one (Kühn, 1968; Eastaugh *et al.*, 2004; Seccaroni, 2006). The very high contents of lead oxide (>50 wt%) also contribute to the yellow colouring (Wedepohl *et al.*, 1995).

The colour of the two red glazes (Afr 36 and Sam 17) cannot be fully explained with one of the analysed matrix components. The Fe_2O_3 contents of 1.2 wt% may contribute to the red appearing. The red tile glaze from Samarkand of the 13th century has a lighter red or orange colour. The brightening can be explained with a high amount of SnO_2 precipitates in the glaze.

The glazed tableware from Afrasiab dates into the 10th and 11th century, when tile glazing was not yet well established (Watson, 1985). In this time, a new calligraphic style of black colour on white background is reported from the 9th and 10th century in Central Asia (Samanid time; Fehervari, 2000; Mason, 2004). Black and white colours are found in the glazes Afr 37, Afr 38, and Afr 39 from Afrasiab.

7.3 Afghan glazes

The Afghan glazes originate from tableware from the 13th to the 17th century from the ancient site Herat. The oldest glazes from 13th and 14th century have turquoise and ochre colour; the younger ones from the 15th to the 17th century have additionally blue, green, white, and black colours.

The colouring in the blue glazes is produced by 0.1-0.4 wt% CoO. These CoO contents are low if compared to most of the other blue glazes which are investigated in this study (0.2-1.3 wt% CoO).

Enhanced contents of 0.5-0.6 wt% CuO are also found in the green samples Her 45 and Her 55. Together with the high lead content of 53.8-61.8 wt% PbO in these samples, the resulting colour is a light green. The CuO content is comparatively low compared to other investigated green samples of this study, which have an average value of 2.6 wt% CuO.

Table 19: Analyses of selected chromium-rich particles of the glazes Her 49 and Her 52 in wt%.

Glaze	Her 49		Her 52	
Oxide	Particle 1	Particle 2	Particle 1	Particle 2
SiO_2	0.7	0.4	0.1	0.5
Fe_2O_3	4.7	5.9	4.8	9.4
Al_2O_3	10.0	12.2	13.9	8.4
CaO	0.1	0.2	0.1	0.1
MgO	15.4	16.3	18.4	15.3
Na_2O	0.1	<0.05	<0.05	0.1
K_2O	0.1	0.1	<0.05	0.1
TiO_2	0.2	0.2	0.3	0.2
CuO	**8.7**	**8.2**	**3.8**	**4.1**
Cr2O3	**59.6**	**55.7**	**57.2**	**55.7**
MnO_2	0.6	0.3	2.5	3.3
ZnO	0.5	0.3	0.1	0.1
Cl	<0.05	<0.05	<0.05	<0.05
Sum	99.7	99.8	101.5	97.6

The turquoise sample Her 59a has a CuO value of 2.0 wt% in alkali glaze matrix, which leads to the greenish blue colour. In contrast to turquoise glazes from other localities, no SnO_2 and consequently no SnO_2 crystals are found. Instead, various crystal grains are detected. Most of these grains have a high silica content of up to 78.1 wt% and a sodium oxide content of 4.4-6.1 wt% (particles in the samples Her 53, and Her 58). In the turquoise glazes Her 49 and Her 52, particles with 55-60 wt% chromium oxide and ca. 9 wt% CuO are detected (fig. 49 a, tab. 19). One turquoise glaze, Her 56a, shows very tiny and rather homogeneously distributed inclusions (fig.49 b). It is difficult to determine the exact compositions because of the small size of the inclusions. The indistinct shape of the inclusions could suggest a second glassy phase, which can arise from de-mixing of glass phases during the cooling step. The high amount of phase boundaries in the glaze is assumed to have a whitening effect.

Quartz grains as opacifying crystals are found in the white glazes Her 43 and Her 46.
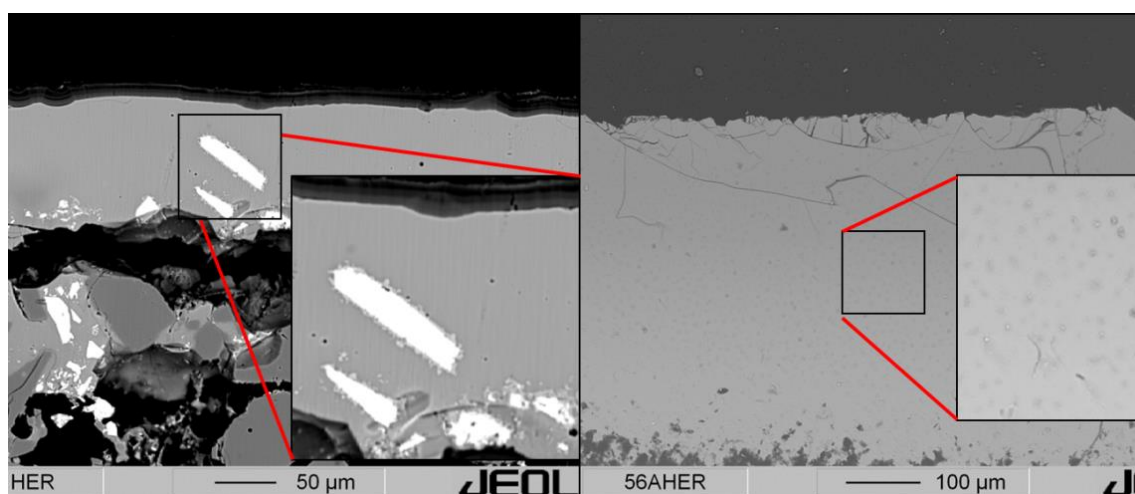
Figure 49 a and b: Two backscattered electron pictures of turquoise glazes Her 52 and Her 56a from Herat. In figure a, the glaze matrix contains large, chromium-rich crystals of 10-50 µm, which show reaction products in the contact zone with the matrix. Figure b shows small inclusions of a darker phase which are ascribed to decomposition of the glaze into two glassy phases.

The colour of the black glazes cannot be ascribed to an oxide of the measured matrix composition or to a special pigment. One black sample (Her 56b) has a blue hue which can be ascribed to the higher content of 2.4 wt% CuO. This CuO content can be ascribed to a mixing process of Her 56b with the turquoise glaze Her 56a, which are on the same ceramic sherd and probably fired in a common heating step.

The ochre glazes from Herat have enhanced values of 3.3-5.0 wt% Fe_2O_3, in comparison with the average value of 1.0 wt% Fe_2O_3 in the blue, turquoise, green, and white coloured glazes. The ochre glazes have enhanced lead oxide of 31.8-52.8 wt% PbO, which contribute to the yellow hue in the ochre colour, as mentioned in chapter 7.2. Further, they contain 6.4-8.2 wt% Al_2O_3 which is higher than the average value of 3.6 wt% in the other glazes. Further, the Al_2O_3 contents correlate with the Fe_2O_3, which suggests an input of one part of the Al and Fe from the clay-rich body, as shown in chapter 8.3.2.

7.4 Iranian glazes

The glazes from the Iranian building complex Takht-i-Suleiman are blue, green, turquoise, white, brown, yellow, and red. The majority are blue and turquoise glazes with each ten glaze samples

of the total number of 37. The two younger samples from the prayer niche in Isfahan from the 20th century are light blue and black. The blue, turquoise, and white colours form the traditional ground stock of Iranian tile glazes (O´Kane, 2011). Brown and ochre colours are reported to be introduced in the 14th century tile glazing in Iran (O´Kane, 2011) but they occur here in samples from the 13th century, yet. The glazes in this study have common transition metal ions and particles for the colouring of blue, turquoise, brown, and white glazes.

The blue Iranian glazes contain 0.2-1.3 wt% CoO. Additionally, they are opacified with SnO_2, from which 1.9-3.7 wt% is found as dissolved SnO_2 in the matrix. Due to the SnO_2 particles, the glazes show therefore a lighter hue than the blue glazes of e.g. Uzbekistan, Afghanistan, or Turkey.

The green samples are coloured by 0.6-3.0 wt% CuO and have a lead-rich glassy matrix with 55.7-61.6 wt% PbO. The glaze with 61.6 wt% has with 0.6 wt% the lowest content of CuO and has a greenish-yellow colour. Other studies on historical glass describe that a high content of lead on its own leads to yellow colouring (Wedepohl *et al.*, 1995). Therefore, the combination of high lead content and CuO may affect the greenish yellow colour.

Most of the turquoise glazes are coloured with the combination of Cu^{2+}-ions and SnO_2 particles like e.g. Uzbek samples (fig.45). In the turquoise samples TiS 11b and TiS 23c, CoO is additionally found. The addition of cobalt to the copper-coloured samples is remarkable, because it is not essential for the turquoise colouring. The sample TiS 11b has only 0.1 wt% SnO_2, but it shows small gas bubbles in the glaze matrix, which may cause the opaque turquoise colour. The turquoise samples tend to have higher contents of lead oxide and are opacified with SnO_2. Abu´l-Qasim describes the process of tin addition with a pre-step of mixing and heating with lead (Allan *et al.*, 1973). In Persia and Iraq of the 7th-9th century, the lead content is observed to increase parallel with the upcoming technology of tin opacification (Mason *et al.*, 1997; Hill, 2004). In the investigated Iranian samples, no correlation between the higher SnO_2 values in turquoise samples and the PbO content is found. Nevertheless, the common addition of SnO_2 and PbO is conceivable, when differing batches of lead and tin mixture are used in the tile glazing production. For the works on the fortress Takht-i-Suleiman, different glaze makers, as well as the use of different techniques (*lajvardina* and lustre) are described (Watson, 1985), which can also explain the diversity of compositions. The *lajvardina* technique implies an approach of two separate layers in the glaze (see 2.3.5.5). This can be confirmed in some of the blue, white, and red samples from Takht-i-Suleiman. In contrast, the *lajvardina* characteristic of cobalt enhanced values in the lower glaze layer could not be observed. The underlying glaze of the red colour has

no considerable contents of Co, Cu, Fe, or Mn and is probably intended to be a white glaze base. This is also known as typical characteristic for Iranian *cuerda seca* tiles (O´Kane, 2011).

The white colour is achieved with particles of recrystallized SnO_2; a surplus of Sn is also dissolved in the glassy matrix with contents between 2.4 and 10.6 wt% SnO_2. In two white samples TiS 30a and TiS 30b, the SnO_2 content is below 1.0 wt%, but high SiO_2 contents above 70 wt% are observed. In the BSE pictures of both samples, quartz grain relics with re-crystallised needles as fringes are observed, which result in the white appearing.

The ochre and brown samples TiS 10 and TiS 31 have either a higher Fe_2O_3 content of 4.9 wt% (TiS 10) or are enriched in MnO_2 (3.3 wt%, TiS 31).

One single red coloured glaze (TiS 32) is very rich in SiO_2, but the Na_2O content with 3.8 wt% is lower than the average value of 7.8 wt% in the rest of Iranian samples. Any colouring ions are missing.
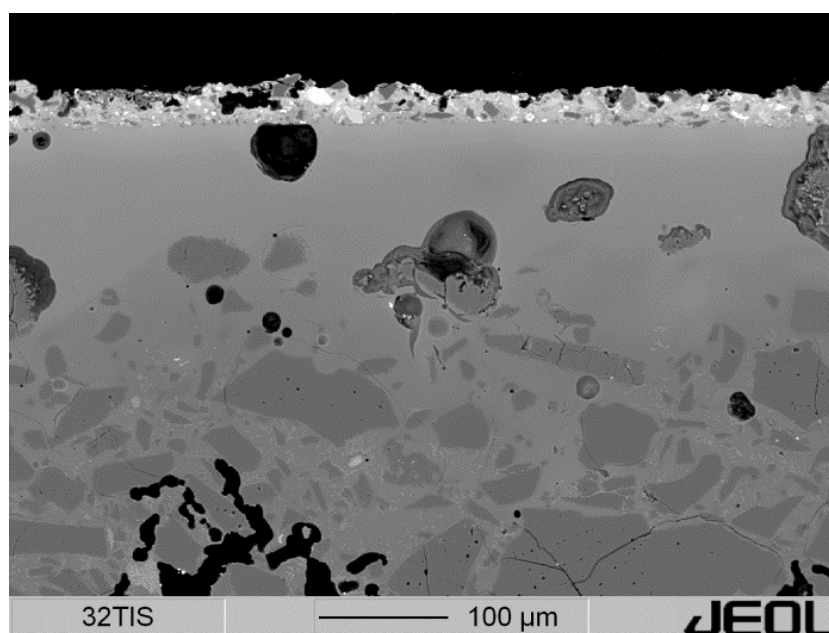
Figure 50: BSE-picture of a red sample of Takht-i-Suleiman (TiS 32). The silica-rich glaze with enhanced values of MgO is covered by a layer of quartz grains and Fe_2O_3-MgO-Al_2O_3 containing minerals. The amounts of copper in the analyses could reveal small cuprite crystals, resulting in the red colour. The dark grey phases in the glaze are again non-dissolved quartz crystals.

The red colour therefore probably originates from the additional layer on the top, which is not included in the bulk measurements of EPMA (fig.50). The matrix of the layer and also some

components of its crystalline phases can hardly be detected with the EPMA due to their small size of partly below 1 µm. The larger grains in the upper layer are quartz crystals and Fe_2O_3/MgO/Al_2O_3-rich crystals (tab.20), but the results of the analysis are poor here. Probably the grains with high content of Fe_2O_3 act as a dark red pigment. Especially the very fine grinding of the iron-rich particles leads to a brighter red colour than the normal ochre hue (Matthes, 1990). Traces of Cu are detected in most of the analysed grains, one of them has even >1 wt% copper oxide. This may suggest the presence of very fine dispersed cuprite, which gives the upper layer the red colour. The presence of cuprite would require a reducing firing step. As can be seen in figure 50, the interface between the upper layer and the glaze is, in contrast to the glaze-ceramic interface, very sharp, suggesting a separate heating step for the upper layer. An additional reducing firing step for the colouring layer is known from the lustre production (chapter 2.2.4) and can be assumed here.

Table 20: Analyses of the upper layer particles of the red sample (TiS 32). The main compounds beside SiO_2 are depicted in bold letters; similar compositions are outlined in columns.

Oxide	Particle 1	Particle 2	Particle 3	Particle 4	Particle 5	Particle 6	Particle 7
SiO_2	53.10	46.69	47.08	54.51	58.73	**84.24**	**80.87**
Fe_2O_3	**22.82**	**31.12**	**15.47**	**14.30**	**12.25**	5.48	7.29
Al_2O_3	**6.21**	**5.41**	**10.03**	**8.95**	**7.39**	1.89	4.31
CaO	3.05	2.63	2.95	3.23	3.98	1.32	1.56
MgO	1.41	1.24	8.21	1.88	1.88	0.80	0.75
Na_2O	**8.96**	**7.38**	8.25	**10.97**	**9.74**	2.32	3.09
K_2O	2.29	2.07	1.50	1.83	1.59	0.73	0.85
TiO_2	0.11	0.24	0.16	0.17	0.15	0.11	0.09
CuO	0.11	0.00	**1.32**	0.16	0.11	0.13	0.11
SnO_2	1.47	1.79	4.76	3.57	3.85	2.41	0.64
SO_3	0.25	0.38	0.18	0.35	0.21	0.13	0.16
Cl	0.29	1.34	0.11	0.10	0.16	0.56	0.34
Sum	100.06	100.30	100.03	100.02	100.04	100.13	100.08

A definite determination of lustre technique cannot be made, because the Cu is not detected as a separate phase, but only in mixed analyses. In the whole sample set of this study, the red colour is far less common than the blue, turquoise, and white colours. Nevertheless, red is used as line colour in the Iranian *cuerda seca* technique of the 14th century whereas Spanish glaze makers used black lines only (O´Kane, 2011).

Further samples with additional surface layers are identified to have a lustre colouring; the sample TiS 29a has a very compact upper layer, consisting primarily of Au. The sample TiS 30a has an upper layer with SnO_2 and PbO amounts, but, due to the highly porous structure, very low totals in the analyses.

7.5 Turkish glazes

The Turkish glazes from the mosque Ata Hanka in Konya are blue, green, turquoise, black, and ochre. The single glaze from Kayseri is turquoise.

The blue glaze from the mosque Ata Hanka in Konya is coloured by 0.4 wt% CoO.

The green glazes of this site have with up to 5.5 wt% the highest CuO contents in the complete analysed sample set of this study.

All turquoise glazes from Konya and Kayseri belong to the alkali lead or lead group and have CuO contents between 0.5-2.2 wt%. The SnO_2 contents of 3.4-4.8 wt% represent the part of tin oxide in solution which is accompanies the precipitations of recrystallized tin oxide in the matrix. The number of turquoise samples is too small to identify a possible correlation between the SnO_2 and lead oxide. This would be expected if both were added together to the glass batch, as it is reported by Abu´l-Qasim (1301; in Allan *et al.*, 1973).

The black and ochre glazes Kon 22a and 20b have higher contents of manganese oxide and iron oxide (4.2 resp. 3.9 wt% MnO_2 and 2.1 wt% Fe_2O_3 both).

7.6 Bulgarian glazes

The Bulgarian glazes originate all from the ancient fortress Dristra and comprise blue, green, white/beige, black, purple, and ochre colour. The oldest glazes from the pre-Islamic epoch of the 12th century are all ochre coloured. The purple glaze occurs only on one of the two polychrome sherds.

Because of the limited variety of colours (brown and green) and the predomination of lead glazes, no correlation of colour with the lead or alkali composition is observable. In the well represented group of green lead glazes from Ottoman period in Bulgaria, contents of 1.2-4.5 wt% CuO are detected. The brown and ochre samples have enhanced values of Fe_2O_3 (1.6-2.7 wt%). In both groups, an exception is formed by an older glaze from the 14th-15th century. In the

green sample BG 8, only 0.3 wt% CuO is found. In a brown sample, BG 7, of the same period, only 0.7 wt% Fe_2O_3 is detected. Together with undissolved quartz grains, which lead to whitening of the colour, a light brown or ochre colour results (fig. 51 a). The black sample BG 16 has no enhanced contents of iron, chrome, or manganese which would explain the black colour. Instead, it has 1.5 wt% CuO, which should give the lead dominated glaze a green colour. With the methods used in this study, the black colour cannot be explained; possible are for example organic components in the glaze or underlying ceramic or the presence of very fine black colouring CuO particles at the interface of glaze and ceramic. In the backscattered electron picture however, no such phase is visible.

There are three beige samples in the sample set from Bulgaria, dating to the Ottoman period. These glazes are not enriched in any transition metal oxide. Considering the lack of any strong colouring additives, the weak brown is assumed to be achieved by the small contents of 0.7-1.1 wt% Fe_2O_3. One of the beiges samples, BG 21, consists of two layers, from which the lower one is silica and alumina-rich and contains enhanced Fe_2O_3 contents of 2.6 wt%. The upper layer of glaze has only 0.7 wt% Fe_2O_3, which contributes only in a minor degree to the beige appearing. The blue glaze samples BG 1 and BG 12 from two polychrome sherds have around 1.0 wt% CoO and CuO (0.9 and 1.1 wt% CoO, 0.9 and 1.0 wt% CuO). The blue sample BG 12 has additionally slightly enhanced MnO_2 values of 0.3 wt%. The green glaze of one painted sherd BG 3 has a very low CuO value of 0.3 wt%. Instead, there is a considerable content of 1.0 wt% Cr_2O_3, resulting in a darker green colour, if compared to the green shade induced by Cu ions in a lead glaze. The highest values of 2.5 wt% Mn_2O_3 are responsible for the purple colour of the painted sherd from the 17th century (BG 13). The two white glazes BG 2 and BG 11 have no significant contents of opacifiers (fig. 51 b). Together with the absence of colouring agents in the glassy matrix, the glazes are likely to have a translucent appearing. They are both part of the polychrome samples from Bulgaria, which have very light ceramic bodies. The white colour can be achieved due to the light ceramic body which shows through the glazes. Analyses of selected Bulgarian ceramic compositions are given in table 9.
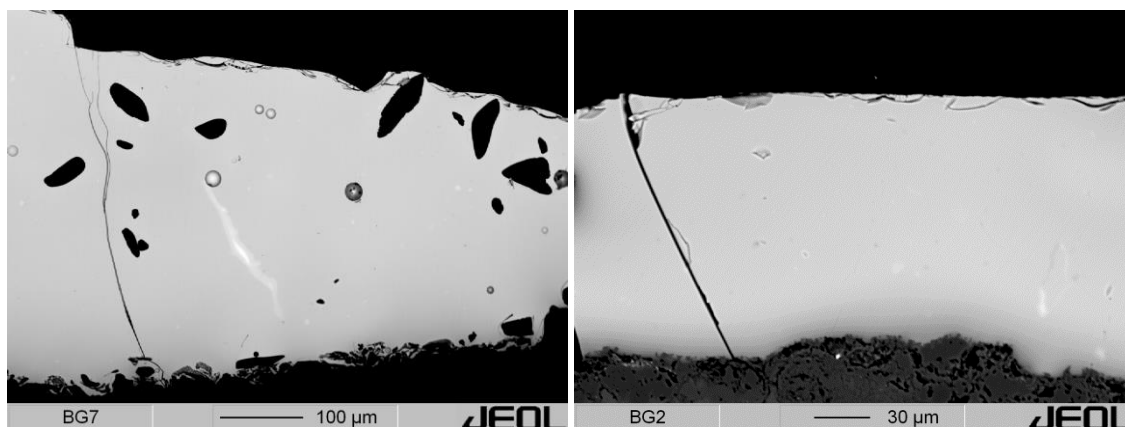
Figure 51 and b: BSE-pictures of two Bulgarian lead-rich glazes; one ochre glaze BG7 with undissolved quartz grains (a), and one white glaze BG2 without any opacifying crystalline parts.

7.7 Moroccan glazes

The Moroccan glazes have blue, green, turquoise, white, black, purple, ochre, and yellow colour. Black and white glazes are in the sample set of all different sampling sites; the Necropolis Chellah, the Marinid School, the madrassas Bou Inania in Fes and Meknes, the madrassa Abu al Hassan, the Saadian tombs the Fountain and the Sultans palace in Tangier and the mausoleum in Tangier. Ochre and turquoise glazes are found at all these sites except for the Marinid School and the Sultans Palace in Tangier. Blue samples occur at all sites except for the Marinid School and the madrassa Abu al Hassan in Salé. Purple glazes are found in the Necropolis Chellah, the madrassa Bou Inania in Fes and the mausoleum in Meknes. Green glazes are found on tiles of these sites and additionally on samples from Marinid School, the madrassa Bou Inania in Meknes and the madrassa Abu al Hassan in Salé. Yellow glaze occur in the Necropolis Chellah, the Marinid School, and the Saadian tombs.

The colourings of Moroccan glazes do not correlate with any specific lead or alkali (earth) contents in the glaze compositions. The CoO contents in the blue coloured samples vary between 0.1 and 0.6 wt%. They cover various different shades of blue, of which the lighter ones are opacified with SnO_2 pigments, which also occurs in the glaze matrix in high values of up to 41.2 wt% SnO_2. Three blue glazes (Nec 13, InM 59, and Sad 70) additionally show minor contents of 0.1-0.3 wt% CuO which is not correlating with a geographical or historical classification.

The green samples all have significant values of 1.1-3.9 wt% CuO, from which especially those of the 14th century from the Marinid School in Salé stand out with 3.1 and 3.9 wt% CuO. The continuously high lead contents in Moroccan glazes cause the green colour together with the

Cu^{2+} ions. A few green samples from the Necropolis Chellah, Bou Inania Meknes, and Fes, show contents of about 1.1-1.4 wt% Fe_2O_3. Because of the very low values of <0.6 wt% Fe_2O_3 in other samples, this content can be assumed to be intentionally brought in.
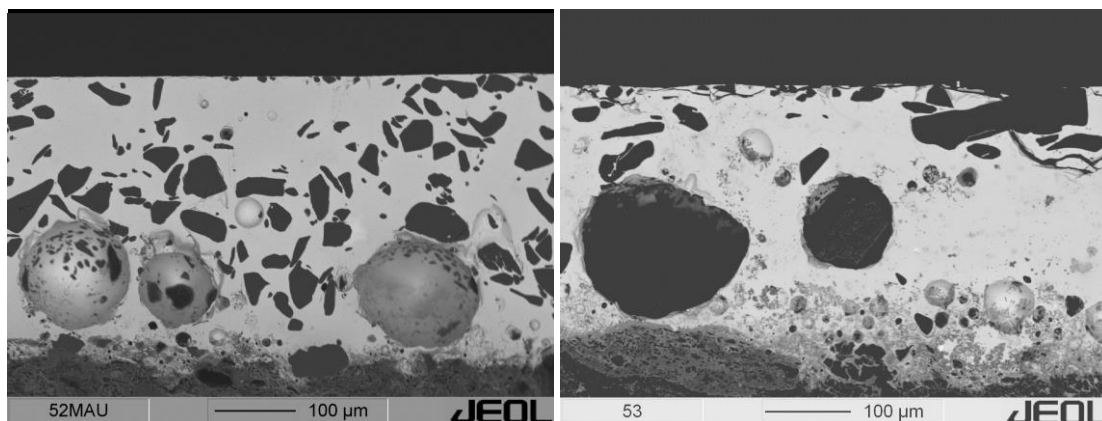
Figure 52 a and b: BSE-pictures of two glazes from the mausoleum of Moulay Ismail in Meknes. The left one (a) is a white glaze (Mau 52), the right one (b) is an ochre coloured one (Mau 53). Both have high contents of bubbles and quartz grains which brighten the glaze´s colour. The pictures are matched in contrast and brightness with the reference to the dark quartz grains colour.

Undissolved quartz grains in the matrix lead to whitening as it is seen in one white and one turquoise Moroccan glaze (Ina 37 and Mau 52, fig.52 a and b). A combination of quartz grains with recrystallized SnO_2 is observed in the samples from the mausoleum Moulay Ismail and the madrassa Bou Inania in Meknes.

The turquoise samples are primarily coloured with a combination of CuO at contents of 0.7-3.4 wt%. The Cu^{2+} appears in the lead containing matrix of 40.4-65.9 wt% PbO in a more greenish blue. Again, recrystallized particles of tin oxide opacify and brighten the initial colour. SnO_2 contents of 1.2-10.4 wt% in the Moroccan turquoise glazes exceed the SnO_2 values of e.g. Iranian samples with ca. 6.5 wt% SnO_2.

The white samples Sad 64 and Sad 72 from Saadian tombs in Marrakesh show very high SnO_2 contents and SnO_2-precipitations in the lead-rich glass matrix. A significant content of MnO_2 in the which could act as decolorizing agent (Nassau, 2001) is not detected.
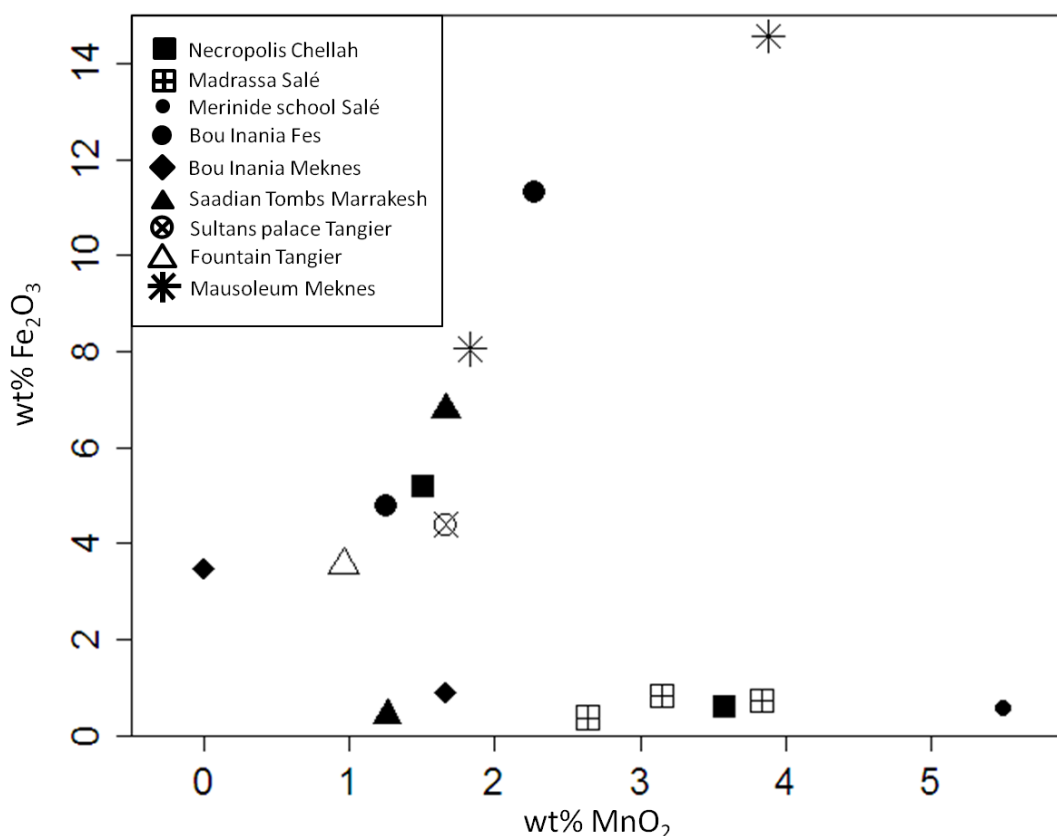
Figure 53: Fe₂O₃ and MnO₂ in Moroccan black glazes. The glazes split into two groups of a) enhanced Fe₂O₃ contents at moderate MnO₂ values and b) low Fe₂O₃ contents of <1 wt% and partly enhanced MnO₂ contents of 2-4 wt%. The black colour is caused by the MnO₂; the Fe₂O₃ produces a brown hue in the black colour.

The largest group of samples is formed by black coloured glazes, which are commonly dyed by either only MnO₂ or a combination of MnO₂ and Fe₂O₃ in concentrations of 1.0-5.6 wt% MnO₂ and 3.5-14.6 wt% Fe₂O₃ (fig.53). The migration of iron oxide from the ceramic body can be neglected, regarding the consistently white stone paste tile bodies in Moroccan samples.

The Fe₂O₃ gives the black, manganese-coloured glaze a brown hue. In one glaze from the madrassa Abu Al Hassan in Salé, Sal 6, the MnO₂ is present as idiomorphic Mn-rich crystals, additionally to the MnO₂ content in the glaze matrix (fig.54). The samples of the 14th century from the madrassa Abu Al Hassan in Salé are completely free of Fe₂O₃ and instead have high contents of MnO₂. One sample of the madrassa Bou Inania in Meknes from the 14th century has 3.6 wt% Fe₂O₃ and 0.0 wt% MnO₂. The black glazes tend to have with 1.7 wt% in average higher potash values than the rest of the sample set with 1.4 wt%.
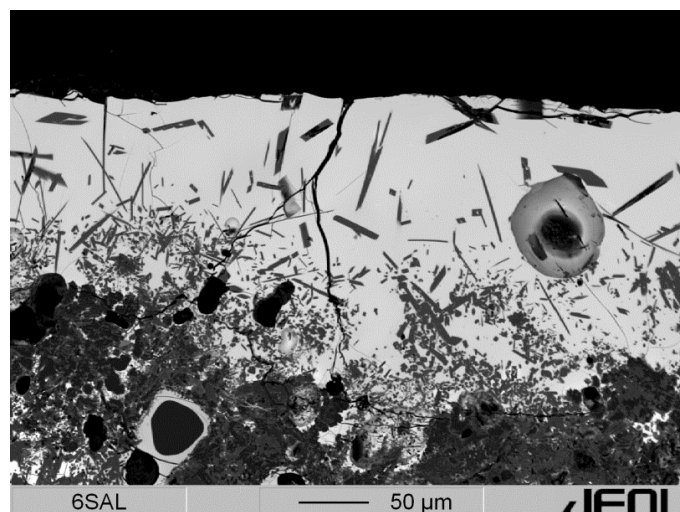
Figure 54: BSE-image of a black glaze from the madrassa Abu Al Hassan in Salé (Sal 6). The long prismatic precipitates are manganese-rich crystals with about 14.0-15.0 wt% MnO_2 beside the major components SiO_2 (37-45 wt%), CaO (ca. 22 wt%), PbO (ca. 13 wt%), and MgO (0.5-3 wt%).

Varying manganese oxide contents of 1.0-3.1 wt% Mn_2O_3 are found in the purple samples and result in different gradations of intensity in the violet colour. In the violet samples of the madrassa Bou Inania in Fes, precipitates of SnO_2 lighten and opacify the purple colour. The matrix composition has 10.8-11.5 wt% SnO_2. From the same site, a sample with only 0.2 wt% SnO_2 and no SnO_2 precipitations shows a more intensive, deeper hue of purple. The brown and ochre samples from all sites show Fe_2O_3 contents of 2.7-5.8 wt%. One of the two ochre samples from the mausoleum Moulay Ismail in Meknes, Mau 53, has additionally 1.3 wt% MnO_2 and 0.13 wt% CoO. This combination is also used for darker or black samples from the Sultans palace in Tangier. But compared to the glazes with black appearing, the sample from Meknes is brightened by the high content of bubbles, quartz pebbles and other crystalline phases in the glaze (fig.52 a and b). The two ochre glaze Ina 34 and Ina 41 from the madrassa Bou Inania in Fes contain additional SnO_2 pigments, resulting in an opaque and lighter appearance of the glaze colour.

8 Discussion

In the following part, the observations of interaction between ceramic body and glaze from chapter 5.2 are discussed at first place. Further, the behaviour of the calculated firing temperatures of the different subgroups is outlined. In the main part, the characteristics of alkali and alkali earth contents, other minor elements, and main colorants are compared with other Islamic glazes. The discussion includes relations and possible technology transfer in Islamic glazing tradition and differences to comparable glass analyses.

8.1 Ceramic-glaze interaction

As described in chapter 5.1, backscattered electron pictures give information about the interaction between the ceramic body and the overlying glaze layer. Additionally to the pictures, line scans through the cross section of ceramic and glaze reveal diffusion processes between the both.

The widths of the ceramic-glaze interfaces are evaluated on BSE pictures of all samples. In the BSE pictures can be observed, that the alkali and alkali lead glazes have broader transition zones to the ceramic (160-170 μm in average) than the lead rich glazes with ca. 90 μm transition zone. This is attributed to the generally higher processing temperatures of the alkali-rich glazes, which result in more interaction with the ceramic components. A broader interaction zone can also be the result of lower cooling rates, so the reaction between ceramic and glaze can be assumed to be enhanced (Rehren & Yin, 2012). Another reason can be found in the melting behaviour of multi-component systems. In a system with few major elements such as pure lead silica glaze, the melting process can be assumed to be in a smaller temperature interval than in a multicomponent system. In some cases, where the lead/silica ratio is close to the eutectic point of ca. 40 mol% PbO (Jak *et al.*, 1997), most of the glassy material melts in a very short temperature interval. In multi-component systems such as alkali glazes with Si, Na, K, Ca, and Mg, the melting process is commonly over a wider temperature range. That means that initially molten parts of the batch already interact with the ceramic body, while the rest of the glaze is still in the process of melting.

Regarding the narrow interaction zones typically 40-150 μm in lead glaze samples, it can be assumed that the application was not carried out by addition of pure lead oxide slurry, but with

a mixture of either pre-frit or raw glaze components including the silica amount of the glaze. The homogeneity of the glassy matrix in the lead glazes gives hint to a pre-step of fritting and milling, before the material is applied as slurry. The production of alkali glazes is assumed to be carried out with slurry of grounded frit (chapter 2.3.1, Allan *et al.*, 1973). Whether the slurry was applied with an additional inorganic clay binder cannot be proven.

The interaction with the ceramic is further investigated in EDX-line-scans over the cross-section of ceramic and glaze (chapter 5.2). Higher silica contents are primarily observed in the alkali glazes close to the ceramic-glaze interface. Mg, Na, and Ca are consequently diluted by the Si input and are therefore relatively depleted close to the ceramic. The line scan profile of Fe shows a flat gradient at very low total values. The line scan profiles of K and Al show enrichment next to the ceramic body or a constant profile, suggesting a compensation of the Si-dilution by migration from the ceramic body. Most likely, the compensation comes from K-feldspar grains in the stone paste ceramic which were detected as constituents in the quartz rich ceramics. The alumina migration from clay-based body can be ascribed to the contents of 10-22 wt% Al_2O_3, found in the average values clay-based bodies. However, a lack of diffusion profile does not exclude a diffusion process. The even distribution of element composition can be explained with a complete homogenization of the glaze in long firing times, or with similar contents of glaze and ceramic in the initial compositions. On the other hand, the input of aluminium from the ceramic body seems to have a minor influence compared to the glaze recipe. The group of polychrome Bulgarian glazes has low Al values in the glaze (1-2.5 wt%), but high contents in the average value of ceramic body composition (21 wt%). In contrast, the monochrome Bulgarian glazes are high in Al_2O_3 (1.5-8.5 wt%) but the average ceramic composition is at 13 wt%.

For more detailed statements, the ceramic body composition must be further investigated. In the present case of minimally invasive sampling, the measurements on the small ceramic part adhering to the glaze do not serve as representative investigation. In the work of Pernicka (1979), parts of alumina from the clay-based ceramic are assumed to be solved in glazes. Rehren & Yin (2012) can show based on ceramic body and wood ash analyses, that the glaze compositions of lime rich glazes are strongly influenced by the interaction of Ca-poor ceramic body and the Ca-rich wood ash for glaze production.

The enrichment of silica is also reported from lead glazed slipware of Uzbek tableware ceramic from the 10th-11th century (Henshaw *et al.,* 2007). Molera *et al.* (2001) reveals in an experimental approach, that the glazes of recipes with different lead/silica ratios are surprisingly

homogeneous in their final composition. This is explained by Si-diffusion from the quartz frit into the lead glaze. The forming of wollastonite precipitates in glazes in the vicinity of the ceramic body is reported for Islamic glazes (Simsek *et al.*, 2010; Pradell *et al.*, 2010). In the present study, wollastonite crystals are observed in samples from Samarkand of the 13th century and in Iranian glazes. The formation of the wollastonite is ascribed to an excess concentration of Si and Ca in the glaze, which originates from thermal decomposition of mineral phases in the ceramic body (Casellato *et al.,* 2007; Doménech-Carbó *et al.,* 2008; Coentro *et al.,* 2014).

In Uzbek and Iranian glazes, feldspar minerals are found. They form at high firing temperatures above 1000 °C in the presence of Al (Pradell *et al.,* 2010; Coentro *et al.,* 2014). Further, Molera *et al.* (2001) states a higher degree of interaction with an illitic than a kaolinitic clay body, which result in a broader interaction layer. The small amount of ceramic body material does not allow the comparison of clay compositions and interaction in the present set of samples.

8.2 Processing temperature

On the basis of the glaze composition, the minimal processing temperatures of the glazes were calculated (chapter 2.1.5).

In history, the processing temperature of a glaze could not be easily predicted by the craftsmen, but was probably an experience-based estimation. Especially the natural variation of the raw materials in glaze production makes the prediction of melting behaviour difficult. The portion of sodium carbonates, hydrogen carbonates, and sodium chloride in the lake Wadi-el-Natrun for example underlie seasonal fluctuations, and probably also long-term changes due to climate variations (Shortland, 2004). The plant ash compositions have differences due to the regional soil and the harvesting time (Clemens, 2002) and the silica sources may vary in their composition due to inhomogeneities in the deposit (Shugar & Rehren, 2002). In general, it is reasonable to have glaze processing temperatures below those of ceramic heating in order to avoid volume changes in the ceramic body and further reaction of one of the ceramic components. The out-gassing of reaction products from the ceramic would lead to bubble formation in the glaze. The technology process of Islamic Middle East ceramics is simulated with 900-1200 °C by Tite *et al.* (2011). For alkali glazes, Tite *et al.* (1998) suggest a temperature range from 950 to 990 °C at 10^4 P process viscosities for medieval Islamic glazes. Hill (2004) calculates temperatures of 800-900 °C for Iranian alkali dominated glazes and around 650 °C for Iranian lead glazes. These values are

supported by Hallett *et al.* (1988), who report processing temperatures of about 850 °C for alkali glazes and 640 °C for lead-based glazes from northern Yemen (Hallett *et al.*, 1988; Hill, 2004; Tite, 2011).

In the present study, the firing temperatures of the alkali glazes are generally in the upper range of the mentioned reference values. The highest process temperatures up to 1200 °C are found in the alkali glazes from Uzbekistan with ca. 7 wt% (ca. 5 mol%) of Na_2O and K_2O sum. The lowest values of Islamic glazes are found in the lead rich glazes from Morocco with ca. 570 °C and 65 wt% PbO (35 mol%, fig.55 a-c).

Compared to the scattering of the younger Uzbek samples of 660-960 °C processing temperature in lead glaze compositions, the lead glazes from Iran and Turkey from the 13th century have with 680-770 and 900-930 °C narrower windows of processing temperatures. Nevertheless, the small number of each three Iranian and Turkish samples does not allow any assumptions about the standardisation of the technology.

It is reported from the period of the Seljuq and Khwarazmian dynasty, that a certain standardization of techniques took place (Golombek, 1996). The narrow distribution of process temperatures in Iranian and Turkish glazes of this period confirms this observation. An exchange of craftsmen in the Middle East is described in detail for the Timurid and Safavid potters in Turkish cities and Syrian craftsmen in Samarkand in the middle ages until the 16th century (Golombek, 1996; Beşer, 2009). The exchange of potters and glaze makers could be one reason for the coherence.

The alkali and alkali lead glazes from Iran and Turkey scatter all between 820 and 1140 °C. This can be ascribed to the larger variation in alkali raw materials than in the lead source (Tite *et al.*, 1998).

In the samples from the ancient Bulgarian fortress Dristra, the process temperatures split into two major domains. The larger part of the glazes is lead-rich and shows a wide spectrum of 630 and 860 °C processing temperature, including the glazes from the Second Bulgarian Empire of the 11th-13th century. The narrow field between 1020 and 1080 °C represents the probably imported glazes with medium lead content. The investigated Iranian and Turkish glazes in this study show similar alkali lead compositions and calculated firing temperatures above 1000 °C. Assuming that processing techniques are similar in neighbouring regions, the imported glazes found in Bulgaria could originate in the eastern parts of the Ottoman Empire, i.e. the present day´s Turkey or Iran.

In contrast, the lead glazes from Morocco reveal a wide scatter of alkali amounts and wide scattering of process temperatures between 570 and 920°C.
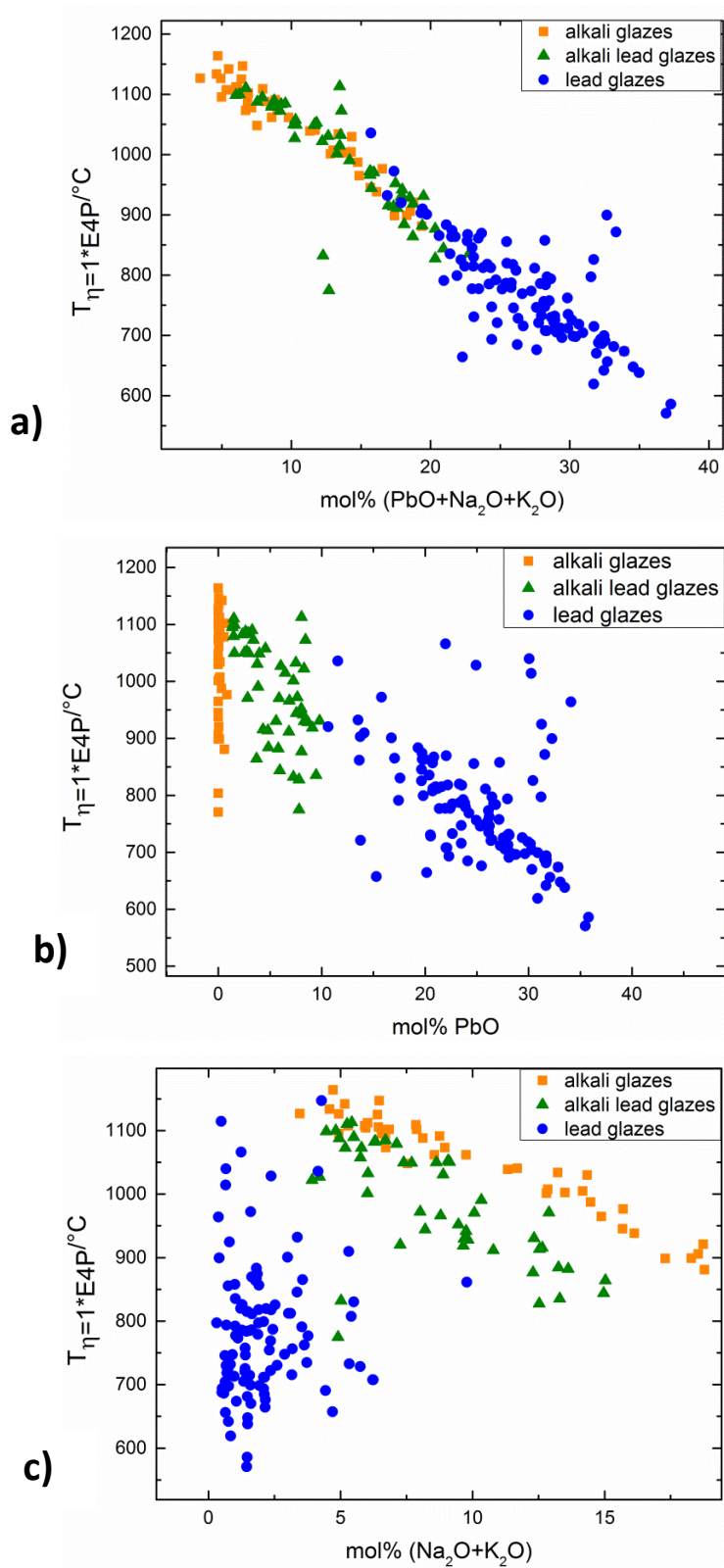
Figure 55 a-c: Calculated processing temperatures of the main glaze groups, depicted versus the sum of the mol% of main flux components PbO, Na$_2$O, and K$_2$O (figure a), separately versus PbO (figure b) and versus alkali oxides (figure c).

Figures 55 a-c show the processing temperatures of versus the molar contents of lead and alkali oxides. The processing temperatures show a good negative correlation with the total of alkali oxides and lead oxide.

The group of alkali lead glazes show scattering in the processing temperatures similar to the alkali glaze group. The small influence of lead contents up to 10-15 mol% PbO can be explained with the phase diagram of SiO_2 and PbO, where the first eutectic point lays at ca. 40 mol% PbO (fig.56). However, the temperature lowering influence of alkali earth oxide contents below 5 mol% is even harder to observe. As can be seen in figure 55 c, the effect is superimposed by high lead oxide contents and it first occurs alkali glazes.
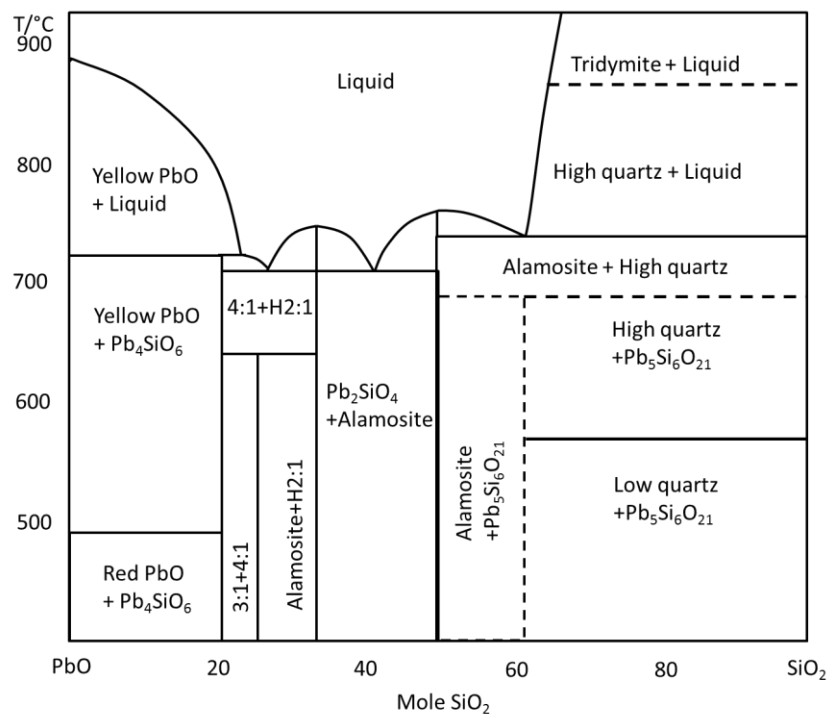
Figure 56: Excerpt of the phase diagram of PbO and SiO_2 after Smart & Glasser (1974)

8.3 Source of alkalis and alkali earth

In order to get insight to regional characteristics and preferences, the alkali sources of the different localities are discussed. Where alkali and alkali earth values are opposed without the lead content, the compositions are re-cast to lead free composition as it is described in chapter 5.3. In the alkali lead glaze compositions of Uzbek and Iranian sample, even the simple dilution

of alkali composition by lead oxide is likely. Therefore, the re-cast alkali and alkali earth contents have to be compared. At first, possible influences of the melting process, diffusion during heating and weathering to the alkali composition are outlined.

In an overview, the alkali glazes are compared considering their alkali and alkali earth contents and the accompanying elements. Afterwards, the different localities are treated separately in detail.

As discussed in chapter 2.1.4, alkali oxides as flux additives may originate from two main raw material sources. First, plant ash flux, which has been used from the earliest glaze production on, and second, mineral natron which was introduced since the 10th century BC in Egypt and the Levant. The Na- content itself is not diagnostic for the alkali source; both mineral and plant ash sources can result in a high or low Na_2O content. The ratio of sodium oxide to potash in contrast, is much higher in mineral natron sources (up to factor 30) than in plant ash glazes (high variation, commonly between 1 and 10; Brill, 1999). Certain factors that influence the Na_2O/K_2O ratio in the plant ash and further in the glaze melt make it difficult to retrace the exact raw material. The K_2O values can scatter due to different parts of a plant or the soil composition. The alkali characteristic of a plant ash normally represents the availability of cations in the regional soil and does not vary significantly from one plant species to the other within one type of soil (Clemens, 2002).

As an additional source of uncertainty, the Na_2O in glaze can be depleted by weathering processes. Glass corrosion, which is comparable to glaze corrosion, is commonly described in two main processes; the incorporation of water molecules in the glassy network and the migration of alkali ions to the surface (Sanders & Hench, 1973). The alkali elements are leached out which proportionally enriches the remaining components in the glass. Especially in the case of low contents of CaO and Al_2O_3 as stabilizing agents, the sodium migration is enhanced (Bacon, 1968; Fluegel, 2007). In order to investigate the leaching-out of the sodium, the contents are compared with the amount of stabilizing agent. This consideration does not reveal a significant effect of glaze stability and thereby of Na_2O decrease (fig.57). Furthermore, the question if underlying clay ceramics strongly influence the alkali and alkali earth oxide contents cannot be entirely resolved. The EPMA profiles through glazed ceramic show enhanced SiO_2 values close to the ceramic and presumably a diffusion of Al and K in the case of quartz bodies.
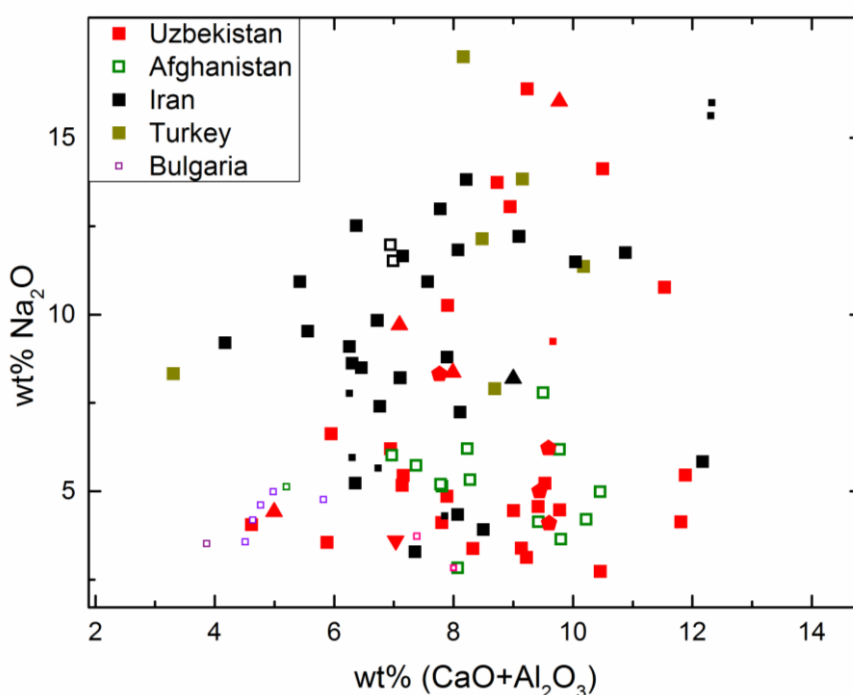
Figure 57: Depiction of the lead free re-cast values of sodium oxide versus the stabilizing ingredients CaO and Al_2O_3 in in alkali and lead alkali glazes. Depletion of Na_2O due to weathering effects would lead to a correlation of Na_2O with CaO and Al_2O_3. The tableware glazes are empty symbols, tile ware is depicted in full symbols. Glazes on clay ceramics are plotted in small points compared to the glazes on quartz frit bodies. Uzbek samples are subdivided into squares (mosque Khoja Zainuddin), circles (Ishrat Khane), triangles top up (madrassa Mir-i Arab), triangles top down (Samarkand), and pentagons (madrassa Abdul Aziz Khan). The Iranian data points are subdivided into squares (Takht-i-Suleiman) and triangles (restoration glazes from Isfahan).

However, the oxides of K, Mg, or Ca in glazes of clay ceramic do not show any systematic shift to higher values in glazes on clay bodies, as it will be shown later in this chapter. The distribution of Na_2O/K_2O values can therefore be taken as more or less original and up to a certain point representative for glaze recipes of the respective region and period.

For the alkali glazes in the present study, the overall characteristic is Na_2O dominated. Only three glazes from Herat, Afghanistan, have high K_2O values and Na_2O/K_2O ratios below 1. The ratios of the remaining alkali glazes are commonly between 1 and 8. This accords to the general observation that Islamic alkali glazes are commonly enriched in soda relative to potassium (Brill, 1999; Shortland *et al.,* 2006). However, even the re-cast absolute Na_2O values are in part surprisingly low (down to 1.6 wt%). The low sodium values have to be regarded concerning the

analytical totals measurements in order to estimate the influence of weathering and sodium depletion of the glaze. The Afghan glaze with 1.6 wt% re-cast Na_2O has an analytical total of 98.1 wt%, allowing theoretically an original Na_2O value of 3.5 wt% Na_2O, which is still low. Three Uzbek alkali glazes with lead contents below 1 wt% and re-cast Na_2O values below 4.3 wt% have analytical totals between 95.1 and 95.8 wt% (samples KhZ 199, KhZ 244, KhZ 250). Other sodium-poor Uzbek glazes with 4.5-5.5 wt% re-cast Na_2O have analytical totals of 97.8-100.3 wt% (samples KhZ 031, KhZ 161, KhZ 162, KhZ 171, and KhZ 246). In general, the depletion of the glaze material seems to be not the sole reason for the low sodium values.

The alkali lead glazes are also made by using sodium dominated alkali flux, which is accompanied by varying contents of lead oxide. In the alkali and alkali lead glazes, Na_2O re-cast contents are between 1.6 and 17.3 wt%, K_2O contents are between 0.3 and 5.9 wt%.

A discrimination between mineral natron and sodium-rich plant ash as flux was previously established by Lilyquist & Brill (1993) for Early Egyptian glass on the basis of K_2O and MgO contents. They suggest a characteristic composition of the mineral natron flux glass, with K_2O below 2.0 wt% and less than 2.0 wt% MgO. The composition of the glass with plant ash flux is determined to have 2.2-4.0 wt% MgO and 2.5-6.5 wt% K_2O.

The considerations of alkali and alkali earth contents for glazes differ from those for glass composition in the influence of the underlying ceramic body in glaze compositions. In the recent study, it could be shown that at least some elements in the glaze like Si, Al, and K are influenced by the ceramic body. However, the general trends in the MgO and K_2O contents of the investigated glazes are considered in the following, assuming the migration of MgO and K_2O from the ceramic body to be minor compared with the original glaze composition (chapter 5.2). The compositional ranges of the presumably plant ash glazes are broader, including samples with K_2O contents of 0.3 to 5.9 wt% and MgO contents of 2.0 to 5.3 wt% (re-cast composition). The K_2O variation may be attributed to the time of plant harvesting, the use of different species and parts of the plants, different soil compositions, and the type of the alkali-bearing chemical compound in the plants (Mohr & Schopfer, 1978; Clemens, 2002). The compositional variation of mineral natron fluxed glazes exceeds the suggested range too, showing much higher K_2O values up to 4.6 wt% (re-cast composition). An impure mineral natron source with varying amounts of additional potassium salts could be one reason for the K_2O scattering in a mineral natron flux. Conclusively, in the present data set, K_2O contents (but also CaO, not shown here) scatter too much to be used as an indicator for the source of the sodium flux (fig.58 a). The

influence of the ceramic body on the K_2O and MgO contents in the glazes could be estimated by line scans through the glaze cross section. The influence is primarily seen in the glazes on stone paste ceramic, where the silica is enhanced in the vicinity of the ceramic. Al and K are not diluted by the enhancement of silica and are also assumed to migrate from the ceramic to the glaze. The lack of a diffusion profile can also be due to e.g. complete homogenization through diffusion or a too low concentration gradient between ceramic and glaze. In figure 58 a and b, the glazes with clay body are marked with smaller plot size. The number of clay based ceramic is small compared to the stone paste ceramics (53 of 243), and a general trend in MgO or K_2O contents in glazes on one or the other ceramic type is not observed.

According to the MgO values, the glazes can be subdivided into two groups, showing a gap between 1.3 and 2.0 wt% MgO, which allows the distinction between plant ash flux and mineral natron flux (fig.58 a). Alkali glazes from the 12th century Iran, from the 13th century Uzbekistan (Samarkand) and from the 13th century Turkey have a mineral natron flux signature (0.3-0.9 wt% MgO, re-cast values). A few of the 13th century Iranian glazes, but also Uzbek glazes (Bukhara) from the 15th and 16th century have plant ash characteristic (2.4-4.5 wt% MgO, re-cast values). For Afghan glazes from the 13th/14th to the 17th century, plant ash flux was used, with one exception, dated to the 15th century. This discrimination on the basis of MgO values is consistent with earlier studies of Islamic glazes from the 10th-13th century from Egypt, Syria and Iran (Pradell *et al.*, 2008; Doménech-Carbó et al., 2008), of medieval glazes from Yemen (Hallett *et al.*, 1988) and Jordan (Al-Saad, 2002) and of glazes from the 17th century from India (fig.58 a, Gill & Rehren, 2011). The occurrence of mineral natron compositions in medieval Central Asian glazes is reported from the Indian alkali glazes of the 14th – 17th century (Gill *et al.*, 2014) and from Syrian and Iranian alkali glazes from the 8th -14th century (Mason, 2004). In contrast, Uzbek alkali glazes from Akshiket, (Henshaw, 2007), early Islamic alkali glazes from Iran (Hill *et al.*, 2004), lustre ware alkali glazes from Syria, Iran (13th century), Iraq and Egypt (10th-11th century, Pradell et al., 2010), alkali glazes from Iraq of the 3rd century BC to the 15th century AD (McCarthy, 1996), and a selection of alkali tile glazes from Takht-i-Suleiman analysed by Osete-Cortina *et al.* (2010) show high MgO contents, which characteristic for plant ash flux.

A discrimination of both flux types is supported by P_2O_5 measurements (fig. 58 b). Almost all mineral natron flux glazes have P_2O_5 values at or below the detection limit of the microprobe (<0.05 wt%). A few Uzbek, Iranian, and Afghan plant ash alkali glazes have re-cast P_2O_5 contents of 0.1 - 0.8 wt% and five samples from the mosque Khoja Zainuddin have even higher P_2O_5
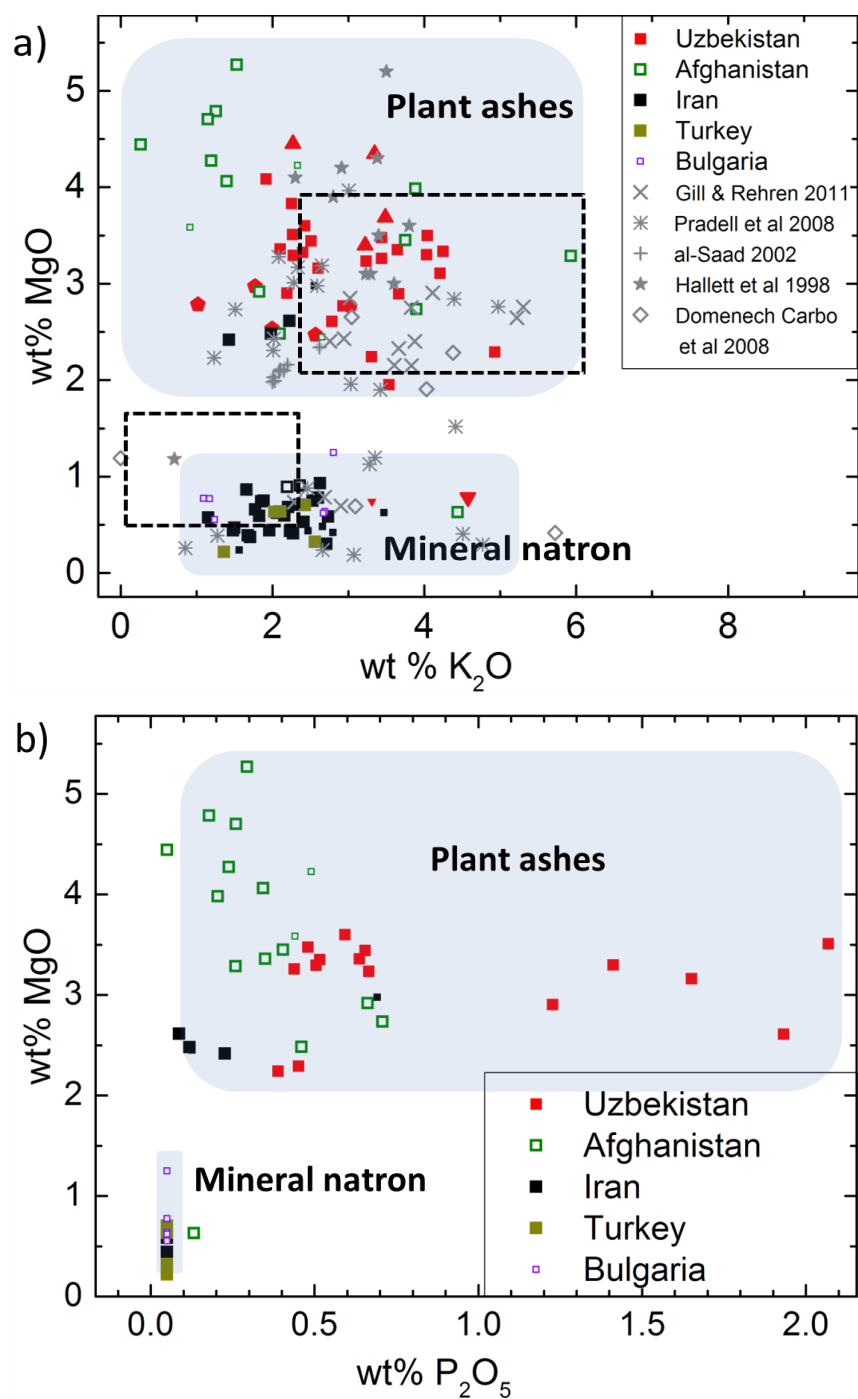
Figure 58a: Re-cast MgO versus K_2O and b: re-cast MgO versus P_2O_5 for alkali and alkali lead glazes. The dotted rectangles in 58a are the suggested composition categories for mineral natron and plant ash flux after Lilyquist & Brill (1993). Lead-free recalculated data from India (Gill & Rehren, 2011), Egypt, Syria and Iran (Pradell *et al.*, 2008, Doménech-Carbó *et al.*, 2008), Yemen (Hallet *et al.*, 1988) and Jordan (Al-Saad, 2002) are added for comparison. The tableware glazes are empty symbols, tile ware is depicted in full symbols. Glazes on clay ceramics are plotted in small points compared to the glazes on quartz frit bodies. In figure 58a, Uzbek samples are subdivided as in fig. 57.

contents of 1-2 wt%. Three of the five samples, two turquoise and one white one (KhZ 133.2, KhZ 196, and KhZ 032.1) are opacified with SnO_2 particles and have dissolved SnO_2 in the glaze matrix. In contrast, SnO_2-opacified glazes are also within the glazes of 0.1-0.8 wt% P_2O_5. An opacification with bone ash, which would result in high phosphate values, could not be proved. An associated higher level of re-cast mean CaO values is not observed (4.3 wt% in P_2O_5 rich glazes, 5.5 wt% in P_2O_5-poor ones). A bone ash slip between ceramic and glaze cannot be found either. Possibly, the high phosphate values are part of one type of plant ash material, related with phosphate bearing subsoil. Unfortunately, the P_2O_5 discrimination cannot be tested by data from the previous studies because of the lack of reported P_2O_5 values. A common distinction of flux types considers the ratio of Na_2O/K_2O and is based on the assumption of higher K values and therefore lower Na_2O/K_2O ratios in plant ash glazes (Shortland *et al.,* 2006; Tite *et al.*, 2006; Rehren, 2008).
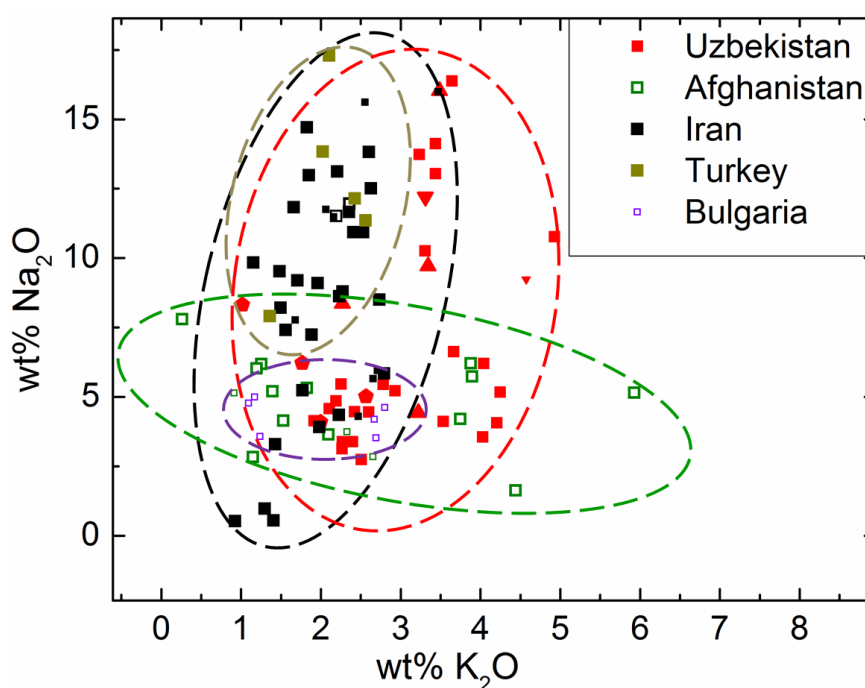
Figure 59: Depiction of the re-cast Na_2O and K_2O values of alkali and lead alkali groups. The tableware glazes are empty symbols, tile ware is depicted in full symbols. Glazes on clay ceramics are plotted in small points compared to the glazes on quartz frit bodies. Uzbek samples are subdivided into squares (mosque Khoja Zainuddin), circles (Ishrat Khane), triangles top up (madrassa Mir-i Arab), triangles top down (Samarkand), and pentagons (madrassa Abdul Aziz Khan). The Iranian data points are subdivided into squares (Takht-i-Suleiman) and triangles (restoration glazes from Isfahan).

With regard to the wide scattering of K_2O values in both types of alkali sources, this approach is not suitable for the samples investigated here. Nevertheless, the ratio of alkali oxides can be compared with known plant ash compositions and gives hint to particular plant species.

The depiction of K_2O versus Na_2O of alkali-rich samples is shown in figure 59 for the groups of alkali and re-cast alkali lead samples. The Na_2O/K_2O ratios of Uzbek alkali glazes are with 2.0-6.0 within the range of Uzbek plant ash raw material (Brill, 1999). In the Afghan alkali samples, the ratio is even below 1.0, suggesting very high K_2O contents in the used plant species. A plot of Na_2O/K_2O ratios in alkali and alkali lead glazes versus their approximate geographical locality is depicted in figure 60.
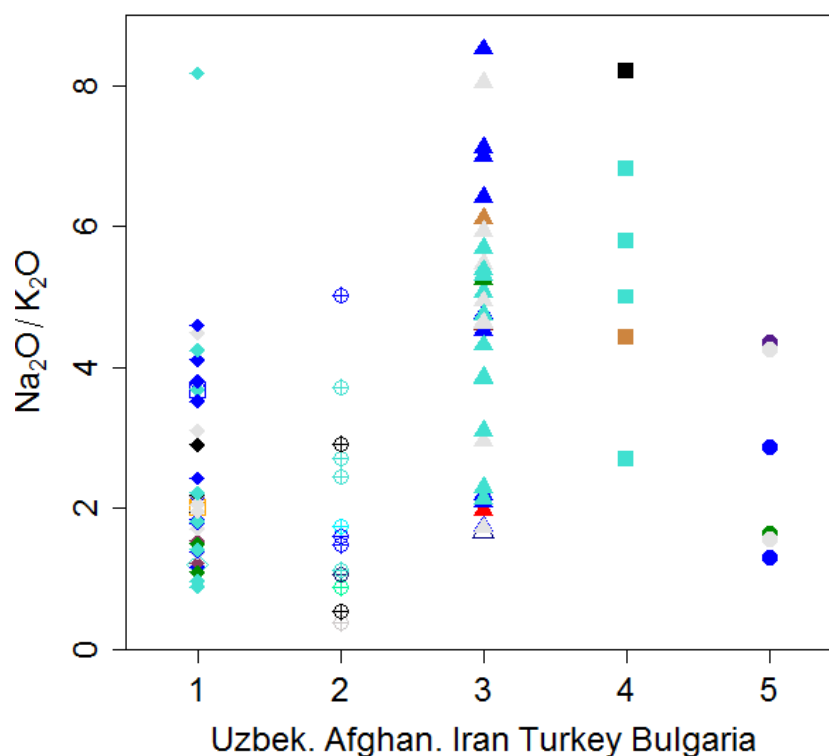
Figure 60: Distribution of the Na_2O/K_2O ratios in alkali and alkali lead glazes depending on their geographical site. The data points are coloured according to the approximate glaze colours.

One particular plant, called *Ishkor,* was analysed in another study and shows a Na_2O/K_2O ratio of 7.7 with a potash content of 4.6 wt% (Brill, 1999). The Iranian and Turkish samples show very similar behaviour of the K_2O and Na_2O distribution with re-cast K_2O values between 1.2 and 5.0 wt%, re-cast Na_2O values of 3.3-17.3 wt% and Na_2O/K_2O ratios of 1.7-8.5.

147

The Na_2O/K_2O ratio distribution of the coloured, probably imported ware of Bulgaria cannot be assigned unambiguously to one of the other locality groups. Henshaw (2010) mentions an enhanced ratio of Na_2O/K_2O of glazes from Middle East regions in comparison to the Central Asian samples from Akhsiket, Kuva, and Tashkent. In her analyses, medieval plant ash glazes from Akshiket, Uzbekistan are lower in sodium oxide and higher in potash than Iranian and Iraqi ones of the same period. This cannot be confirmed in the present sample set. Figure 60 reveals higher average values in the Turkish and Iranian glazes than in Uzbek, Afghan and Bulgarian ones. Within the Uzbek glazes, only one outlier has a Na_2O/K_2O ratio of above 8. Henshaw (2010) also states a general decrease of the alkali oxide sum in Central Asian glazes. Low alkali oxide sums are also observed in the Uzbek samples of the present study.

The CaO and MgO contents of alkali and alkali lead glazes can result from the sand part in the glaze as well as from a plant ash flux or from diffusion from the ceramic body. If CaO and MgO are ascribed to the sand source, the contamination is likely to be a calcareous or dolomitic part. Primarily calcareous characteristics can originate from coastal sands with seashell contaminations or from the seashells as separately added ingredient (Freestone, 2006). If the CaO and MgO contents originate from the plant ash part in the glaze, the input has to be ascribed to the soil on which the plants have grown. Because a plant takes up the water-dissolved ions from the ground, its alkali, and alkali earth composition mirrors the composition of the underlying soil (Clemens, 2002).

The glazes of the 16th century from Uzbekistan, most of the Afghan glazes and the four painted samples from Takht-i-Suleiman, Iran belong to the group of higher CaO/MgO values. The higher MgO re-cast values of >1 wt% in this group suggest a plant ash source for the alkali earth oxides and therefore an input of CaO and MgO from the soil on which the plants have grown. The proximity to the dolomite ratio of some glaze compositions is therefore likely to be caused by a dolomitic part of the soil. Pernicka & Malissa (1976) observe a dolomitic ratio of MgO and CaO contents in Persian glazes from 12th-14th century from Afghanistan. Here, the dolomitic part is ascribed to a separately added ingredient. Possibly, the "qamsari" stone, which is mentioned in the ancient treatise of glaze making of Abu´l-Qasim stands for this dolomitic ingredient (Allan *et al.*, 1973; Pernicka & Malissa, 1976). Assuming that the application of glaze slurry could have taken place with inorganic binder such as clay, this application vehicle could enhance the alkali and alkali earth contents. The small volume of binder material and the partly very low values of

alkali and alkali earth oxides suggest a minor role of the possible binder material in alkali and alkali lead glazes.

Lower MgO re-cast values below 1 wt% are found in most Iranian and Turkish glazes. Additionally, two Uzbek glazes from Samarkand (13th century) and most of the Bulgarian alkali lead glazes are in the low MgO group. In all these glazes, the CaO content is assumed to be brought in with a calcareous contamination of the used sand source.

8.3.1   Uzbekistan

The earliest Uzbek sample from the 11th-12th century are consistently lead glazes, and will be treated in chapter 8.4. For the flux in the alkali and alkali lead glazes from Samarkand of the 13th century, a mineral natron source is assumed because of the low MgO re-cast content of <0.8 wt%. The mineral natron is commonly very low in alkali earth contents, so the CaO re-cast contents of 5.7-7.3 wt% must be brought in as a contamination of the sand or an additional ingredient. In the random analyses of the clay-based ceramics from Samarkand, the CaO values are below 1 wt% and are therefore assumed to contribute only little to the enhanced CaO value in the glassy phase.

For the alkali and alkali lead glazes from Bukhara from the 15th century and younger, a plant ash source is assumed because of the high re-cast MgO values of 3.2 wt% in average (fig. 58 a; Sayre & Smith, 1974; Freestone, 2006). Although the ratio of alkali oxides is not diagnostic for mineral natron or plant ash source, it can be compared with plant ash analyses from the same region. The Na_2O/K_2O ratio for the alkali-rich samples is between 1.3 and 3.5, which is in good agreement with the analysed ratio of 3.3 in one of the plant ashes of the *salsola grassi* from the Uzbek desert (tab.21; Brill, 1999).

Table 21: Na_2O and K_2O contents of plant ashes from Uzbekistan, Brill, 1999.

Ref.-No.	Description of plant ash	Na_2O	K_2O	Na_2O/K_2O
4446	Ashes of *salsola grassi*, small stems with foliage and pod debris. Final firing at 800°C for 1h	40.30	12.30	3.28
4447	Samarkand, alkali used by tile glazers. Hard, dark gray lumps. Final firing at 800°C for 1h to remove unburned carbon	42.10	7.01	6.01
4449	Uzbekistan plant ashes black powder containing many relict stems, re-fired at 750°C for 1h	8.12	25.80	0.31

The subgroup of the Uzbek samples from the madrassa Mir-i Arab from the 16th century has values of Na_2O/K_2O = 3.1 in average, which also matches the ratios of analysed plant species (Brill, 1999). The enhanced P_2O_5 content in alkali and alkali lead glazes of Uzbek glazes can also be attributed to the plant ash source, in particular to the soil from which it was harvested (Clemens, 2002).

8.3.2   Afghanistan

The Afghan alkali glazes show, with one exception, plant ash characteristic with MgO re-cast values of 2.4-5.3 wt% (fig.26). The low re-cast sodium oxide values of 1.6-6.2 wt% Na_2O resemble the alkali glaze group of the Uzbek tiles with re-cast sodium oxide contents of 3.1-6.2 wt% Na_2O. Both alkali groups with low sodium oxide contents date into the 15th-16th century, when Uzbekistan was ruled by the Sheibanid dynasty and Afghanistan by the Timurid dynasty. It is known that Timurid craftsmen were hired in other regions and cities in order to build up imposing monuments (Golombek, 1996). An exchange of Afghan and Uzbek craftsmanship could be also the reason for the parallels in the alkali glaze compositions. Kleinmann (1986) reports similar compositions in glazes with plant ash flux from various sites in Mesopotamia, Egypt, north-eastern Persia and Turkestan, and Turkey of the 8th-12th century.

The Na_2O/K_2O ratios in the Afghan alkali glazes between 0.5 and 5.6 are within the wide scatter of the plant ash analysis of Afghan species (*ishkor* and *tezab*) with ratios of 1.2 and 7.7 (Brill 1999; Tite *et al.*, 2006). One older sample from the 13th/14th century (Her 58) is with a Na_2O/K_2O ratio of 2.7 within the general range, too.

An exception is the white sample Her 46 from the 15th century with mineral natron characteristic. It is evidence for the use of mineral natron parallel to plant ash as flux in the 15th century. Nevertheless, the K_2O value is with 4.4 wt% considerably high and results in a Na_2O/K_2O ratio of 0.4. The mineral natron sources Wadi-el-Natrun or Lake Van in eastern Anatolia with Na_2O/K_2O ratios of >10 (Shortland, 2004; Reimer *et al.*, 2008) must be ruled out as a possible sodium source because of this low Na_2O/K_2O ratio. The database on evaporite compositions from salt lakes and salt stocks is unfortunately too small for a comprehensive comparison. A purified plant ash source is also unlikely, because the depletion of MgO would simultaneously reduce the CaO content (chapter 2.1.4). However, the CaO value is with 9.4 wt% remarkably high. The origin of the potash rich and magnesia poor flux cannot be clarified here.

8.3.3   Iran

The Iranian glazes date into the 12th and 13th century, i.e. the Khwarazmian and the Ilkhanate dynasty. In the alkali and alkali lead glazes, high re-cast sodium oxide contents up to 15.6 wt% Na_2O are found. Most of the glazes have low MgO compounds, which is characteristic for the use of mineral natron. Possible sources of mineral natron could be either the salt lakes in Egypt (Wadi-el-Natrun and el-Barnuj) or salt lakes in the Middle East (Lake Van). The origin of mineral natron outside of the Wadi-el-Natrun is not easy to determine because of the small amount of analysed data (chapter 8.3.2). Most of the sources seem to have about 99% Na_2O content and almost no K_2O (Shortland *et al.*, 2006) and do not fit the re-cast K_2O contents up to 3.5 wt% at re-cast Na_2O contents of 4.3-16.0 wt% in the alkali and alkali lead glazes.

Four Iranian glazes, TiS 31-34, reveal from painted tiles with lustre or *ladjvardina* decoration. These alkali and alkali lead glazes have a clear plant ash characteristic with enhanced MgO re-cast values of 2.4-3.0 wt%. The Na_2O/K_2O ratios are between 1.7 and 6.1. Analyses of Iranian plant ashes, called *osnan,* show Na_2O/K_2O ratios of 3.5-9.2 (Tite *et al.*, 2006) indicate the wide variability of the plant ash compositions and overlap with the mentioned ratios of Iranian glazes. On the building complex Takht-i-Suleiman, which is the origin of the glazes, craftsmen from different parts of the Middle East were taking part in the building process (Mason, 2004). This may be the reason for the parallel use of mineral natron and plant ash flux in the tile glaze production. For the region of present day´s Iraq, the use of plant ash for alkali glazes in lustre ware is reported from the 7th-11th century; whereas mineral natron is used in one part of Iranian lustre ware glazes from the 7th- 14th century (Mason, 2004).

The two glazes from the restored samples from the 20th century Isf 18 and Isf 19 have PbO, SiO_2, Na_2O, and alkali earth oxide contents within the range of older Iranian glazes from Takht-i-Suleiman. One of the glazes differs with a higher re-cast K_2O value of 4.9 wt% from the glazes from the 13th century which have 2.2 wt% in average, and 3.5 wt% as maximum re-cast K_2O value. The modern restoration glazing obviously uses another alkali flux than the craftsman of former times.

8.3.4   Turkey

The Turkish alkali and alkali lead glazes from the sites Konya and Kayseri have re-cast sodium oxide values up to 17.3 wt% Na_2O, similar to the Iranian glazes. The very low MgO contents of

<1 wt% suggest the use of mineral natron as a flux. The re-cast K_2O values are between 1.4 and 3.1 wt%. In the later glazed pottery from *Iznik* of the 15th-16th century, similar compositions are found but with lower K_2O values (Paynter *et al.*, 2004). In the here analysed Turkish glazes from Konya and Kayseri, the Na_2O/K_2O ratios are with 2-8 lower than those from the salt compositions from Wadi-el-Natrun or from the lake Van in Turkey (Shortland, 2004; Reimer *et al.*, 2008). The Turkish salt lake Tuz Gölü is 100 km in the north-east of Konya, but the high purity of 89-99 % Na-minerals (Kilic & Kilic, 2010) does not fit to the analysed compositions. Therefore, the mineral natron of the glaze has to originate from a further salt lake or salt stock.

The alkali and alkali lead glazes from Turkey have re-cast CaO values of 2.0-8.0 wt%. These contents are unlikely to result from the mineral flux, but probably originate from contaminations in the sand as e.g. calcareous or anorthite parts. Low Ca contents of < 1 wt% CaO in the analysed stone paste body grains rule out a large influence of Ca- migration from the body. The Al_2O_3 contents of the glazes scatter between 1.3 and 6.0 wt% and also have to be ascribed to sand contamination or alumina migration from the stone paste ceramic bodies.

8.3.5 Bulgaria

The larger part of the 27 Bulgarian samples from the Ottoman and all ten from the Second Bulgarian Empire are lead samples which are not discussed here.

Six glazes, BG 1-3 and BG 11-13, have alkali lead compositions and originate from two painted sherds which are assumed to be imported tableware (chapter 3.5; Atanasov, pers. com. 2013). The glazes have medium lead contents of 16.8-23.3 wt%, which are similarly observed only in the Iranian and the Turkish glazes of this sample set (9.7-27.1 wt% respectively 12.2-27.5 wt% PbO). The re-cast K_2O contents of 1.1-2.8 wt% and the mineral natron characteristic of 0.6-1.3 wt% MgO (re-cast composition) especially resemble the Iranian re-cast alkali lead glaze compositions with 1.2-2.7 wt% K_2O and 0.3-0.9 wt% MgO. Nevertheless, the re-cast values of 3.5-5.0 wt% Na_2O and 1.8-4.0 wt% CaO are lower than in the Iranian glazes (4.3-13.8 wt% Na_2O and 2.9-9.0 wt% CaO re-cast composition). The Na_2O/K_2O ratios are with 2.7 ± 1.4 in the range of the other alkali and alkali lead glazes from Uzbekistan, Afghanistan, Iran, and Turkey (fig.57). As possible origin for the imported sherds, the Middle East may be considered because of the medium lead content of 16.8-23.2 wt% PbO and the similar K_2O and MgO values.

8.3.6   Morocco

The Moroccan samples are consistently high lead glazes and have no independent alkali or alkali earth component. The input of minor elements will be discussed in the chapter 8.4.6.

8.4   Minor elements in lead glazes

This chapter treats the minor parts of e.g. alumina, alkali, and alkali earth oxide contents in lead glazes. Lead glaze compositions occur in the sample set of each of the investigated locality: The oldest, consistently lead rich glazes are from Afrasiab. The younger Uzbek glazes from the 13th-17th century, as well as the Afghan, Iranian, and Turkish glazes have only in part lead compositions. Within the younger glazes of Ottoman period, 21 of 27 glazes have lead composition. The glazes of the Second Bulgarian Empire and the Moroccan glazes have all lead compositions.

Lead glazes consist in up to 95 % of their composition of PbO and SiO_2. Colouring agents, alkali oxides, alkali earth oxides and different impurities as Fe_2O_3 represent only a few weight percent each. Due to the narrow interfaces between ceramic and glaze in lead glazes compared to alkali and alkali lead glazes, the application is assumed to have been in a mixture of lead and silica component rather than in a pure lead slurry reacting with the siliceous ceramic body (chapter 8.1). The low contents of alkali and alkali earth contents in lead glazes on clay bodies also contradict the application of pure lead oxide slurry. Because the lead component is assumed to be purified and pre-treated in a roasting step (Tite *et al.*, 1998), the input of alkali and alkali earth contents can originate from a diffusion process from the ceramic body or from a component of the glaze slurry. This component can be contaminations of the SiO_2 source, the colouring agent, or another separately added mineral. Considering that the application of the glaze slurry was in some cases realised with a clay binder (chapter 2.3.1), the backtracking of alkali and alkali earth sources becomes even more difficult. Because of the low contents and different input possibilities, Pernicka (1979) deny the suitability of alkali and alkali earth oxide contents in lead glazes for classification. A correlation of alkali and alkali earth oxides with the SiO_2 content suggests a contamination of the sand source. If the minor elements are added with the colouring mineral, a correlation between colouring agent and the accompanying elements is expected. Such a correlation between CoO and MgO is observed in one subgroup and will be discussed in chapter 8.7.1.

The ceramic body composition can influence the contents of alkali and alkali earth oxides in the glaze, as well as the alumina content. Especially in the case of clay-based ceramic bodies, diffusion of the Al_2O_3-component into the glaze is assumed (Pernicka, 1989). In figure 61, the depiction of CaO and Al_2O_3 is given for the lead glazes of different locations. Regarding the ceramic body type (small data points), a statistical enhancement of alumina values on clay-based ceramic can be confirmed. An enhanced Ca-value cannot be observed.

From the description of SiO_2 sources for glassmaking, which are assumed to be similar for the glaze production, quartz pebbles, chert, riverine and coastal sand, and inland deposits are known (Henderson, 2013). For the traditional glaze making in Iran, the Khwarezmian scholar Abu Raihan al-Buruni mentions the gathering of quartz pebbles from dry river beds as silica source (Allan *et al.*, 1973).
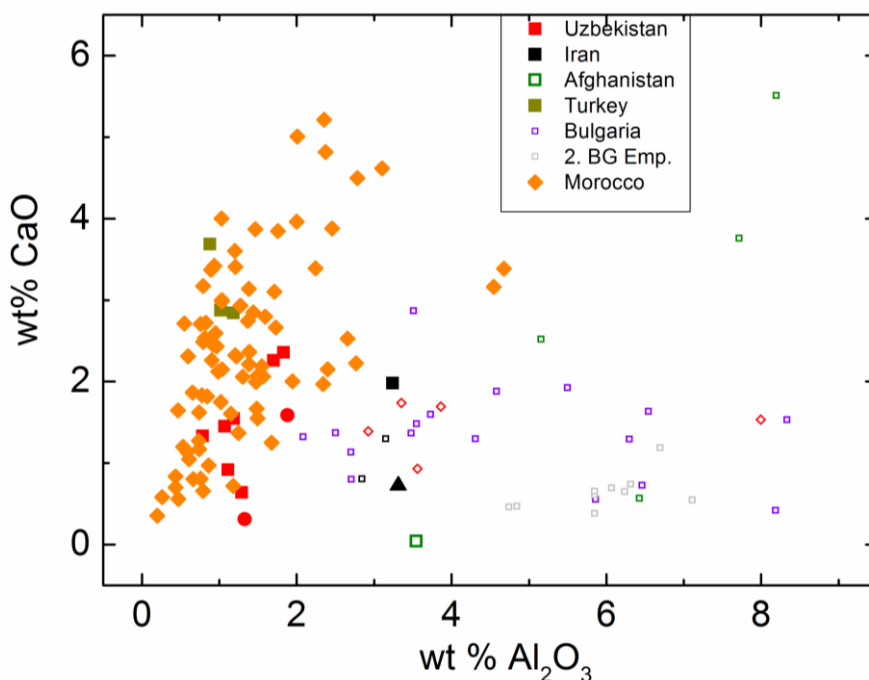
Figure 61: CaO and Al_2O_3 contents in lead glazes, which are caused either by different sources of used silica or separately added minerals. A distinct correlation of CaO and Al_2O_3 with colouring agents cannot be observed (chapter 8.7). Glazes on clay ceramics are plotted in small points compared to the glazes on quartz frit bodies. The Uzbek data points are subdivided into diamonds (Afrasiab), squares (mosque Khoja Zainuddin), and circles (Ishrat Khane). The Iranian data points are subdivided into squares (Takht-i-Suleiman) and triangles (restoration glazes from Isfahan).

The purity of quartz pebbles and chert is commonly higher, the purity of sand deposits depends on the type of rock they originate from, and on the medium and the distance they are transported. Fluvio-glacial transported sand deposits are commonly less sorted and more contaminated than deposits which are transported by aeolian processes (Henderson, 2013). The longer the sand is transported the lower is the fraction of light minerals with low stability against weathering like e.g. carbonates. Heavy minerals, which resist against chemical and physical weathering, are e.g. iron oxides, iron titanites and silicates with high Mohs scale like zircon (Henderson, 2013). Alumina and aluminium silicates are also stable against weathering and can be found in sand deposits. MacCarthy (1933) assigns high CaO values in sand to the contents of shell fragments in coastal sands. However, sands from calcareous-rich sand bars of delta areas can also contain high CaO values. Pernicka & Malissa (1976) suggest limestone or dolomite as a separately added mineral in Islamic glazes.

The alkali and alkali earth contents of the lead glazes are in most cases around 1 wt%, only the CaO values are at 2.2 wt% in average. Higher values of CaO are primarily found in the large number of Moroccan lead glazes (fig.61).

8.4.1   Uzbekistan

The compositions of the lead glazes from Afrasiab have total alkali contents below 4 wt% which are dominated by K_2O. Within the alkali and alkali earth oxides, Na_2O, K_2O, and MgO show rough correlations. The values of 0.4-1.1 wt% Na_2O, 0.3-3.0 wt% K_2O and 0.3-1.2 wt% MgO seem to be too low for addition of a separate mineral but point to a contaminated Si-source or the diffusion input by the clay-based ceramic body. The correlation of MgO and CaO values in the Uzbek lead glazes on clay-bodies (Afrasiab) and stone paste bodies (mosque Khoja Zainuddin, the madrassa Mir-i Arab and the mausoleum Ishrat Khane) contradicts the theory of element input of MgO and CaO from the ceramic body (fig. 62). The alumina contents are between 2.9 and 8.0 wt%, whereof the highest values are found in Afghan and Bulgarian glazes. They can result e.g. from an aluminium silicate in the sand component or from the use of clay-binder in the glaze application process. In the random analyses of ceramic grains, Al_2O_3 values of up to 10 wt% are detected, which are assumed to contribute to the Al content in the glaze (see also chapter 5.2). Regarding the mol fractions of alkali, alkali earth oxides, iron oxide and alumina, potassium feldspars as well as plagioclase, mica minerals, chain silicates or garnets come into question. The

sums of Na_2O and K_2O for example, can result from potassium feldspar, which is formed with the high Al_2O_3 contents. The molar contents of the oxides are listed in table 22. The contents in weight percent are given in table 11.

Table 22: Minor elements in the lead glazes from Afrasiab, given in mol%.

sample	colour	Na_2O	K_2O	CaO	MgO	Fe_2O_3	Al_2O_3	SiO_2
36 Afr	red	0.68	0.60	1.73	0.67	0.19	3.64	65.72
37 Afr	white	0.93	1.18	2.83	1.66	0.49	3.55	69.23
38 Afr	white	1.45	1.21	2.89	1.43	0.33	3.06	68.62
39 Afr	black	1.46	2.70	2.27	2.38	1.84	6.50	71.01
40 Afr	green	0.72	0.92	2.58	0.99	0.86	2.99	63.45
41 Afr	green	1.26	0.85	3.44	1.84	0.46	3.26	62.54
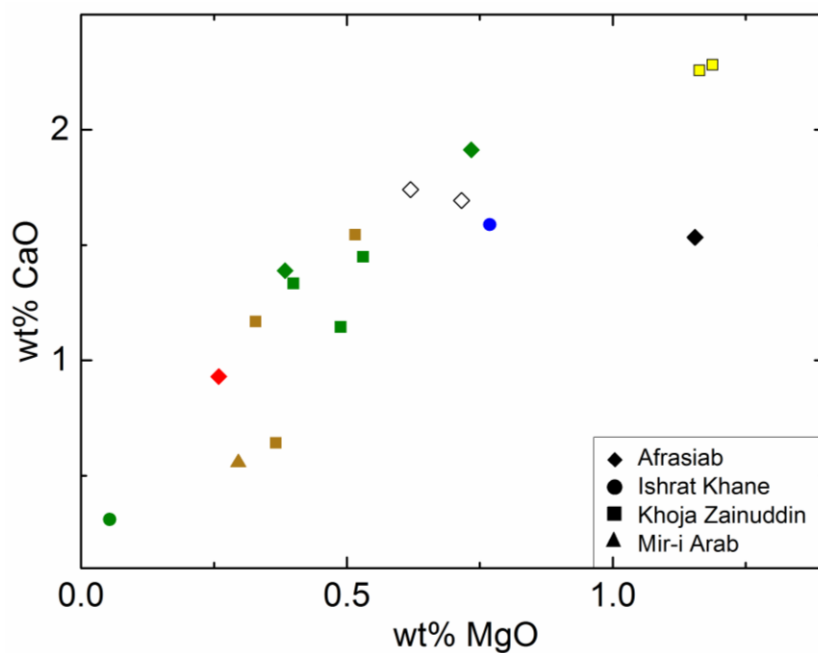
Figure 62: CaO and MgO correlation in lead-rich samples on clay-based bodies from Afrasiab, 10th/11th century, from the stone paste glazes from mausoleum Ishrat Khane from the 15th century, the mosque Khoja Zainuddin, Bukhara, and from the madrassa Mir-i Arab, Samarkand, both from the 16th century. The colours display the colouring of the glaze.

The lead glazes from the mosque Khoja Zainuddin and from the mausoleum Ishrat Khane, Samarkand, show very low values of 0.8-2.0 wt% Al_2O_3 and 0.6-2.4 wt% CaO, which can be ascribed to a very pure SiO_2 source. Quartz stones gathered from ravines, dry river beds, or flints,

as it is described by the medieval Islamic scholar Al-Biruni (Allan *et al.*, 2000) presumably build the silica source in Uzbek glazes.

8.4.2 Afghanistan

In the Afghan set of tableware glazes, lead-rich compositions are found in almost all sampled centuries (14th-17th). The lack of intermediate glazes in the sample set suggests the continuous coexistence without mixing of the technologies of alkali and lead glazes. The Afghan lead glazes have all clay-rich ceramic bodies. The glazes show a wide spread of Al_2O_3, which is due to its magnitude unlikely to result only from clay body migration or clay binder material. Together with the scattering of K_2O, MgO, and CaO, different sand sources or different mineral additions are suggested. Because of the popular role of tableware ceramics as trading objects (Fragner, 2007), the localities of production are much harder to encircle here than in the case of tile ceramics. In two lead glazes from Herat (Her 50 and Her 54), a combination of high CaO and Al_2O_3 values is observed. This high values of 3.8-5.5 wt% CaO and 7.7-8.2 wt% Al_2O_3 represents a contamination of Ca-(and maybe Al_2O_3-) contamination of the silica source together with the input of Al_2O_3 from the clay-based ceramic body and a possible addition of clay-binder (fig.62).

8.4.3 Iran

In the historical Iranian samples, only three glazes TiS 12, TiS 13a, and TiS 13b have lead contents above 30 wt% PbO. The glazes TiS 13a and TiS 13b belong to one greenish-yellow polychrome sherd of clay-based tableware ceramic. These glazes from the 10th-13th century are from "*Champlevé*" tableware and show medium Al_2O_3 contents of 2.8-3.2 wt%. The CaO values of 0.8-2.0 wt% are below the average CaO value of alkali and alkali lead glazes from Iran (4.5 wt%), too. Even when the values are re-cast to lead-free compositions, the Iranian lead glazes stay with 2.1-4.4 wt% CaO below the average value of 5.1 wt% CaO in alkali and alkali lead glazes. Both, CaO and Al_2O_3 could be suspected to originate from the ceramic body, but the similar values of Tis 13 a and b on clay-based ceramic and TiS 12 on stone past ceramic (fig. 61) make a wider influence unlikely. Assuming that the alkali and alkali lead glazes are produced with a similar silica source as the lead glazes, the additional CaO in alkali and alkali lead glazes has to result from the natron flux or a separate mineral, which was e.g. added as binder for the slurry application. The majority of the Iranian alkali and alkali lead glazes have mineral natron

composition, which has no significant alkali earth contents. The CaO is therefore assumed to be brought in with a separate ingredient. Pernicka & Malissa (1976) suggest the separate addition of a calcareous or dolomitic ingredient also for Afghan glazes from the 12th-14th century (chapter 8.3).

In the younger lead glazes from the 20th century the CaO and MgO values are similar to those of the historical samples. As a peculiarity, the lead glaze has a high K_2O value of 4.2 wt% K_2O, which is exceeded only by a few lead glazes from the Marinid time in Morocco.

8.4.4   Turkey

The three lead glazes from Turkey are from one tile of the mosque Ata Hanka in Konya. In the lead free, re-cast compositions, the CaO average value is with 11.4 wt% higher than the average value of 4.8 wt% CaO in the alkali and alkali lead glazes from Turkey. Compared to the CaO average values of re-cast lead glaze compositions from Uzbekistan, Afghanistan, Iran, Bulgaria, and Morocco (2.8-4.6 wt%), the CaO values are also enhanced and reflect a contamination of the sand with e.g. carbonatic minerals or the addition of a calcareous mineral (fig.61). Assuming a common silica source of alkali, alkali lead, and lead glazes, the addition of a separate calcareous mineral is likely.

8.4.5   Bulgaria

The glazes from the Second Bulgarian Empire of the 11th-12th century and the monochrome glazes from Ottoman Bulgaria are lead glazes. It seems that the lead glaze technology is the dominating if not the only technique in this period. Only the six glazes from polychrome sherds have alkali lead compositions, which are assumed to be imported tableware. A possible explanation for the lack of alkali and alkali lead compositions could be a continuity of glazing tradition from the Roman culture. The Second Bulgarian Empire followed close upon the Byzantine Empire, which implies the Roman tradition. A minor influence of the occupying Ottomans in the 14th century on the glazing craftsmanship would explain the continuity of lead glaze compositions.

The ratio of silica to lead contents are with around 1:2 constant in the Second Bulgarian Empire and Ottoman epoch in Bulgaria. Glazes from both epochs have high Al_2O_3 contents of 1.6-8.3 wt% and CaO contents of 0.4-2.9 wt%. A correlation of CaO and SiO_2 can be detected, which can

be due to a contamination of the sand raw material or due to an addition of Ca-rich mineral (fig.63). With regard to the normalised CaO values of 0-1 wt% in sherds from the Second Bulgarian Empire and 4-8 wt% in the Ottoman samples, a contribution of Ca migration from the ceramic seems also likely. The Al_2O_3 values show broader scattering and no specific correlation can be observed. The Al_2O_3 input is assumed to be at least in parts from the clay body ceramic, regarding the high Al_2O_3 values of up to 20 wt% in analysed ceramic grains. According to Pernicka (1979), the values of Al_2O_3 do not suit as parameter for glaze classification due to the input by the ceramic body.
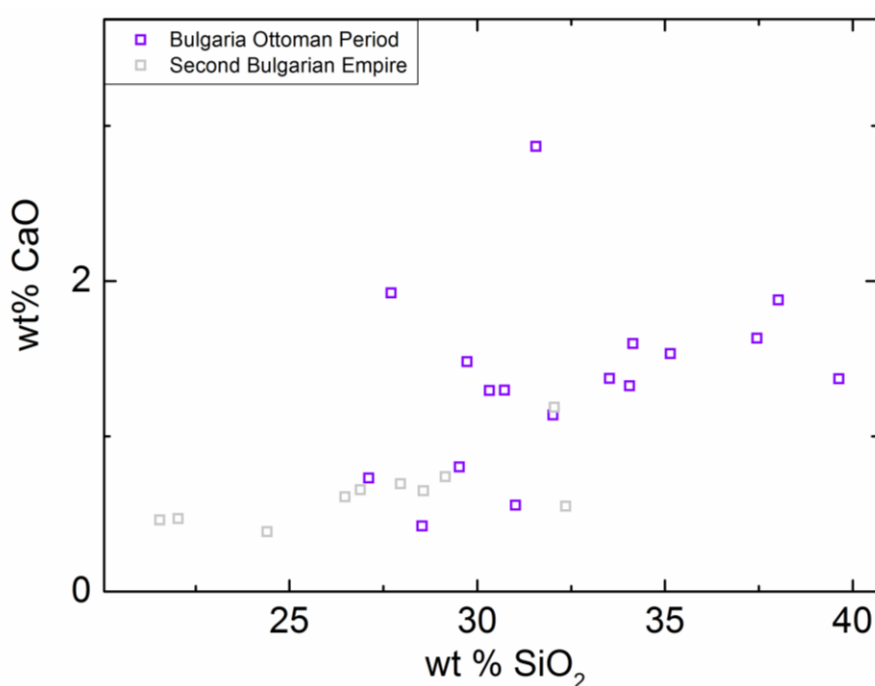
Figure 63: Correlation of CaO and SiO_2 in the monochrome lead glaze sherds from Ottoman Bulgaria and the glazes from Second Bulgarian Empire.

The elements Na_2O, K_2O, and MgO have values of below 1 wt% in the glazes from the Second Bulgarian Empire; in the glazes of the Ottoman period the values are even below 0.5 wt%. These values are too small to expect a separate alkali oxide or alkali earth oxide ingredient. Although, there is no distinct correlation between the alkali (earth) oxides and the SiO_2 content, the input of these oxides is likely to be the sand component. Possibly, the use of different sand deposits for the glaze production in the Second Bulgarian Empire and Ottoman period is reason for the lack of SiO_2 correlations.

Further, the lead glazes from the Second Bulgarian Empire and Ottoman Bulgaria show a correlation of Fe_2O_3 and MgO with Na_2O (fig.31). These oxides cannot be ascribed to a certain mineral. Possibly, they belong to a pyroxene or amphibole mineral, or to clay minerals which were added to the glazing slurry.

The TiO_2 in monochrome Ottoman and glazes from the Second Bulgarian Empire correlates with the Al_2O_3 contents (fig.32) and roughly with the Fe_2O_3 contents. The Ti values can be explained with Ti contents in the ceramic body. Random analyses of ceramic material reveal Ti contents of 0.3-0.9 wt% in ceramics of monochrome and polychrome sherds of Ottoman Bulgaria, and Ti contents of 0.1-1.2 wt% in sherds from the Second Bulgarian Empire. The TiO_2 contents in the ceramic material and possibly the glaze raw material in the glazes from the Second Bulgarian Empire and the Ottoman time reveal certain continuity in the glaze production over different centuries and regimes in Bulgaria.

In contrast, the glazes from the painted sherds with alkali lead composition do not fit into the correlations. The two polychrome sherds with the glazes BG 1-3 and BG 11-13 are assumed to be imported tableware (pers. comm. Atanasov, 2013). The lower PbO and Al_2O_3 values and the higher Na_2O contents in the polychrome paintings underline this assumption (figs. 30 and 32).

8.4.6   Morocco

The general compositions of the Moroccan glazes are lead-rich, even if the lead content varies between 29.7-64.9 wt% PbO from locality to locality. Alkali and alkali earth oxides are in average 0.8 wt% Na_2O, 1.5 wt% K_2O, 0.5 wt% MgO and 2.4 wt% CaO. In most of the glaze compositions, the Na_2O and K_2O ratios show no special characteristics and vary between 0.4 and 0.8. The low total content of alkali oxides and the missing correlation to any colouring agent or SiO_2 suggest that the alkali contents originate from different sand sources or from a separately added component. The homogeneity of flux application in Moroccan glazes cannot be unambiguously attributed to an availability of raw materials or a cultural influence. The rule of Romans in the northern part of Morocco from the 1st-5th century AD can be one reason for a continuously preferred use of lead as flux. A similarity of Moroccan glazes to the lead-rich tile glazes from Spain and Portugal reveals a cultural vicinity to the southwestern European craftsmanship (Iñañez *et al.*, 2008; Guilherme *et al.*, 2013).

Remarkable are the three groups of glazes with enhanced contents of up to 2.5 K_2O and 1.4 Na_2O from the necropolis Chellah, from the Marinid School in Salé and of the madrassa Abu Al Hassan in Salé. Simultaneously, they have the lowest lead oxide values within the Moroccan samples.

Between Na_2O and K_2O as well as between CaO and MgO, a correlation is observed in all Moroccan glazes (fig.34). A diffusion of alkali and alkali earth elements from the ceramic glaze could result in the rough correlation. The Moroccan samples have continuously stone paste ceramic bodies, which also contain feldspar grains. However, the analyses of ceramic are not statistically corroborated, because of the small material amount per sample. The already mentioned values of glazes from buildings from Salé and Rabat play again a different role and do not fit in the correlation of Na_2O and K_2O. It cannot be decided whether the glazes from the other localities Meknes, Tangier, Fes, and Marrakesh have a common silica source, or just sources of similar alkali and alkali earth ratios. Statistical differences in the ceramic compositions, which could lead to the increased Na_2O and K_2O values, cannot be detected.

The Al_2O_3 values of Moroccan glazes are with 1.3 wt% in average comparatively low compared to the average values of Uzbek and Afghan samples (3.2 wt%), Iranian and Turkish glazes (2.3 wt%), and the Bulgarian group (4.3 wt%, fig.63). The CaO values instead scatter from 0 to more than 5 wt%. Regarding the contents of Al_2O_3 in context with the body type, the alumina values are strongly influenced by the diffusion of alumina from the underlying ceramic. The stone paste ceramic bodies of Moroccan glazes obviously do not introduce considerable amounts of alumina into the glaze.

The ZnO content of the Moroccan samples is with 0.3-0.4 wt% slightly enhanced compared to the other localities with around 0.1 wt%. The highest values are found in the glazes from the fountain and the sultan´s palace in Tangier. The glazes from Tangier include black, white, blue, turquoise, green, and ochre colours, so the ZnO cannot be ascribed to a particular colouring agent, but is assumed to originate from the silica source.

8.5 Comparison of Islamic glazes

This chapter puts the results into context of previous investigations of Islamic glazes. It can be concluded from this study, that different glazing technologies existed contemporaneously at different localities and during several centuries.

In almost every epoch and locality, lead glazes can be verified. This is also observed in investigations of samples from Iraq, Jordan, and Iran (McCarthy, 1996; Al-Saad, 2002; Holakooei *et al.*, 2014). The earliest Uzbek tableware glazes of the Seljuq and Samanid period of the 10th-11th century have a consistent lead flux characteristic (fig.64). The lead glaze technology is probably brought to Central Asia in the course from Iraq in the 9th century (Henshaw, 2010). As locations for ceramics and glazed tiles in Central Asia of these epochs, the following four main production centres are stated (Allan *et al.*, 2000; Naymark, 2006; Pugachenkova *et al.*, 2009); the Fergana region in eastern Uzbekistan, the Khorezm region in western Uzbekistan, the Bukhara and Samarkand region, and the city of Tashkent. It is known, that from the 10th-12th century in Uzbekistan, the black and white calligraphic style is used for tableware (Henshaw, 2010), which occurs in two samples of Afrasiab from the 10th and 11th century. Two other lead glazes from Afrasiab have green colour and prove the early occurrence of green in the decorative styles of tableware in Uzbekistan, outreaching the reported black and white decoration. Possibly, these are predecessors of the "Haft rang" technique, which was developed by the Khwarazmians in the Iranian region in 12th century (Allan *et al.*, 1973).

This is a decorative style of seven different glaze colours which was later extensively used in the in Iran (Holakooei *et al.*, 2013). The name "Haft rang" is a literally translation of "seven colour". Assuming that the use of plant ash flux in glass production was continuously carried out in Central Asia through the Roman time (Sayre & Smith, 1974), the occurrence of mineral natron compositions in glazes is remarkable. In this study the earliest glazes with mineral natron characteristics are Iranian alkali glazes from the 12th century (fig.64). Mason (2004) show that few alkali glazes from Syrian lustre ware from 700-1250 AD and Iranian lustre ware from 700-1340 AD have mineral natron characteristic. The somewhat younger tiles from Turkey and Samarkand of the Mongol period in the 13th century also have alkali glazes with mineral natron flux. The youngest sample with mineral natron is the single tableware glaze from Afghanistan from the 15th century. This single mineral natron glaze attracts attention by its high alumina value of 13.3 wt%. High alumina alkali glazes with mineral natron characteristic also occur in Indian Islamic tile glazes from the 14th-17th century, but with at most 7.4 wt% Al_2O_3 wt% (Gill *et al.*, 2014). In contrast, the Iranian tile glazes from the Ilkhanate dynasty of the 13th century are the earliest plant ash alkali glazes in the entire set of samples with enhanced MgO values of 1.8-3.0 wt% MgO (fig.64). Henshaw *et al.* (2007) reveal the use of plant ash in Uzbek tableware (*Ishkor* ware) from the 10th-11th century synchronously to the lead glaze tableware.
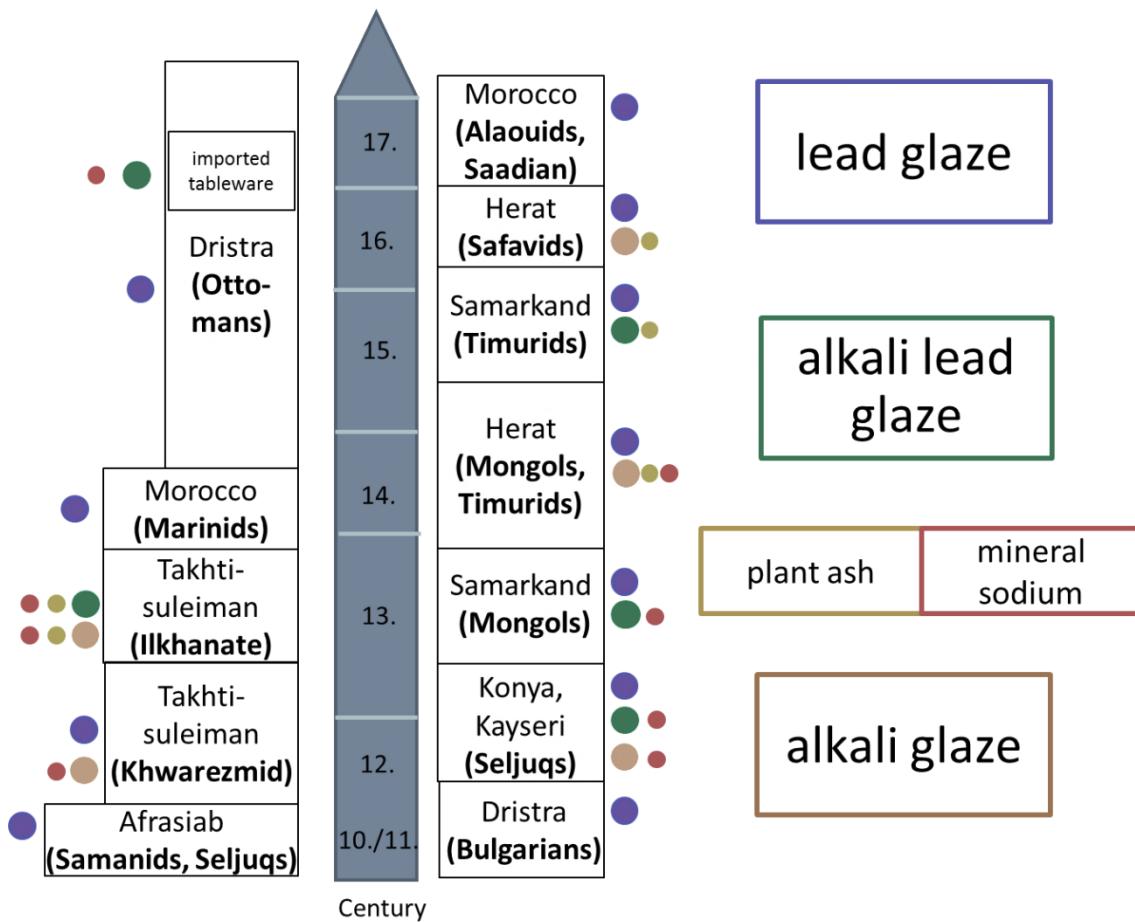
Figure 64: Basic compositions of glazes during the medieval centuries of Islamic culture.

Uzbek and almost all Afghan glazes from the 15th to 17th centuries also have plant ash compositions with up to 16.5 wt% Na_2O, 4.1 wt% K_2O, 4.4 wt% MgO, and 7.0 wt% CaO. Similar characteristics are known from the so-called *Ishkor* plant ash glazes from Central Asia from the 12th century and earlier (Pérez-Antegui *et al.*, 1999; Vandiver *et al.*, 2010). The plant ash technology is also reported for other Islamic tile glazes, e.g. from the 17th century in Pakistan (Gulzar *et al.*, 2013) and confirms the trading and transfer of knowledge in the Timurid Central Asia (Henshaw *et al.,* 2007).

One subgroup of the plant ash alkali glazes from the mosque Khoja Zainuddin has Na_2O values below 6.0 wt% and an average value of 4.5 wt%. The tableware glazes from Herat, Afghanistan also have plant ash compositions with lower Na_2O values, similar to the sodium-poor alkali glazes from Uzbekistan. Similar low Na_2O values are reported from medieval plant ash glazes

from Akshiket, Uzbekistan (Henshaw, 2010). Other Islamic glazes from e.g. India or Jordan have commonly Na_2O values between 10 and 19 wt% (Al-Saad, 2002; Gill & Rehren, 2011).

In the 16th/17th century, the imported tableware from Bulgaria also has mineral natron flux in the alkali lead composition. Unfortunately, it cannot be assigned to a specific cultural origin. An analogy is found in one part of Indian tile glazes of the 17th century, where the use of mineral natron is assumed (Gill *et al.,* 2014).

One of the Uzbek tiles of the madrassa Abdul Aziz Khan, Samarkand, from the 17th century is decorated with the so-called *cuerda seca* technique, where adjacent areas of glazes are heated together in one firing step (Brill, 1999; Pérez-Antegui *et al.*, 1999; Tite *et al.*, 2006). This technique was introduced and widespread during the Timurid period in the 14th century, but also continued after the death of the ruler Timur in 1405 in important part of buildings (Golombek, 1996; O´Kane, 2011). For the well-defined ornaments of decoration, it is necessary that the glazes stay at a high enough viscosity without running into the adjacent colour. Lower Na_2O flux contents, as they are for example observed in the Uzbek *cuerda seca* glazes, avoid the runny texture of the glaze. The chemical compositions of the *cuerda seca* glazes fit into the groups of Uzbek alkali and alkali lead glazes. It can be assumed, that the glazed tile is a local product, although its decoration differs from the commonly monochrome tiles from Uzbekistan. In the Moroccan and Bulgarian glazes from the 14th- 18th century, lead oxide seems to be the only important flux in the present data set, which may be caused in the Roman influence in northern Morocco and the adjacent south eastern Europe.

8.6 Comparison with glass

This chapter compares the compositions of tile and tableware glazes with analysed glass samples from similar regions and periods. The differences between glaze and glass compositions can be ascribed to the availability of raw materials, but also to cultural reasons as tradition and different groups of craftsmen.

8.6.1   Lead content

As a general tendency a temporal shift in lead use between glass and glazes is observed; the prevalent use of lead as flux seems to be earlier introduced in glaze than in glass production in this part of ancient Central Asia. The oldest glazes of the sample set for example; the lead-rich

tableware glazes from Afrasiab in Uzbekistan from the 10th-11th century show almost no Na_2O and MgO and low concentrations of K_2O and CaO. In contrast, the well-developed glass production of this time is reported to be still based on alkali and alkali earth fluxes (Lukens, 1965; Bezborodov & Zadneprovskii, 1976). Glass from the same period in the close-by regions Surhandarja and Kashkadarja valley, Khorezm also has high Na_2O and CaO, even moderate MgO and K_2O values and a negligibly low lead content. A similar picture is drawn in the Eastern European glazes and glass findings; the glazes from the Ottoman period in Bulgaria show lead flux domination. The Bulgarian glass of these times however, is commonly Na- or Na-Ca-dominated without lead content (Bezborodov, 1975). Also in Ottoman glass samples from Turkey, soda-lime characteristics with higher Ca contents are reported (Akyuz *et al.*, 2012, Rehren *et al.*, 2015).

In one part of medieval Islamic bead glass from North Africa and Mali from the 11th century on, lead contents of 32-87 wt% are found. However, the rest of the glass objects have 20 wt% Na_2O and up to 9 wt% CaO without lead (Robertshaw *et al.*, 2010). In contrast to the glass findings, the Moroccan glazes of the present study show no alkali-rich compositions but consistently lead rich recipes, so the prevalence of lead flux in glazes is again confirmed. Other studies of Islamic glass describe the use of lead only as colouring agent but not as a flux (Colomban *et al.*, 2011; Akyuz *et al.*, 2012).

8.6.2 Alkali flux in glass and glazes

As described in chapter 2.1.4, mineral natron and plant ash flux are known from the Early Egyptian glass production on (Sayre & Smith, 1961; Shortland, 2006). Plant ash compositions are found in glass from ancient Mesopotamia, Greece, and Persia of the 2nd millennium BC (Sayre & Smith, 1974). The mineral natron flux was introduced in the first millennium BC and was widely distributed by the Roman glass production. In the 7th-9th century AD, the glazing recipes in Egypt shifted from the use of mineral natron toward a subsequent substitution of mineral natron by plant ash flux (Shortland *et al.*, 2006). According to Henderson *et al.* (2004), the replacement of mineral natron by plant ash in glasses from Syria was nearly complete.

For early Islamic glazes from Iran, Syria, and Jordan, Sayre & Smith (1974) revealed soda-lime characteristic and high MgO values in in early Islamic glass. These plant ash characteristics give rise to the assumption that in the some parts of the Roman Empire and outside the same; the glass production was continuously carried out with plant ash flux, without interruption by the

Roman mineral natron recipes (Sayre & Smith, 1974). Consequently, Islamic glasses from the 8th and 9th century are found have plant ash characteristics (Bezborodov, 1975; Wedepohl *et al.*, 1995). For Islamic glazes, there is evidence for the use of plant ash in Iraqi tableware glazes from the 8th-9th century with considerable contents of 2-5 wt% K_2O and 1-4 wt% MgO (Mason, 2004). In the tile glazes of this study, plant ash compositions are observed in the 13th century in Iranian glazes from Takht-i-Suleiman. But here, the plant ash is used synchronously to mineral natron flux (fig.64). The glazes from later centuries from Uzbekistan and all but one from Afghanistan have also plant ashes as alkali source. The one Afghan glaze with low MgO content of 0.6 wt% (Her 46) dates to the 15th century and is an indication of the parallel use of mineral natron and plant ash flux in this period. This continuous use of mineral natron in the 15th century discriminates the glaze production from the glass making technology, where plant ash had completely replaced the minerals natron flux in the 11th century (Henderson *et al.*, 2004). In the alkali and alkali lead glazes from younger centuries, no more mineral natron compositions are found.

In general, the glass compositions seem to be richer in flux amount than the glaze compositions. This is ascribed to the lower processing viscosity, which is needed for the moulding of glass: a viscosity of about 10^3 P is necessary for the shaping and blowing of glass melts. In contrast, a glaze melt´s viscosity has to be around 10^4 P, to avoid running from the ceramic sherd (Tite *et al.*, 1998).

8.6.3 High alumina compositions in glass and glazes

A group of glass compositions from Central Asian, described by Bezborodov (1975), has a mixed alkali composition with up to 9.1 wt% Al_2O_3, named Na_2O-K_2O-CaO-MgO-Al_2O_3-SiO_2-glass.

Some of the plant ash glazes from Uzbekistan from the 15th century and the plant ash glazes from Afghanistan show similar recipes: additionally to their enhanced MgO and K_2O values, they also have CaO contents of up to 8 wt% and Al_2O_3 contents of up to 7 wt%. However, the total alkali content is with about 6 wt% lower in the glazes than in the glass compositions with about 20 wt%.

Similar high Al_2O_3 values of 4.4-8.3 wt% and lower CaO values of 1.8-5.8 wt% are reported from glass findings from the 10th-11th century from Kuva in the Ferghana valley in Uzbekistan (Rehren *et al.*, 2010). High alumina glasses with up to 11.4 wt% Al_2O_3 and CaO values of 4.3-7.4 wt% are found in glasses from the late Byzantine and Islamic times from the ancient city Pergamon,

Turkey (Rehren *et al.*, 2015). Dussubieux *et al.* (2010) report from a group of glass findings with high-Al around 9.8 wt% Al_2O_3 but mineral natron characteristic from medieval Indian and Southeast Asian production sites. Glazes with mineral soda characteristic and high alumina contents up to 8.7 wt% are found in a group of Indian tile glazes from the 16th and 17th century from different buildings in Delhi, India (Gill *et al.*, 2014). A characteristic with 13 wt% Al_2O_3 and mineral natron composition is found in one of the Afghan tableware glazes from the 15th century (Her 46). A connection or knowledge transfer between the Timurid dynasty and the Southeast and Indian regions would have to be proved by a larger sample set. High alumina glazes are also reported from Chinese GE ware and longquan celadon glazes from the 14th-17th century and from Taiwanese proto-porcelain and celadon glazes from the 13th-17th century (Liem *et al.*, 2000; Xie *et al.*, 2007). However the compositions are with around 20 respectively 30 wt% Al_2O_3 and very low Na_2O contents of 0.4-2.0 wt% distinctly different from the Afghan glaze.

8.7 Colours

The characteristics concerning the colouring agents in the different sites and cultures will be presented and compared with other investigations of Islamic glaze and glass colours.
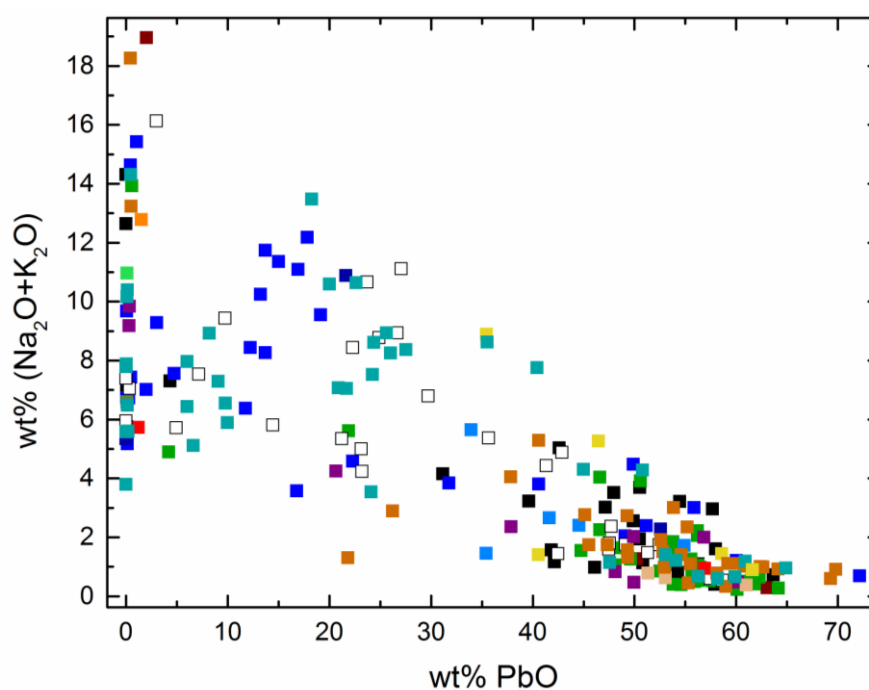
Figure 65: Alkali oxide and PbO contents with data point colours according to the glaze colours.

In the glazes of some of the locations, correlations between the matrix composition and the glaze colours are found. The characteristics of the black, green, blue, turquoise, and white samples from different sites are depicted in figs. 65 and 66.
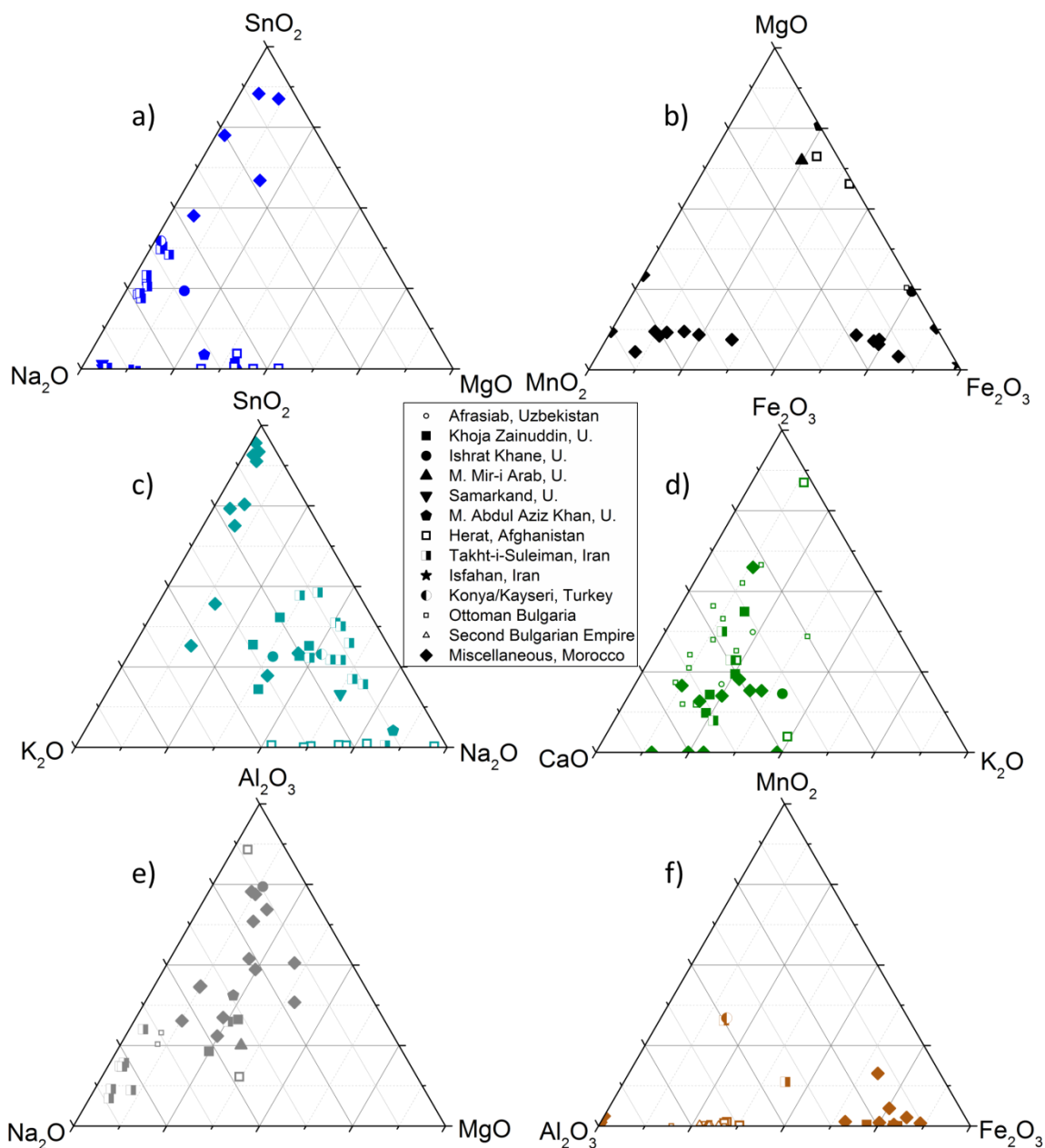
Figures 66 a-f): Differences in minor and colouring elements between the localities within one type of glaze colour. The grey colour represents the white-coloured glazes.

8.7.1 Blue

The blue samples are consistently coloured by Co^{2+} ions, which is in some cases accompanied by Cu^{2+}. Henshaw *et al.* (2007) reports on pure copper coloured glazes from ancient Islamic alkaline glazes in Akshiket, Uzbekistan, however, those cannot be identified in this sample set. The Co has to be present in an oxidic or siliceous compound in order to form the blue colouring CoO_4-complex in the glass (Nassau, 2001). Kleinmann (1990) therefore assumes for Islamic glaze production a pre-heating and oxidation of the Co-sulphide linneite before it is added to the glaze frit.

The blue samples in this study can be distinguished regarding their Na_2O, SnO_2, and MgO content as it is depicted in fig.66a.

In the blue glazes from Morocco, the SnO_2 contents are with 7.6 wt% in average higher than in the remaining blue glazes (1.1 wt% SnO_2 in average). The reason for the higher SnO_2 content of Moroccan blue glazes is assumed to be an intentional lightening of the blue colour. It neither correlates with the lead content nor with any other of the main composition elements. The correlation of Co with Zn, Mn, or Al, known from ancient Egyptian vitreous materials and attributed to a Co source of alum in western Egypt oases (Shortland & Tite, 2000; Shortland & Eremin, 2006) is not observed. Wen & Pollard (2016) states the use of an iron and arsenic-rich cobalt ore in Qamsar, Iran for Iranian and Egypt Minai glazes from the 12th and 13th century. In the present data set, no distinct correlation could be found in Co and Fe contents and the As-contents were not quantitatively determined.

8.7.2 Black

The black glazes can be subdivided into two groups, from which the first one is primarily coloured with MnO_2 and the other one with MnO_2 and additional Fe_2O_3 (fig.66b). The group with primarily MnO_2 comprises the Moroccan glazes from Salé and Rabat, the madrassa Bou Inania in Fes and the Mausoleum in Meknes. The high Mn content cannot be explained with the geographical proximity to the manganese deposits near Marrakesh (Thein, 1990) nor with a specific dynasty in which the manganese was preferably exploited.

The Moroccan black glazes show higher levels of K_2O in glazes with manganese oxide, suggesting a Mn ingredient which is accompanied by K_2O contents. A separate addition of K_2O-rich sand and Mn ingredient is nonetheless possible.

High values of Fe_2O_3 are found in the other Moroccan black glazes, the Turkish, Iranian, Bulgarian, and the old Uzbek sample from Afrasiab. The samples from Morocco still have up to 4.0 wt% MnO_2 additionally to the high Fe_2O_3 contents of 4.8-8.6 wt%. The younger black glazes from Bukhara and the Afghan black glaze are not distinctly rich in MnO_2 or Fe_2O_3.

Besides the matrix colouring with transition metal ions, different pigments were used for the black glaze colour: chromite as pigment is found in the black glaze KhZ 090 of the mosque Khoja Zainuddin beside 0.3 wt% Cr_2O_3 and 0.9 wt% MnO_2 contents in the matrix. Chromium particles are also reported from imported Persian glazed ceramic of the 12th-14th century from Afghanistan (Pernicka & Malissa, 1976). The historical craftsman Abu´l-Qasim described 1301 in his treatise of glaze production the use of "muzarrad" which originates from the region Khorasan, today the northern part of Iran. In the treatise, "muzzarad" is added as an ingredient in black glazes (Allan et al., 1973). Wulff et al. (1968) considers a mineral mine in the area of Nain, Persia, which contains high contents of chromite and manganese and could be the origin for the black colouring chromite in the Uzbek glaze. In Iranian and Egyptian Minai ware from the 13th century, the black colour of glaze paintings is reported to be produced by variable contents of chromium, iron, and copper (Wen & Pollard, 2016).

In the same glaze of the mosque Khoja Zainuddin, crystallites of iron-rich clino-pyroxene are detected, which could also contribute to the black-colouring. The manganese- and iron-rich particles in the Moroccan black glazes are presumably precipitated from the matrix, because of their vicinity to the ceramic body and their consistently elongated shape with characteristic surface angles. This idiomorphic appearance points to a particle formation from the glaze matrix by recrystallization.

8.7.3 Turquoise

The turquoise colour in the glazes is commonly produced by a combination of copper ions, which are integrated in an alkali-rich glassy matrix, and opacifying pigments. The opacifiers are commonly recrystallized SnO_2 or in few cases non-dissolved quartz grains, which whitens the light blue colour of the copper coloured glaze.

The alkali-rich compositions of the matrix of the turquoise glazes are realised with alkali and alkali earth contents of 10.0-21.3 wt%, dominated by Na_2O.

In turquoise glazes from Uzbekistan, Turkey and Morocco, contents of ca. 3 wt% SnO_2 are found. The turquoise glazes from Meknes and Fes from the Moroccan set of glazes show higher SnO_2

contents of 8.7 wt% in average, and slightly lower CuO average values of 1.0 wt% than the other Islamic turquoise glazes with 2.5 wt% SnO_2 and 1.7 wt% CuO in average. The differences in alkali oxide contents and matrix integrated SnO_2 are shown in figure 66 c.

The dissolved SnO_2 in the glaze matrix precipitates to cassiterite already at lower contents, when the remaining glass composition has higher amount of impurities (Paynter *et al.*, 2004). Those impurities can be Al_2O_3, Fe_2O_3, or the presence of different alkali and alkali earth oxides in amounts of a few wt%. The opposite pertains for high purity glazes with high SiO_2 contents and only few alkali and alkali earth oxides. These glazes can dilute high contents of SnO_2 without forming of a crystalline phase (Paynter *et al.*, 2004). This is for examples the case in the glazes from Iznik, Turkey, which contain 20-40 wt% PbO and 8-14 wt% Na_2O as flux, but only around 1 wt% K_2O, CaO, MgO, Al_2O_3 and Fe_2O_3. In these glazes, 3.0-8.5 wt% SnO_2 is dissolved, without opacifying cassiterite precipitations (Paynter *et al.*, 2004).

In the Turkish glaze Kon 20a, the Na_2O content is with 6.1 wt% lower, and the Cu^{2+} is accompanied by CoO. The occurrence of CoO in turquoise glazes is also observed in two Iranian glazes TiS 11b and TiS 23c, which gives the glaze a darker hue of blue colour. In the Iranian glazes with Cu and Co mixed composition, the Na_2O values fit with 9.1 and 12.0 wt% into the range of 8-14 wt% Na_2O in turquoise glazes. In Uzbek glazes, the mixing of CuO and CoO oxide is also observed without deviations from the flux composition of the remaining turquoise glazes. The addition of Co to the Cu-colorant in one part of glazes from one location reveals certain experimentation with the colouring agents.

One peculiarity is found in the turquoise glazes from Afghanistan, where tin oxide is neither found in the matrix nor as cassiterite crystals. This is astonishing regarding the fact that SnO_2 opacification with cassiterite precipitates is already known from the pre-Islamic period (Moorey, 1999; Mason *et al.*, 1997; Brill, 1999; Paynter *et al.*, 2004; Tite *et al.*, 2006). The Afghan glazes without SnO_2 precipitations date primarily into the Timurid dynasty of the 14th-15th century, when the opacifying technique was already wide spread. In the Uzbek glazes which are also assigned to the Timurid Empire, the technology was well established (chapter 2.3). One explanation for the lack of SnO_2 could be the availability of a tin compound in this part of the empire, but also a deliberate distinction from other craftsmen tradition is possible. Regarding the evidences for tin raw material in Central Asia, the first explanation seems unlikely. Tin bearing deposits are known from the Uzbek semi-desert (Karnab), from the valleys in Tajikistan (Mushiston) and Kyrgyzstan (Fergana valley; van Gorder, 2008; Garner, 2011), and even in the

area of present day´s Afghanistan (Weeks, 1999; Peters, 2011). In the 15th century, under the rule of Shahrukh Mirza, Herat supersedes Samarkand as capital of the Timurid Empire. An intentional cultural deviation from the old capital could be the reason for the change in colouring agents.

In the two Afghan glazes Her 49 and Her 52, the turquoise colour is attained with chromium and copper-rich crystals, which also lead beside the green-turqousie colouring to the opacification. The exact compositions of the pigments are subject of further investigations. The crystals with grain sizes between 10 and 50 μm are not idiomorphic and unevenly distributed, which suggests a separate addition to the melt. Small reaction zones around these crystals underpin the assumption of deliberately added crystals (fig.49). Precipitated crystals would have been formed during cooling, where a further reaction with the glass matrix is unlikely. One white sample (Her 56a) shows two different, finely dispersed phases of glass in the glaze. These two phases are likely the result of immiscibility of silica-rich compositions at a distinct temperature (Parmelee & Harman, 1973). They are assumed to contribute to the bright appearing of the glaze, because of the high amount of phase boundaries on which the light is scattered (chapter 7.3).

8.7.4 Green

Almost all green samples are coloured with copper contents between 1.0 and 5.5 wt% Cu^{2+}, integrated in a lead containing matrix. The highest CuO-values are observed in Turkish and Bulgarian glazes. The iron content is also enhanced in the green glazes from Morocco and Afghanistan and partly Bulgaria (figure 66d, 1.5-3.7 wt% Fe_2O_3), which can be either attributed to an iron rich mineral in the sand source, or iron diffusion from the ceramic body. The ceramic bodies of Bulgarian glazes are entirely clay-based, whereas the two Afghan green glazes are each on one clay-, and one silica-based ceramic body. The Moroccan glazes have silica based bodies. The compositions of green glazes from different sites also al differ in their K_2O contents and partly in the CaO contents (figure 66d).

The green sample BG 3 of a painted sherd has 1.0 wt% Cr_2O_3, which distinguishes this glaze composition further from the ones from the Second Bulgarian Empire and Ottoman Bulgaria. In the Afghan glaze Her 49 of the 15th century, Cr_2O_3 particles are detected, contributing to the turquoise glaze colour. The element is also found in one black tile glaze from Uzbekistan (chapter 7.2). Wen & Pollard (2016) mention the occurrence of chromium in an Iranian green glaze from

a Minai sherd of the 13th century, but it is not proved to be intentionally brought in for green colour.

8.7.5 White

None of the common colouring ions of Mn, Co, Cu, or Fe are present in white glazes. This reveals a very clean production procedure without unintentional mixing. In order to whiten the glaze to cover the underlying ceramic body, the glaze can be opacified. In chapter 2.2.2, different techniques of opacification with SnO_2 precipitations, SiO_2 pigments, or gas bubbles are described.

Compositional differences in the white glazes from different sites can be observed in the relative contents of Na_2O, Al_2O_3, and MgO, as it is shown in figure 66e. The white glazes from Iran have enhanced PbO values and precipitates of cassiterite. The white glazes from Uzbekistan from the 13th and younger centuries show very high SiO_2 contents in addition to added SnO_2. With only 0.0-9.6 wt% PbO they stand in contrast to the high lead glazes of Iran.

In the Moroccan glazes, the white samples have either quartz grains, cassiterite precipitates or a combination of both. The Marinid glazes of the 14th century contain only calcium and lead-rich precipitates, whereas the glazes from the northern Moroccan cities Fes and Meknes show in part cassiterite opacification. Also the white tile glazes from the Saadian Tombs of the 16th century from Marrakesh show cassiterite precipitations. This could indicate that the northern cities Fes and Meknes already used the cassiterite opacification technique, before it came into use on the western coast of Morocco.

8.7.6 Brown/Ochre

In the brown and ochre glazes, Fe_2O_3 in the glassy matrix is the main colouring agent. A rough correlation of the colouring Fe_2O_3 with Al_2O_3 can be found in samples from Bulgaria and the two samples of Afghanistan (fig.67). The samples from Uzbekistan, Iran, and Turkey also fit this correlation but are too few for a separate statistical analysis. One explanation for the correlation of Fe_2O_3 and Al_2O_3 is a diffusion process of both elements from the ceramic body into the glaze. This claim is supported by the fact that the brown coloured glazes with Al_2O_3-Fe_2O_3 correlation all belong to clay-based ceramics. The ochre and brown glazes from Uzbekistan and Morocco

have stone paste ceramic as body. However, the iron is in average higher in the brown and ochre coloured samples in general, so a second source of Fe_2O_3 is likely.

Another explanation for the occurrence of high iron oxide with high alumina content could be the use of a Fe_2O_3 and Al_2O_3 bearing mineral. This could be for example a common source of ochre colour. The mineral bauxite has high amounts of Fe_2O_3 and Al_2O_3 and can be used as ochre colouring agent. It is formed when aluminium rich silicate rocks are exposed to extreme weathering conditions, changing between very humid and very dry periods (Yamaguchi, 2010). In the weathering process, silica, alkali, and alkali earth components are leached out and a residual accumulation of iron and aluminium minerals remains. Large deposits of bauxite are found in the United States, in Brazil, Australia, and India; smaller ones are known from e.g. Kazakhstan and Afghanistan (Bray, 2009; Renaud *et al.*, 2015) and could have been available for the ancient glaze makers in Central Asia.

The Moroccan and the majority of Uzbek ochre glazes do not show any correlation of Fe_2O_3 with Al_2O_3 or any other values.
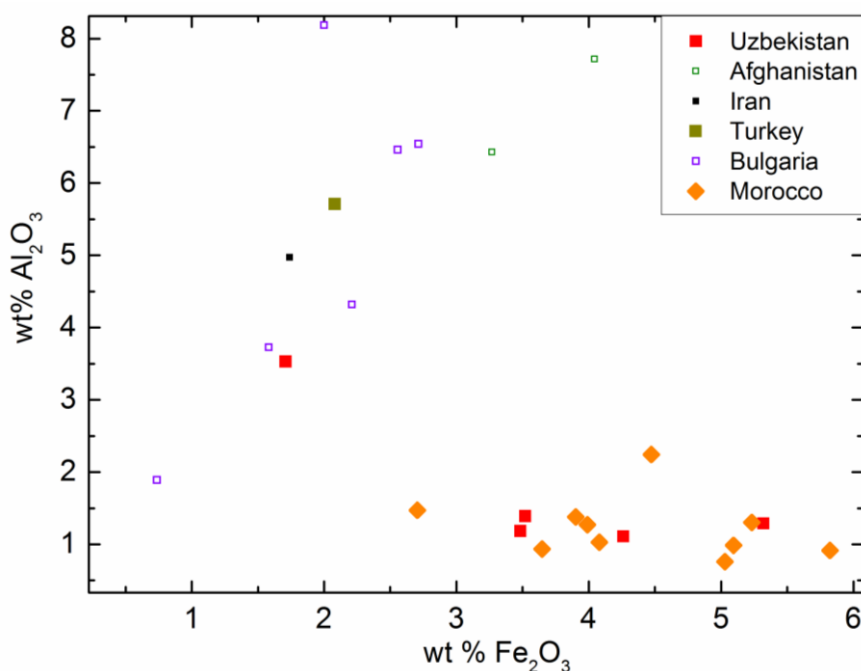
Figure 67: Alumina and iron oxide content of ochre and brown coloured samples. The rough correlation includes the ottoman samples of Bulgaria, Herat, Turkey, and Takht-i-Suleiman. The tableware glazes are empty symbols, tile ware is depicted in full symbols. Glazes on clay ceramics are plotted in small points compared to the glazes on quartz frit bodies. Uzbek samples are subdivided into squares (mosque Khoja Zainuddin) and triangles top up (madrassa Mir-i Arab).

8.7.7 Yellow

The number of yellow glazes in this sample set is too small to make statistically proved statements. The five yellow samples KhZ 029, MAKg, TiS 13a, Nec 19, and Eco 78 all have high in lead oxide, which is assumed to be one reason for the yellow colouring (Wedepohl, 1995). Some of the samples are iron-rich, but the presence of a yellow amber colouring of $Fe_2O_{3-X}S_x$ with sulphur on the oxygen place (chapter 2.2.1) can hardly be proven. The exact position of the sulphur in the glassy network cannot be determined with the EPMA or XRD methods and makes further investigations needed.

Crystalline compounds of lead tin oxide and lead silicate are found in the Uzbek glaze MAKg from the madrassa Abdul Aziz Khan. The lead tin oxide $Pb_2Sn_2O_6$ produces a yellow colour, whereas the lead silicate has a whitening effect (Eastaugh *et al.*, 2004). The lead silicate is listed in the international Colour Index (1971), but is not yet known as a historical pigment (Bradford, 1971; Eastaugh *et al.*, 2004). The particles of the detected $Pb_2Sn_2O_6$ phase are agglomerated in clusters, as can be seen in BSE pictures (fig.47 b). This phenomenon is observed in other yellow glazes from medieval India and is ascribed to a separate production of the pigments being subsequently added to the glaze frit powder (Gill *et al.*, 2014). The $Pb_2Sn_2O_6$ particles are in the size of several μm, which is unlikely to be milled separately. More likely is the addition of tin oxide to the lead-rich frit. During the heating, the tin oxide melts and crystallises in the cooling process with the lead rich environment to form lead tin oxide (Heck, 2000).

The composition of the $Pb_2Sn_2O_6$ can give some hints to the production conditions of the yellow glaze: the precipitations of the $Pb_2Sn_2O_6$ are favoured in the presence of Si and have a thermal stability field of 600-900 °C (Heck, 2000). At 850-900 °C, a silica containing lead tin phase forms synchronously so that a formula of $Pb(Sn,Si)O_3$ is favoured (Martin & Duval, 1990; Gulzar *et al.*, 2014). In the yellow glaze from Bukhara, no such silica-containing lead tin oxide is found, so the processing temperature was probably below 850 °C. Unfortunately, the analysis of the glaze matrix for processing temperature estimation is difficult in this sample, because of the very fine dispersed pigments. However, the high lead content >50 wt% confirms the low processing temperature.

The additional orange coloured lead tin pigments with zinc content from the study of Gill *et al.* (2014) are not found in the present glazes.

8.7.8 Purple

There are nine samples of purple coloured glazes; two from the mosque Khoja Zainuddin from Bukhara, Uzbekistan, one from a painted sherd from Bulgaria, and six from different sites in Morocco. The manganese contents are between 0.8 and 3.1 wt% Mn_2O_3 from which the Uzbek glazes from the mosque Khoja Zainuddin have with 0.8-0.9 wt% the lowest values; the Moroccan glazes from the madrassa Bou Inania in Fez and the necropolis Chellah in Rabat have with 2.3-3.1 wt% the highest values. The manganese content does not correlate with any of the major and minor elements, neither in Uzbek nor in the other samples.

8.7.9 Red

There are very few samples with red colour, namely Afr 36 from Uzbekistan and TiS 32 from Iran. Fe_2O_3 or Cu_2O as crystalline pigments would result in a red colour of the glaze, but are not detectable in both of the glazes. Contents of dissolved iron or copper oxide are neither found in the glaze matrices. In the case of TiS 32, different Fe-rich crystallites are found in an upper layer of the glaze, partly combined with up to 1.3 wt% copper oxide. It can be assumed from the resulting colour, that the copper is present as crystalline Cu_2O and contributes to the red appearance. However, further investigations are needed for the specification of the oxidation state of the transition metal. The content of CuO in the Afghan glaze instead, is with 0.1 wt% too low to produce any colouring effect (Nassau, 2001).

9 P-XRF element analysis

In this chapter, the specific suitability of the p-XRF device for glaze measurements shall be investigated. The method of p-XRF is a tool which has its benefits primarily in the fast and easy handling which makes the quick major element analysis of large amounts of sample material possible. Furthermore, accessory elements like colouring and purifying agents of a glass can be determined down to about 0.5 wt%, depending on the element and the overall composition. A challenging aspect in the compositions is the occurrence of light elements (Mg, Al, Si, and P) simultaneous with up to a few percent heavier elements like Sn or Pb. The higher absorption coefficient of the heavy elements makes the matrix correction for the lighter elements difficult. Therefore, satisfying results for samples with Pb content are difficult to obtain.

9.1 Measurement settings

In the p-XRF measurements, the elements of the main composition Pb, Sn, Cu, Co, Fe, Mn, Ca, K, Cl, P, Si, and Al are detected. The measurement values are converted into oxide compounds and normalized to 100% in order to attain comparability with the EPMA analyses. Most of the trace elements (Ce, Cd, Ag, U, Nb, Zr, Y, Sr, Rb, Au, Se, Ni, Cr, V, and Ti) are below the detection or quantification limit (Armbruster & Pry, 2008). The elements As, S, Te, Hg, and Th have to be disregarded in the lead containing samples because of strong interferences with the lead spectrum (e.g. Pb Lα at 10.449 keV and As Kα = 10.544 keV). The measurements of Mg are only qualitative, because the device is used without helium flush and the energy of the Mg signal is too low to be detected under air atmosphere.

In the case of thin alkali glazes, the analyses cannot be undoubtedly assigned to the glaze layer, but can be influenced by the underlying ceramic body. For the estimation of the influence of the ceramic bodies, the depth of the detected fluorescence signals is very important, which depends largely on the specific glaze composition (Gerward, 1993; Hubbell & Seltzer, 1996; Kleinknecht, 2005). The emitted signal of an element is partly absorbed by the layers between emitting atom and detector (glaze composition and atmosphere), which decrease the intensity of the detected signal. The higher the atomic number of an element, the higher is its absorption. The attenuation coefficients of the absorbing elements in turn, are a function of the energy of the incident photon (Gerward, 1993). In the present case, the material of original glaze contains

177

predominantly light elements (Na, Mg, Al, Si, K, Ca, and O), optional lead and tin and a few transition metals (Mn, Fe, Co, Cu).

The underlying ceramic or quartz frit is in general made of silica, mica, carbonates, or a mixture of them. In all cases, it also consists of primarily light elements, which are low in fluorescence energy. The radiated fluorescence energy of lighter elements is lower and the depth from which the radiation reaches the detector window is less (Duve & Schmottlach, 2012). Therefore, the signals of these light elements penetrate, if at all, only weakly the overlying glazes. For testing the influence of the underlying substrate material on the analysis of a glaze, layers of alkali glass in different thicknesses are measured, mounted on lead metal. In this testing array, the lead substrate replaces the ceramic of the original tile, because the lead signals can be easily separated from that of the overlying alkali glass. Additionally, the Pb Lβ signal which is used in the p-XRF evaluation is with 12.614 keV higher energetic than the utilized Kα line of ceramic elements like Si Kα = 1.740 keV, Al Kα = 1.487 keV, Ca Kα = 3.692 keV and K Kα = 3.314 keV (Thompson & Vaughan, 2001). Therefore, the signals of the light elements of the real ceramic body are definitely lower than the lead signal in the test array. In case of iron-containing ceramic bodies, the influence of the Fe with a Kα line of 6.4 keV and higher penetration power can be elevated in the glaze analysis. Iron contents of up to 5.3 wt% are detected in ceramic of clay-based bodies (tab. 10, Second Bulgarian Empire) which can influence the alkali glaze measurements on these ceramics. In the stone paste bodies, the Fe_2O_3 values are commonly below 1 wt%.

The composition of the upper glass layers is a common object slide with ca. 72 % wt% SiO_2, 14.5 wt% Na_2O, 1.3 wt% K_2O, 6.5 wt% CaO, 4.5 wt% MgO, 1.0 wt% Al_2O_3 and 0.3 wt% SO_3 (Menzel, 2014). For a thickness of 340 µm of alkali glaze, the signal of lead fluorescence is reduced from the 100% Pb signal without glass layer down to ca. 21 % of the Pb signal; if a thickness of 1300 µm is used, only ca 2 % of the original lead signal is measured (fig. 68). When the data points are fitted with the exponential function y=y0+A*exp(R0*x), the lead signal is reduced to ca. 10 % of the initial value through a layer of 500 µm alkali glass. The parameter values for the fit are y0 = 0.01 and R0 = 0.0045±0.0001 with a coefficient of determination (R^2) of 0.9992. The initial value is set to 100%. A ceramic body at the place of lead is assumed to affect the glaze analysis less than the here used lead material, due to the lower radiation energies of the ceramic components. In the case of lead containing glaze on calcareous, quartz, or clay bodies, the substrate signal is completely negligible.

Modell	Exponential		
Equation	y = y0 + A*exp(R0*x)		
COD (R^2)	0.99919		
		value	St. Err.
Pb/%	y0	0.00998	0
Pb/%	A	100	0
Pb/%	R0	-0.00447	1.19987E-4
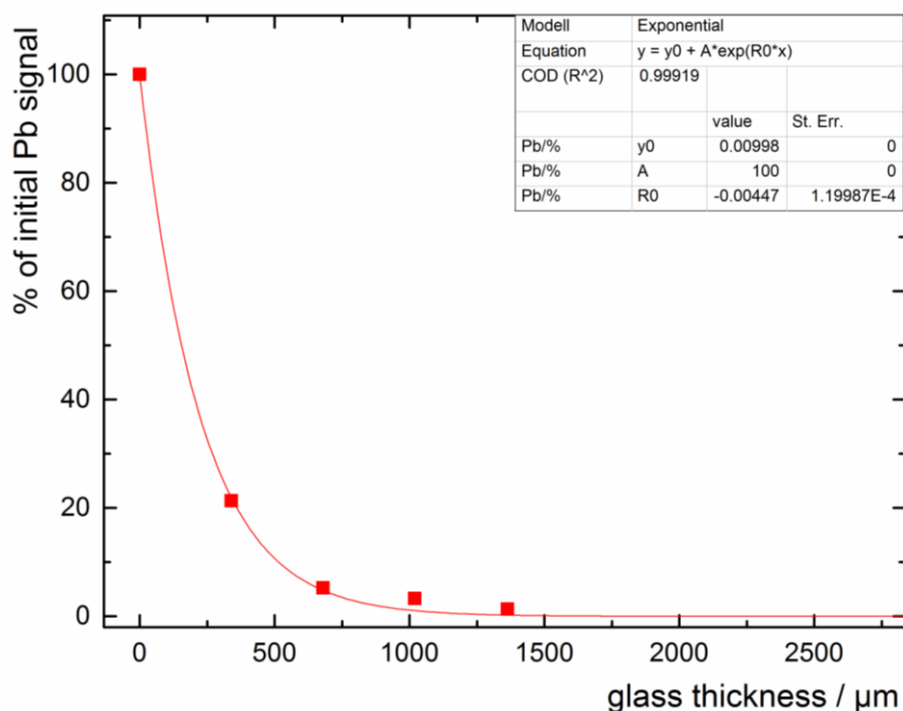
Figure 68: Reduction of lead XRF signal through the absorption of alkali glass layers

9.2 Sample preparation and measurement

For the investigation of the measurement accuracy, historical and synthetically produced glazes with varying contents of alkali oxides and lead oxide are measured with EPMA and p-XRF (tab.15). In addition, concentration series of colouring ions are realised in the synthetically produced glass.

In the investigation of p-XRF measurements, the two different measurement programs, "mining" and "soil" are tested. The default program "mining" is appropriate for the measurement of lighter elements Si, Al, and P (chapter 4.3) and is used for the part of original glaze samples which have a sufficient surface area of at least 7 mm^2. Those are 17 samples of the Uzbek tiles with lead contents between 0 and 56 wt% PbO, and eleven samples of Moroccan lead glazes with PbO > 30wt%. The Moroccan glazes are additionally measured with the "soil" program. In this program, minor contents of the heavier elements between W and U are measured more precisely, foregoing the measurement of the light elements Mg, Si, and Al. The transition metal ions of Mn, Fe, Co, Ni, Cu, and Zn are detected in both measuring programs.

Both, "mining" and "soil" program are also applied on the synthetically produced glass samples. The synthetic glass is measured in two sample preparation modifications; first, as bulk material as it is derived from the glass casting process, second, as thin polished films of 200-400 µm, mounted on calcareous substrates in order to investigate the influence of the underlying ceramic body and the surface texture to the glaze measurement (fig.69).

The calcareous body is chosen as substrate in order to imitate the original ceramic body compositions of light elements. The influence of the calcareous substrate can be assumed to be in the upper range of the influence of original ceramic bodies, because the predominant Ca in the calcareous body has higher signal energy (Ca Kα = 3.69 keV) than the rest of the common ceramic elements (Si Kα = 1.74 keV, Al Kα = 1.49 keV, and K Kα = 3.31 keV). In the case of iron containing ceramic body however, the iron signal energy of Fe Kα = 6.40 keV can enhance the influence of ceramic signal in the glaze analysis.

To the synthetic glass compositions, different concentrations of 0.5-3 wt% MnO_2, 0.1-0.4 wt% CoO and 0.5-3 wt% CuO are added (tab.23).

Table 23: Analysed glass compositions with historical recipes, three glass compositions have different matrix or copper content, 15 glass samples have only varying CoO, MnO and CuO and corresponding Na_2O values.

	Glass recipes of historic glass in wt%			Glass recipes of glass with different transition metal oxide contents		
Oxide	Green	Ochre	Turquoise	Blue	Violet	Light blue
SiO_2	34.0	34.0	60.0	55.0	55.0	55.0
Al_2O_3	3.0	3.0	3.0	6.0	6.0	6.0
Fe_2O_3	2.0	5.0	1.0	-	-	-
MgO	4.0	2.0	4.0	-	-	-
CaO	2.0	4.0	4.0	12.0	12.0	12.0
PbO	45.0	45.0	8.0	-	-	-
MnO	-	-	-	-	0.5 and X; X=1-3	-
CoO	-	-	-	0.X; X=1-4	-	-
CuO	3.0	-	3.0	-	-	0.5 and X; X=1-3
Na_2O	4.0	4.0	12.0	1.X; X=6-9	14.5 and 1X; X=2-4	14.5 and 1X; X=2-4
K_2O	3.0	3.0	5.0	12.0	12.0	12.0

Figure 69: Glaze imitation samples with concentration series of CuO, CoO, and MnO₂ as colouring agents as given in table 23.

The concentrations are in the range of the colouring agents in the investigated historical glazes. All synthetic glass samples are also measured with the EPMA device, in order to investigate the accuracy of colouring agents' measurements of the p-XRF.

9.3 Comparison of "mining" and "soil" programs with EPMA

9.3.1 "Mining" program on Uzbek glazes

The historical tile glazes from Bukhara and Samarkand are measured with the "mining" program of the p-XRF. The data reveal partly high deviations from the EPMA values: The p-XRF data for SiO_2 and Al_2O_3 are 20-30% lower than the EPMA values, the SnO_2 values under-determine the EPMA data even with 40% (tab.24 a and b and fig.70).

The p-XRF measurements of CaO, PbO, and K_2O in contrast show an over-determination of the EPMA values of 90% in average in the CaO values and over 100% in the PbO and K_2O values.

In the determination of the transition metal ions CuO and CoO, the "mining" data of the p-XRF exceeds the EPMA data with 20% (CuO) and 60% (CoO) in average. The data of Fe_2O_3 show in average a good accordance to the EPMA data with less than 5% deviation (fig.71).

Tables 24 a) and b): EPMA and p-XRF analyses of a) SiO_2, SnO_2 Al_2O_3, CaO, PbO and K_2O b) transition metal oxides from glazes of the mosque Khoja Zainuddin (KhZ) and the mosque Baland (bb) in Bukhara n.d. stands for not determined.

a)	SiO_2		SnO_2		Al_2O_3		CaO		PbO		K_2O	
Sample	EPMA	p-XRF	EPMA	p-XRF	EPMA	p-XRF	EPMA	p-XRF	EPMA	p-XRF	EPMA	p-XRF
KhZ 032	65.7	67.8	6.4	5.7	2.2	1.8	4.3	6.7	9.6	10.0	2.6	7.1
KhZ 090	65.5	70.5	0.2	0.0	8.2	3.4	3.2	12.0	0.0	0.1	4.9	8.6
KhZ 134	35.4	27.4	0.1	0.1	1.3	1.3	0.9	1.8	49.1	66.4	0.9	1.2
KhZ 171	77.3	75.8	0.0	0.0	3.8	2.3	5.2	9.3	0.4	0.7	2.6	9.0
KhZ 196	67.5	56.2	3.0	3.8	3.5	2.7	3.8	9.7	7.6	15.7	2.0	5.1
KhZ 198	67.0	68.9	3.7	1.3	3.4	2.5	6.4	8.9	5.2	5.5	2.3	8.5
KhZ 201tü	65.7	66.0	3.5	1.7	2.8	2.6	4.5	9.2	8.3	9.4	2.1	5.8
KhZ 201oc	50.1	27.4	n.d.	0.1	1.1	1.3	0.9	1.8	38.2	66.4	0.7	1.2
KhZ 244	71.2	72.8	n.d.	0.0	4.2	2.8	7.0	10.2	0.1	0.6	1.8	9.6
KhZ 246	74.5	74.0	n.d.	0.0	4.2	3.0	5.4	9.5	0.1	0.2	2.4	9.9
KhZ 247	69.9	72.7	0.2	0.1	4.5	3.1	6.9	9.0	0.6	1.1	2.2	9.6
KhZ 250	74.6	72.7	n.d.	0.1	4.1	3.1	4.8	9.0	0.1	1.1	2.2	9.6
bb001	34.7	23.3	0.0	0.0	2.0	1.5	1.1	0.9	56.0	70.8	0.5	0.9

b)	Fe_2O_3		CuO		CoO		MnO_2	
Sample	EPMA	p-XRF	EPMA	p-XRF	EPMA	p-XRF	EPMA	p-XRF
KhZ032	0.9	0.5	n.d.	0.0	n.d.	0.0	n.d.	0.4
KhZ090	1.6	2.1	0.3	0.4	0.0	0.0	0.9	1.6
KhZ134	3.4	1.8	0.1	0.1	n.d.	0.0	0.0	0.1
KhZ171	1.2	1.4	n.d.	0.1	n.d.	0.0	n.d.	0.0
KhZ196	1.2	1.1	1.9	4.6	n.d.	0.0	0.0	0.1
KhZ198	1.2	1.1	2.6	2.3	n.d.	0.0	n.d.	0.1
KhZ201	1.2	1.0	2.4	3.0	0.0	0.0	n.d.	0.1
KhZ201	4.3	1.8	0.1	0.1	0.0	0.0	0.0	0.1
KhZ244	1.9	2.4	0.1	0.1	0.4	0.4	n.d.	0.1
KhZ246	2.1	2.2	0.1	0.1	0.3	0.3	n.d.	0.1
KhZ247	2.5	2.6	0.1	0.2	0.4	0.4	n.d.	0.1
KhZ250	1.1	2.6	0.1	0.2	0.2	0.4	n.d.	0.1
bb001	0.4	0.2	2.1	2.1	0.0	0.0	0.0	0.1

Although the p-XRF data show high relative deviations from the EPMA values, the element fractions within the "mining" measurement are in good agreement with the relative amounts in the EPMA data. A comparison of main elements of the "mining" p-XRF data with EPMA results is depicted in figure 72.
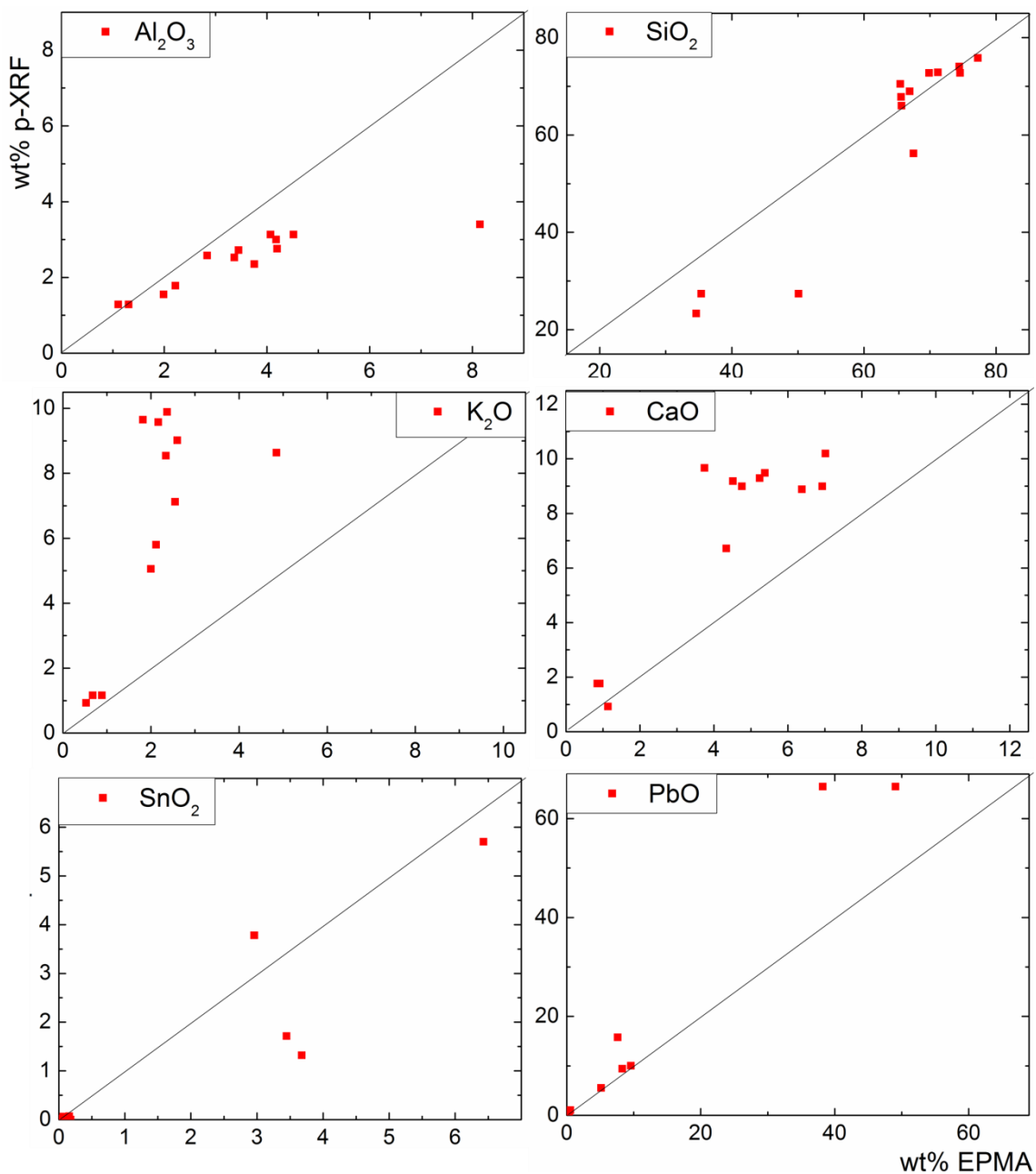
Figure 70: p-XRF values measured with the "mining" program versus the EPMA data of major element oxides in Uzbek tiles. A tendency to over-determination is observed in the metal oxides with an oxidation state of +1 and +2 K_2O, CaO, and PbO. The oxides of Al^{3+} and Sn^{4+} are distinctly underdetermined, whereas SiO_2 has only a slight under-determination.
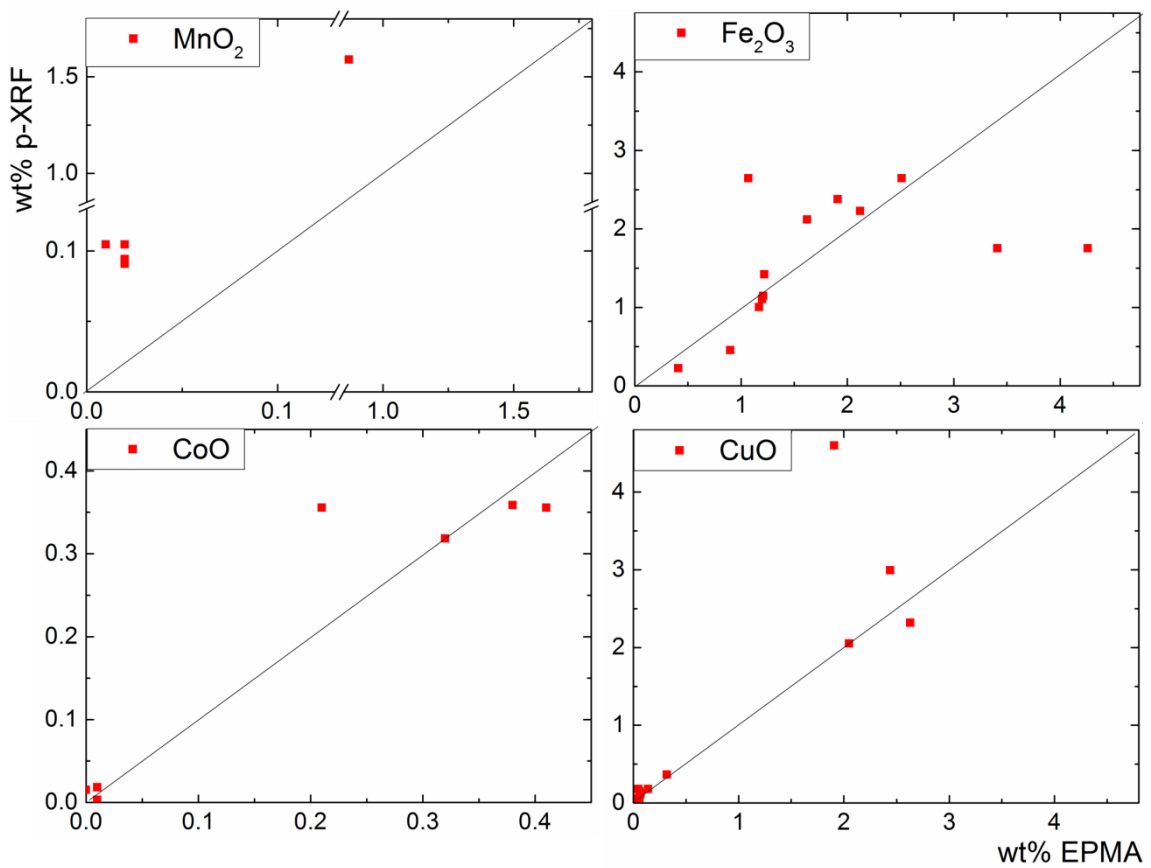
Figure 71: p-XRF values of "mining" program versus the EPMA data of transition metal oxides in Uzbek tiles.
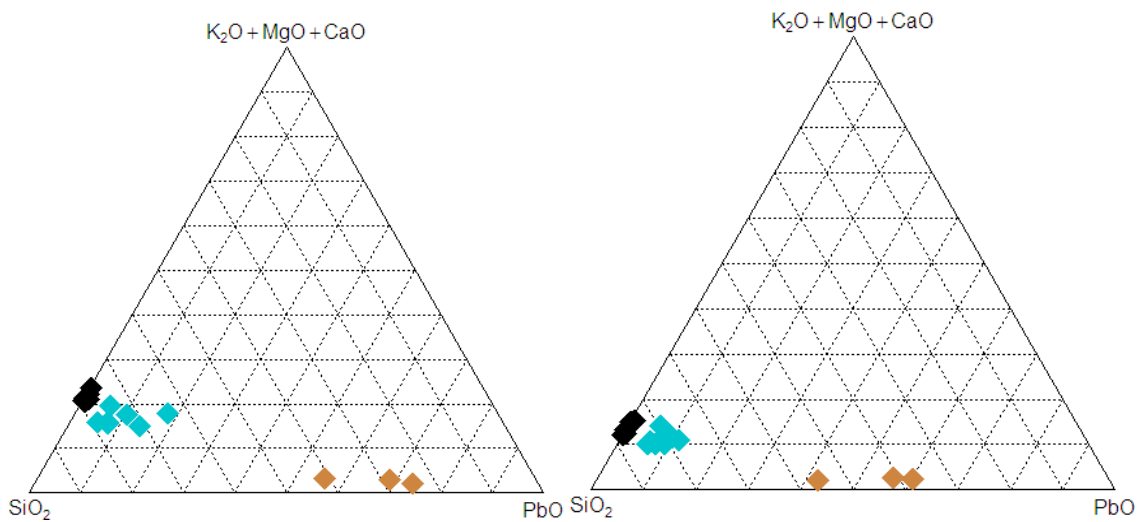
Figure 72: Major element composition in Uzbek glazes, measured with the "mining" program of p-XRF (left) and EPMA (right). The three major compositional types (alkali, alkali lead, and lead, chapter 5.2.1.) are clearly visible from both methods.

The measurement results of p-XRF "mining" and EPMA are depicted in ternary diagrams of the three main glaze components silica, lead, and alkali (earth) oxides. The classification into three different groups of lead contents, which is described in chapter 5.3, is also found in the values of p-XRF measurements.

9.3.2 "Mining" and "soil" program on Moroccan glazes

The differences between "mining" and "soil" are most substantial in the lead glazes from Morocco (fig.73): the Fe_2O_3, MnO_2, CuO, and CoO data of the "soil" program exceed the EPMA values with partly more than 100%, whereas the average deviations of the "mining" data of these oxides are with 54%, 51%, 25%, 49%, and 70% much lower (tab.25). The "soil" measurements of PbO scatter with 76% in average around the EPMA values; the "mining" values instead are with 56% in average consistently lower than in the EPMA data. For CaO and K_2O, the values of "mining" and "soil" program do not differ significantly and scatter with more than 100% deviation around the EPMA values. In the p-XRF data of SnO_2, measurements of both programs are in the lower range <1wt% SnO_2 more than 100% higher than the EPMA values; in the range >1wt% SnO_2, they are 30% lower than the EPMA values in average. The "mining" data of SO_3 partly exceeds the EPMA values with more than 100%, the "soil" data show even higher values (fig.73).

SiO_2, Al_2O_3, and P_2O_5 are measured only with the "mining" program and exceed the EPMA values with 60% in the case of SiO_2 and more than 100% in the case of Al_2O_3 and P_2O_5 (fig.73, tab.25).
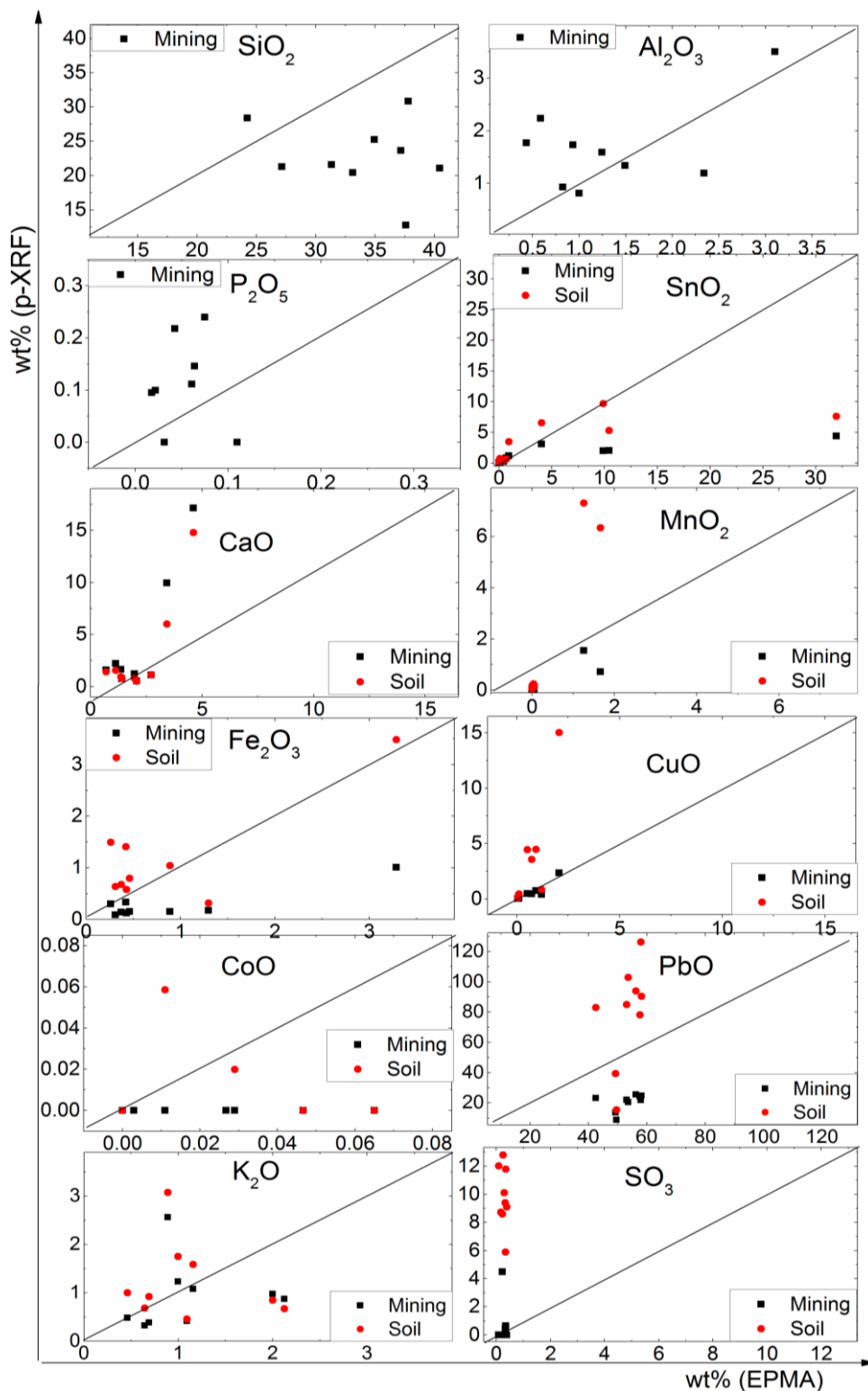
Figure 73: Mining and soil data from Moroccan lead rich glazes. Both measurement methods over-determine the values of EPMA measurement in most cases. Only the p-XRF values of SnO_2 are in average lower than the EPMA values. The soil-program data exceeds the EPMA value usually more than the mining-program data.

Table 25: The EPMA and p-XRF analyses of three Moroccan tile glazes, from the mausoleum Meknes (Mau), the madrassa Bou Inania in Meknes (InM) and the Saadian tombs in Marrakesh (Sad). "n.d." stands for not determined.

	Mau 54			InM 62.1			Sad 70		
	turquoise			white			light blue		
Oxide	**EPMA**	Mining	Soil	**EPMA**	Mining	Soil	**EPMA**	Mining	Soil
SiO$_2$	**27.16**	21.27	n.d.	**37.81**	30.84	n.d.	**38.04**	44.59	n.d.
Al$_2$O$_3$	**0.59**	2.23	n.d.	**0.82**	0.93	n.d.	**0.47**	2.01	n.d.
P$_2$O$_5$	**0.04**	0.22	n.d.	**0.03**	0.00	n.d.	**0.01**	0.15	n.d.
SnO$_2$	**10.43**	1.98	5.29	**4.04**	3.06	6.50	**1.48**	3.59	6.57
CaO	**1.14**	2.20	1.55	**2.72**	1.10	1.13	**0.56**	1.45	1.43
MnO	**0.01**	0.00	0.20	**0.00**	0.00	0.19	**0.01**	0.00	0.14
FeO	**0.37**	0.14	0.68	**0.43**	0.12	0.58	**0.41**	0.23	1.07
CuO	**0.93**	0.73	4.46	**0.07**	0.02	0.18	**0.10**	0.02	0.12
CoO	**0.03**	0.00	0.09	**0.05**	0.00	0.00	**0.23**	0.09	0.53
PbO	58.16	24.72	90.28	53.04	22.08	84.93	55.86	23.56	80.80
K$_2$O	**0.46**	0.48	1.00	**1.16**	1.08	1.59	**2.50**	1.15	1.89
SO$_3$	**0.35**	0.65	11.78	**0.39**	0.00	9.09	**0.15**	0.00	5.91

9.3.3 "Mining" and "soil" measurements on bulk glass and glaze imitation

The "soil" and "mining" programs were also tested on bulk glass and glaze imitations of the synthetic glass compositions. In general, the comparison of measurements on bulk glass and glaze imitations shows higher values on glaze imitations than on the bulk glass samples. Further, the deviations from the EPMA values are generally higher in "soil" than in "mining" results. The relations to the reference values of the EPMA analysis are shown in figs.74 and 75.

9.3.3.1 Major element composition

The synthetic glass compositions which are measured as bulk glass and as glaze imitations consist of SiO$_2$, Al$_2$O$_3$, Na$_2$O, K$_2$O and CaO as major elements and MnO$_2$, CoO, and CuO as colouring agents. In tendency, the highest values are obtained in the "mining" measurements on glaze imitations. The "soil" measurement on bulk glazes is consistently the lowest value, under-determining the EPMA value with about 10-80%.

Al$_2$O$_3$ and SiO$_2$ are measured only with the "mining" program. The Al$_2$O$_3$ measurements on glaze imitations exceed the bulk glass data with 20-60%, over-determining the EPMA values with more than 100% (fig.74). The bulk glass values are with an over-determination of about 70% closer to

the original values. In the SiO₂ measurements, the difference between glaze imitation and bulk glass measurements is only between 45 and 60% over-determination.

The contents of K₂O and CaO are measured with both programs. In the K₂O data of "soil" program, the measurements are consistent for glass and glaze imitations and match the EPMA values in a range of <5%. The "mining" analyses on bulk glass gives similar K₂O values, whereas the glaze imitation data of the "mining" program over-determines the EPMA values with 16-20%.
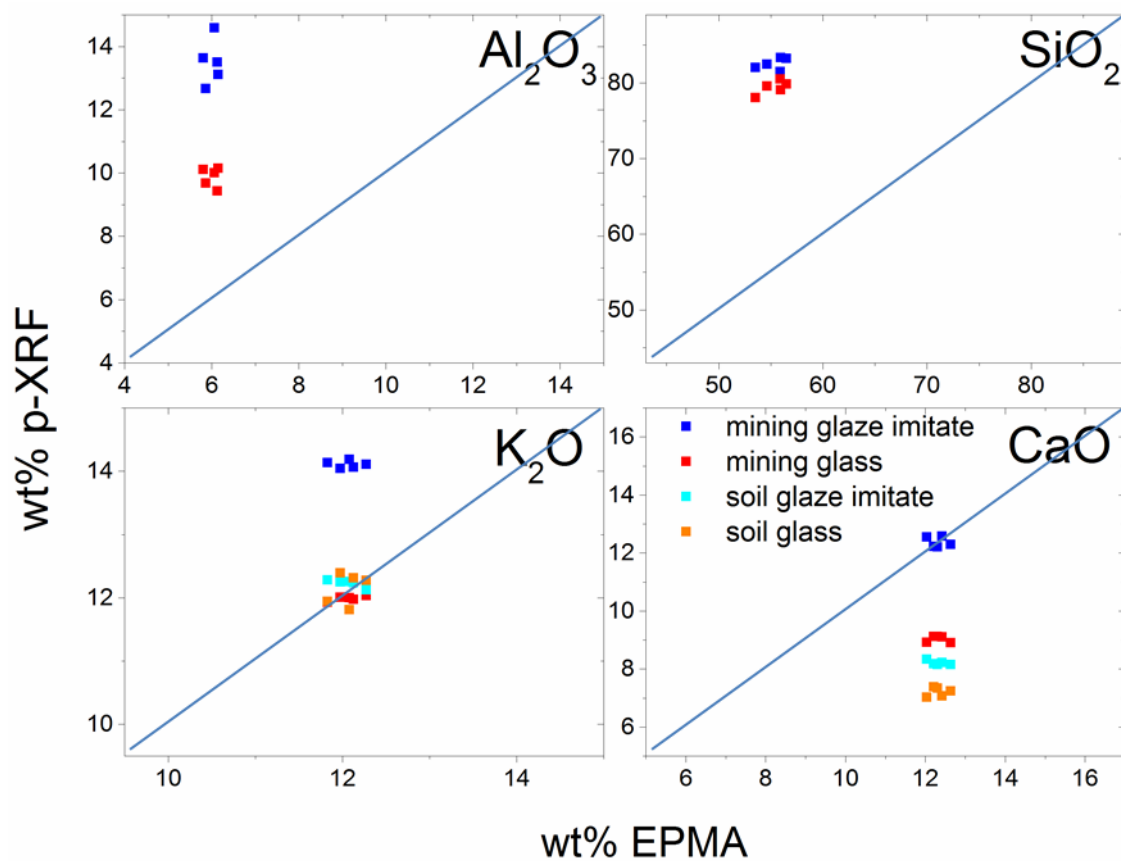
Figure 74: P-XRF measurements of bulk glass and glaze imitations versus the respective EPMA values. K₂O and CaO are measured with "mining" and "soil" program, SiO₂ and Al₂O₃ only with "mining" program.

In the CaO data, the "soil" measurements on both sample preparations give results which are 31-42 % under the EPMA value. The data from the "mining" measurements on bulk glass are 25-30 % under the EPMA value; the "mining" data from glaze imitations match the EPMA values in a range of 0-4%; the data from bulk glass and from the "soil" measurements under-determine the EPMA values.

9.3.3.2 Colouring agents in p-XRF and EPMA

The calibration rows of transition metal oxides consist of 15 samples of bulk glass and glaze imitations with identical compositions in spite of the content of MnO_2, CoO, and CuO respectively. The Na_2O content is set anti-proportional to the colouring ion contents (tab.26).
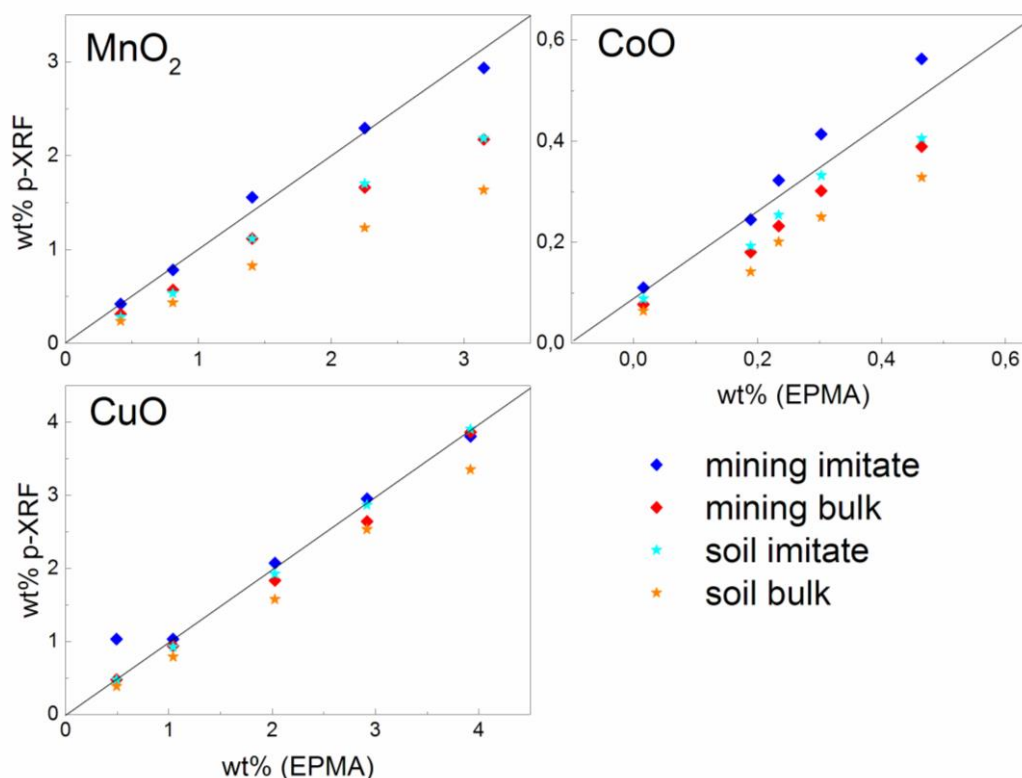
Figure 75: Depiction of the calibration series of CoO, CuO, and MnO_2 given in table 24.

The CuO, MnO_2 and CoO values of the "mining" program are consistently higher than in the "soil" data. In most cases, the "mining" program matches the EPMA values with a good accuracy (fig.75, tab.26). In the measurements on glass compositions with 0.5-3.9 wt% CuO, the data of different programs and sample preparations show no large differences and matches the EPMA values with a deviation of below 10%.

In CoO coloured glass with CoO concentrations between 0 and 0.5 wt%, the high "mining" values from the glaze imitation samples exceed the EPMA values. Here, the "mining" program on bulk glass and the "soil" program on glaze imitations match the EPMA values the best with an average deviation of 0-16%.

Table 26: Concentrations of colouring agents CuO, CoO and MnO$_2$, measured with EPMA and p-XRF. The p-XRF measurements are carried out on glaze imitations (calcareous substrates with thin layers of glass) and bulk glass samples. The p-XRF measurements show good results with a relative error of <10 %.

	wt% CuO					wt% CoO					wt% MnO$_2$			
	glaze imit.		bulk glass			glaze imit.		bulk glass			glaze imit.		bulk glass	
EPMA	Min.	Soil	Min.	Soil	EPMA	Min.	Soil	Min.	Soil	EPMA	Min.	Soil	Min.	Soil
0.50	0.55	0.48	0.48	0.38	**0.02**	0.11	0.09	0.08	0.06	**0.42**	0.42	0.28	0.31	0.24
1.04	1.03	0.92	0.94	0.79	**0.19**	0.24	0.19	0.18	0.14	**0.81**	0.78	0.54	0.57	0.44
2.03	2.07	1.92	1.84	1.58	**0.23**	0.32	0.25	0.23	0.20	**1.41**	1.56	1.11	1.12	0.83
2.92	2.95	2.87	2.64	2.53	**0.30**	0.41	0.33	0.30	0.25	**2.25**	2.30	1.70	1.66	1.23
3.92	3.81	3.91	3.86	3.35	**0.47**	0.56	0.41	0.39	0.33	**3.15**	2.94	2.19	2.17	1.63
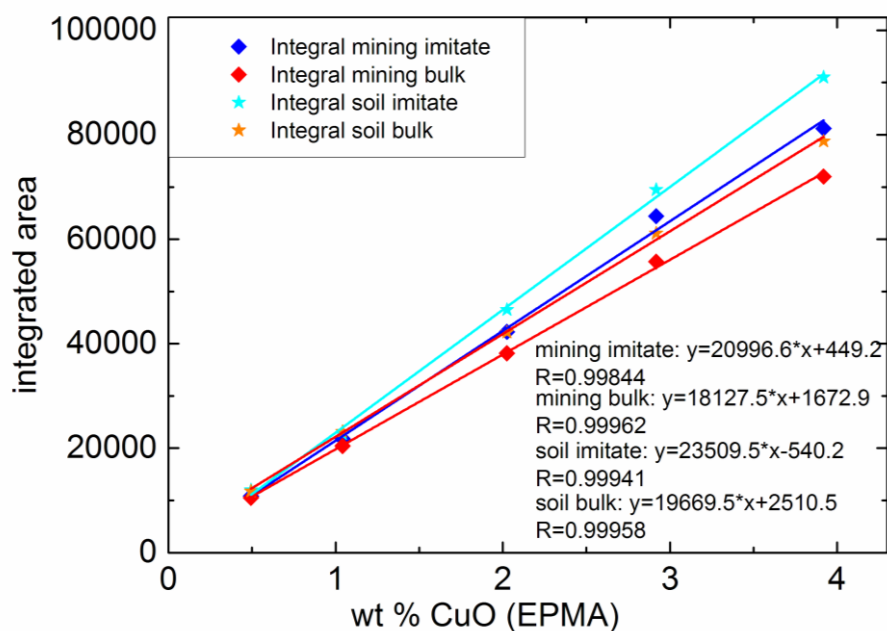
Figure 76: Correlation of integrated Cu-peaks of both measuring programs and material specimens with the data from EPMA analysis.

Figure 77: Comparison of the calculated CuO-data of Moroccan glazes on basis of the integrated peaks of the p-XRF spectra with the program-intern calculated values for both measurement programs.

In case of violet coloured glass with 0.4-3.2 wt% MnO_2, the "mining" measurement on glaze imitations matches the EPMA value the best with deviations of 2-7%.

A further approach of data evaluation is to calculate the contents of a minor element directly from the recorded spectrum of the p-XRF. This has the advantage of avoiding the intern data correction which is not adapted to the particular chemical composition and cannot be controlled by the user.

The peaks from the Cu-Kα radiation in the XRF spectrum are exemplarily integrated and correlated with the EPMA data (fig.76). The data interval for integration is set in the low background scattering, each 0.4 eV below and above the Cu-Kα peak at 8.055 eV.

The resulting regression lines are then used for the calculation of CuO contents in original glazes from Morocco based on the raw spectra from the p-XRF measurement (fig.77). The calculated values of Cu contents in Moroccan are consistently lower than the data of the device intern evaluation. They under-determine the EPMA values with 50-70%; the device evaluation of "mining" measurement match the EPMA values with 40% accuracy. The device evaluation of the "soil" program deviates in average more than 100% from the EPMA.

9.3.4 Discussion

A few general trends can be observed in the data of p-XRF measurements. At first, there is an exceeding of measurement values of glaze imitations over those of bulk glass. This can be attributed to a smoother surface on the glaze imitations than on the bulk glass. The samples of bulk glass have a plain surface, but are not polished after solidification like the glaze imitations. The original glazes have a surface which is plane in contrast to the bulk glass samples, but not as smooth as the polished glaze imitations. A smooth surface is an important criterion for a valuable measurement of p-XRF. The out-coming signal reaches the detector window most homogeneously, when the escape from the material is in the same level. Within the data, the "soil" program seems to be less affected by surface texture and is therefore more suitable for not polished glass surfaces. In the original glazes, the differences in the measurements due to the sample surface are also slightly lower in the data of the "soil" program. This can be explained with to the calculation method of the "soil" program, which uses the scattered Compton peak as reference and is therefore less sensible to the surface scattering effects, which influence the X-ray fluorescence signal.

An influence of surface corrosion would be expected to enrich the PbO contents in the p-XRF results of historical glazes (Orfanou & Rehren, 2015), which cannot be distinctly observed.

An influence of the underlying calcareous ceramic in glaze imitations compared to bulk glass samples could not be detected. The higher values of CaO in the "mining" measurement of glaze imitations compared to the measurements on bulk glass, do not differ from the exceeding of Al_2O_3 and K_2O in glaze imitation measurements. The pure calcareous body would have elevated only the CaO values. In the "soil" program data, no distinct exceed of CaO values is observed.

In the lead free calibration glass samples, the elements K and Ca are with 0-20 % better determined than in the lead containing Moroccan and synthetic glazes with 50 % deviation. In the tiles from Bukhara and Samarkand, the analysis for Ca is with about 30 % deviation better in the glaze compositions with lower lead content. The determination of the transition metals in original glazes and glaze imitations is also poorer in accuracy when heavy elements lead and tin are present alongside light glass elements in considerable amounts. It is assumed, that the combination of light elements with considerable amount of heavy elements like PbO is a problem for the internal matrix correction of the device. Al_2O_3 and PbO are better determined in the Uzbek than in Moroccan tiles, whereas Fe_2O_3, CuO, and SnO_2 are more precisely determined in the lead-rich Moroccan samples.

The glass samples of the calibration series with CuO and MnO_2 contents show a good precision in p-XRF measurements, especially the "mining" program on the glaze imitations which is the most reliable measuring tool here. In the CoO values, the "soil" measurement is the more accurate program with a calibration factor to EPMA data of 1.03 in contrast to a factor of 0.78 in "mining" data.

9.3.5 Conclusion

As first aspect, an influence of glaze measurement by an underlying light-element material could be widely ruled out.

The comparison of bulk glass and polished glaze imitations shows the importance of a smooth surface for p-XRF measurement. The "soil" data seems to be less affected by the surface properties than the "mining" program.

The manual evaluation of the raw spectra does not further improve the results of colouring agent determination.

The deviations of "soil" and "mining" measurements from the EPMA data are substantial, especially in the analysis of lead or tin containing compositions.

As a general tendency, the values of "mining" program data exceeds the "soil" program values, which is attributed to the different methods of matrix correction (chapter 4.3). In comparison of the two measurement programs, the "mining" is more suitable for the determination of PbO, CuO, MnO_2, and SO_3. The oxides of light element SiO_2, Al_2O_3, and P_2O_5 are only determinable with the mining "program". The "soil" program gives the better results for CaO, Fe_2O_3, SnO_2, and CoO. The K_2O contents are determined more precisely in the Moroccan lead glazes with the "mining" program, but in the synthetic alkali glazes better matched with the "soil" program.

As an example for semi-quantitative analysis, the p-XRF data of the Uzbek samples are plotted in a ternary diagram opposed to the corresponding EPMA data, shown in figs. 72a and b. The distinction into three groups of main composition can be observed in the p-XRF data, too. This shows that the measurement precision is sufficient for the semi-quantitative analysis of the major elements. For the Moroccan original tiles, the grouping is limited to one lead-rich group, which is reproducible with the p–XRF data but with a shift to higher SiO_2 values.

The colouring agents CuO and MnO_2 in concentrations of 0.5-4 wt% can be determined with a precision of less than 10% deviation. The EPMA values of CoO between 0.1-0.5 wt% are matched

with a accuracy below 16%. The measurement of colouring agents is again more precise on smooth, polished surfaces of glaze imitation samples.

10 ORMOCER® composites

This chapter treats former and new approaches of the adaption of ORMOCER® material to historical glaze colouring agents. As a former approach, the result of a restoration of enamelled terracotta medallions was investigated after the 6 year exposure to northern Germany weathering condition (Furmanek, 2006). For the restoration of Islamic glazes, the ORMOCER® material was combined with different fillers. In the colouring of ORMOCER® with pigments, augmentation of phase boundaries was accepted with the advantage of high colour intensity and fidelity to the original glaze compositions. Glass powders with historical composition were used in one approach; another approach used particles of historical colouring agents. In the case of Fe_2O_3 and CuO, particles of sub-micrometre scale were used. Because of their small particle sizes, they have to be treated with a surface modification in order to stabilize the particle suspension.

Different methods of particle dispersion were tested on all ORMOCER® materials with mineral pigments. All coatings were tested in outdoor weathering or climate chamber. The colour stability was tested in the change of UV-Vis transmission before and after weathering. The adhesion of the coatings was also tested before and after weathering, under the pulling force of an adhesion tape with the so-called Sellotape™-test.

10.1 Coloured ORMOCER® in former restorations

In the year 2006, a historical building with several medallions of glazed terracotta in Lüneburg, northern Germany, was restored by the institute for conservation and restoration of Peter Furmanek in Hannover, Germany (Furmanek, 2006). After 6 years of weathering and air pollution, a few of the terracotta medallions with different colours showed chipped parts of coloured ORMOCER® (figs.78 a and b).

a)   b)

Figures 78 a and b: One of the restored medallions from the IHK-building in Lüneburg, Germany. Just restored (a; Furmanek, 2006) and six years after restoration (b, kindly provided by F. Schlütter). The arrows mark the points of sampling.

The restoration approach by Furmanek is documented as follows: the medallions were delivered from old restoration layers; loose parts of the original glaze were consolidated with ORMOCER® G. Damaged parts of the underlying terracotta were patched with Paraloid® B 72 in ethyl acetate, mixed with chamotte flour. Holes in the ceramic were filled with a mortar replacement, consisting of Syton® X 30, Acematt® HK, Tween®, water and SiO_2 flour of quartz and cristobalite. A supplement of old slip was done with several layers of Syton® X 30, Acematt® HK and quartz flour in different grain sizes. The imitation of the original glaze was performed with the ORMOCER® G material, combined with different colours of fine glass powders of <63 μm and mineral pigments of the company "KREMER Pigmente".

The parts of coloured ORMOCER® which were chipped-off were investigated with the micro-Raman method. In order to reveal the changes of the chemical bondings in the material over time, a just cured ORMOCER® G was taken as a reference material. Additionally, the Raman spectrum of the main ORMOCER® component, Paraloid 72 B was separately recorded.
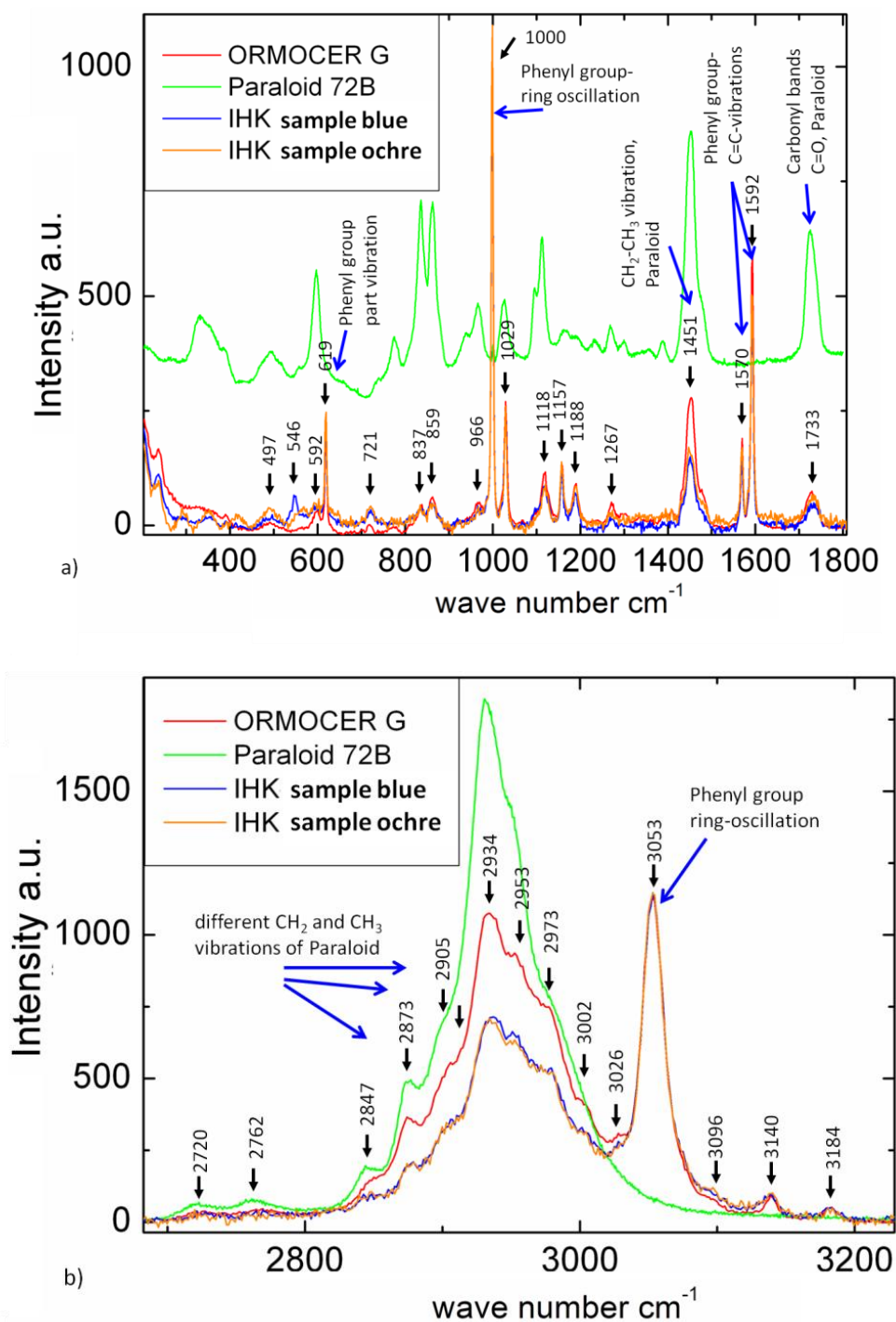
Figure 79 a) and b): Two excerpts of the Raman spectra of one blue and one ochre sample, a just cured ORMOCER® G and component Paraloid 72 B. The spectra were calibrated to the phenyl group ring oscillation at 1000 and 3053 cm^{-1} (Riegel *et al.*, 1998; Posset *et al.*, 2002).

The Raman spectra were normalised to the oscillation peaks of the phenyl group at 1000 and 3053 cm^{-1} which are known to be very stable bondings (Riegel *et al.*, 1998; Posset *et al.*, 2002). The micro-Raman spectra of the older ORMOCER® compounds and the new ORMOCER® G are very similar (figs. 79 a and b). Most of the peaks of the Paraloid 72 B are well distinguishable in both spectra. According to former investigations of ORMOCER® degradation, an aging effect is assumed to change the carbonyl and C-H bondings at 1733 cm^{-1} (pers. comm. K. Egly, 2012), which is not observed here. Instead, differences between the new and the aged material are seen in one CH$_2$-CH$_3$ vibration of the Paraloid 72 B at 1451 cm^{-1} and in the region between 2800 and 3000 cm^{-1} in figure 78b. The reduction of the Paraloid B 72 signal in the pigmented material is unusual for the aging of ORMOCER®. Paraloid B 72 is known from other restoration approaches as stabilising material without vulnerability to weathering (Vaz *et al.*, 2008). The relative reduction of the peak is ascribed to the high portion of particles in the mixture. The portions of pigment particles in the ORMOCER® material were not documented in the restoration process (Furmanek, 2006), but it can be assumed that a high amount of solid phase reduced the ORMOCER® part and therefore the adherent and stabilizing properties of the coating. This may explain the chipping of the glaze supplement. The underlying kit was not investigated at this point and cannot be excluded as a further reason of vulnerability.

10.2 ORMOCER® G with historical glass particles

In the present study, experiments were carried out for the further adaption of the ORMOCER® to the colours of original Islamic glazes. The properties of weathering resistance and colour fastness were tested in outdoor weathering and climate chambers.

The ORMOCER® G material is already an adaption to the glass composition in terms of its amorphous silica-based network. There are different options to increase the part of silica content in the material, such as adding silica gel to the silicon-alkoxide or adding a pre-molten glass in the form of flakes or powder. The latter alternative has the advantage of matching of historical the glass composition and was carried out as a first adapting step.

For this approach, the analysed ratios from the original glazes were taken for the melting of bulk glass bars of 100 ml (tab.27). As basis for the imitated glass, the average values of the three different compositional groups in the Bukhara glazes from the 15th-17th century were taken (chapter 5.3). The added compounds are SiO$_2$, Pb$_3$O$_4$, Al$_2$O$_3$, Na$_2$CO$_3$, K$_2$CO$_3$, MgCO$_3$, CaCO$_3$ from

which the oxides were obtained by *Unimin* cooperation and the carbonates by the *Merck* Company. A pre-homogenisation was carried out for 15 min in a tumble mixer. Then, the powders were gradually given into the platinum-rhodium or Al_2O_3 crucibles during heating process in order to avoid an over-foaming of the melt. Crucibles of Pt-Rh-alloy in the proportion of 80 vol% Pt and 20 vol% Rh have the advantage of high stability and tensility, but can only be used for glass compositions with low lead content. For high lead compositions, Al_2O_3 as crucible material was taken in order to avoid corrosion of the platinum.

Table 27: Glass recipes of historical composition. The analysed values are normalised to a sum of 100 %.

	Alkali glass		Alkali lead glass		Lead glass	
Oxide	pre-set	analysed	pre-set	analysed	pre-set	analysed
SiO_2	79.0	79.0	70.7	70.3	41.7	43.8
PbO	0.00	<0.05	8.2	9.1	53.5	49.8
Al_2O_3	4.94	4.9	3.4	3.5	1.4	1.9
Na_2O	5.3	5.1	6.7	5.9	0.9	1.3
K_2O	3.0	3.0	3.3	3.4	0.9	1.1
MgO	3.5	3.5	3.3	3.3	0.5	0.9
CaO	4.3	4.5	4.3	4.6	1.1	1.5
sum	100.00	100.00	100.00	100.00	100.00	100.00

A mechanical mixing or stirring of the glass melt was not carried out, because the small quantities of the batch can easily be contaminated. For the same reason, gas bubbles were driven out by convection and not by stirring. A sufficient homogeneity shall be achieved through the heating convection after 4 hours heating at 1650 °C for alkali glass, after 2 hours at 1650 °C for alkali lead glass and after 2 hours at 1550 °C for the lead glass, each realised in a HTK 40-17 *Thermconcept* furnace. The cooling was performed in a *Nabertherm* N11 furnace with a cooling rate below 10 K/h in order to avoid strains in the bulk glass. During the cooling process, further driving out of gas bubbles is not possible.

The lead free composition showed the highest viscosity as a melt and has a streaky appearing in the cooled bulk. The glass samples with low and high lead contents are less streaky but have bubbles in the bulk material. The results show, that the homogenization of glass with historical

glaze composition is difficult to realize in small batches and needs long heating times. This can be ascribed to the low contents of natron flux, which were taken from the average values of historical glazes from Bukhara. The glaze compositions are on the lower edge of processability for glass batches.

The glass samples were analysed in a powder diffractometer in order to detect potential crystalline phases or long range order structures. The diffractograms show only the scattering of short range order, which confirms the choice of cooling temperatures and rates in the process.

The ready molten and cooled glass was ground in a ball mill to form a powder of 25-50 μm grain size. The grain size distribution was determined by laser diffraction measurement. The particle size has to be optimised in order to avoid undesired sedimentation of too large particles in the suspension of ORMOCER® G on the one hand, and too high effect of light scattering on phase boundaries with too small particles on the other hand.

In order to reduce the effects of phase boundary refraction, the optical density of the ORMOCER® G was adapted to the refraction index of the glass. The refraction indices of the three glass compositions were determined with an Abbé refractometer to 1.494±0.003 in the alkali glass, 1.517±0.003 for the alkali lead glass and 1.600±0.003 in the lead glass. The values were measured at the standardized wavelength of 633 nm. In a first step, the synthetic alkali glass was mixed with the ORMOCER® G in different portions of 9.8±0.5-99.6±0.5 vol% (0.06-0.6 wt%, tabs. 28 and 29). The ORMOCER® G has a refractive index of 1.45±0.3 close to the alkali glass; the ORMOCER® E lies with a refraction index of 1.54±0.3 between the alkali and the lead glass composition (Streppel, 2005; Declerck, 2010). The refractive indices of ORMOCER® materials are adjusted by the variation of the content of epoxy resin (Kron *et al.*, 2001).

The compounds were homogenized by manual stirring. In order to test the materials as a glaze substitution, they were applied to silica-rich ceramic substrates which represent the later base material of building tiles. Then, the coatings were cured for one day at room temperature. The stability of the coatings was tested with a so-called Sellotape™-test, in which an adhesion tape is stuck on the surface and then pulled away in right angular. The better the stability, the less particles of the coating remain on the tape. The amount of particles on the pulled-away Sellotape™ was determined by measuring the weight of the tape before and after contact with the coating. The differences in the amount of removed particles were also visible with the unaided eye, but can be quantified in the increase of the Sellotape™ weight. On the Sellotape™

strips, which were pulled from the coatings with less than 30.6 vol% particle amount, no weight increases were observed. From the coatings with 48.1 vol% particle amount and more, the additional weight of particles on the Sellotape™ strips was up to 10 mg.

Table 28: Contents and volume proportion of alkali glass powder in 2 ml ORMOCER® G, calculated with the glass density of 0.718±0.063 g/ml and an ORMOCER® density of 1.20±0.03 g/ml.

Glass powder (mg) per 0.2 ml ORMOCER® G	14	30	44	69	85	101	124	143
vol %	9.8	20.9	30.6	48.1	59.2	70.3	86.4	99.6

Table 29: Table of mg/ml-values of glass powder in ORMOCER® G.

	Alkali glass	Alkali lead glass	Lead glass
specific weight (g/cm^3)	2.40±0.07	2.70±0.07	3.85±0.07
Glass surface	weighed portion (mg/ml)	weighed portion (mg/ml)	weighed portion (mg/ml)
Rough	100	150	300
	290	500	650
	100<x<290		
Smooth	290	150	>300
		>150	650
		>500	
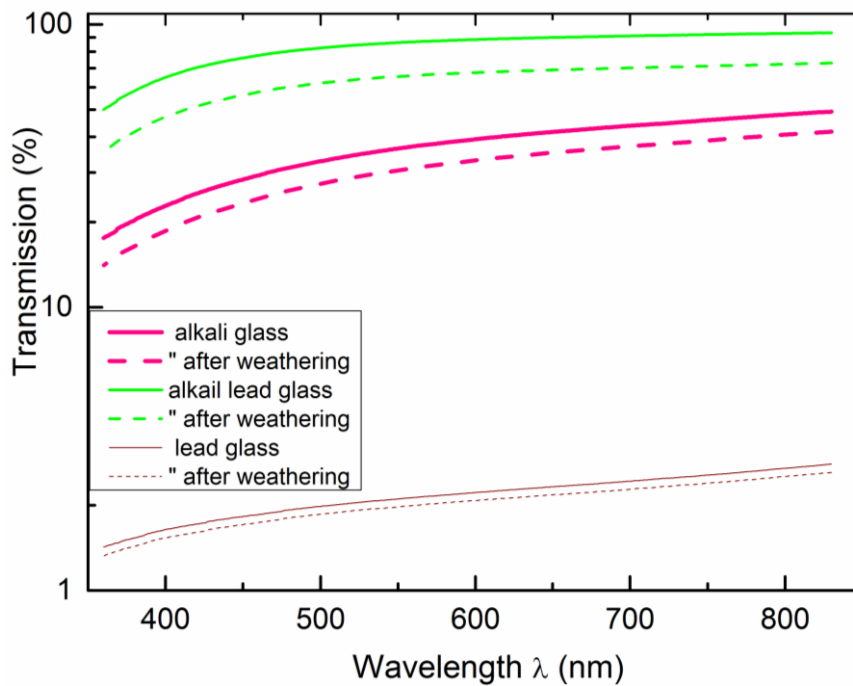
Figure 80: Transmission characterization of the three different glass compositions in ORMOCER® G, before and after one month weathering. The alkali lead glass shows the highest transmission before weathering, but also the highest loss through weathering.

The investigation of the dependence of weathering stability and particle amount in the coating was carried out with glass particles of alkali lead and lead composition. In order to monitor changes in the transparency of the material, the coatings with different particle amounts were applied to glass substrates and measured with UV-Vis spectroscopy before and after weathering. The surfaces of the glass substrates were in one part smooth and in the other part the surfaces were roughened, in order to investigate the adherence properties on different surfaces. After curing, the coatings were exposed 4 weeks to an outdoor atmosphere of -6.4 to 11.9 °C and 55-100 % RH. The transmission measurements were carried out with an UV-Vis spectrometry Cary® 100 Bio of Varian® within a wavelength range of 360 to 830 nm (chapter 4.6).

The general observation is a higher loss of transparency and less adhesion in the ORMOCER® G - glass compositions on the plain glass than on the rough surfaces. The application of the Sellotape™-test removes parts of up to 50 mg of the coating from the smooth glass surfaces, whereas no detachment measured from the coatings on roughened surfaces. The coatings with alkali and alkali lead glass lose 5-10 % transparency after weathering, whereas the

lead glass compounds have a milky appearing already before the exposure and do not show distinct change after weathering (fig.80).

10.3 ORMOCER® G and E with coloured glass particles

In order to test the effect of milled coloured glass in the two different ORMOCER® variations, G and E, glass compositions similar to the historical alkali glazes were molten. For better processability, the alkali values were increased compared to the glaze recipes. Exemplarily, a milled turquoise alkali glass was used for the colouring with glass particles. The pre-set composition and the corresponding EPMA analysis values show the good predictability of the glass composition (tab.30)

Table 30: Composition of the recipe and the EPMA measurements of the molten glass.

Oxide	Na_2O	Al_2O_3	K_2O	MgO	Fe_2O_3	SiO_2	CaO	CuO	PbO	Total
wt% pre-set	12.00	3.00	5.00	4.00	1.00	60.00	4.00	3.00	8.00	100.0
wt% EPMA	10.19	3.22	5.20	1.02	0.93	59.06	4.40	3.20	10.86	98.11

The processes of milling, processing, and characterisation were the same as for colourless glass (chapter 10.3). In contrast to the colourless glass, the application on plain glass substrates was skipped, because of the poor stability results.

The turquoise colour of the glass got lighter in the milling process because of the high amount of grain boundaries on which light is reflected. By integration into the ORMOCER® material, a homogeneous turquoise coating was achieved after curing. In the case of ORMOCER® E, the glass powder tended to agglomerate and resulted in an inhomogeneous coating surface.

Both materials ORMOCER® G and E were tested in a the climate chamber for six days with relative humidity levels between 0 and 70 % and temperatures between 0 and 46 °C (fig.81). The outdoor weathering is omitted here, in favour of the reproducibility of the climate conditions. The profile is based on original weathering data from north India (National Capital Territory of Delhi), where a restoration of glazed tiles from historical Islamic buildings was envisaged.
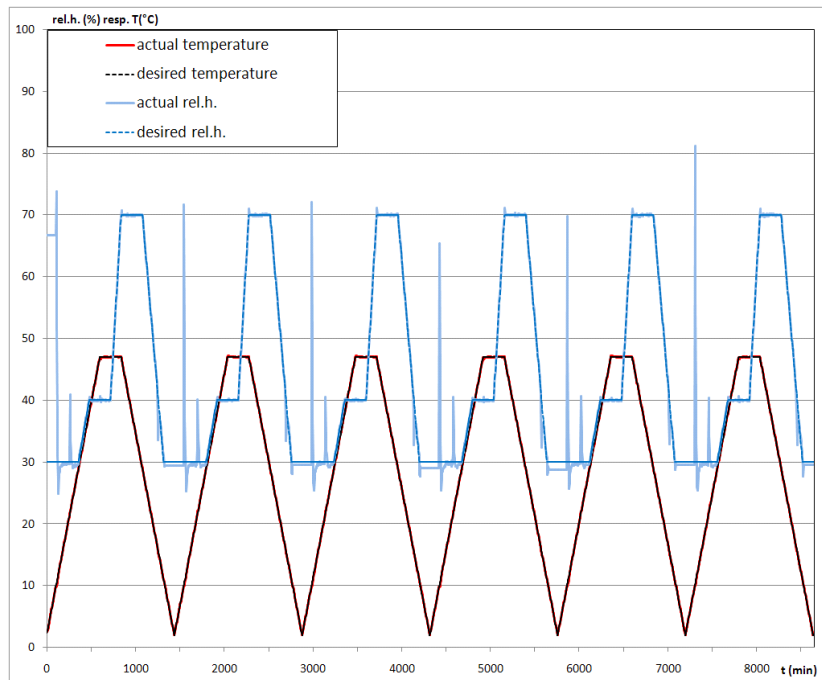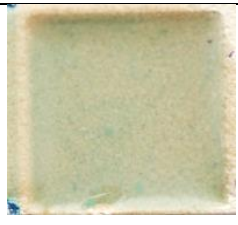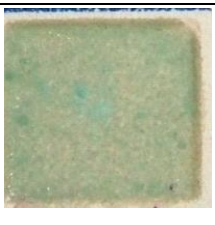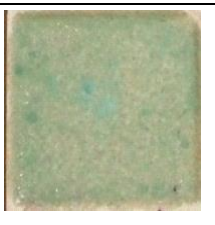
Figure 81: Six-times 24h-run of the climate chamber in relative humidity and temperature. The humidity is not measurable at the point of T=0 °C, which leads to the disturbance in this area.

Table 31: Weathering stability of the powder of turquoise coloured glass in ORMOCER® E and G. Especially in the ORMOCER® E coating the surface is very inhomogeneous and the adhesion is not satisfying.

	ORMOCER® G	ORMOCER® E
Before weathering		
After weathering		

The colour hues of both materials did not show any change after weathering treatment (tab.31). The ORMOCER® G compound showed good adhesion before and after weathering. In contrast, a loss of stability is observed in the ORMOCER® E material after weathering. Here, the Sellotape[TM]-test compound showed the detachment of parts of 5-10 mg of the coating after weathering. For a better surface quality, both coatings were covered with a layer of pure ORMOCER® G respectively E. After curing of the added layer, the surface structures were smooth, but the adhesion behaviour was unaltered.

10.4 ORMOCER® with mineral pigments

The use of glass powder as pigmentation is close to the original chemical composition, but does not fulfil the requirement of high colour intensity. Therefore, an approach of colour matching was carried out by addition of colouring agents to the ORMOCER® matrix. As colouring agents, solvable organic dyes as well as non-solvable, inorganic pigments are common for implementation (Kron *et al.*, 2001). Here, pigment colouration was favoured, because of its higher intensity and better light fastness. The metal ion compounds in particular, have good colour intensity because of their high refractive index (Nassau, 2001). It is desired, that the pigments contain colouring ions in the same oxidation state and coordination sphere as in the original glaze. As far as possible, the original pigments were taken. In the case of ion colouring, pigments with the same transition metal ion complex were used.

Both types of ORMOCER®, G and E, were combined with a number of mineral pigments from μm to nm size. The pigments are inexpensive and easily available as chemical agents, e.g. at "KREMER Pigmente".

Similar to the former applications on terracotta medallions in northern Germany, the ORMOCER® material was mixed with historical pigments. As pigments, cobalt blue pigment $CoAl_2O_4$, Egyptian blue $CaCuSi_4O_{10}$, manganese violet $Mn(NH_4)P_2O_7$, tin oxide SnO_2 for whitening and a lead tin oxide Pb_2SnO_4 as yellow pigment were used. A combination of Pb_2SnO_4 and the $CaCuSi_4O_{10}$ was used to produce a green colour. The weighed portions of ORMOCER® and pigment material are given in table 32.

To avoid segregation of pigments during the application of the restoration material, the suspensions of ORMOCER® and pigments had to be dispersed and de-agglomerated. In one

approach, a roller mill with a pre-step of ultrasonic treatment was used; in the other approach a bead grinding mill dispersed the particles.

The ultrasonic finger de-agglomerated the pigments, which was in particular necessary for the sub-micrometre sized particles (Pohl *et al.*, 2004). The ultrasonic finger (Sonics Vibra-Cell) was used with a power of 47 W with 30 periods of 1 sec ultrasonic exposure and 5 sec break. A roller mill is composed of three parallel cylindrical rollers.

Table 32: Grain sizes and contents of pigments, ORMOCER® G and E, and the hardening agent.

Pigment	$CoAl_2O_4$	$CaCuSi_4O_{10}$	$Mn(NH_4)P_2O_7$	Pb_2SnO_4	$CaCuSi_4O_{10}$ + Pb_2SnO_4	SnO_2
Grain size (µm)	4.2	<120	2.3	1-63	1-120	0.5
ORMOCER®G (mg)	119	204	197	261	235	179
Pigment (mg)	45	68	16	115	45+76	53
ORMOCER®E (mg)	120	209	195	260	223	175
Hardening agent (mg)	0.6	1.0	0.9	1.3	1.1	0. 9
Pigment (mg)	48	67	16	113	45+76	53

In one "run", the suspension is put on the slot between the first and the second cylinder, from where it is transported through the first and the second slot to the third cylinder. The material was first treated in 2-3 runs of gap setting with slot width of 5 µm between the rollers at 200 rpm, and afterwards in one run of "force" setting with a defined pressure of 5 N/mm and a slot width of 5 µm at 130 rpm. The thickening of the solution during the milling process had to be compensated with subsequent addition of 2-Butoxyethanol as organic solvent.

In the second approach, the bead grinding mill is used, which simultaneously homogenized and grinded the particles in ORMOCER® material. It has the disadvantage of the beads as grinding aid which has to be separated from the ORMOCER® material after the milling process. As bead grinding mill, the version SL-C5-25 Dispermat® of the company VMA-Getzmann was used with a milling slit of 0.3 mm and 100 ml glass beads of 1-1.25 mm diameter. The grinding process was carried out for 2 h at a frequency of 3750 rpm and a maximal temperature of 35 °C.

The homogeneity and stability of the dispersions were tested by sedimentation experiments. In order to observe potential segregation of particles, the differently treated dispersions were left

for about one week (187 h, 7.8 days) without any movement or stirring. The materials showed different behaviours depending on the dispersion method; in the compounds dispersed with ultrasonic finger and roller mill, no sedimentation of the mineral pigments was observed (fig.82 a). In contrast, segregation was observed in the dispersions which were treated with the bead grinding mill. On the bottom of the glass ampullae, the particles settled after the sedimentation time of 187 h (fig.82 b).

Figure 82 a) and b): Sedimentation behaviour of pigments manganese violet, cobalt blue, cobalt green and lead tin oxide yellow (from left to right) in ORMOCER® G after 187 h. The treatment with a roller mill and ultrasonic finger produces homogeneous compounds (a) whereas dispersion with a bead grinding mill leads to clearly visible sedimentation (b).

Both ORMOCER® compositions, G and E were than applied to ceramic substrates, cured for one day at room temperature, and weathered for six days in the climate chamber. The weathering conditions were the same as described before. The coatings of $CoAl_2O_4$ and $CaCuSi_4O_{10}$, $Mn(NH_4)P_2O_7$, and SnO_2 were homogeneous with both types of ORMOCER®. The Pb_2SnO_4 pigments and the combinations with $CaCuSi_4O_{10}$ showed coarse surfaces in the ORMOCER® G material and even lumps and flakes in the ORMOCER® E material.

The SellotapeTM-tests, which were carried out after the described weathering, revealed a better adhesion on the ORMOCER® G coatings than the tests on the ORMOCER® E ones. In the ORMOCER® coatings, the Sellotape[TM] broke away parts of 1-4 mg of the coating and left holes and inhomogeneities behind (tab.33).

Table 33: Coatings on ceramic substrates; depicted before and after weathering and with a final pure ORMOCER® layer after weathering. For a test of visualization of the coating in REM cross section image, two samples were partly cut.

	$CoAl_2O_4$	$CaCuSi_4O_{10}$	$Mn(NH_4)P_2O_7$	Pb_2SnO_4	$CaCuSi_4O_{10}$ $+ Pb_2SnO_4$	SnO_2
ORMOCER®G						
Before weathering						
After weathering						
With add. ORM. layer						
ORMOCER®E						
Before weathering						
After weathering						
With add. ORM. layer						

The less homogeneous performance of the mineral particles was smoothened with a final layer of uncoloured, pure ORMOCER® after curing of the pigmented layer. The results showed a plane and homogeneous surface with glassy transparent appearing in both ORMOCER® materials.

After curing and weathering of the final layer, the Sellotape^{TM}-test was carried out again. The weathering was carried out with the same six runs of relative humidity between 0 and 70 % and temperatures between 0 and 46 °C as before.

The results were comparable to those before the addition of the last layer. In the ORMOCER® G coating, good adhesion was observed before and after weathering. In the ORMOCER® E approach, the coatings were vulnerable to the pulling force of the Sellotape^{TM} and stick in parts to the tape after removal.

10.5 ORMOCER® coloured with nano-particles

In order to improve the homogeneous distribution of particles, nano-particles of colouring oxides were incorporated into the ORMOCER® material. Concerning the results of adhesion tests with mineral pigments, ORMOCER® G was chosen as a host matrix. With the use of nano-particles, the content of solid phase in the ORMOCER® could be reduced without loss of the colour intensity. Beside the improved homogeneity, the coatings were expected to reveal higher stability because of the higher content of ORMOCER® with high chemical and physical stability (Haas *et al.*, 1999).

As nano-particle colours, the transition metal oxides Fe_2O_3 and CuO were used, which also occur in the historical glazes: Fe^{3+} is known as ochre or red colouring ion from historical glazes and was added here as oxide particle. Cu^{2+} occurs as a colouring ion in turquoise and green glazes, but was also found in a copper-chromium-magnesium oxide as black pigment in an Uzbek glaze (chapter 7.2). Here it was applied as oxide pigment to the ORMOCER®. The used Fe_2O_3 particles have grain sizes of 92 nm and 99% purity; the CuO particles have 40-80 nm grain size and 99.9 % purity; both were obtained by the company *Iolitec*. Other nano-particles of cobalt-, copper-, manganese-, tin- and lead-tin-oxides are also commercially available.

The agglomeration of the nano-sized particles is supposed to be avoided with a chemical modification of the particle surfaces. The treatment connects a silane molecule with the surfaces of the metal oxide particles. In our case, 3-Methacryloxypropyltrimethoxysilan (MEMO) was used as silane which forms a strong connection to the rest of the ORMOCER® network (Gellermann *et al.*, 2007). The surface modification of an inorganic particle is sketched in figs. 83 and 84.
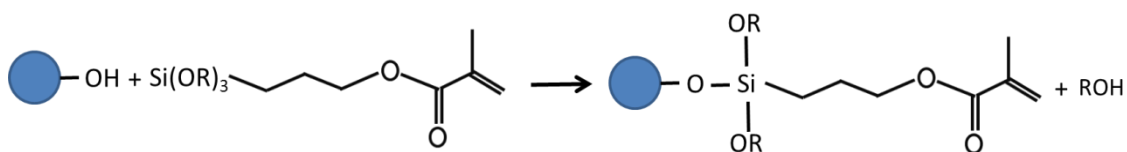
Figure 83: Depiction of particle modification with 3-Methacryloxypropyltrimethoxysilan (MEMO) with R = methyl group (CH_3) adapted from Althues *et al.* (2007).

Unmodified particles

After polymerization

Modified particles

After polymerization
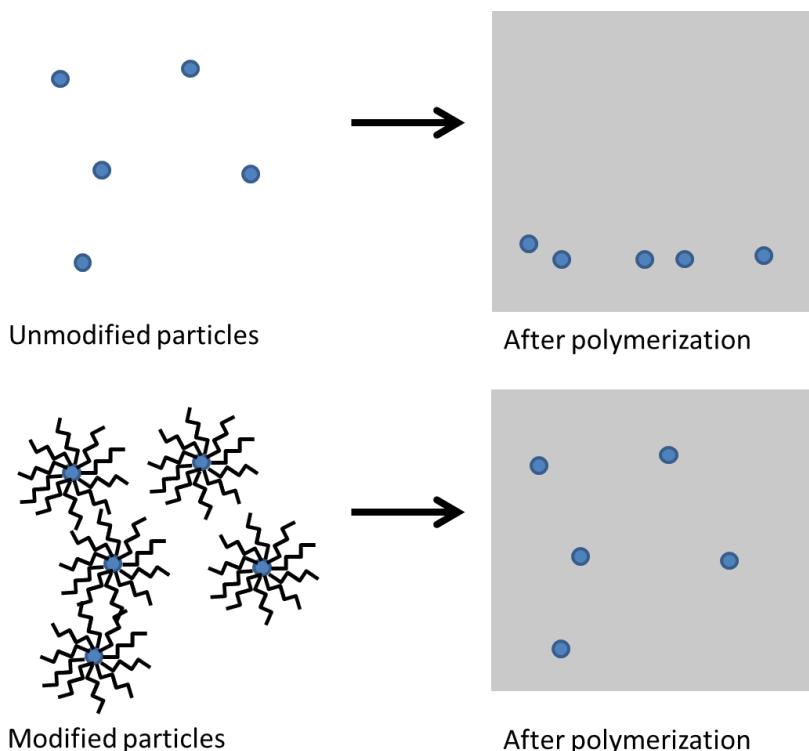
Figure 84: Behaviour of unmodified particles in a sol-gel material (upper picture) and modified particles in a polymerized matrix (lower picture; Althues *et al.*, 2007).

Table 34: Contents of nano-particle volumes and ORMOCER® material with ethyl acetate. The volumes of nano-particles are calculated into a weight with a density of 5.2 for Fe_2O_3 and 6.4 for CuO for easier handling (data of the producer).

	Fe_2O_3		CuO	
Ingredients	0.5 vol%	1.0 vol%	0.5 vol%	1.0 vol%
Particle volume (cm^3)	0.025	0.051	0.025	0.005
ORMOCER solution (ml)	13.50	13.50	13.50	13.50
Ethyl acetate (ml)	1.50	1.50	1.50	1.50

The Fe_2O_3 and CuO nano-particles, modified and unmodified ones, were mixed in 0.5 and 1.0 vol% concentrations into the ORMOCER® G with ethyl acetate as solvent (tab.34). A treatment with ultrasonic finger and roller mill was carried out. The less suitable dispersion process with bead grinding mill was not applied here (chapter 10.4).

Measurements with Fourier transform infra-red spectrometry (FT IR) were carried out in order to control the integration of the MEMO-modifier into the dispersion. The FT IR measurements confirmed the inclusion of the MEMO-modifier in the particle solution as it is seen in figure 85; the spectra of modified particles are superimposed by the overlying spectrum of pure MEMO, which is especially seen in the range of 500-1750 cm^{-1}.
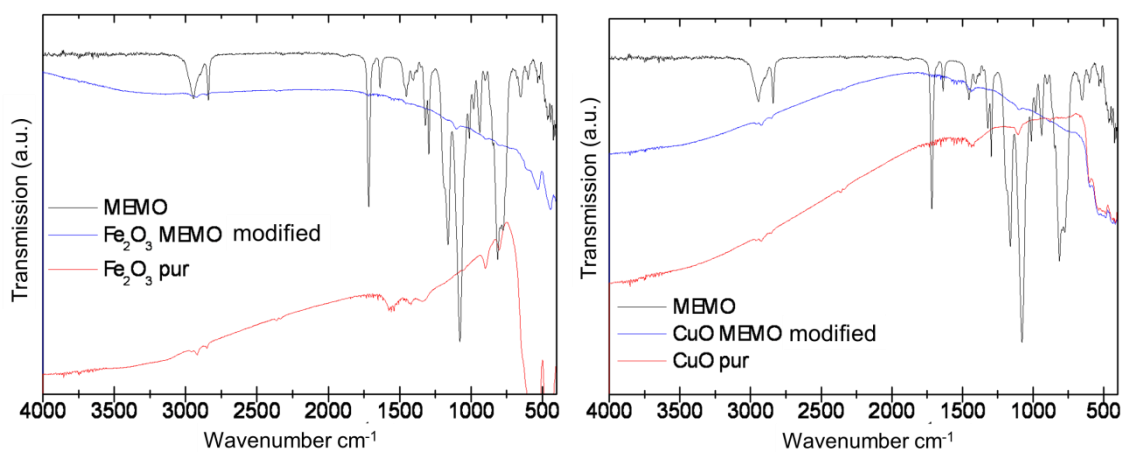
Figure 85: FT IR measurement of ORMOCER® G and modified particles of Fe_2O_3 (left) and CuO (right) in a concentration of 0.5 vol%, dispersed with ultrasonic finger and roller mill. The modification of the ORMOCER® by MEMO is obvious.
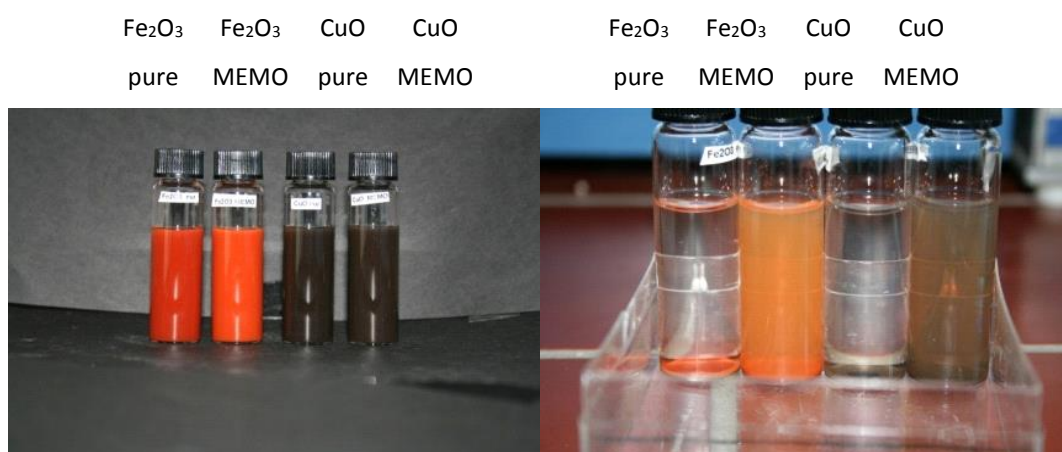
Figure 86 a) and b): Batches of 0.5 vol% modified and unmodified particles of Fe₂O₃ and CuO in an ethyl acetate solution, homogenized with ultrasonic finger and roller mill before and after 187 h.

Before application, the sedimentation behaviour of modified and unmodified particles in ORMOCER® G was observed in an ethyl acetate dilution in a time span of 187 h. In comparison to the suspensions with unmodified particles, the approaches with modified particles showed a much better result after the defined sedimentation time (fig.86 a and b). The unmodified particles instead showed agglomeration on the ampulla bottom.

The unmodified and modified particles in ORMOCER® G were applied to ceramic substrates and rough glass substrates in order to investigate transmission and adhesion. The coatings underwent a weathering of six runs of 12 h periods with relative humidity levels between 30 and 98 % and temperatures between -20 and 46 °C. Because of difficult realisation of humidities below 30 %, the minimum value was increased in comparison to former simulations. The upper limit was set to the maximum of realisable relative humidity of 98 %; the temperature range was expanded to the minimum limit of -20 °C in the used climate chamber. Before and after the weathering treatment, the coatings were investigated with UV-Vis spectroscopy.

The measurements of UV-Vis spectrometry show different changes in transparency before and after weathering, depending on the particle content and the particle modification (fig.87). In the coatings with 0.5 wt% particle amount, the surface modifications of CuO and Fe₂O₃ increase the transparencies before and after weathering. In the case of 1.0 wt% particle amount, the increase of transparency due to modification is observed before weathering but disappears after weathering treatment.
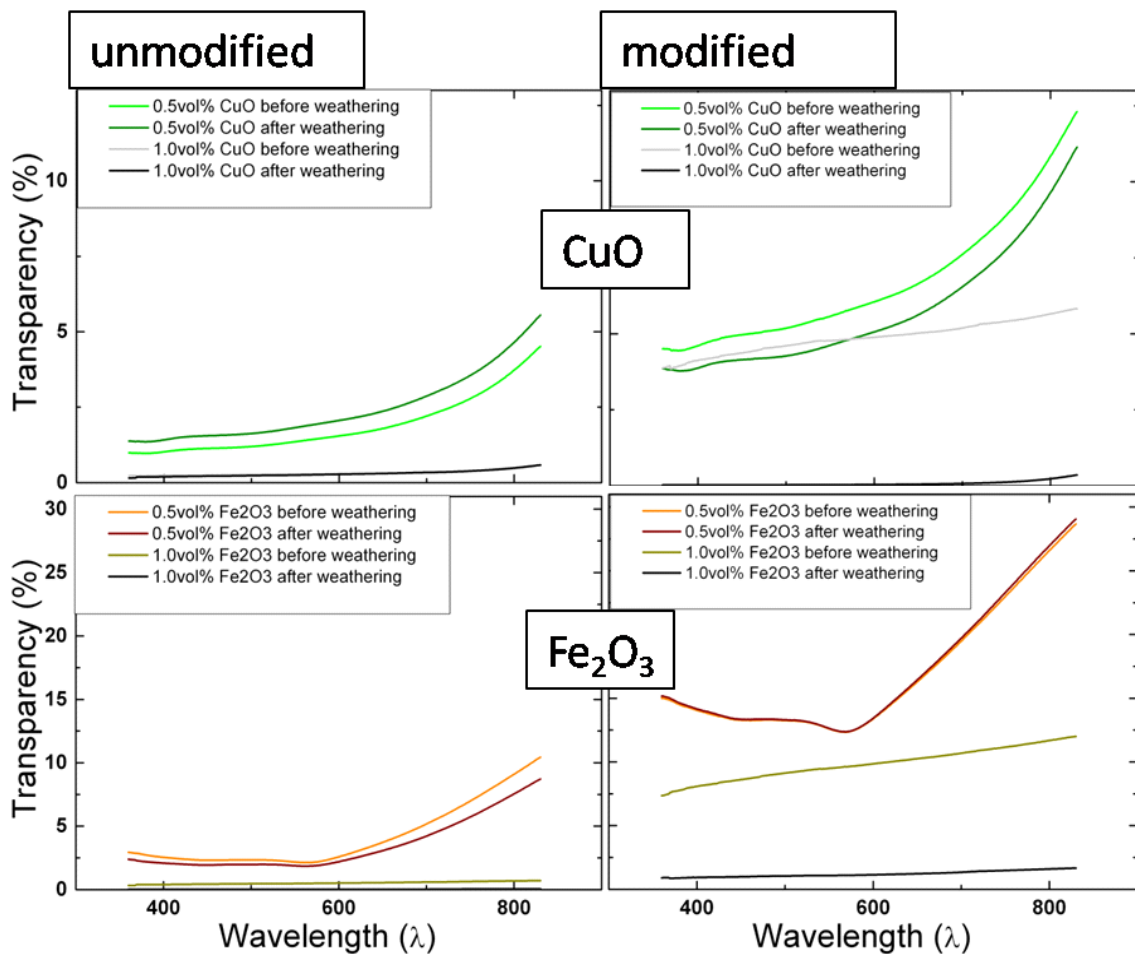
Figure 87: Transparency of the modified and unmodified compounds of 1.0 and 0.5 vol% pigments before and after a weathering treatment of 30 to 98% RH and -20 to 46 °C. The transparency increases with the particle modification. In 1.0 vol% materials, the increase is lost after weathering.

The change of transparency in coatings with 0.5 wt% (modified and unmodified) particles and the coating with 1.0 wt% unmodified particles is between 0 and 1 %.

The coatings with 1.0 wt% content of MEMO-modified particles show up to 5 % loss in transparency (fig.87). All coatings show good stabilities in the Sellotape^TM-test without any removed parts on the pulled-away Sellotape^TM-strip. The adhesion does not differ with the modification treatment or the volume ratio of integrated particles.

10.6 Summary of results

The investigations with Raman spectroscopy on former restoration approaches reveal the good stability of the ORMOCER® part of the coatings. The decrease of the content of Paraloid 72B can be ascribed to a too high fraction of colouring particles.

According to these results, the influence of particle fraction in ORMOCER® G is investigated. In the experiments of historical glass particles in ORMOCER®, it is shown that the fraction of solid material may not exceed ca. 30 vol% for a good adhesion on the substrate. The Sellotape™-test shows that lower contents of particles and therefore less grain boundaries increase the mechanical stability of the coating.

The application of the material on smooth glass and rough glass surfaces demonstrates a higher transparency loss in the coatings on smooth surfaces. The loss can be explained with the smaller adhesion area on smooth surfaces than on the roughened ones. It can be expected, that the coatings profit from the rough surfaces of ceramic tiles in on-site application.

The tests of ORMOCER® G and E coatings, combined with milled glass and mineral pigments, reveal better adhesion of the ORMOCER® G material to the underlying ceramic material. The weathering experiments underscore the good stability of ORMOCER®G as matrix material, whereas the ORMOCER® E tends to form lumps of agglomerated glass particles. The agglomerated particles are partly detached by the adherent Sellotape™-strip.

In the investigation of different dispersion methods, the homogenization with ultrasonic finger and roller mill results in a more stable dispersion than the use of the bead grinding mill. This can be ascribed to the de-agglomeration, achieved by the ultrasound and by the shear forces in the roller mill. The compounds treated with bead grinding mill show sedimentation of the particles after one week and poor adhesion to ceramic surfaces. The poor adhesion can be explained by the settlement of particles within the coating layer. The bottom of the layer is enriched in the particle amount, which reduces the adhesion properties of the ORMOCER® matrix.

The benefits of mineral particles as colorants are the readily accessible pigments and the intensity of colouring. The nano-particles show the same results in adhesion and stability as the µm-sized mineral pigments. Especially in the reduced amount of particle volume of 0.5 vol%, good results in weathering stability are achieved. A disadvantage of the nano-particle application is the complex process of particle modification, which impedes a large scale and low cost production.

11 Conclusion

11.1 Glaze compositions

Glazes from tiles of imposing Islamic buildings and some tableware glazes of the medieval epoch in Central Asia, the Middle East, Asia Minor, and North Africa are analysed regarding their main composition and colouring agents. Three major production recipes can be distinguished, i.e. alkali glazes, alkali lead glazes, and lead glazes. In the work of Tite (2011), Islamic glazes from Egypt, Iran, Iraq, and Syria are subdivided into four groups of composition, being partly consistent with those of this work. The alkali lime glazes with <2 wt% PbO correspond to the alkali glazes, but with higher content of CaO. The second and third group of low lead alkali and lead alkali glazes (2-10 wt% PbO and 10-35 wt% PbO) can be subsumed to the alkali lead group described here. Tite´s high lead group has PbO contents >35 wt% and is comparable to the lead glazes (>30 wt% PbO) of this study. The lead and the alkali oxides serve as a flux for the lowering the melting point.

In the interaction of ceramic body and glaze, primarily an influence from Si, Al, and K is observed in the line scans from the cross section of ceramic and glaze. However, the input of ceramic material doesn't seem to be critical for the classification of glazes according to their alkali and alkali lead compositions.

In every epoch and locality, except of the Ilkhanate dynasty in Iran, lead glaze samples can be verified. This is also observed in previous investigations e.g. from medieval Iraq, Jordan and Iran (McCarthy, 1996; Al-Saad, 2002; Holakooei *et al.*, 2014). In the Moroccan and Bulgarian glazes, lead seems to be the only important flux. In part, the lead flux is supplemented by additional alkali contents. The lack of alkali and alkali lead glazes in Bulgarian and Moroccan glazes (assuming that the Ottoman alkali lead glazes are imported tableware) seems to affect the regions with Roman-influenced history and with geographical distance to the Near East alkali flux tradition.

For the alkali lead glazes and alkali glazes, the overall characteristic is sodium dominated, although the absolute soda values are in part surprisingly low. Samples from Bukhara, Takht-i-Suleiman and the Turkish localities have the highest, but still moderate Na_2O values up to 15 wt%, compared to other analyses from e.g. India (Gill & Rehren, 2011).

The source of the alkali flux is either mineral natron or plant ash. The source can be determined regarding the MgO values, limited to 1.3 wt% in mineral natron and exceeding 2.0 wt% in the case of plant ashes. In the samples of the present study, the K_2O component is not suitable for the indication of the flux-relevant alkali source due to its broad scattering. The P_2O_5 contents are also enhanced in the plant ash compositions but the data set is not sufficient for statistical evaluation. An influence of the ceramic body on the glaze composition is observed only for SiO_2, Al_2O_3, and K_2O in quartz frit ceramics with slight K-feldspar content.

The earliest Uzbek tableware glazes from the 10th-11th century (Seljuq period) were generally produced using a lead flux. The same applies to part of the Uzbek tile glazes which were produced between the 13th and 16th century. In Iran, glazes from the 12th century (Khwarezmid period) are lead glazes, but also alkali-fluxed glazes with mineral natron characteristics can be found. Although the production of lead-rich glazes was established from the 8th-9th century on in Iraq, Syria, and Egypt (Henshaw, 2010; Tite *et al.*, 2011), alkali glazes are found in almost all regions except of Bulgaria and Morocco.

Plant ash-fluxed alkali glazes are found in 13th century glazes from Takht-i-Suleiman. The plant ash flux technology is assumed to be continuously used in Mesopotamia, Iran, and Central Asia (Sayre & Smith, 1974; Henderson, 2009), but it could be shown that a parallel use of mineral natron parallel existed in the alkali glaze production from the 12th-15th century from Uzbekistan to Afghanistan. Mineral natron characteristics are also reported by Mason (2004) for Syrian and Iranian alkali glazes on lustre ware of the 8th-14th century. Tile glazes with partly mineral natron compositions are found in the Mughal architectural glazes from the 14th- 17th century from India (Gill *et al.*, 2014).

Alkali and alkali lead tile glazes from Samarkand from the 13th century (Mongolian period) have mineral natron flux characteristics, but samples from the 15th century (Timurid period) show plant ash signature. Alkali fluxed Uzbek glazes from Bukhara from the 16th century (Sheibanid dynasty) are also made by plant ash flux and are subdivided into two groups with high and low sodium oxide content. The Afghan alkali glazes have sodium oxide contents similar to the sodium-poor Uzbek subgroup, which points to a possible exchange of glaze makers or glaze making technology from Uzbekistan and Afghanistan in the 15th-17th century. Regarding the extensive exchange of Timurid craftsmen in Central Asia, this option seems to be even more likely (Golombek, 1996). One sample from the 15th century from Afghanistan with mineral natron reveals that this material was parallel used in these centuries.

Concerning the colouring of the glazes, it has to be distinguished between pigments and colouring ions which are incorporated in the glassy matrix. The colouring agents for translucent glazes are cations of various transition metals. As ions, Co^{2+} (blue), Cu^{2+} (green in a lead rich matrix), Fe^{3+} (brown/black), Mn^{4+} (brown/black) and Mn^{3+} (violet) are determined by EPMA. For opaque yellow, white, and turquoise glazes, different pigments were used. The crystalline pigments are investigated by a μ-XRD[2] device with the result of SnO_2, SiO_2, and $PbSiO_4$ as whitening agents. $PbSiO_4$ and $Pb_2Sn_2O_6$ are found in the yellow glaze, from which only the lead tin oxide causes the yellow colour. In the black glazes, different Cr-rich pigments, Cu-Cr-Mn-oxides and iron containing clinopyroxenes are found, even in samples of the same period and region. Cr-rich particles are also detected in two turquoise Afghan glazes from the 15th and 16th century. The use of the ions of Fe, Cu, Co, Cr, and Mn seems to be widely common in the Islamic glazes and corresponds to the described colouring agents in e.g. the study of Tite (2011). The use of opacifying SnO_2 particles is widespread as it is reported from different Islamic glazes from Iraq, Iran, Egypt, and Syria (Henshaw, 2010; O´Kane, 2011; Tite, 2011). The colouring agents are known already from former, e.g. Egyptian, Roman and pre-islamic periods, but especially SnO_2 pigments became increasingly widespread in the Islamic glazing tradition. The use of yellow and black pigments instead varies already within the buildings from Bukhara from Cr crystals and clino-pyroxenes in the mosque Khoja Zainuddin to a Cu-Cr-Mn-oxide in the madrassa Mir-i Arab of the same epoch.

Regarding the matrix compositions connected with the colouring, a certain assignment within the different locations and epochs can be seen. It is noticeable that e.g. the content of lead in turquoise glazes in Uzbekistan is in the range of 0.0-9.2 wt% Pb, whereas blue glazes are mostly alkali ones with PbO contents <2.0 wt%. The turquoise glazes show, that this restriction is not influenced by any defaults of availability and processability. The assumption of common addition of lead and tin to the glaze, which is already described for Iranian glazes of the 13th century (Allan *et al.*, 1973) cannot be confirmed by correlations of tin and lead oxide in the compositions.

11.2 Portable XRF measurement

With the p-XRF, semi-quantitative information about the major element compositions is generated. The depth of the detectable signals depends on the analysed sample setup. The p-XRF data are collected with the XL3 Hybrid device of the company *Analyticon Instruments*. In the

comparison of p-XRF results of the "mining" program from Uzbek glazes with EPMA results, the same major composition groups can be distinguished. The Moroccan glazes, all lead rich, are measured with the "mining" as well as with the "soil" program, revealing a better performance in the "mining" measurements. The deviations are nevertheless high, because of the high lead contents, which make the calculation of matrix correction difficult.

The measurement of the colouring oxides MnO_2, CoO, and CuO is satisfying with the internal calibration of the device and even improved with the "mining" program measurement, if compared to the results of the "soil" program. The measurements of glaze imitations lead to better results than that of bulk glass. This can be attributed to the smoother surface texture.

In spite of the accuracy limits in the measurements of particular elements in glazes, the classification of flux composition into three groups could be confirmed with the p-XRF analysis. The measurement precision is therefore sufficient for the semi-quantitative analysis of the flux characteristic of glazes. Especially for the on-site measurement of large sample quantities on historical buildings, the device is a suitable tool.

11.3 Restoration material

The ORMOCER® fulfils the requirements of stability, reversibility, and transparency, which are imposed to a modern restoration material. As pigments, historically coloured glass, cobalt blue, Egyptian blue, lead tin yellow, manganese violet, iron oxide, copper oxide, and cassiterite were used. The metal compounds have higher colour intensities than the pigments of coloured glass. It has to be considered that the proportion of ORMOCER® in the batch must be high enough (70 vol%) to guarantee the ORMOCER® properties of weathering and mechanical stability. The adhesion properties of the ORMOCER® and the homogeneity of the mixture are the best in a fraction of max. 30 vol% particles per ORMOCER®.

With integrated particles, the ORMOCER® G materials show homogeneous coatings, whereas the particles in the ORMCOER® E show more agglomeration. In the sedimentation and weathering experiments, the use of an ultrasonic finger in combination with a roller mill is favourable compared to the treatment with bead grinding mill. The treatments with ultrasonic finger and roller mill result in less sedimentation and better adhesion of the dispersions. The treatment of the dispersions in the bead grinding mill does not result in sufficient adhesion,

certainly due to the sedimentation behaviour and a congregation of particles on the bottom of the coating.

The modification of dispersed nano-particles by 3-methacryl-oxypropyltrimethoxysilan leads to a further homogenization in the sedimentation tests. It is therefore approved for the use in coloured glaze supplements. In weathered coatings of nano-particle compounds, the surface modification shows certainly no enhancement of stability.

The treatment of pigmented coatings with an additional layer of pure ORMOCER® results in a bright and transparent appearing, which is closer to the original optical appearance of the glaze. A long-time test application on a historical building will be the next step to validate the suitability of the restoration material.

11.4 Outlook

The investigation of main element composition allows some assumptions of raw materials choice and raw materials origins. Especially in the case of cobalt or manganese, the number of known deposits in the historical periods is limited. Nevertheless, it would be highly interesting to compare more data of trace elements and isotope ratios in order to allocate the raw materials to known deposits. For example the amount of Sr in the glaze compositions can give hints to the origin of the Ca component in the sand, in the cases where sand is assumed as silica source. Enhanced Sr contents together with enhanced ratios of $^{87}Sr/^{86}Sr$, point to an input of shells, as it is the case in coastal sands (Freestone, 2006).

The Na_2O/K_2O ratio should be also further investigated, concerning the potential sources of mineral natron. The high K_2O values in some Uzbek, Afghan, and Iranian glazes, which exceed 2.0 wt% K_2O, could be explained with particular K-rich salts of lakes or deposits. More information about salt composition of different relevant salt lakes would help to assign the glaze raw materials.

The few cases of high alumina glazes in Afghan and Uzbek glazes with mineral natron and plant ash characteristic could not be definitely assigned to a related culture or to a certain alkali source. Assuming, that the influence Al diffusion from ceramic body does is not solely responsible for amount of 8-13 wt% Al_2O_3, the similarity to Indian tile glazes of the Mughal architecture (Gill *et al.*, 2014) should be followed. A larger data set of Afghan and Uzbek tableware and tile glazes from the medieval and early modern period would be helpful here.

Another point of interest is the mineral natron composition of the Central Asian glazes, particularly the Iranian, some Uzbek, and one Afghan glaze. The use of mineral natron stands in contrast to the continuously plant ash based glass production of medieval Central Asia and is observed only in a few other glaze findings. A broader sampling and an investigation of possible mineral natron deposits in Central Asia would lead to a deeper understanding.

In the examination of colouring agents it has to be admitted that in the cases of different possible oxidation states, the measurements of EPMA are not sufficient to determine the exact valence of the colouring ions. In some cases such as Cu^{2+} and Cu^{1+}, the differentiation can be simply made according to the visible colour of the glaze. In the case of Fe-ion instead, the states of Fe^{2+} and Fe^{3+} can be present at the same time and only the dominating oxidation state is decisive for the glaze colour. As a further example, the upper, copper-containing layer of the red Iranian glaze from Takht-i-Suleiman should be investigated concerning the oxidation states of the metal ions. Here, e.g. investigations with photoemission spectroscopy (PES) could illuminate further the colouring effect and the intentional application of reducing and oxidizing firing conditions. Furthermore, possible traces of sulphur atoms in oxygen positions in the matrix should be investigated, examining the yellow colour of iron-rich glazes. The substitution of the bridging oxygens by several hundred ppm of sulphur already shifts the transmission of Fe^{3+} to an amber yellow colour but is difficult to prove.

The method of portable XRF is shown to be suitable for semi-quantitative analysis of large scales of samples on site. The limitations of measurement precision are primarily in the combination of light and heavy elements in considerable amounts in one composition. More knowledge about the intern calibration and matrix correction process could deliver more precise explanations for the feasibility and limitations in the semi quantitative analysis.

The investigations of colouring the ORMOCER® as a restoration material show the good performance of the material composition, when the particle amount does not exceed a certain limit of volume fraction. A stable, adhering coating with historically based pigments could be developed for future glaze restorations. The material is ready for a test application on a historical site and can be easily produced with commercially available inorganic pigments and ORMOCER® G material from the Fraunhofer Institute for Silicate Research. The contact and cooperation with a north Indian restoration project for buildings in Orchha, Pradesh is already appointed but has to await the administrical process. There are good reasons to be optimistic that the very good suitability of the material can be demonstrated on original historical objects.

List of symbols and abbreviations

Symbol/Abbreviation	Unit	Explanation
χ		electronegativity
T_g	°C	glass transition point
T_m	°C	melting point
C	g/mol	concentration
η	P	viscosity
ORMOCER®		ORganically MOdified CERamic
TFP-TMOS		3,3,3-trifluoropropyltrimethoxysilane
MEMO		3-Methacryloxypropyltrimethoxysilan
d		lattice distance
θ	°	angle of X-ray incidence in XRD measurement
rpm		Rotations per minute
RH	%	Relative humidity
ε	L/mol*cm	Molar extinction coefficient

List of figures

List of tables

Literature

Abd-Allah, R. (2009). Solarization behaviour of manganese-containing glass: an experimental and analytical study. *Mediterranean Archaeology and Archaeometry,* **9**, 37-53.

Abdurazakov, A. A. (2009). *Central Asian Glassmaking During the Ancient and Medieval Periods*. In G. Fuxi, R. Brill, & T. Shouyun Eds., *Ancient Glass Research along the Silk Road*. Singapore, World Scientific Publishing Company, Incorporated, **1**.

Abri, M., & Wallasch, S. (2008). Die Medrese Abdul Aziz Khan. *Projekte.* 2008: http://www.abriundraabe.de/node/55

Achaari, M. (2010). Monuments, sites et zones classés "patrimoine national" *Sites et Monuments classés* 2010: http://www.minculture.gov.ma/fr/index.php

Adas, M. (2001). *Agricultural and Pastoral Societies in Ancient and Classical History*, Philadelphia, Pennsylvania, Temple University Press, 363.

Agency, U. S. E. P. (2006). XRF Technologies for measuring trace elements in soil and sediment. *Innovative technology verification report,* **540**, 1-204.

Akyuz, S., Akyuz, T., Mukhamedshina, N. M., Mirsagatova, A. A., Basaran, S., & Banu, C. (2012). Characterization of ancient glass excavated in Enez (Ancient Ainos) Turkey by combined Instrumental Neutron Activation Analysis and Fourier Transform Infrared spectrometry techniques. *Spectrochimica Acta Part B: Atomic Spectroscopy,* **71/72**, 75-79.

Al-Saad, Z. (2002). Chemical Composition and Manufacturing Technology of a Collection of Various Types of Islamic Glazes Excavated from Jordan. *Journal of Archaeological Science,* **29**, 803-810.

Allan, J. W., d´Errico, E., Kondratenko, V., Moghaddarn, F. T., Porter, Y., & Rakhimov, A. (2000). The blue of Samarkand. *Proceedings of the international symposium on revitaleation of traditional ceramic techniques in central asia,* **2**, 11-14.

Allan, J. W., Llewllin, L. R., & Schweizer, F. (1973). The history of so-called egyptian faience in islamic persia: Investigations into Abu'l-Qasim's Treatise on Ceramics. *Archaeometry,* **15**, 165-173.

Althues, H., Henle, J., & Kaskel, S. (2007). Functional inorganic nanofillers for transparent polymers. *Chemical Society Reviews,* **36**, 1454-1465.

Angell, C. A., Ngai, K. L., McKenna, G. B., McMillan, P. F., & Martin, S. W. (2000). Relaxation in glassforming liquids and amorphous solids. *Journal of Applied Physics,* **88**, 3113-3157.

Anslyn, E. V., & Dougherty, D. A. (2006). *Modern physical organic chemistry*, Texas, Austin, University Science Books, 1104.

Arjomand, S. A. (1999). The Law, Agency, and Policy in Medieval Islamic Society: Development of the Institutions of Learning from the Tenth to the Fifteenth Century. *Comparative Studies in Society and History,* **41**, 263-293.

Armbruster, D. A., & Pry, T. (2008). Limit of blank, limit of detection and limit of quantitation. *Clin Biochem Rev,* **29**, 49-52.

Atkins, P. W., & Friedman, R. (2011). *Molecular quantum mechanics*, Oxford, Oxford university press, 560.

Attin, T., Buchalla, W., Kielbassa, A., & Helwig, E. (1995). Curing shrinkage and volumetric changes of resin-modified glass ionomer restorative materials. *Dent. Matter,* **11**, 359-362.

Avramov, I., & Milchev, A. (1988). Effect of disorder on diffusion and viscosity in condensed systems. *Journal of Non-Crystalline Solids,* **104**, 253-260.

Bacon, F. (1968). The chemical durability of silicate glass. *Glass Ind,* **49**, 554-559.

Badr, J., Drewello, R., Huck-Stiasny, C., & Schuessler, U. (2010). Materialwissenschaftliche Untersuchung des Fliesendekors an der Moschee Khoja Zainuddin in Buchara (Usbekistan). *Metalla, Archäometrie und Denkmalpflege,* **3**, 172-174.

Bamford, C. R. (1977). *Colour generation and control in glass*, New York, Elsevier, **2**.

Barkoudah, Y., & Henderson, J. (2006). Plant ashes from Syria and the manufacture of ancient glass: ethnographic and scientific aspects. *Journal of Glass Studies,* **48**, 297-321.

Bernar, M. D., & Martín, M. d. M. M. (1987). Materiales hispano musulmanes del" Cerro del Castellón"(Vélez Rubio-Almería). *Revista velezana,* **6**, 101-132.

Berthold, C., Bjeoumikhov, A., & Brügemann, L. (2009). Fast XRD^2 Microdiffraction with Focusing X-Ray Microlenses. *Particle and Particle Systems Characterisszation* **26**, 107-111.

Beşer, E. (2009). *Archaeometrical Investigation of Some Medieval Glass Samples from Alanya Region.* (PhD), Orta Doğu Teknik Üniversitesi, Ankara, Turkey.

Bezborodov, M. A. (1975). *Chemie und Technologie der antiken und mittelalterlichen Gläser*, W. B. (1975) Ed., Mainz, Philipp von Zabern Verlag, 327.

Bezborodov, M. A., & Zadneprovskii, Y. A. (1967). Ancient and medieval glass of Central Asia. *Archaeological Chemistry*, 29-57.

Bosworth, C. E. (2004). *The New Islamic Dynasties: A Chronological and Genealogical Manual*, Edinburgh Edinburgh University Press, 263.

Bottinga, Y., & Weill, D. F. (1972). The viscosity of magmatic silicate liquids; a model calculation. *American Journal of Science,* **272**, 438-475.

Bowley, H. J., Gardiner, D. J., Gerrard, D. L., Turrell, G., Louden, J. D., & Graves, P. R. (1989). *Practical Raman Spectroscopy*, Heidelberg, Springer-Verlag, 157.

Bradford, E. (1971). *Colour index international*, S. o. D. a. Colourists Ed., American Association of Textile Chemists and Colorists.

Bragg, W. H., & Bragg, W. L. (1915). *X rays and crystal structure*, Bell.

Brandi, C., Schädler-Saub, U., & Jakobs, D. (2006). *Theorie der Restaurierung*, International Council on Monuments and Sites, 213.

Bray, L. (2009). Bauxite and alumina. *Mining Engineering,* **62**, 40-41.

Brill, R. H. (1999). *Chemical Analyses of Early Glasses*, T. C. M. o. Glass Ed., New York, The Corning Museum of Glass, **2**, 553.

Brill, R. H. (1999). *Chemical Analyses of Early Glasses*, T. C. M. o. Glass Ed., New York, The Corning Museum of Glass, **1**, 335.

Brinker, C. J., & Scherer, G. W. (1990). *Sol-gel Science: The Physics and Chemistry of Sol-gel Processing*, London, UK, Academic Press, 912.

Brow, R. K. (2004). Structural Theories of Glass Formation. *CER103.* 2004: www.umr.edu/~brow/index.html

Bukharaev, R. (2000). *Islam in Russia: The Four Seasons*, London, UK, St. Martin's Press, 334.

Caiger-Smith, A. (1991). *Lustre Pottery: Technique, Tradition and Innovation in Islam and the Western World*, London, UK, Herbert Press, 246.

Campbell, M. (1983). *An introduction to medieval enamels*, Gilsum, NH, Stemmer House, 48.

Casellato, U., Fenzi, F., Riccardi, M. P., Rossi Osmida, G., & Vigato, P. A. (2007). Physico-chemical and mineralogical study of ceramic findings from Mary City–Turkmenistan. *Journal of Cultural Heritage,* **8**, 412-422.

Cassius, A. (1685). *De Extremo Illo Et Perfectissimo Naturae Opificio Ac Principe Terraenorum Sidere Auro; De admiranda eius natura, generatione, affectionibus, effectis, atque ad operationes artis habitudine*, Georgius Wolffus, 164.

Chapoulie, R., Déléry, C., Daniel, F., & Vendrell-saz, M. (2005). Cuerda seca ceramics from al-andalus, islamic spain and portugal (10th− 12th centuries ad): Investigation with sem–edx and cathodoluminescence. *Archaeometry,* **47**, 519-534.

Chase, W. T. (1971). Egyptian blue as a pigment and ceramic material. *Science and archaeology, Cambridge, Mass*, 80-90.

Clemens, S. (2002). Understanding engineering plant metal accumulation. *Trends in plant science,* **7**, 309-315.

Coentro, S., Trindade, R. A. A., Mirão, J., Candeias, A., Alves, L. C., Silva, R. M. C., & Muralha, V. S. F. (2014). Hispano-Moresque ceramic tiles from the Monastery of Santa Clara-a-Velha (Coimbra, Portugal). *Journal of Archaeological Science,* **41**, 21-28.

Colomban, P. (2013). *The Destructive/Non-Destructive Identification of Enameled Pottery, Glass Artifacts and Associated Pigments—A Brief Overview.* Paper presented at the Arts, 77-110.

Colomban, P., Tournié, A., Caggiani, M. C., & Paris, C. (2012). Pigments and enamelling/gilding technology of Mamluk mosque lamps and bottle. *Journal of Raman Spectroscopy,* **43**, 1975-1984.

Colomban, P., Tournié, A., M.C., C., & Paris, C. (2011). Pigments and enamelling_gilding technology of Mamluk mosque lamps and bottle. *Journal of Raman Spectroscopy,* **43**, 1975-1984.

Conradt, R. (2011). Chemische beständigkeit - eine Einführung. https://www.yumpu.com/de/document/view/21550054/chemische-bestandigkeit-eine-einfuhrung-r-conradt-der-ghi/7

Conradt, R. (2011). Glass Chemistry. Chemical Bonds. Short-Range Order Structure Composition-Property Relations Chapter 2. *Feuerfestkolloquium.* 2011: Aachen

Conradt, R. (2012). *Werkstoff Glas Glastechnik.* München, Deutsches Museum, 80-98.

D'Amour, M., & Bélanger, D. (2003). Stability of substituted phenyl groups electrochemically grafted at carbon electrode surface. *The Journal of Physical Chemistry B,* **107**, 4811-4817.

Davison, S., & Newton, R. G. (2008). *Conservation and Restoration of Glass*, Oxford, UK, Taylor & Francis, 392.

Debenedetti, P. G., & Stillinger, F. H. (2001). Supercooled liquids and the glass transition. *Nature,* **410**, 259-267.

Debevoise, N. C. (1934). *Parthian pottery from Seleucia on the Tigris*, Michigan, US, **32**, 132.

Declerck, P. (2010). *Synthesis and technological processing of hybrid organic-inorganic materials for photonic applications.* (PhD), Julius Maximilian University Würzburg, Würzburg, Germany.

Doménech-Carbó, M. T., Doménech-Carbó, A., Yusá-Marco, D. J., & Ahmadi, H. (2008). Characterization of Iranian Moarraque glazes by light microscopy, SEM-EDX and voltammetry of microparticles. *Journal of Cultural Heritage,* **9**, e50-e54.

Dussubieux, L., Gratuze, B., & Blet-Lemarquand, M. (2010). Mineral soda alumina glass: occurence and meaning. *Journal of Archaeological Science,* **37**, 1646-1655.

Duve, M., & Schmottlach, A. (2012). Leistungsverzeichnis Fluoreszenzanalyse. Retrieved 23.07.2105, 2015: http://indikator-labor.de, Wuppertal

Eastaugh, N. (2004). *The Pigment Compendium: A Dictionary of Historical Pigments*, Routledge Chapman & Hall.

Eastaugh, N., Walsh, V., Chaplin, T., & Sidall, R. (2004). *Pigment Compendium: A Dictionary of Historical Pigments: A Dictionary of Historical Pigments*, Elsevier Science, **1**, 512.

Eshel, G., Levy, G., Mingelgrin, U., & Singer, M. (2004). Critical evaluation of the use of laser diffraction for particle-size distribution analysis. *Soil Science Society of America Journal,* **68**, 736-743.

Fehervari, G. (2000). *Ceramics of the Islamic World in the Tarec Rajab museum*, I.B.Tauris, 448.

Fehervari, G. (2012). The Lajvardina technique. *Overglaze-Painted* http://www.trmkt.com/ogpaint.html#laj

Fernández, A. L., & Pablo, L. d. (2002). Formation and the colour development in cobalt spinel pigments. *Pigment & Resin Technology,* **31**, 350-356.

Figueiredo, M. O., Silva, T. P., & Veiga, J. P. (2009). Ancient glazed ceramic tiles: a long-term, study from the remediation of environmental impacts to the non-destructive characterization of materials.

Fisher, T. S. (2014). *X-Ray Fluorescence*. Elemental analysis. http://www.thermoscientific.de/eThermo/CMA/Images/Various/151Image_15772.gif.

Fjellvåg, H., & Kjekshus, A. (2001). Orbital Ordering. *Theoretical Acitivity in Solid stata Chemistry and Material Science.* 2015: http://folk.uio.no/ravi/activity/ordering/orbitalordering.html

Fluegel, A. (2007). Glass viscosity calculation based on a global statistical modelling approach. *Glass Technology-European Journal of Glass Science and Technology Part A,* **48**, 13-30.

Fluegel, A. (2007). Global Model for Calculating Room-Temperature Glass Density from the Composition. *Journal of the American Ceramic Society,* **90**, 2622-2625.

Fluegel, A. (2007). Global Model for Calculating Room-Temperature Glass Density from the Composition. *Journal of the American Ceramic Society,* **90**, 2622-2625.

Fragner, B. G. (2007). Hochkulturen und Steppenreiche Der Kulturraum Zentralasien. *Osteuropa -Stuttgart- deutsche Verlagsanstalt,* **57**, 27-52

Freestone, I. (2006). *Glass production in Late Antiquity and the Early Islamic period: a geochemical perspective Geomaterials in Cultural Heritage.* Florence, Italy, The Geological Society: London, UK, 201-216.

Freestone, I., Meeks, N., Sax, M., & Higgitt, C. (2007). The Lycurgus cup—a roman nanotechnology. *Gold Bulletin,* **40**, 270-277.

Freestone, I. C. (1987). *Composition and microstructure of early opaque red glass Early vitreous materials*, British Museum, 173-191.

Freestone, I. C. (1991). Technical Examination of Neo-Assyrian Glazed Wall Plaques. *Iraq,* **53**, 55-58.

Frost, R. L., Ding, Z., Kloprogge, J. T., & Matrtens, W. N. (2002). Thermal stability of azurite and malachite in relation to the formation of mediaeval glass and glazes>. *Thermochimia Acta,* **390**, 133-144.

Furmanek, P. (2006). Dokumentation Lüneburg am Sande 1 +2, 35 Terrakottamedaillons 55

Garner, J. (2011). *Pre-Islamic tin mining in Central Asia* (PhD), TU Bergakademie Freiberg, Bochum.

Gellermann, C., Ballweg, T., & Wolter, H. (2007). Herstellung von funktionalisierten oxidischen Nano- und Mikropartikeln und deren Verwendung. *Chemie Ingenieur Technik,* **79**, 233-240.

Gerward, L. (1993). X-ray attenuation coefficients: Current state of knowledge and availability. *Radiation Physics and Chemistry,* **41**, 783-789.

Ghoneim, N. A., & El Badry, K. (1983). Thermal expansion of high lead silicate glasses in relation to structure. *Thermochimica Acta,* **60**, 253-263.

Gianoncelli, A., & Kourousias, G. (2007). Limitations of portable XRF implementations in evaluating depth information: an archaeometric perspective. *Applied Physics A,* **89**, 857-863.

Gill, M., Rehren, T., & Freestone, I. (2014). Tradition and indigeneity in Mughal architectural glazed tiles. *Journal of Archaeological Science,* **49**, 546-555.

Gill, M. S., & Rehren, T. (2011). Material Characterization of Ceramic Tile Mosaic from Two 17th-Century Islamic Monuments in Northern India. *Archaeometry,* **53**, 22-36.

Golombek, L. (1996). Timurid potters abroad. *Oriente moderno,* **15**, 577-586.

Gradmann, R., Badr, J., & Schüssler, U. (2012). *Charac-iszation of glazed tiles with EPMA and mobile XRF for the development of adapted conservation materials.* Paper presented at the 39th International Symposium on Archaeometry: "50 years of ISA", Leuven, Belgium, 208-214.

Grazhdankina, N. S., Rakhimov, M. K., & Pletnev, I. E. (2006). Architectural ceramics of uzbekistan. 142

Green, L. R., & Hart, F. A. (1987). Colour and Chemical Composition in Ancient Glass: An examination of some Roman and Wealden Glass by means of Ultraviolet-Visible-Infrared Spectrometry and Electron Microprobe analyses. *Journal of Archaeological Science,* **14**, 271-282.

Grousset, R. (1970). *The Empire of the Steppes: A History of Central Asia*, New Brunswick, NJ, Rutgers University Press, 718.

Guilherme, A., Manso, M., Pessanha, S., Zegzouti, A., Elaatmani, M., Bendaoud, R., . . . Carvalho, M. L. (2013). Micro-XRF for characterization of Moroccan glazed ceramics and Portuguese tiles. *Journal of Instrumentation,* **8**, C02055-C02055.

Gulzar, S., Wörle, M., Burg, J.-P., Chaudhry, M. N., Joseph, E., & Reusser, E. (2013). Characterization of 17th Century Mughal tile glazes from Shahdara Complex, Lahore-Pakistan. *Journal of Cultural Heritage,* **14**, 174-179.

Haas, K. H., Amberg-Schwab, S., & Rose, K. (1999). Functionalized coating materials based on inorganic-organic polymers. *Thin Solid Films,* **351**, 198-203.

Hall, A. W., Godber, M. J., Blackwood, K. M., Milne, P. E., & Goodby, J. W. (2004). The photoinitiated cyclopolymerization of dienes in the creation of novel polymeric systems and three-dimensional networks. *Journal of Materials Chemistry,* **14**, 2593-2602.

Hallett, J. R., Thompson, M., Keall, E. J., & Mason, R. B. (1988). Archaeometry of medieval Islamic glazed ceramics from North Yemen. *Canadian Journal of Chemistry,* **66**, 266-272.

Hamer, F., & Hamer, J. (2004). *The Potter's Dictionary of Materials and Techniques*, A & C Black, 375 ff.

Han, X. Y., Zhuo, S. J., Shen, R. X., Wang, P. L., & Ji, A. (2006). Comparison of the quantitative results corrected by fundamental parameter method and difference calibration specimens in X-ray fluorescence spectrometry. *Journal of Quantitative Spectroscopy and Radiative Transfer,* **97**, 68-74.

Hansen, T. (2008). Ceramic Stains. *Stain.* 2008: http://digitalfire.com/4sight/material/stain_2451.html

Heck, M. (2000). *Chemisch-analytische Untersuchungen an frühmittelalterlichen Glasperlen.* (PhD), TU Darmstadt, Darmstadt.

Heide, K., Hartmann, E., Gert, K., & Wiedemann, H. G. (2000). MS-TGA of ancient glasses: an attempt to determine the manufacturing conditions. *Thermochimia Acta,* **365**, 147-156.

Henderson, J. (1985). The Raw Materials of Early Glass Production. *Oxford Journal of Archaeology,* **4**, 267-291.

Henderson, J. (2004). Radical changes in Islamic glass technology: evidence for conservatism and experimentation with new glass recipes from early and middle islamic raqqa, syria. *Archaeometry,* **46**, 439-468.

Henderson, J. (2013). *Ancient Glass: An Interdisciplinary Exploration*, Cambridge, UK, Cambridge University Press, 450.

Henshaw, C., Rehren, T., Papachristou, O., & Anarbaev, A. A. (2007). Lead-glazed slipware of 10th-11th century akshiket, Uzbekistan. *BAR International Series,* **8**, 145-148.

Henshaw, C. M. (2010). *Early islamic ceramics and glazes of Akhsiket, Uzbekistan.* (PhD), University College London, London, UK.

Herron, M. M. (1988). Geochemical classification of terrigenous sands and shales from core or log data. *Journal of Sedimentary Research,* **58**, 820-829.

Hildburgh, W. L. (1936). *Medieval Spanish enamels and their Relation to the Origin and the Development of Copper champlevé enamels of the Twelfth and Thirteenth Centuries*, Oxford, UK, Oxford University Press, H. Milford, 146.

Hill, D. V. (2004). *The materials and technology of glazed ceramics from the deh luran plain, southwestern Iran: A study in innovation.* (PhD), University of Michigan, Michigan.

Hillenbrand, C. (2005). Ravandī, the Seljuk court at Konyaand the Persianisationof Anatolian cities. *Mesogeios (Mediterranean Studies),* **25**, 157-169.

Hinz, W. (1970). *Silikate: Grundlagen der Silikatwissenschaft und Silikattechnik. Die Silikate und ihre Untersuchungsmethoden. B. 1*, Berlin, Verlag für Bauwesen, 868.

Holakooei, P., Tisato, F., Vaccaro, C., & Petrucci, F. C. (2014). Haft rang or cuerda seca? Spectroscopic approaches to the study of overglaze polychrome tiles from seventeenth century Persia. *Journal of Archaeological Science,* **41**, 447-460.

Holleman, A. F., & Wiberg, E. (1995). *Lehrbuch der anorganischen Chemie*, Berlin, Walter de Gruyter.

Hoover, H. C. (2003). *Georgius Agricola De Re Metallica 1912*, Kessinger Publishing, **12**, 640.

Hubbell, J. H., & Seltzer, S. M. (1996). Tables of X-Ray Mass Attenuation Coefficients and Mass Energy-Absorption Coefficients from 1 keV to 20 MeV for Elements Z = 1 to 92 and 48

Additional Substances of Dosimetric Interest. *National Institute of Standards and Technology, 5632*.

Hull, D., & Clyne, T. W. (1996). *An Introduction to Composite Materials*, Cambridge, UK, Cambridge University Press, 326.

Iñañez, J. G., Speakman, R. J., Buxeda i Garrigós, J., & Glascock, M. D. (2008). Chemical characterization of majolica from 14th–18th century production centers on the Iberian Peninsula: a preliminary neutron activation study. *Journal of Archaeological Science, 35*, 425-440.

International Council on Monuments and Sites, I. (1964). Venice Charter. *Proceedings of the IInd International Congress of Architects and Technicians of Historical Monuments, 1*, 1-4.

'Izzatī, A. F., & Ezzati, A. (2002). *The Spread of Islam: The Contributing Factors*, London, UK, Saqi Books, 560.

Jak, E., Hayes, P., Degterov, S., Pelton, A., & Wu, P. (1997). Thermodynamic optimization of the systems PbO-SiO2, PbO-ZnO, ZnO-SiO2 and PbO-ZnO-SiO2. *Metallurgical and Materials Transactions B, 28*, 1011-1018.

Jones, D., & Michell, D. J. (1976). *The arts of Islam*, London, Arts Council of Great Britain, 396.

Kaczmarczyk, A., & Hedges, R. E. (1988). Ancient Egyptian faience: an analytical survey of Egyptian faience from Predynastic to Roman times. *Journal of Near Eastern Studies, 47*, 138-140

Kasch, M. (2009). *Usbekistan 2009: eine Architekturreise nach Zentralasien; Taschkent, Buchara, Samakand, Sha-ri Sabz*, Dresden, Germany, Professur für Denkmalpflege und Entwerfen, 149.

Kasemann, R., Krug, H., & Schmidt, H. K. (2010). *ORMOCERe (ORganically MOdified CERamics) als Werkstoffe in Mikrotechniken*. Paper presented at the Werkstoffe der Mikrotechnik : Basis für neue Produkte, Karlsruhe, 303-312.

Kilic, O., & Kilic, A. M. (2010). Salt crust mineralogy and geochemical evolution of the Salt Lake (Tuz Gölü), Turkey. *Scientific Research and Essays, 5*, 1317-1324.

Kleinknecht, K. (2005). *Detektoren Für Teilchenstrahlung*, Stuttgart, Germany, Teubner B.G. GmbH, 260.

Kleinmann, B. (1986). *History and development of early Islamic pottery glazes.* Paper presented at the Proceedings of the 24th international archaeometry symposium, 73-84.

Klockmann, F., Ramdohr, P., & Strunz, H. (1978). *Klockmann's Lehrbuch der Mineralogie*, Ferdinand Enke Verlag, 876.

Kreibig, U., & Vollmer, M. (1995). *Optical properties of metal clusters*, Springer, 532

Kreimeyer, R. (1987). Some notes on the firing colour of clay bricks. *Applied Clay Science, 2*, 175-183.

Kron, J., Schottner, G., & Deichmann, K.-J. (2001). Glass design via hybrid sol–gel materials. *Thin Solid Films, 392*, 236-242.

Kucuk, A., Clare, A. G., & Jones, L. (1999). An estimation of the surface tension for silicate glass melts at 1400°C using statistical analysis. *Glass Technology, 40*, 149-153.

Kühn, H. (1968). Lead-tin yellow. *Studies in Conservation, 13*, 7-33.

Kühn, H., & Feller, R. L. (1986). Artists' Pigments: A Handbook of Their History and Characteristics. *National Gallery of Art, Washington, Cambridge University Press*, 169-186.

Lakatos, T., Johansson, L.-G., & Simmingsköld, B. (1972). The effect of some glass components on the viscosity of glass. *Glasteknisk tidskrift, 27*, 25-28.

Lamm, C. J. (1941). *Oriental glass of mediaeval date found in Sweden and the early history of lustre-painting*, Stockholm, Wahlström & Widstrand i.komm., 116.

Lane, A. (1947). *Early Islamic pottery: Mesopotamia, Egypt and Persia*, London, UK, Faber and Faber, 52.

Lapidus, I. M. (2002). *A History of Islamic Societies*, Cambridge University Press, 374.

Leißner, J., Drewello, R., & Weißmann, R. (1998). Glassmalereien mit dem Excimerlaser behandeln? Modelluntersuchungen zur Abnahme von Korrosions-krusten, organischen Polymeren und Mikroorganismen. *Restauro, 104*, 324-329

Lemke, C. (1998). Reflections of the Roman Empire: the first century glass industry as seen through traditions of manufacture. *The prehistory and history of glass and glassmaking technology*, 269-291.

Lewis, I. R., & Edwards, H. (2001). *Handbook of Raman Spectroscopy: From the Research Laboratory to the Process Line*, CRC Press, 1072.

Liem, N. Q., Sagon, G., Quang, V. X., Tan, H. V., & Colomban, P. (2000). Raman study of the microstructure, composition and processing of ancient Vietnamese (proto) porcelains and celadons (13-16th centuries). *Journal of Raman Spectroscopy, 31*, 933-942.

Lilyquist, C., & Brill, R. H. (1993). *Studies in early Egyptian glass*, New York, Metropolitan Museum of Art, New York, 80.

Lilyquist, C., Brill, R. H., & Wypyski, T. (1993). *Studies in Early Egyptian Glass*, Metropolitan Museum of Art.

Liu, S., Li, Q. H., Gan, F., Zhang, P., & Lankton, J. W. (2012). Silk Road glass in Xinjiang, China: chemical compositional analysis and interpretation using a high-resolution portable XRF spectrometer. *Journal of Archaeological Science, 39*, 2128-2142.

Liz-Marzan, L. (2007). Farbenfroh: Plasmonenschwingungen massgeschneiderter Metall-Nanopartikel in Kolloiden. *Photonik-Stuttgart, 39*, 58.

Lukens, M. G. (1965). Medieval Islamic Glass. *The Metropolitan Museum of Art Bulletin, 23*, 198-208.

MacCarthy, G. R. (1933). Calcium carbonate in beach sands. *Journal of Sedimentary Research, 3*, 64-67.

Martin, E., & Duval, A. R. (1990). Les deux variétés de jaune de plomb et d'étain: étude chronologique. *Studies in Conservation, 35*, 117-136.

Mason, R. B. (2004). Shine Like the Sun. *Bibliotheka Iranica, Islamic Art and Architecture Series, 12*, 1-142.

Mason, R. B. (2004). Shine Like the Sun. *Bibliotheka Iranica, Islamic Art and Architecture Series, 12*, 31 pp.

Mason, R. B., & Tite, M. (1997). The beginnings of tin-opacification of pottery glazes. *Archaeometry, 39*, 41-58.

Mason, R. B., Tite, M. S., Paynter, S., & Salter, C. (2001). Advances in Polychrome Ceramics in the Islamic World of the 12th Century AD. *Archaeometry, 43*, 191-209.

Masters, B. R. (2009). CV Raman and the Raman effect. *Opt. Photonics News, 20*, 41-45.

Matthes, W. E. (1990). *Keramische Glasuren: Grundlagen, Eigenschaften, Rezepte, Anwendung*, Augustus-Verlag, 499.

Mauro, J. C., Yue, Y., Ellison, A. J., Gupta, P. K., & Allan, D. C. (2009). Viscosity of glass-forming liquids. *Proceedings of the National Academy of Sciences, 106*, 19780-19784.

McCarthy, B. (1996). *Microstructural and compositional studies of the technology and durability of ceramic glazes from Nippur, Iraq, ca. 250 B.C.-1450 A.D.* (PhD), John Hopkins University, Ann Abor, USA.

McNaught, A. D., & Wilkinson, A. (1997). *Compendium of chemical terminology*, International Union of Pure and Applied Chemistry, 450.

Menzel, G. G. (2014). Microscope Slides. http://www.menzel.de/Produkte.655.0.html

Meyer, H.-P., Varychev, A., Grimm, J., & Steinmann, L. (2014). *p-ED-XRF analyses including Na and Mg of ancient glasses.* Paper presented at the 92nd Annual Meeting Deutsche Mineralogische Gesellschaft, Jena, Germany, 82.

Meyer, J. (2014). The Timurids and the Turkmen. *Central Asia, Afghanistan, and Iran, 1370-c. 1500.* 2015: http://www.davidmus.dk/en/collections/islamic/dynasties/timurids-and-turkmen

Mohr, H., & Schopfer, P. (1978). *Physiologie des Ionentransports Lehrbuch der Pflanzenphysiologie*, Springer Berlin Heidelberg, 476-479.

Molera, J., Bayés, C., Roura, P., Crespo, D., & Pradell, T. (2007). Key Parameters in the Production of Medieval Luster Colors and Shines. *Journal of the American Ceramic Society, 90*, 2245-2254.

Molera, J., Pradell, T., Salvadó, N., & Vendrell-Saz, M. (2001). Interactions between clay bodies and lead glazes. *Journal of the American Ceramic Society, 84*, 1120-1128.

Molera, J., Pradell, T., & Vendrell-Saz, M. (1998). The colours of Ca-rich ceramic pastes: origin and characterization. *Applied Clay Science, 13*, 187-202.

Moorey, P. R. S. (1999). *Ancient mesopotamian materials and industries : the archaeological evidence*, New York Eisenbrauns, 415.

Morgan, D. (1988). *Medieval Persia, 1040-1797*, Longman, 72.

Mostafawy, S. (2007). *Islamische Keramik: aus der Sammlung des Badischen Landesmuseums Karlsruhe*, Karlsruhe, Badisches Landesmuseum Karlsruhe, 127.

Müller-Weinitschke, C. (1995). *Experimente zur Kontursicherung: verschiedene Sicherungsmaterialien im Vergleich*, Berlin, Germany Ernst, Wilhelm & Sohn, Verlag für Architektur und technische Wissenschaften GmbH, **5**, 10.

Nadali, D. (2006). Esarhaddon's glazed bricks from Nimrud: The Egyptian campaign depicted. *Iraq, 68*, 109-119.

Nassau, K. (1987). *The physics and chemistry of color: the fifteen causes of color*, Wiley, 98.

Nassau, K. (2001). *The physics and chemistry of color: the fifteen causes of color, 2nd ed*, Wiley-VCH, 496.

Naymark, A. (2006). *A Note on Sogdian Coroplastics: Two Ossuary Fragments from Afrasiab Ēran ud Anērān, Studies presented to Boris Il'ic Marsak on the occasion of his 70/th birthday*. Venice, Italy, Libreria Editrice Cafoscarina, 718.

Neri, A. (1663). *L' arte vetraria*, Florence, Italy, Batti, Apresso Giacomo, 261.

Newman, A. J. (2006). *Safavid Iran: Rebirth of a Persian Empire*, I. B. Tauris, 281.

Nicholson, P. (2010). Kilns and Firing Structures. *UCLA Encyclopedia of Egyptology*, 11.

O´Kane, B. (2011). Tiles of Many Hues - The development of iranian cuerda seca tiles and the transfer of tilework technology. *Colour in Islamic art and Architecture, 189*, 175-203.

Orfanou, V., & Rehren, T. (2015). A (not so) dangerous method: pXRF vs. EPMA-WDS analyses of copper-based artefacts. *Archaeological and Anthropological Sciences, 7*, 387-397.

Osete-Cortina, L., Doménech-Carbo, M. T., Doménech, A., Yusa-Marco, D. J., & Ahmadi, H. (2010). Multimethod analysis of Iranian Ilkhanate ceramics from the Takht-e Soleyman palace. *Anal Bioanal Chem, 397*, 319-329.

Padovani, S., Borgia, I., Brunetti, B., Sgamellotti, A., Giulivi, A., D'Acapito, F., . . . Battaglin, G. (2004). Silver and copper nanoclusters in the lustre decoration of Italian Renaissance pottery: an EXAFS study. *Journal Applied Physics A, 79*, 229-233.

Padovani, S., Sada, C., Mazzoldi, P., Brunetti, B., Borgia, I., Sgamellotti, A., . . . Battaglin, G. (2003). Copper in glazes of Renaissance luster pottery: Nanoparticles, ions, and local environment. *Journal of Applied Physics, 93*, 10058-10063.

Parmelee, C. W., & Harman, C. G. (1973). *Ceramic glazes*, Boston, US, Cahners Books, 612.

Pauling, L. (1960). *The Nature of the Chemical Bond and the Structure of Molecules and Crystals: An Introduction to Modern Structural Chemistry*, Cornell University Press, 69.

Paynter, S. (2009). *Links between glazes and glass in mid-2nd millennium BC Mesopotamia and Egypt*, na.

Paynter, S., Okyar, F., Wolf, S., & Tite, M. S. (2004). The production technology of Iznik pottery—a reassessment*. *Archaeometry, 46*, 421-437.

Pernicka, E. (1979). *Chemischer Analyse glasierter Keramik aus Carnuntum*. In Ö. A. d. Wissenschaften (Ed.), *Die Gefäßkeramik des Legionslagers von Carnuntum*. Vienna, Mathilde Grünewald, **29**, 9.

Pernicka, E., & Malissa, H. (1976). *Examination of Islamic glazes with the electron microprobe*. Paper presented at the Nature, Aim and Methods of Microchemistry; International Microchemical Symposium, 55.

Pernicka, E., Malissa, H., & Krejsa, P. (1977). Analytisch-chemische Untersuchungen an glasierter Islamischer Keramik. *Berichte der Österreichischen Studiengesellschaft für Atomenergie Ges. m. b. H., 2838*, 45

Peters, S. G. (2011). *Summary of the Daykundi Tin, Tungsten, and Lithium Area of Interest*, USGS, 294-312.

Philon, H., Walford, T. T., Stamford, V., & Benakē, M. (1980). *Early Islamic ceramics: ninth to late twelfth centuries*, Islamic Art Publications, 176-177.

Pilz, M., & Römich, H. (1997). Sol-gel derived coatings for outdoor bronze conservation. *Journal of Sol-Gel Science and Technology,* **8**, 1071-1075.

Pilz, M., & Römich, H. (1998). Germany Patent No.: F.-G. Z. F. D. A. F. E.V.

Pinder-Wilson, R. (1995). *The islamic lands and China*. In H. Tait (Ed.), *Five thousands years of glass*. London, 112-143.

Pohl, M., Hogekamp, S., Hoffmann, N. Q., & Schuchmann, H. P. (2004). Dispergieren und desagglomerieren von nanopartikeln mit ultraschall. *Chemie Ingenieur Technik,* **76**, 392-396.

Posset, U., Gigant, K., Schottner, G., Baia, L., Kiefer, W., & Popp, J. (2002). *The benefit of raman spectroscopy for the study of sol-gel-derived hybrid materials*. Paper presented at the Organic-Inorganic Hybrids, University of Surrey, Guildford, UK.

Pradell, T., Molera, J., Bayés, C., & Roura, P. (2006). Luster decoration of ceramics: mechanisms of metallic luster formation. *Applied Physics A,* **83**, 203-208.

Pradell, T., Molera, J., Salvadó, N., & Labrador, A. (2010). Synchrotron radiation micro-XRD in the study of glaze technology. *Applied Physics A,* **99**, 407-417.

Pradell, T., Molera, J., Smith, A. D., & Tite, M. S. (2008). Early Islamic lustre from Egypt, Syria and Iran (10th to 13th century AD). *Journal of Archaeological Science,* **35**, 2649-2662.

Pradell, T., Molera, J., Smith, A. D., & Tite, M. S. (2008). The invention of lustre: Iraq 9th and 10th centuries AD. *Journal of Archaeological Science,* **35**, 1201-1215.

Priven, A. (2004). General method for calculating the properties of oxide glasses and glass forming melts from their composition and temperature. *Glass Technology-European Journal of Glass Science and Technology Part A,* **45**, 244-254.

Pugachenkova, G. A., & Rtveladze, È. V. (2009). Afrāsīāb. *Encyclopædia Iranica,* **1**, 576-578.

Raman, C. V. (1928). A new radiation. *Indian Journal of physics,* **2**, 387-398.

Rasteiro, M. G., Gassman, T., Santos, R., & Antunes, E. (2007). Crystalline phase characterization of glass-ceramic glazes. *Ceramics International,* **33**, 345-354.

Rawson, H. (1967). *Inorganic glass-forming systems*, Academic Press, 317.

Reade, W., Freestone, I., & Simpson, S. J. (2005). *Innovation or continuity? Early first millennium BCE glass in the Near East: the cobalt blue glasses from Assyrian Nimrud.* Paper presented at the Annales du 16e Congres de l'Association Internationale pour l'Histoire du Verre, 23-27.

Rehren, T. (2008). A review of factors affecting the composition of early Egyptian glasses and faience: alkali and alkali earth oxides. *Journal of Archaeological Science,* **35**, 1345-1354.

Rehren, T., Connolly, P., Schibille, N., & Schwarzer, H. (2015). Changes in glass consumption in Pergamon (Turkey) from Hellenistic to late Byzantine and Islamic times. *Journal of Archaeological Science,* **55**, 266-279.

Rehren, T., Osório, A., & Anarbaev, A. (2010). *Some Notes on Early Islamic Glass in Eastern Uzbekistan*. In V. d. R.-G. Zentralmuseums (Ed.), *Glass Along the Silk Road from 200 BC to AD 1000*. Mainz, Römisch-Germanisches Zentralmuseum, **9**, 93.

Rehren, T., & Yin, M. (2012). Melt formation in lime-rich proto-porcelain glazes. *Journal of Archaeological Science,* **39**, 2969-2983.

Reimer, A., Landmann, G., & Kempe, S. (2008). Lake Van, Eastern Anatolia, Hydrochemistry and History. *Aquatic Geochemistry,* **15**, 195-222.

Renaud, K. M., Wardlaw, B. R., & Hubbard, B. E. (2015). Assessment of bauxite, clay, and laterite deposits in Afghanistan. *Open-File Report*, 49

Riegel, B., Blittersdorf, S., Kiefer, W., Hofacker, S., Müller, M., & Schottner, G. (1998). Kinetic investigations of hydrolysis and condensation of the glycidoxypropyltrimethoxysilane/aminopropyltriethoxy-silane system by means of FT-Raman spectroscopy I. *Journal of Non-Crystalline Solids,* **226**, 76-84.

Robertshaw, P., Benco, N., Wood, M., Dussubieux, L., Melchiorre, E., & Ettahiri, A. (2010). Chemical analysis of glass beads from medieval Al Basra (Morocco). *Archaeometry,* **52**, 355-379.

Ross, K. A., Arntfield, S. D., & Cenkowski, S. (2013). *A Polymer Science Approach to Physico-Chemical Characterization and Processing of Pulse Seeds*. In F. Yılmaz (Ed.), *Polymer Science*. Rijeka, Croatia, InTech, 3.

Rottländer, R. C. A. (2000). *Plinius Secundus d.Ä., Über Glas und Metalle*, Germany, Scripta Mercaturae Verlag, 407.

Rousseau, R. M. (2004). Some considerations on how to solve the Sherman equation in practice. *Spectrochimica Acta Part B: Atomic Spectroscopy, 59*, 1491-1502.

Sanders, D., & Hench, L. (1973). Mechanisms of glass corrosion. *Journal of the American Ceramic Society, 56*, 373-377.

Savory, R. (2007). *Iran Under the Safavids*, Cambridge University Press, 29.

Sayre, E. V., & Smith, A. D. (1974). Analytical Studies of Ancient Egyptian Glass. *Recent advances in the science and technology of materials, 3*, 47-70.

Schmidt, H., Mennig, M., Burkhart, T., Fink-Straube, C., Jonschker, G., Schmitt, M., & Bauer, A. (1998). Germany Patent No.: I. F. N. M. G. Gmbh.

Schmidt, H. K. (2010). Sol-Gel-Techniken für neue Materialien der Mikrotechnik.

Scholze, H. (1965). *Glas: Natur, Struktur, und Eigenschaften*, Vieweg, 370.

Seccaroni, C. (2006). *Giallorino: storia dei pigmenti gialli di natura sintetica*, Tivoli, Italy, De Luca Editori d'Arte, 399.

Sentance, B., Polledo Carreño, M., & Torreclavero. (2008). *Cerámica: sus técnicas tradicionales en todo el mundo*, San Sebastián, Nerea, 216.

Shelby, J. E. (2005). *Introduction to glass science and technology*, Cambridge, UK, Royal Society of Chemistry, 291.

Shokouhi, F., Oliaiy, P., Rahighi, J., Lamehi-Rachti, M., Roohfar, Z., & Durali, S. (2002). Elemental Analysis of Ancient Iranian Luster Decorated Pottery. *International Journal of PIXE, 12*, 253-258.

Shortland, A., & Eremin, K. (2006). The analysis of second millennium glass from Egypt and Mesopotamia Part1: New WDS Analyses. *Archaeometry, 48*, 581-603.

Shortland, A., & Tite, M. (2000). Raw materials of glass from amarna and Implications for the origin of egyptian glass.pdf>. *Archaeometry, 42*, 141-151.

Shortland, A. J. (2004). Evaporites of the Wadi el Natrun. *Archaeometry, 46*, 497-516.

Shortland, A. J., Schachner, L., Freestone, I., & Tite, M. S. (2006). Natron as a flux in the early vitreous materials industry: sources, beginnings and reasons for decline. *Journal of Archaeological Science, 33*, 521-530.

Shugar, A., & Rehren, T. (2002). Formation and composition of glass as a function of firing temperature. *Glass Technology C, 43*, 145-150.

Simsek, G., Colomban, P., & Milande, V. (2010). Tentative differentiation between Iznik tiles and copies with Raman spectroscopy using both laboratory and portable instruments. *Journal of Raman Spectroscopy, 41*, 529-536.

Skoog, D. A., & West, D. M. (1992). *Principles of instrumental analysis*, Bel Air, CA, Saunders College Philadelphia, 700.

Smart, R. M., & Glasser, F. P. (1974). Compound Formation and Phase Equilibria in the System PbO-SiO2. *Journal of the American Ceramic Society, 57*, 378-382.

Sparavigna, A. C. (2012). Faience: the ceramic technology of ancient Egypt. *ARCHAEOGATE, 12*.

Spuler, B., & Marcinkowski, M. I. (2003). *Persian historiography and geography: Bertold Spuler on major works produced in Iran, the Caucasus, Central Asia, India, and early Ottoman Turkey*, Singapore, Pustaka Nasional Pte Ltd, 96.

Stilgebauer, J. (1996). *Kolloide, Anorganischer Experimentalvortrag*. Chemie in der Schule. http://chids.online.uni-marburg.de/dachs/expvortr/562.pdf.

Streppel, U. (2005). *Selbstorganisierte Strukturbildung in UV sensitiven optischen Polymeren.* (PhD), Friedrich Schiller Universität Jena, Jena, Germany.

Tanimoto, S., & Rehren, T. (2008). Interactions between silicate and salt melts in LBA glassmaking. *Journal of Archaeological Science, 35*, 2566-2573.

Thein, J. (1990). Paleogeography and Geochemistry of the "Cenomano-Turonian" Formations in the Manganese District of Imini (Morocco) and their Relation to Ore Deposition. *Ore Geology Reviews, 5*, 257-291.

Thiemsorn, W., Keowkamnerd, K., Phanichphant, S., & Hessenkemper, H. (2006). *Effects of glass structure on the optical absorption of transition ions in industrial soda-lime-silica glasses (session: Glass).* Paper presented at the Asian Symposium on Materials and Processing, 19.

Tholey, M. J., Berthold, C., Swain, M. V., & Thiel, N. (2010). XRD2 micro-diffraction analysis of the interface between Y-TZP and veneering porcelain: Role of application methods. *Dental Materials, 26*, 545-552.

Thompson, A. C., & Vaughan, D. (2001). *X-ray data booklet*, Berkeley, US, University of Berkeley, 457.

Thomson, G. (1986). *The Museum Environment*, Oxford, UK, Butterworth Heinemann, 293.

Tite, M. S. (2002). Invasive Sampling versus Object Integrity: A Final Response. *Papers from the Institute of Archaeology*.

Tite, M. S. (2008). Ceramic Production, Provenance and Use—a Review. *Archaeometry, 50*, 216-231.

Tite, M. S. (2011). The Technology of Glazed Islamic Ceramics Using Data Collected by the Late Alexander Kaczmarczyk. *Archaeometry, 53*, 329-339.

Tite, M. S., & Bimson, M. (1986). Faience: an investigation of the microstructures associated with the different methods of glazing. *Archaeometry, 28*, 69-78.

Tite, M. S., Freestone, I., Mason, R., Molera, J., Vendrell-Saz, M., & Wood, N. (1998). Lead glazes in antiquity - methods of production and reasons for use. *Archaeometry, 40*, 241.

Tite, M. S., Shortland, A., Maniatis, Y., Kavoussanaki, D., & Harris, S. A. (2006). The composition of the soda-rich and mixed alkali plant ashes used in the production of glass. *Journal of Archaeological Science, 33*, 1284-1292.

Tite, M. S., & Shortland, A. J. (2003). Production technology for copper- and cobalt blue vitreous materials from the new kingdom site of amarna- a reappraisal. *Archaeometry, 45*, 258-312.

Tite, M. S., Shortland, A. J., Schibille, N., & Degryse, P. (2016). New Data on the Soda Flux Used in the Production of Iznik Glazes and Byzantine Glasses. *Archaeometry, 58*, 57-67.

Turnbull, S. R. (2003). *Crusader Castles of the Teutonic Knights (1): The red-brick castles of Prussia 1230-1466*, Osprey Publishing, **1**.

Turner, W., & Rooksby, H. (1961). Further historical studies based on X-ray diffraction methods of the reagents employed in making opal and opaque glasses. *Jb RGZM, 8*, 1-6.

Turner, W. E. S. (1956). Studies in Ancient Glasses and Glassmaking Processes: Raw Materials and Melting Processes, part V. *Journal of the Society of Glass technology, 38*, 436-444.

van Gorder, C. (2008). *Muslim-Christian Relations in Central Asia*, New York, Routledge, 31.

Van Grieken, R., & Markowicz, A. (2001). *Handbook of X-Ray Spectrometry, Second Edition*, CRC Press, 1016.

van Sprang, H. (2000). Fundamental Parameter in XRF Spectroscopy. *JCPDS International Center for Diffraction Data, 42*, 1-10.

Vandiver, P. (2005). *Craft and Knowledge as an Inangible Cultural Property: A Case study of Samarkand tiles and Traditional Potters in Uzbekistan.* Paper presented at the Material Research Society Symposium, Boston, Massachusetts, USA, 331-352.

Vandiver, P., Rakhimov, A., & Rakhimov, A. (2010). *Ishkor glazes from Uzbekistan.* Paper presented at the Proceedings of the Second International Conference on the Conservation of Grotto Sites, 234-248.

Vaz, M., Pires, J., & Carvalho, A. (2008). Effect of the impregnation treatment with Paraloid B-72 on the properties of old Portuguese ceramic tiles. *Journal of Cultural Heritage, 9*, 269-276.

Victoria and Albert Museum, L. (2014). Champlevé Enamelling, 1100-1250. *The world's greatest museum of art and design.* 2014: http://www.vam.ac.uk/content/articles/c/champleve-enamelling-1100-1250/

Viñas, S. M. (2002). Contemporary theory of conservation. *Studies in Conservation, 47*, 25-34.

Volceanov, A. (2008). Basicity or Ionicity–A New Approach for Understanding Glass Properties. *Advanced Materials Research, 39*, 129-134.

Wang, K. W. (2009). *The study of Early Islamic Alkali Glaze in Medieval Central Asia.* Paper presented at the European Meeting on Ancient Ceramics, London, 99.

Watson, O. (1985). *Persian lustre ware*, London, Faber and Faber Limited, *1*, 23.

Wedepohl, K. H., Krueger, I., & Hartmann, G. (1995). Medieval lead glass from northwestern europe. *Journal of Glass Studies, 1937*, 65-82.

Weeks, L. (1999). Lead isotope analyses from Tell Abraq UAE new data regarding the tin problem in Western Asia. *Antiquity, 73*, 49-64.

Wen, R., & Pollard, A. M. (2016). The Pigments Applied to Islamic Minai Wares and the Correlation with Chinese Blue-and-White Porcelain. *Archaeometry, 58*, 1-16.

Weyl, W. A. (1967). *Coloured glass*, Society of Glass Technology, *1*, 557.

Winkelmann, A., & Schott, O. (1894). Ueber thermische Widerstandscoefficienten verschiedener Gläser in ihrer Abhängigkeit von der chemischen Zusammensetzung. *Annalen der Physik, 287*, 730-746.

Wolf, S., Stos, S., Mason, R., & Tite, M. (2003). Lead isotope analyses of islamic pottery glazes from Fustat, Egypt. *Archaeometry, 45*, 405-420.

Wolff, S. R., Liddy, D. J., Newton, G. W. A., Robinson, V. J., & Smith, R. J. (1986). Classical and Hellenistic black glazenext term ware in the Mediterranean: A study by epithermal neutron activation analysis. *Journal of Archaeological Science, 13*, 245-259.

Wulff, H. E., Wulff, H. S., & Koch, L. (1968). Egyptian faience-a possible survival in Iran. *Archaeology, 21*, 98-107.

Xie, G., Feng, S., Feng, X., Wang, Y., Zhu, J., Yan, L., . . . Han, H. (2007). Study on ancient Chinese imitated GE ware by INAA and WDXRF. *Nuclear Instruments and Methods in Physics Research Section B: Beam Interactions with Materials and Atoms, 264*, 103-108.

Yamaguchi, K. E. (2010). Iron isotope compositions of Fe-oxide as a measure of water-rock interaction: An example from Precambrian tropical laterite in Botswana. *Frontier Research on Earth Evolution, 2*, 4.

Yousef Jameel Centre, I. a. A. A. (2013). Ottoman ceramics. *Eastern Art Online: Yousef Jameel Centre for Islamic and Asian Art.* 2015: http://www.jameelcentre.ashmolean.org/collection/4/653/834

Zucchiatti, A., Azzou, A., El amraoui, M., Haddad, M., Bejjit, L., & S., A. l. (2009). Pixe analysis of moroccan architectural glazed ceramics of 14th-18th centuries. *International Journal of PIXE, 19*, 175-185.